



Asphalt Research Consortium

Quarterly Technical Progress Report July 1-September 30, 2010

October 2010

Prepared for
Federal Highway Administration
Contract No. DTFH61-07-H-00009

By
Western Research Institute
Texas A&M University
University of Wisconsin-Madison
University of Nevada-Reno
Advanced Asphalt Technologies

www.westernresearch.org
www.ARC.unr.edu

TABLE OF CONTENTS

INTRODUCTION	1
GENERAL CONSORTIUM ACTIVITIES	3
PROGRAM AREA: MOISTURE DAMAGE.....	5
Category M1: Adhesion.....	5
Category M2: Cohesion.....	14
Category M3: Aggregate Surface	15
Category M4: Modeling.....	16
Category M5: Moisture Damage Prediction System	23
PROGRAM AREA: FATIGUE.....	27
Category F1: Material and Mixture Properties	27
Category F2: Test Method Development.....	58
Category F3: Modeling.....	77
PROGRAM AREA: ENGINEERED MATERIALS.....	111
Category E1: Modeling.....	111
Category E2: Design Guidance.....	132
PROGRAM AREA: VEHICLE-PAVEMENT INTERACTION.....	163
Category VP1: Workshop.....	163
Category VP2: Design Guidance.....	163
Category VP3: Modeling.....	165
PROGRAM AREA: VALIDATION	175
Category V1: Field Validation.....	175
Category V2: Accelerated Pavement Testing.....	176
Category V3: R&D Validation	177
PROGRAM AREA: TECHNOLOGY DEVELOPMENT.....	187
PROGRAM AREA: TECHNOLOGY TRANSFER.....	189
Category TT1: Outreach and Databases	189

INTRODUCTION

This document is the Quarterly Report for the period of July 1 to September 30, 2010 for the Federal Highway Administration (FHWA) Contract DTFH61-07-H-00009, the Asphalt Research Consortium (ARC). The Consortium is coordinated by Western Research Institute with partners Texas A&M University, the University of Wisconsin-Madison, the University of Nevada Reno, and Advanced Asphalt Technologies.

The Quarterly Report is grouped into seven areas, Moisture Damage, Fatigue, Engineered Paving Materials, Vehicle-Pavement Interaction, Validation, Technology Development, and Technology Transfer. The format of the report is based upon the Research Work Plan that is grouped by Work Element and Subtask.

This Quarterly Report summarizes the work accomplishments, data, and analysis for the various Work Elements and Subtasks. This report is being presented in a brief summary form. Please note that in many cases the report is briefer than in the past at the request of FHWA AOTR Mr. Eric Weaver. The Quarter of July 1 to September 30, 2010 is second quarter of the Year 4 contract year. Reviewers may want to reference the Year 4 Work Plan and perhaps the earlier Work Plans. There is also background information regarding the research plan contained in the Revised Year 2 Work Plan. The more detailed information about the research such as approaches to test method development, data collection, and analyses will be reported in research publications as part of the deliverables. All of the Work Plans, as well as many other documents, including quarterly reports, are posted on the ARC website, www.ARC.unr.edu.

SUPPORT OF FHWA AND DOT STRATEGIC GOALS

The Asphalt Research Consortium research is responsive to the needs of asphalt engineers and technologists, state DOT's, and supports the FHWA Strategic Goals and the Asphalt Pavement Road Map. More specifically, the research reported here supports the Strategic Goals of safety, mobility, and environmental stewardship. By addressing the causes of pavement failure and thus determining methods to improve asphalt pavement durability and longevity, this research will provide the motoring public with increased safety and mobility. The research directed at improved use of recycled asphalt pavement (RAP), warm mix asphalt, and cold mix asphalt supports the Strategic Goal of environmental stewardship.

GENERAL CONSORTIUM ACTIVITIES

PROGRESS THIS QUARTER

Several ARC members attended and made presentations at the 47th Petersen Asphalt Research Conference and the 2010 Pavement Performance Prediction Symposium in Laramie, Wyoming in July.

The ARC Asphalt Microstructural Modeling team members Mr. Troy Pauli, Dr. Michael Greenfield, Dr. Linbing Wang, and Dr. Jeffrey Bullard met during the week of the Petersen Conference to discuss project progress, coordination, and work plans.

The Asphalt Research Consortium members submitted many papers for presentation and/or publication at the 90th Annual Transportation Research Board meeting in January 2011. The papers submitted are listed in the Technology Transfer section (Work Element TT1c) of this report.

Several ARC members attended and made presentations at the Binder, Mix & Construction, and Fundamental Properties & Advanced Models ETG meetings in Madison, Wisconsin during the week of September 13 – 17, 2010.

Dr. Ramon Bonaquist continues to work with Mr. Frank Fee to coordinate sampling of materials for the Mixtures and Construction ETG's flow number study and will assist with coordination of the testing at the National Institute of Standards and Technology (NIST) and the University of Nevada, Reno.

WORK PLANNED FOR NEXT QUARTER

ARC members, Dr. Hussain Bahia, Dr. Elie Hajj, Dr. Eric Kalberer, and Mr. Michael Harnsberger are planning to attend the RAP Expert Task Group meeting in Oklahoma City, Oklahoma on October 26 & 27, 2010. An update on the RAP research being conducted by the ARC will be presented. In addition to the above ARC members, Dr. Ramon Bonaquist is planning on attending the Warm-Mix Technical Working Group meeting being held in conjunction with the RAP ETG on October 27 & 28, 2010.

Dr. Ramon Bonaquist of Advanced Asphalt Technologies will continue to work with Mr. Frank Fee of NuStar Energy to coordinate sampling of materials for the flow number study requested and approved by the Mixture and Construction ETG.

PROGRAM AREA: MOISTURE DAMAGE

CATEGORY M1: ADHESION

Work Element M1a: Affinity of Asphalt to Aggregate (UWM)

Work Done This Quarter

In this quarter, the research group focused its efforts on validating the effectiveness of the Bitumen Bond Strength (BBS) test for moisture damage evaluation. A comparison between the BBS test results and the modified Dynamic Shear Rheometer (DSR) strain sweep test was conducted. The comparison shows that the BBS test can rank materials similarly to a more sophisticated and time-consuming test. The materials used are listed in table M1a.1.

Table M1a.1. Materials used to compare BBS with DSR strain sweep tests.

Solution	Tap Water
Mineral Surface	Granite
Asphalt Binders	FH 64-22 & CRM 58-28
Modified Asphalt Binders	FH 64-22 + 0.7% Elvaloy (ELV) + 0.17% Polyphosphoric Acid (PPA) & CRM 58-28 + Styrene-Butadiene-Styrene (SBS)

The strain sweep tests in the DSR are performed using a cored rock disk of 25 mm in diameter and 5-mm thick as the bottom plate (i.e., substrate). The rock disk and the asphalt binder simulate the asphalt-aggregate interface in the asphalt mixture. In this test, a water cup specially manufactured for the DSR is used for water conditioning. In order to monitor moisture damage in the asphalt-aggregate interface, rheological responses were measured using oscillatory loads with shear strains varying from 1% to 100% at a frequency of 1.6 Hz frequency (i.e., 10 rad/sec) and 40 °C, for both dry and wet (using tap water) conditioning. Two replicates were tested for each condition and test type.

Figure M1a.1 shows a typical result obtained from the DSR strain sweep procedure. It can be seen that water conditioning significantly affects the rheological properties of asphalt-aggregate systems.

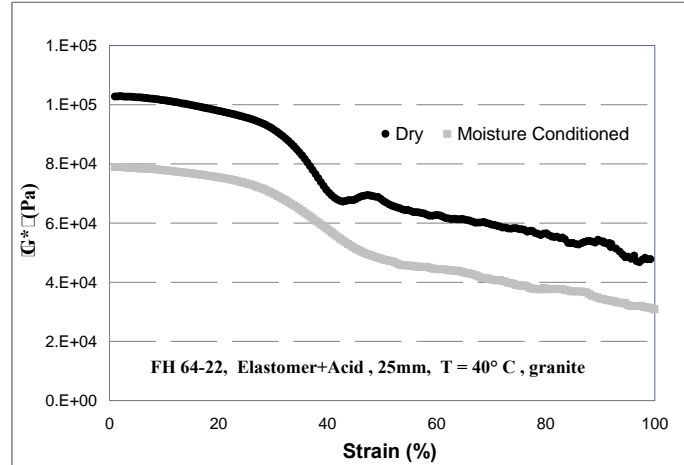


Figure M1a.1. Graph. Strain sweep test in DSR for FH 64-22+ELV+PPA and granite in dry and wet conditions.

Comparison of the BBS and DSR procedures involved the calculation of the percent loss of a specific property after water conditioning for 6 hours. In the case of the BBS test, the pull-off tensile strength (POTS) was used to calculate moisture susceptibility. On the other hand, for the DSR strain sweep test, the complex modulus $|G^*|$ at a strain of 1% was selected as the parameter. Note that similar results were obtained when selecting the complex modulus at higher strain levels (i.e., $\gamma=100\%$). The following equation was used to compute moisture damage in the BBS test:

$$\%Loss_After_Moisture_BBS = 1 - \frac{POTS_{WET}}{POTS_{DRY}} \quad (M1a.1)$$

where $POTS_{DRY}$ and $POTS_{WET}$ are the pull-off tensile strength from BBS test in dry and moisture conditioning after 6 hours, respectively. To calculate the moisture damage in the strain sweep test, the following equation was used:

$$\%Loss_After_Moisture_DSR = 1 - \frac{|G^*|_{\gamma=1\%,_WET}}{|G^*|_{\gamma=1\%,_DRY}} \quad (M1a.2)$$

where $|G^*|_{\gamma=1\%,_WET}$ and $|G^*|_{\gamma=1\%,_DRY}$ are the complex modulus at a shear strain of 1% from DSR testing in dry and moisture conditioning after 6 hours, respectively.

Table M1a.2 shows the results for the three asphalt-aggregate systems tested in the BBS and DSR. It can be seen that the moisture susceptibility ranking from the BBS test and the DSR strain sweep test are the same.

Table M1a.2. Ranking moisture susceptibility of three different asphalt-aggregate systems with BBS and DSR testing.

Asphalt-Aggregate System Description	%Loss_DSR	%Loss_BBS	Ranking DSR	Ranking BBS
CRM 58-28 neat Granite	10%	24%	2	2
CRM 58-28+SBS Granite	8%	22%	1	1
FH 64-22+ELV+PPA Granite	23%	26%	3	3

In addition to the work on BBS and DSR, the team started the training on measuring the surface energy using the atomic force microscope (AFM) equipment at UW–Madison. The team has conducted a detailed literature search and identified the AFM as a possible method to explain and verify the changes in bond strength measured in the BBS and/or DSR.

Significant Results

The research team obtained promising results regarding the feasibility of the BBS test for the characterization of the asphalt-aggregate interface. Limited results on the validation/verification of the BBS test procedure with the modified DSR strain sweep test indicates that the BBS test can rank the asphalt-aggregate systems with respect to moisture damage similarly to more sophisticated and time-consuming tests. Note that results are preliminary and a more extensive test matrix needs to be performed for such comparison. It is clear that the BBS test is a simpler and more practical test. The comparison is needed only for validation of the results in terms of ranking of aggregate-binder systems. A draft AASHTO standard for the BBS test procedure was submitted in this quarter for final approval.

Significant Problems, Issues and Potential Impact on Progress

None.

Work Planned Next Quarter

The research team will continue testing the experimental matrix in the Year 4 work plan. Emphasis will be given to continuing the validation/verification of the BBS test procedure by performing Tensile Strength Ratio (TSR) tests of asphalt mixtures and by extending the experimental matrix which compares BBS with the modified DSR strain sweep test.

Efforts will also focus on understanding the mechanisms of adhesion between asphalt and aggregate based on surface energy measurements with the AFM. The team is expecting to show that the BBS test can be used to determine the moisture susceptibility of asphalt-aggregate systems and as a surrogate test for surface energy measurements.

Work Element M1b: Work of Adhesion Based on Surface Energy

Subtask M1b-1: Surface Free Energy and Micro-Calorimeter Based Measurements for Work of Adhesion (TAMU)

Work Done This Quarter

The main goal of this subtask is to provide material property inputs required in other work elements as required. Any data obtained from this subtask will be included in the material properties database. In the last quarter surface free energy of some aggregates and asphalt binders that are being used to develop test methods were measured.

Significant Results

None.

Significant Problems, Issues and Potential Impact on Progress

None.

Work Planned Next Quarter

Work on this subtask will be conducted in conjunction with and as required by other work elements.

Subtask M1b-2: Work of Adhesion at Nano-Scale using AFM (WRI)

Work Done This Quarter

During this past quarter experiments were conducted in which glass substrates were bonded together with a thin film of asphalt and then subjected to moisture to determine the effect of exposure to water on the adhesive bond between asphalt and glass. Samples were prepared as “sandwiches” with asphalt between two glass microscope slides. SHRP core asphalts AAD-1 and AAK-1, representing a soft and a hard asphalt respectively, were used for these experiments. Samples were prepared by placing a small spot of asphalt on the center of a clean microscope slide, covering with a second clean side, and then heating in an oven at $\sim 120^{\circ}\text{C}$ for about one-half hour with a small weight on top of the stack. The prepared samples had an asphalt film thickness of $\sim 10\text{-}\mu\text{m}$. One set of the prepared slides was exposed to water in the liquid phase by placing the slides in a container and submerging them in water. The second set was placed in a small sealed enclosure along with a pan of water to expose the sample to moisture in the vapor phase. Samples were in contact with moisture for 18-hours before they were removed from their respective containers and allowed to air dry on the bench for $\sim 4\text{-hours}$. A third set of control samples was prepared for both asphalts. Control samples were not exposed to moisture. After drying, the samples were popped apart by applying a pulling pressure to the top slide in the “sandwich”.

Significant Results

The samples that were submerged in water had little or no strength and popped apart easily with the application of almost no force. The samples that were exposed to the saturated vapor were slightly stronger, but were still very easily separated. Both sets of samples were separated without freezing. Control samples that were not exposed to moisture were much more strongly bonded. An attempt to separate the AAK sandwich (without freezing) that had not been exposed to moisture resulted in breaking of the slide, even though pressure was applied very gradually. The AAD control sample was separated by a very slow and careful pulling motion applied to the top slide. While there was no quantitative measure of the effort needed to separate the slides, it was quite evident that the strength of the asphalt bond was diminished greatly by exposure to water as either liquid or vapor. Separation of the AAD control sample left a significant asphalt film on both of the slides. Both of these residual films appeared to be of about equal thickness and both showed an obvious, and equivalent, patterning. Separation of the control sample at room-temperature left about half of the asphalt on each slide, and was obviously by cohesive failure through a zone near the center of the asphalt film.

In contrast to the control samples and samples separated at low temperature (work conducted in the previous quarter), “sandwich” samples separated at room-temperature after exposure to moisture typically exhibited one substrate surface that appeared to be clean with no evident residual asphalt film. For the samples that were exposed to moisture adhesive failure between the asphalt and the glass substrate appears to be the dominant failure mechanism. AFM imaging of the apparently bare substrate surface after separation showed only a few small patches of residual asphalt on the otherwise clean glass surface after the slides were separated. There was no evidence of the essentially continuous residual asphalt film as was seen when similar samples were separated at low temperature without exposure to moisture. This does not, however, exclude the possibility of a continuous film of water which would not be evident in AFM images of the surfaces.

The force needed to separate two parallel plates held together by a thin liquid film must exceed the sum of the attractive meniscus and viscous forces that hold the plates together. The strength of the meniscus force results from both surface tension around the circumference of the intervening liquid film and Laplace (capillary) pressure and is therefore dependent upon the liquid properties and the size of the meniscus. The viscous force is related to liquid properties and meniscus size as well as the initial thickness of the liquid film and the rate at which the surfaces are separated. The force needed to overcome the attractive forces that hold the two surfaces together can thus be written as:

$$F_a = F_m + F_v$$

Where F_a is the total attractive force of adhesion holding the plates together, F_m is the force contributed by the meniscus, and F_v is the viscous force component. As stated above, the force contributed by the meniscus is composed of a component related to capillary pressure and a component related to surface tension. This simple equation can be expanded as shown below. In this expression the left half of the right side of the equation represents the meniscus force and the right half of the right side of the equation represents the viscous force. Note that the viscous part

of the force contains a time term (t_s) that does not appear in the expression for the meniscus force.

$$F_a = \left[\frac{\pi x_n^2 \gamma (\cos\theta_1 + \cos\theta_2)}{h} + 2\pi\gamma x_n \sin\theta_{1,2} \right] + \frac{3\pi\eta x_n^4}{4t_s} \left(\frac{1}{h_s^2} - \frac{1}{h_0^2} \right)$$

Where: F_a is the total adhesive force, x_n is the radius of the meniscus with respect to an axisymmetric line orthogonal to the plane of the substrate surfaces, γ is the surface tension of the liquid, θ_1 and θ_2 are the contact angles between the liquid and the top and bottom plates, h and h_0 are the initial film thickness (or spacing between the plates), h_s is the spacing between the plates at separation, t_s is the time of separation, and η is the viscosity of the liquid (Cai and Bhushan 2007).

For the case of asphalt adhesive exposed to water, our experiments show that h_s approaches h_0 so that the contribution of the viscous force to the total adhesive force approaches 0. This leaves only the portion of the adhesive force that is related to the meniscus force.

Considering the relative surface energies of glass, asphalt, and water we see that water can be expected to displace the lower surface energy asphalt film when the asphalt glass “sandwich” is exposed to moisture for a sufficient length of time. When this occurs, the glass/asphalt interface is destroyed and in its place we now find a glass/water/asphalt interface. Inspection of the first term on the right hand side of the above equation, the capillary pressure term, indicates that the interface between water and glass can be expected to be rather strong. However, for the water/asphalt interface (where the contact angle approaches 90-degrees) cosine θ approaches 0 as does the contribution from the capillary pressure term. The remaining part of this term ($2\pi\gamma x_n \sin\theta_{1,2}$) represents the contribution of surface tension at the circumference of the meniscus to the overall adhesive bond strength. Again, it is the water/asphalt interface that dominates the adhesive strength since this is the weak link in the chain. Thus, we see that when a glass/asphalt interface is exposed to water, either as liquid or vapor, the contribution of capillary pressure and viscous force to the total adhesive force approaches zero, and the adhesive strength is reduced to essentially represent only the contribution from the surface tension around the circumference of the meniscus.

Figure M1b-2.1, A, B, C, D, E, F shows topography and corresponding phase image of the asphalt surface after the separation of “sandwich” samples under various conditions. All of the images are of SHRP core asphalt AAK-1. Figure M1b-2.1, A and B shows the topography and phase images, respectively, of the asphalt surface for a sample that was frozen, popped apart, and thermally treated (heated at $\sim 120^\circ$ C for 40-minutes and cooled) before imaging. The image shows the familiar “bee-structures” as typically seen for solvent spin-cast samples of this asphalt. Figure M1b-2.1, C and D shows the topography and phase images, respectively, of the asphalt surface for a sample that was frozen and popped apart and imaged without thermal treatment. Figure M1b-2.1, E and F shows the topography and phase images of the asphalt surface for a sample that was exposed to moisture and then popped apart and imaged without thermal treatment.

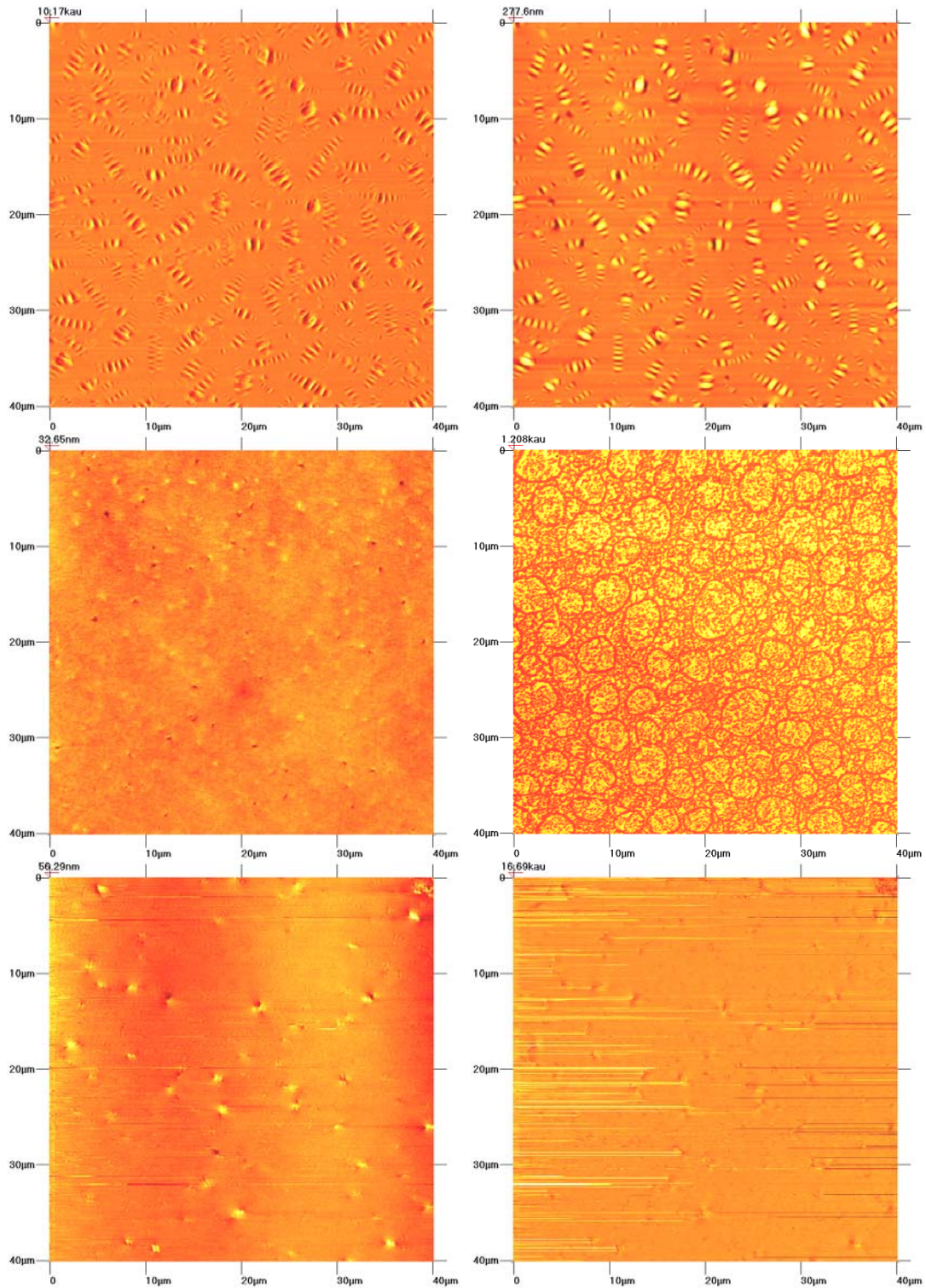


Figure M1b-2.1 A, B, C, D, E, F. Topography and phase images of AAK-1 asphalt surfaces resulting after various preparation techniques.

The images of the AAK asphalt surface resulting after these various preparation techniques show several interesting features. Note that the images shown in figure M1b-2.1 A and B are of the same surface as shown in figure M1b-2.1 C and D. The characteristic “bee-structures” do not appear until after thermal treatment, and the topography is much smoother (~ 33 -nm vs. 278 -nm maximum feature height) for the surface before thermal treatment. The phase image of this surface shows a distinct two-phase patterning with no apparent correlation between the topography and phase images until after the thermal treatment. After heating, the “bee-structures” appear in both the topography and phase images with an obvious correspondence between the two image types. Considering that the “sandwich” samples were prepared under essentially the same thermal conditions as were used for thermal treatment after the “sandwich” was separated, these observations support the concept that the “bee-structures”, as observed by many researchers over the past decade, are a phenomenon associated with the air/asphalt interface. While other factors may be involved in the relative appearances of the two surfaces, a significant difference is that one was heated in contact with air where the other was heated while covered with a glass slide.

Figure M1b-2.1 C and E show topography images of the asphalt surface after “sandwich” samples were popped apart after freezing and after exposure to moisture respectively. Both of the panels show a relatively smooth surface with no obvious “bee-structures”. The sample that was separated after exposure to moisture has a maximum feature height of ~ 56 -nm compared to only ~ 33 -nm for the sample separated after freezing. For comparison, the bare glass slide upon which the samples were prepared typically exhibits ~ 22 -nm of topography in an image of this size. Clearly, these surfaces are quite smooth. If we zoom in on a 20×20 - μm area on the freeze sample surface we obtain an image that looks almost identical to the surface separated after exposure to moisture. That is, features in the moisture sample are approximately twice as large (in the X-Y plane) as the features seen in the freeze sample. A similar scaling also can be applied to the height (Z-axis) of the features.

Figure M1b-2.1 B, D and F show phase images of the asphalt surface after “sandwich” samples were popped apart after freezing followed by thermal treatment, after freezing without thermal treatment, and after exposure to moisture respectively. The three surfaces bear little resemblance to each other and could easily be construed as images of three entirely different materials. Figure M1b-2.1 D exhibits a distinct two-phase structuring with an obvious pattern associated with the phase distribution. The other two images can be interpreted to represent essentially single phase systems in that the “bee-structures” seen in panel B are quite possibly an artifact reflecting the underlying surface topography of this sample. We typically associate the streaked appearance as seen in the phase image of the surface separated after exposure to moisture (panel F) with a sample with considerable liquid characteristics. This type of phase image is often seen for the softer asphalts, but is very unusual for harder asphalts such as AAK-1. A possible explanation for this liquid-like appearance could be that the asphalt in contact with the glass surface was emulsified by exposure to moisture.

Significant Problems, Issues and Potential Impact on Progress

We have experience some delay in obtaining polished aggregate slices for use as solid substrates in adhesion testing.

Work Planned Next Quarter

Experiments conducted this past quarter used a glass substrate as a surrogate for an aggregate surface. Next quarter we hope to obtain specimens of commonly used aggregate materials with different degrees of surface polish and to repeat freezing and moisture experiments using these samples. We will also continue development of nano-rheological techniques which could lead to a much more thorough understanding of the asphalt/aggregate interface.

Cited Reference

Cai, Shaobiao, and B.Bhushan, 2007, Meniscus and viscous forces during normal separation of liquid-mediated contacts. *Nanotechnology*, 18: 1-14.

Subtask M1b-3: Identify Mechanisms of Competition Between Water and Organic Molecules for Aggregate Surface (TAMU)

Work Done This Quarter

This task was temporarily suspended in the last quarter and resources were diverted to the task on the validation of PANDA. We expect to resume work on this task as soon as we complete some of the laboratory work required for the validation of PANDA.

Significant Results

There are no significant results for this quarter.

Significant Problems, Issues and Potential Impact on Progress

Although this task is temporarily suspended, we expect to resume the task in near future and accomplish the objectives as indicated in the work plan.

Work Planned Next Quarter

We expect to resume work on this task as outlined in the work plan.

Work Element M1c: Quantifying Moisture Damage Using DMA (TAMU)

Work Done This Quarter

This work element was completed and findings were reported in previous quarterly reports. There was no activity this quarter. The following paper is accepted for presentation at the TRB (2011).

Sousa, P., E. Kassem, E. Masad, and D. Little, 2011, "New Design Method of Fine Aggregates Mixtures and Automated Method for Analysis of Dynamic Mechanical Characterization Data", The 90th Annual Meeting, Transportation Research Board, Washington, D.C., January 2011 (accepted for presentation).

CATEGORY M2: COHESION

Work Element M2a: Work of Cohesion Based on Surface Energy

Subtask M2a-1: Methods to Determine Surface Free Energy of Saturated Asphalt Binders (TAMU)

Work Done This Quarter

No activity was planned for this quarter.

Work Planned Next Quarter

Work on this task is anticipated to start in year 4 of the project.

Subtask M2a-2: Work of Cohesion Measured at Nano-Scale using AFM (WRI)

Work Done This Quarter

Work which is relevant to this subtask is reported under subtask heading M1b-2 "Work of adhesion at Nano-Scale using AFM".

Significant Results

Please see results reported for subtask M1b-2.

Significant Problems, Issues and Potential Impact on Progress

None.

Work Planned Next Quarter

Work directed toward developing nano-rheology techniques will continue next quarter.

Work Element M2b: Impact of Moisture Diffusion in Asphalt Mixtures

Subtask M2b-1: Measurements of Diffusion in Asphalt Binders and Mixtures (TAMU)

Subtask M2b-2: Kinetics of Debonding at the Binder-Aggregate Interface (TAMU)

Work Done This Quarter

There was no activity this quarter.

Significant Results

None.

Significant Problems, Issues and Potential Impact on Progress

None.

Work Planned Next Quarter

We have accomplished significant portions of this work element including measurement of diffusion through binders and fine aggregate matrix. Further work will be conducted if prioritized based on the requirements from other work elements.

Work Element M2c: Measuring Thin Film Cohesion and Adhesion Using the PATTI Test and the DSR (UWM)

Most work is completed. The remaining activity is reported under Work Element M1a.

CATEGORY M3: AGGREGATE SURFACE

Work Element M3a: Aggregate Surface Characterization (TAMU)

Work Done This Quarter

This work element was completed and findings were reported in previous quarterly reports. There was no activity this quarter.

CATEGORY M4: MODELING

Work Element M4a: Micromechanics Model (TAMU)

A model for predicting and characterizing fracture damage of asphalt mixtures subject to moisture damage has been developed based on cohesive zone concept. This has been attempted by coupling the effect of moisture diffusion with the mechanical performance of asphalt mixtures by means of two key mechanisms: (1) stiffness reduction of the asphalt matrix (also referred to as fine aggregate matrix(FAM) phase); and (2) deterioration of the mechanical and fracture properties of the matrix-matrix interfaces (i.e., cohesive fracture) and matrix-aggregate interfaces (i.e., adhesive fracture); as a function of the amount of moisture present in the mixture.

In the model, different material constitutions (elastic, linear and nonlinear viscoelastic materials), mixture microstructure, and cohesive zone fracture characteristics are implemented within a commercial finite element software, ABAQUS in the form of UMAT (User MAterial) and UEL (User Element), which is intended to simulate material-specific, nonlinear-inelastic microscale fracture and its propagation to complete failure incorporated with moisture damage in asphaltic composites with maximum versatility.

Work Done This Quarter

During this quarter we have mainly progressed fracture tests of semi-circular bend (SCB) specimens with several different levels of moisture conditioning and the numerical simulations of the SCB fracture tests using sequentially coupled moisture diffusion-mechanical analysis. Work progress and significance of each activity can be summarized as follows:

Test Results

The SCB fracture tests were conducted with five different moisture conditioning levels: 0-day, 1-day, 7-day, 13-day, and 30-day submerged in a water bath at 25°C. Unconditioned specimens (i.e., 0-day) were kept inside a dry chamber at the same testing temperature (25°C) to maintain equal testing conditions. For each case, three SCB specimens were tested at a constant loading rate: 100 mm/min. Test results in the form of applied force vs. line point displacement at different levels of conditioning are presented in figure M4a.1. As expected, the figure clearly demonstrates that all cases underwent damage due to moisture conditioning, and the level of damage increased as the conditioning time increased, which implies that the moisture infiltration in the specimens is detrimental to the integrity of asphalt mixtures.

Finite Element Model Simulation

In order to perform the sequentially coupled (i.e., diffusion followed by mechanical loading) simulation, two finite element meshes as illustrated in figure M4a.2, were generated. For the diffusion simulation, no cohesive zone element was embedded in the mesh as shown in figure M4a.2(a), whereas the zero thickness cohesive elements were inserted along the center of the mesh to permit mode I crack growth, as illustrated in figure M4a.2(b).

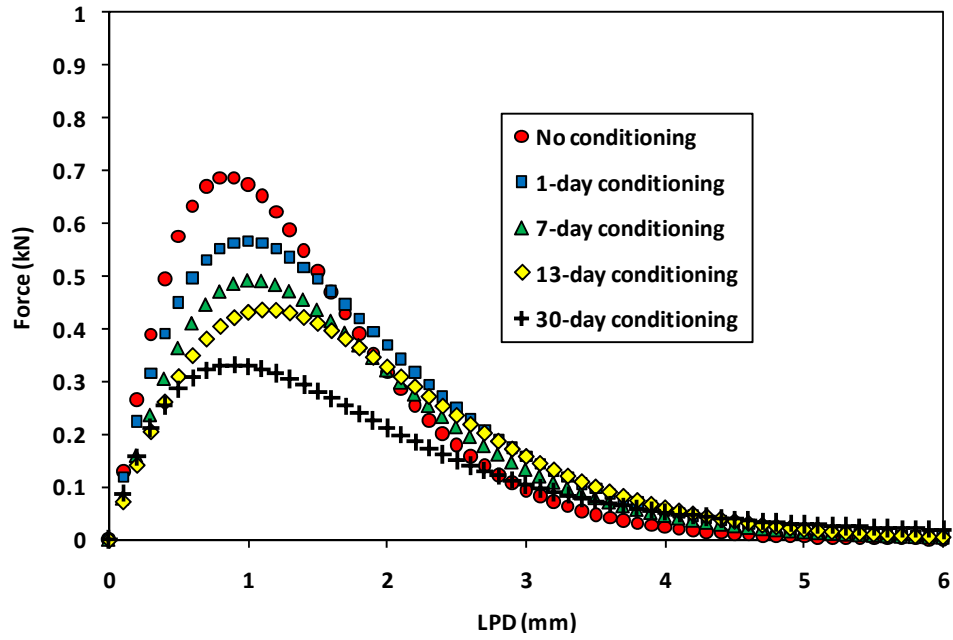


Figure M4a.1. SCB fracture test results at different levels of moisture conditioning.

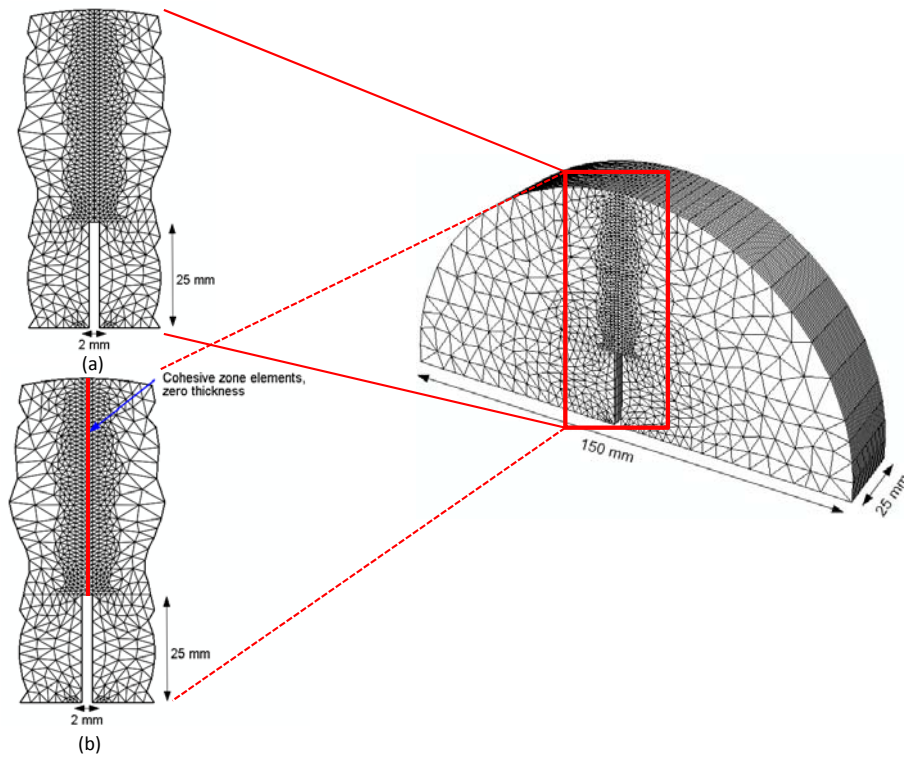


Figure M4a.2. Finite element mesh constructed: (a) diffusion analysis; (b) stress analysis.

Model Simulation Results

In the diffusion analysis, the moisture profile in the SCB specimen was generated by allowing moisture to diffuse in an isotropic manner into the bulk specimen for 1, 7, 13, and 30 days, as presented in figure M4a.3. For the coupling process, the generated moisture profiles shown in figure M4a.3 were then used as initial conditions in the stress analysis.

Figure M4a.4 illustrates a comparison between model simulations and test results plotting the applied load against line point displacements at the five different moisture conditionings. As shown, model simulations could successfully predict the progressive degradation as the level of moisture damage increased, and generally correlate with the experimental data over the whole process from damage initiation to complete fracture.

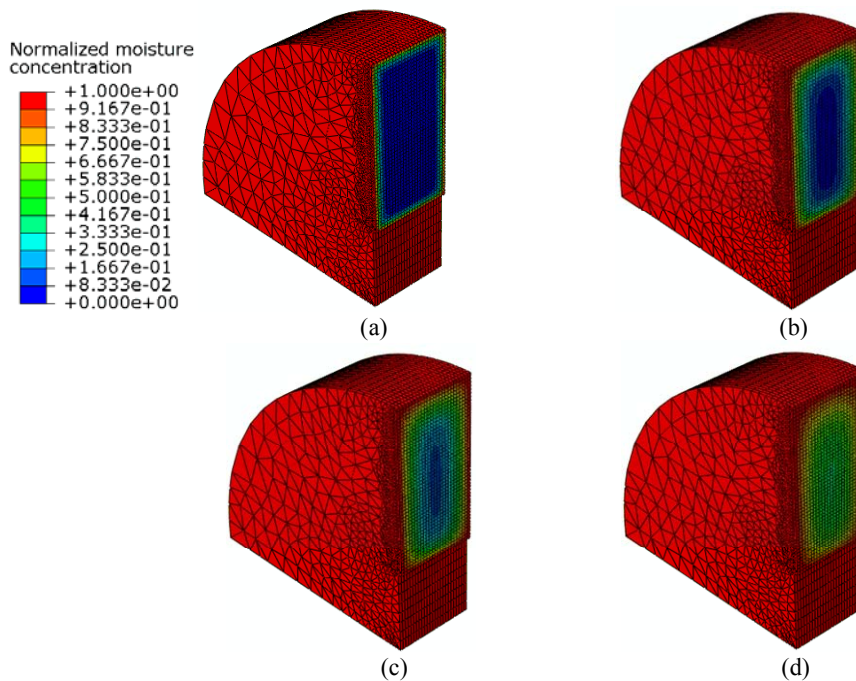
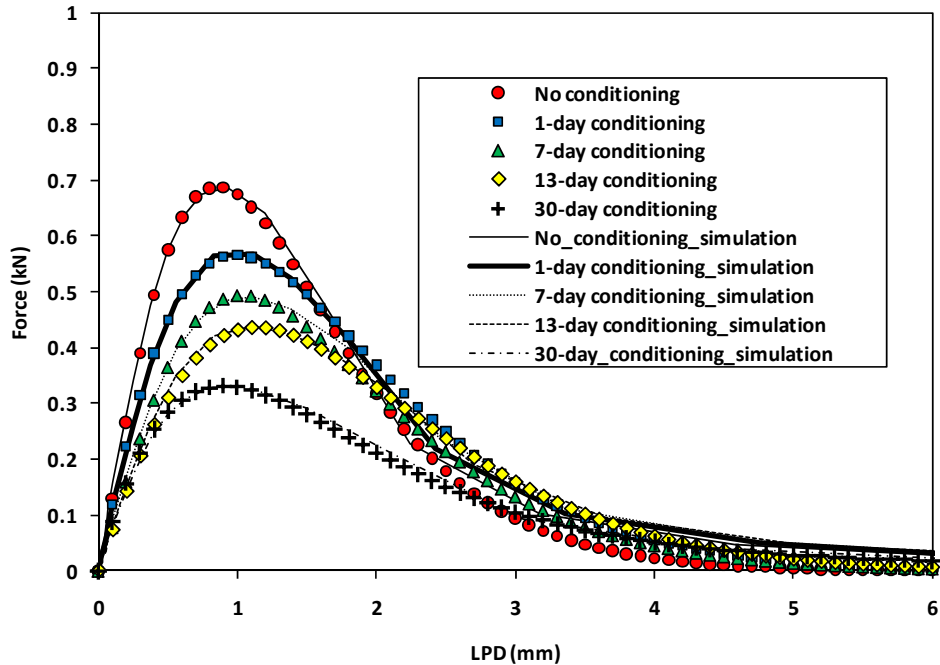


Figure M4a.3. Moisture diffusion profiles: (a) 1-day conditioning; (b) 7-day conditioning; (c) 13-day conditioning; and (d) 30-day conditioning.



FigureM4a.4. Comparison between experimental results and model simulations.

Significant Problems, Issues and Potential Impact on Progress

None.

Work Planned Next Quarter

In the next quarter we will work on the following activities:

- Microstructure modeling of asphalt mixtures with moisture damage through the sequentially coupled moisture diffusion-mechanical analysis.
- Parametric analyses of the microstructure model incorporated with moisture damage characteristics.

Work Element M4b: Analytical Fatigue Model for Mixture Design

This work is addressed under Work Elements F2b.

Work Element M4c: Unified Continuum Model

Work Done This Quarter

In this quarter, the moisture damage model that is implemented into the finite element program PANDA has been verified against a large set of experimental data from the literature. Moreover, the model has been modified to accurately capture the degradation in the mechanical properties due to moisture diffusion. The developed moisture damage model along with the viscoelastic, viscoplastic, and mechanical damage models has been used to predict the damage evolution in micromechanical representative volume elements of the asphalt mixture microstructure. These micromechanical simulations show that the developed continuum-based moisture damage model within PANDA can be used for two purposes: (1) conducting performance simulations on a pavements subjected to complex moisture and other environmental loading conditions; and (2) conducting fairly sophisticated micromechanical simulations that can be used to investigate the effects of microstructural features of an asphalt mixture on their moisture damage response. The later can be used to guide the design of asphalt mix microstructures for improved susceptibility to moisture-induced damage whereas the former can be used to predict the rutting performance and fatigue damage of a pavement and how the level of rutting or fatigue damage is affect by moisture.

In this quarter, numerous micromechanical simulations have been performed to see the effects at a smaller scale which leads to their continuum properties. Though the material model presented in PANDA is developed to model asphalt concretes as continua, it is extremely well-suited to asphalt mastic, which exhibits time-dependent recoverable and irrecoverable deformations, and degrades with loading and moisture exposure. The response of aggregates is usually very stiff and modeled with a simple linear elastic material law. For these simulations, finite element meshes were constructed with three types of regions: aggregates with arbitrary different shape and dimensions, asphalt mastic bulk, and asphalt mastic in the aggregate–mastic bond region. The material properties of mastic bulk and mastic in the aggregate-mastic bond region are the same except the adhesive and cohesive damage degradation properties, which are obtained from previous experimental data.

Significant Results

Figure M4c.1 shows an example of the ability of the continuum moisture-induced damage model in capturing the effect of moisture conditioning on the stress-strain response of an asphaltic mix under monotonic compressive loading. It can be seen from this figure that as the conditioning time increases as the initial stiffness, ultimate strength, and ductility decreases which is in qualitative agreement with experimental trends. Figure M4c.1 shows the corresponding final damage distribution at failure. It is clearly seen that damage localizes within highly moisture diffused regions indicating aggregate stripping from the mastic.

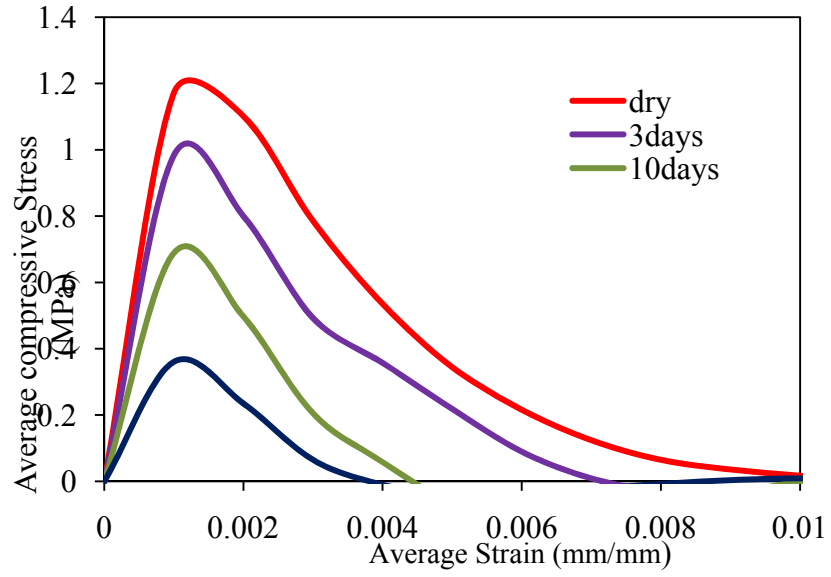


Figure M4c.1. Average stress-strain diagram for compressive loading.

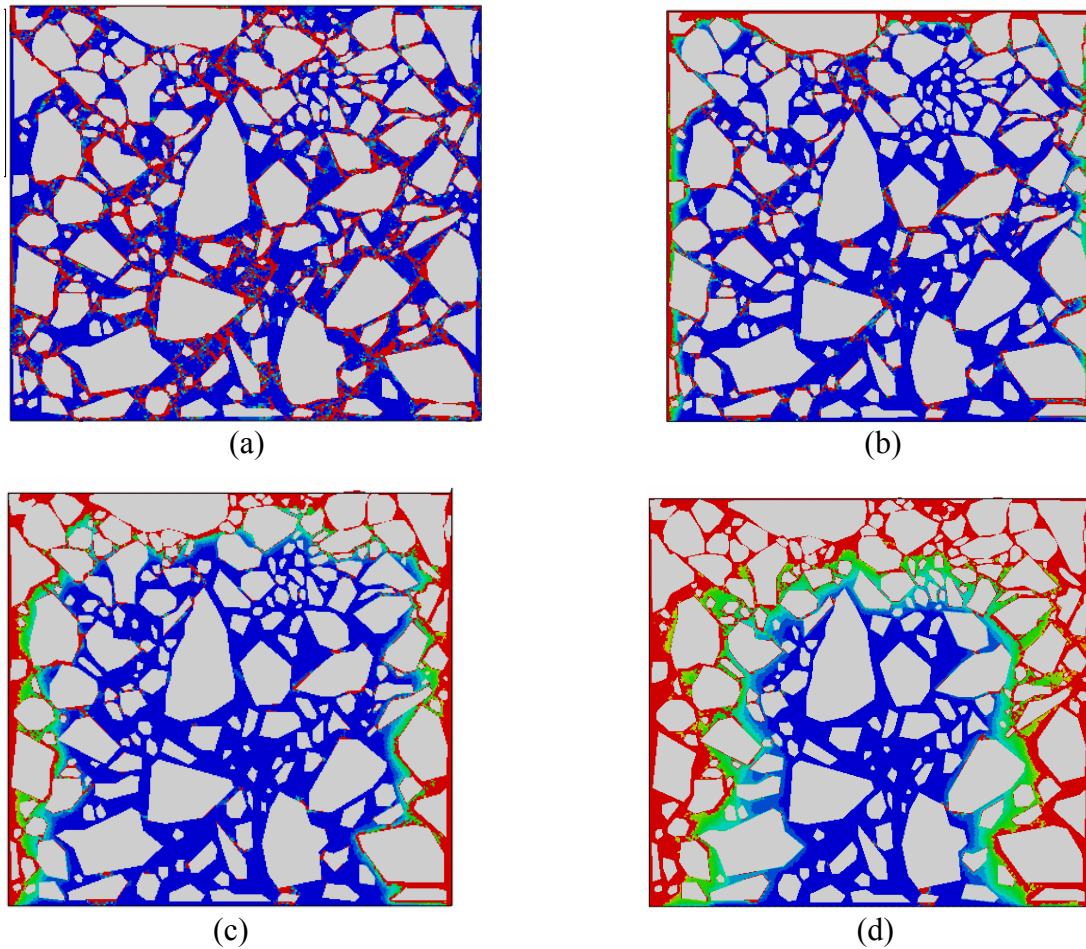


Figure M4c.2. Damage distribution after (a) 0 day, (b) 3 days, (c) 10 days, and (d) 30 days of moisture conditioning time.

The moisture-damage model is found to be capable of predicting damage evolution at the micro and macro scales due to moisture-induced damage. Therefore, one can use the developed models for guiding the design of asphalt mixture as well as to predict the performance of asphalt pavements.

Finally, the thermodynamic modeling for moisture-induced damage has been accomplished for the case of saturated viscoelastic material. For the unsaturated material including the effects of porosity and pore water pressure due to traffic movement will be considered in future work.

Significant Problems, Issues and Potential Impact on Progress

The small-scale pull-off tests that are conducted on an aggregate bonded to the mastic under different moisture conditioning times have resulted in large variability between the specimen replicates. Current efforts are focused on modifying the experimental setup and specimen preparation to reduce the variability. Once this is accomplished, this test will be essential for

further validation of the developed moisture damage constitutive equations and for identifying the material parameters.

Work Planned Next Quarter

A general thermodynamic framework has been developed for deriving complex constitutive equations for asphaltic materials by including moisture-induced damage effects. The focus of the next quarter is on using this thermodynamic framework for deriving constitutive equations that takes more complicated physical mechanisms that occur during moisture-induced damage. Moreover, a systematic procedure is still under development for identifying the material parameters associated with the constitutive models based on well-designed experiments at TAMU. The experiments include moisture conditioned pull-off tests on mastic-aggregate systems using the materials from the ARC 2x2 matrix validation plan.

CATEGORY M5: MOISTURE DAMAGE PREDICTION SYSTEM

Work on individual components such as test methods and micromechanics models required in the system is complete. The components will be put together in the form of a methodology towards the end of this project.

Moisture Damage Year 4		Year 4 (4/10-3/11)												Team
		4	5	6	7	8	9	10	11	12	1	2	3	
Adhesion														
M1a	Affinity of Asphalt to Aggregate - Mechanical Tests													
M1a-1	Select Materials												UWM	
M1a-2	Conduct modified DSR tests													
M1a-3	Evaluate the moisture damage of asphalt mixtures	P				JP						P		
M1a-4	Correlate moisture damage between DSR and mix tests													
M1a-5	Propose a Novel Testing Protocol										JP		F	
M1a-6	Standard Testing Procedure and Recommendation for Specifications							P						
M1b	Work of Adhesion													
M1b-1	Adhesion using Micro calorimeter and SFE												TAMU	
M1b-2	Evaluating adhesion at nano scale using AFM												WRI	
M1b-3	Mechanisms of water-organic molecule competition												TAMU	
M1c	Quantifying Moisture Damage Using DMA					JP				D			F	
Cohesion														
M2a	Work of Cohesion Based on Surface Energy													
M2a-1	Methods to determine SFE of saturated binders												TAMU	
M2a-2	Evaluating cohesion at nano scale using AFM												WRI	
M2b	Impact of Moisture Diffusion in Asphalt													
M2b-1	Diffusion of moisture through asphalt/mastic films			D				F					TAMU	
M2b-2	Kinetics of debonding at binder-aggregate interface													
M2c	Thin Film Rheology and Cohesion													
M2c-1	Evaluate load and deflection measurements using the modified PATTI test												UWM	
M2c-2	Evaluate effectiveness of the modified PATTI test for Detecting Modification													
M2c-3	Conduct Testing													
M2c-4	Analysis & Interpretation													
M2c-5	Standard Testing Procedure and Recommendation for Specifications	see Subtask M1a-6												
Aggregate Surface														
M3a	Impact of Surface Structure of Aggregate													
M3a-1	Aggregate surface characterization			JP					P				TAMU	
Modeling														
M4a	Micromechanics model development							JP					TAMU	
M4b	Analytical fatigue model for use during mixture design													
M4c	Unified continuum model							JP			DP	M&A	TAMU	
M5	Moisture Damage Prediction System												ALL	

LEGEND

Deliverable codes

- D: Draft Report
- F: Final Report
- M&A: Model and algorithm
- SW: Software
- JP: Journal paper
- P: Presentation
- DP: Decision Point
- [x]

-  Work planned
-  Work completed
-  Parallel topic

Deliverable Description

- Report delivered to FHWA for 3 week review period.
- Final report delivered in compliance with FHWA publication standards
- Mathematical model and sample code
- Executable software, code and user manual
- Paper submitted to conference or journal
- Presentation for symposium, conference or other
- Time to make a decision on two parallel paths as to which is most promising to follow through
- Indicates completion of deliverable x

Moisture Damage Year 2 - 5		Year 2 (4/08-3/09)				Year 3 (4/09-3/10)				Year 4 (04/10-03/11)				Year 5 (04/11-03/12)				Team
		Q1	Q2	Q3	Q4	Q1	Q2	Q3	Q4	Q1	Q2	Q3	Q4	Q1	Q2	Q3	Q4	
Adhesion																		
M1a	Affinity of Asphalt to Aggregate - Mechanical Tests																	
M1a-1	Select Materials		DP														UWM	
M1a-2	Conduct modified DSR tests		P		P													
M1a-3	Evaluate the moisture damage of asphalt mixtures				DP		P			P	JP		P					
M1a-4	Correlate moisture damage between DSR and mix tests						P		P									
M1a-5	Propose a Novel Testing Protocol				P				P, D							JP, F		
M1a-6	Standard Testing Procedure and Recommendation for Specifications											P						
M1b	Work of Adhesion																	
M1b-1	Adhesion using Micro calorimeter and SFE						JP										TAMU	
M1b-2	Evaluating adhesion at nano scale using AFM							JP									JP, F WRI	
M1b-3	Mechanisms of water-organic molecule competition				JP												TAMU	
M1c	Quantifying Moisture Damage Using DMA											JP	D	F			TAMU	
Cohesion																		
M2a	Work of Cohesion Based on Surface Energy																	
M2a-1	Methods to determine SFE of saturated binders														JP		TAMU	
M2a-2	Evaluating cohesion at nano scale using AFM							JP									JP, F WRI	
M2b	Impact of Moisture Diffusion in Asphalt																	
M2b-1	Diffusion of moisture through asphalt/mastic films						JP	D	F	D	F						TAMU	
M2b-2	Kinetics of debonding at binder-aggregate interface																	
M2c	Thin Film Rheology and Cohesion																	
M2c-1	Evaluate load and deflection measurements using the modified PATTI test	DP	JP	D	F												UWM	
M2c-2	Evaluate effectiveness of the modified PATTI test for Detecting Modification			D	DP, F													
M2c-3	Conduct Testing						JP											
M2c-4	Analysis & Interpretation				P				D									
M2c-5	Standard Testing Procedure and Recommendation for Specifications					D										see Subtask M1a-6		
Aggregate Surface																		
M3a	Impact of Surface Structure of Aggregate																	
M3a-1	Aggregate surface characterization									JP		P					TAMU	
Models																		
M4a	Micromechanics model development				JP				JP		JP			D	DP	F, SW	TAMU	
M4b	Analytical fatigue model for use during mixture design																TAMU	
M4c	Unified continuum model							JP		JP		DP	M&A	D	DP	F, SW	TAMU	
M5	Moisture Damage Prediction System																ALL	

LEGEND

Deliverable codes

- D: Draft Report
- F: Final Report
- M&A: Model and algorithm
- SW: Software
- JP: Journal paper
- P: Presentation
- DP: Decision Point
- [x]

-  Work planned
-  Work completed
-  Parallel topic

Deliverable Description

- Report delivered to FHWA for 3 week review period.
- Final report delivered in compliance with FHWA publication standards
- Mathematical model and sample code
- Executable software, code and user manual
- Paper submitted to conference or journal
- Presentation for symposium, conference or other
- Time to make a decision on two parallel paths as to which is most promising to follow through
- Indicates completion of deliverable x

PROGRAM AREA: FATIGUE

CATEGORY F1: MATERIAL AND MIXTURE PROPERTIES

Work Element F1a: Cohesive and Adhesive Properties

Work Done This Quarter

The experimental measurement and analysis of the pull-off specimens were completed this quarter. Two aggregate with different lithologies (limestone and andesite) were used as the substrate and the following experiments run:

- Change film thickness: asphalt film was changed to the following thicknesses; 5- μm , 10- μm , 30- μm , 50- μm , and 100- μm . The testing temperature and loading rate were kept constant at 23°C and 0.01-mm/s, respectively.
- Change in temperature and loading rate: Specimens were tested using loading rates of: 0.005-mm/s, 0.01-mm/s, and 0.02-mm/s. For each loading rate the specimens were tested at temperatures of 10°C, 23°C, and 36°C. The asphalt film thickness was kept constant at 30- μm .
- Change in moisture content: Specimens were moisture conditioned after preparation for times of 12-hrs, 24-hrs, and 48-hours. Asphalt film thickness, testing temperature, and loading rate were kept constant at 30- μm , 23°C, and 0.01-mm/s, respectively.

Significant Results

Some of the results found during the analysis are shown below. Figure F1a.1 displays the change in the practical work of fracture as the asphalt film thickness is increased. It was found that an increase in asphalt film thickness caused an increase in the practical work of fracture, which is affected by both the asphalt binder and the aggregate substrate. Figure F1a.2 illustrates how the practical work of fracture changes with changes in loading rate at a constant temperature. The practical work of fracture was found to increase with increases in the loading rate, decrease with increases in testing temperature, and was dependent on the properties of the asphalt binder and aggregate substrate. Figure F1a.3 displays the effect of moisture on the practical work of fracture of an asphalt binder. The resulting practical work of fracture after moisture conditioning was dependent on both the asphalt binder and aggregate substrate and could be predicted using surface free energy and the energy parameter (ER).

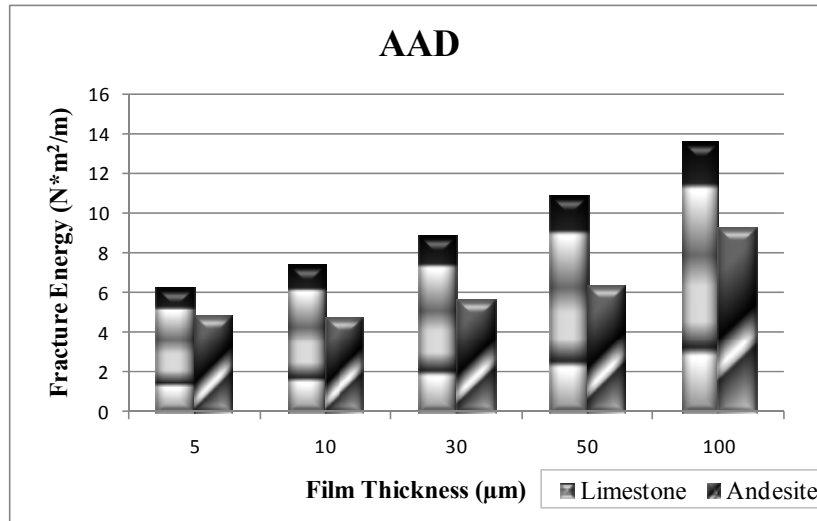


Figure F1a.1. Comparison in practical work of fracture for asphalt binder AAD with both limestone and andesite substrate.

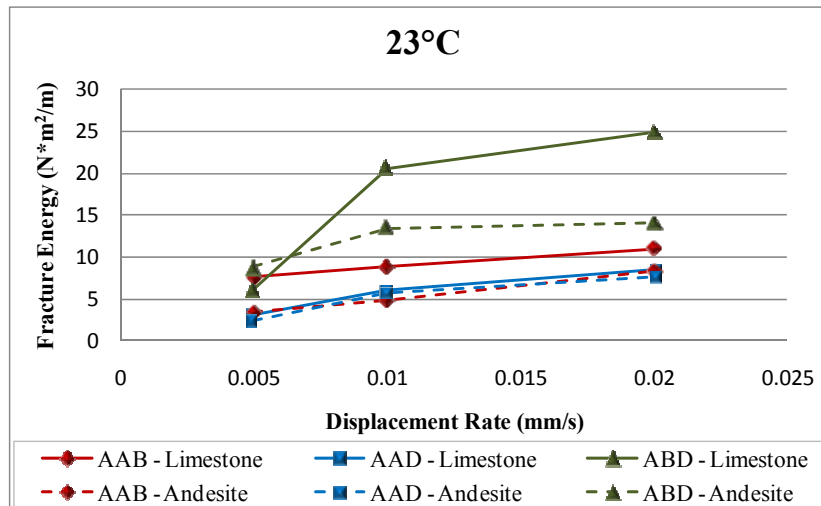


Figure F1a.2. Effect of change in loading rate for asphalt binders AAB for limestone and andesite substrate at 23°C.

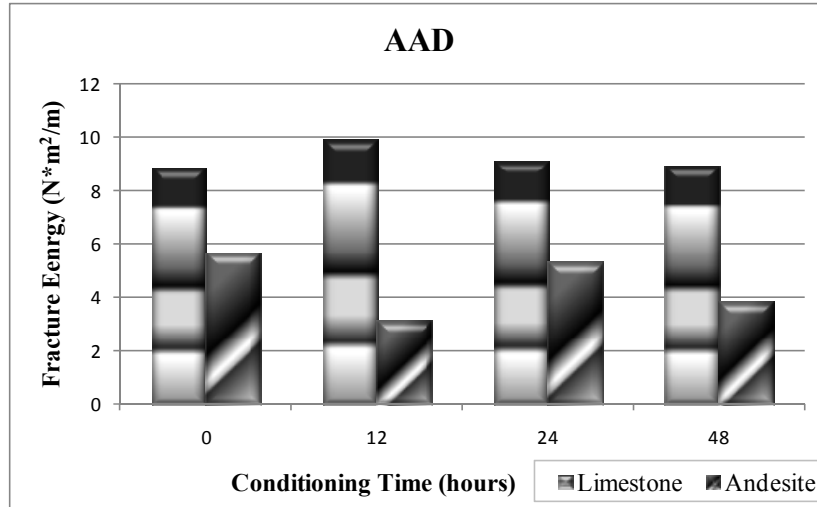


Figure F1a.3. Comparison in practical work of fracture after moisture conditioning for asphalt binder AAD with both limestone and andesite substrate.

Significant Problems, Issues and Potential Impact on Progress

None

Work Planned Next Quarter

Prepare the final report on this task with all major findings. The report will document analytical models that describe the relationship between ideal and practical work of fracture as a function of temperature, film thickness, loading rate and moisture content.

Work Element F1b: Viscoelastic Properties (Year 1 start)

Subtask F1b-1: Viscoelastic Properties under Cyclic Loading

Work Done This Quarter

In the previous quarters we demonstrated that at intermediate to high stress or strain levels, the free volume of the binder increases. A result of this increase is the development of normal stresses under a constrained geometry. The presence of normal and shear stresses together result in interaction non-linearity in the material. In this quarter we focused on a constitutive model to characterize interaction non-linearity and develop a test protocol to determine the model parameters.

Significant Results

The accuracy of micromechanical models to predict the undamaged properties or damaged evolution in an asphalt mixture is contingent on the accuracy of the constitutive relationships

used to describe the properties of its constituent materials. A linear viscoelastic model is commonly used as a constitutive relationship for the matrix in an asphalt composite (binder or mastic). The work in this task will provide a constitutive model (and a method to obtain model parameters) for the asphalt matrix that incorporates the effect of interaction between shear and normal stresses and more accurately reflects the behavior of the material under complex stress states. Preliminary results indicate that it is possible to quantify the interaction non linearity using cone and plate geometry with the DSR using Schapery's non linear model as the basis. The procedure to obtain the model parameters is briefly summarized here.

The linear viscoelastic properties of the binder were measured using a creep test at small stress magnitude. A simple power law was used to describe the linear viscoelastic properties and predict the response. Figure F1b-1.1 shows a single creep recovery curve. The power law parameters were obtained using the creep part of the curve. The recovery part is predicted using superposition and parameters from the creep part. However, when these parameters are used to predict the dynamic response in the presence of a normal force, the predicted strain and stiffness are considerably smaller than the measured strain (figure F1b-1.2). In other words the measured complex modulus was approximately 35% smaller than the expected modulus for a linear material.

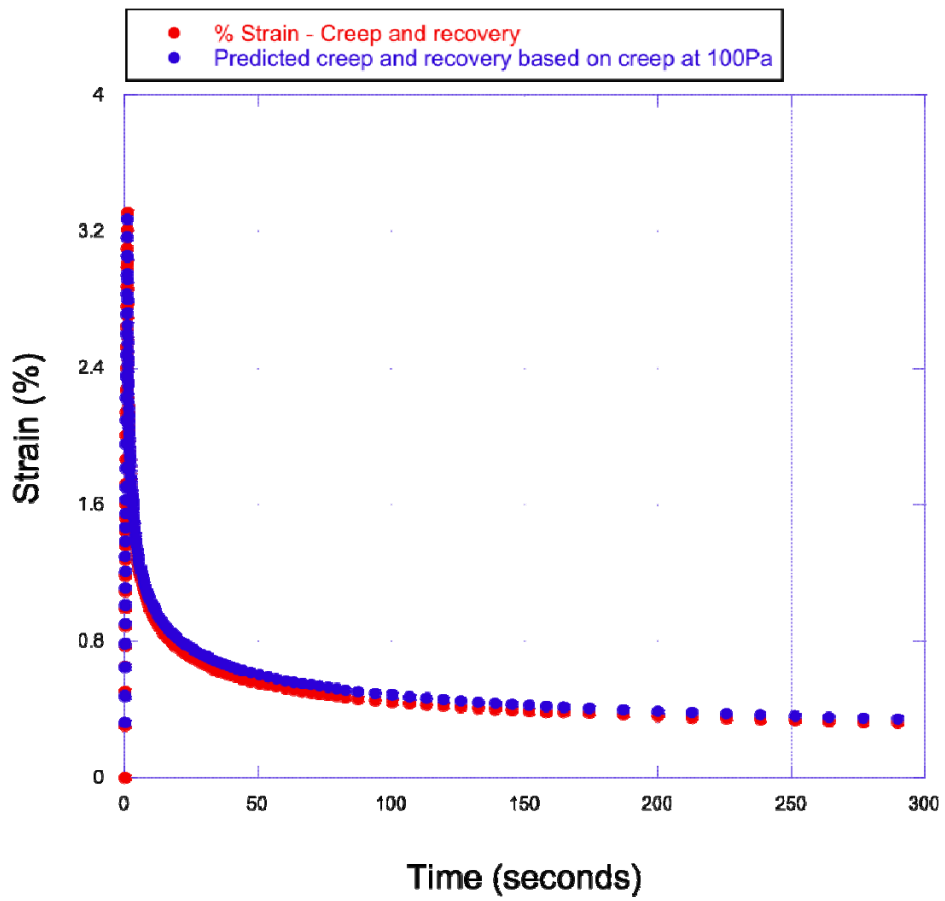


Figure F1b-1.1. Creep portion is used to obtain linear viscoelastic properties and predict creep and recovery at higher stress level using superposition

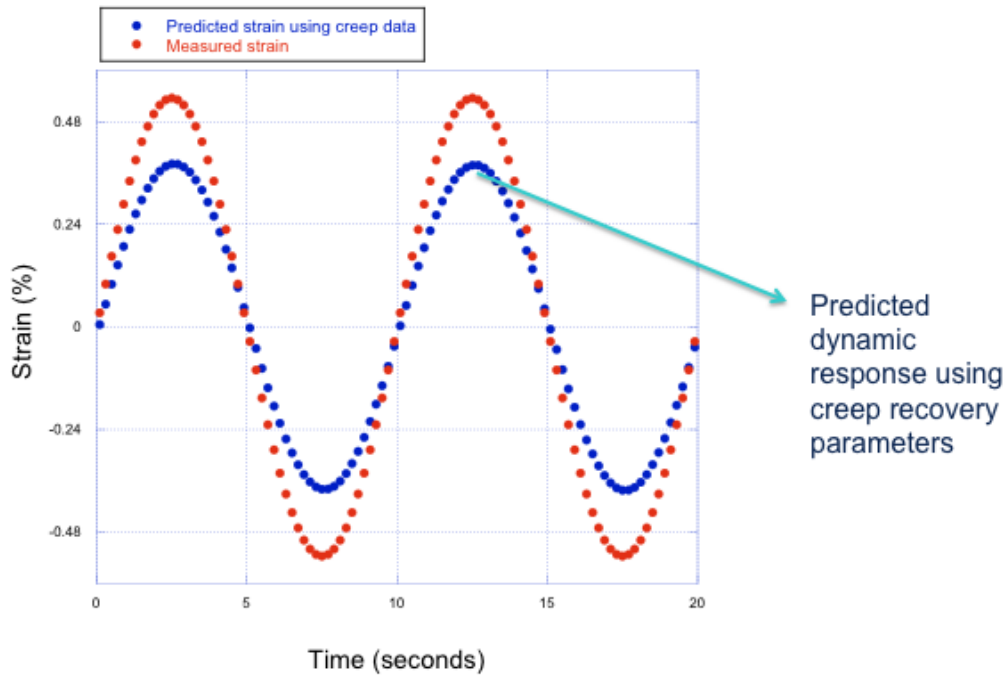


Figure F1b-1.2. Predicted dynamic response when the specimen is subjected to cyclic shear and normal force using linear superposition.

At the end of a short time sweep the specimen has significant normal stress that relaxes slowly (first normal stress due to Wissenberg effect). During this time, several “snap shots” of creep and recovery were captured (figure F1b-1.3 and 4) to calibrate the non-linear viscoelastic model. Finally, the calibrated non-linear viscoelastic model was used to predict the response under a combination of normal stress and cyclic shear stress. Figure F1b-1.5 shows that the model prediction compares reasonably well to the measured cyclic shear strain.

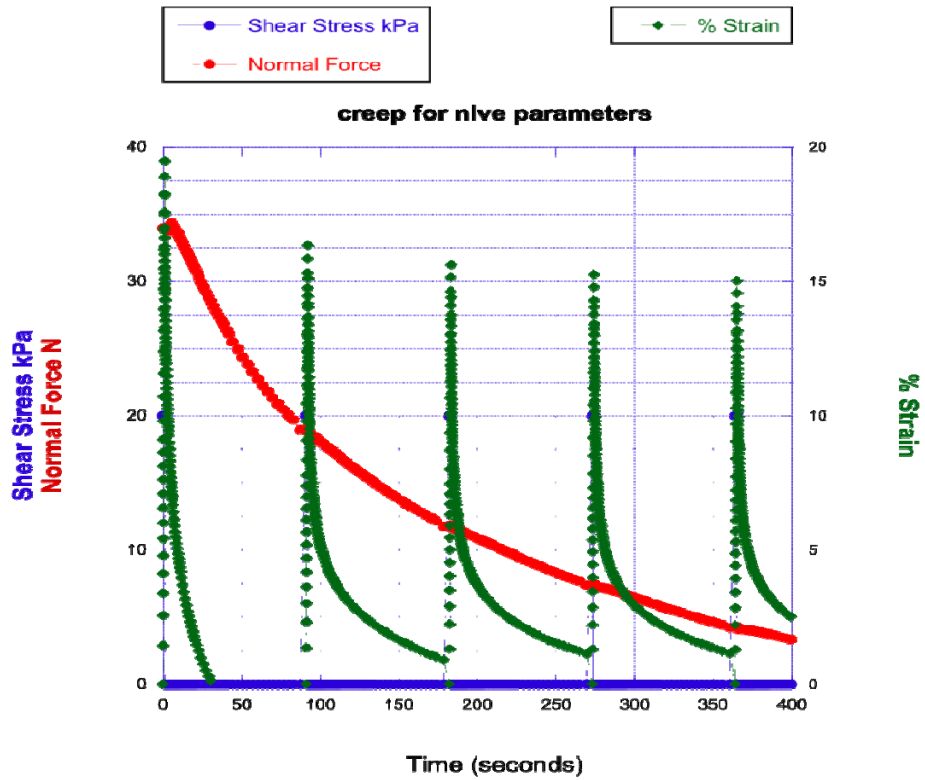


Figure F1b-1.3. Snap shots of shear creep and recovery in the presence of a normal stress to obtain the parameters for the non-linear viscoelastic model.

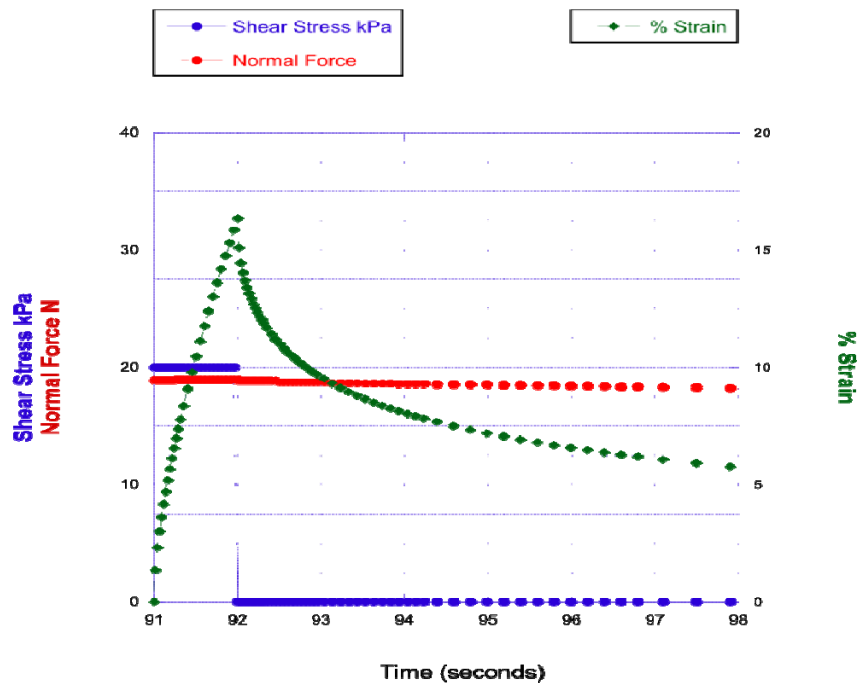


Figure F1b-1.4. Shear creep and recovery in the presence of a normal stress to obtain the parameters for the non-linear viscoelastic model.

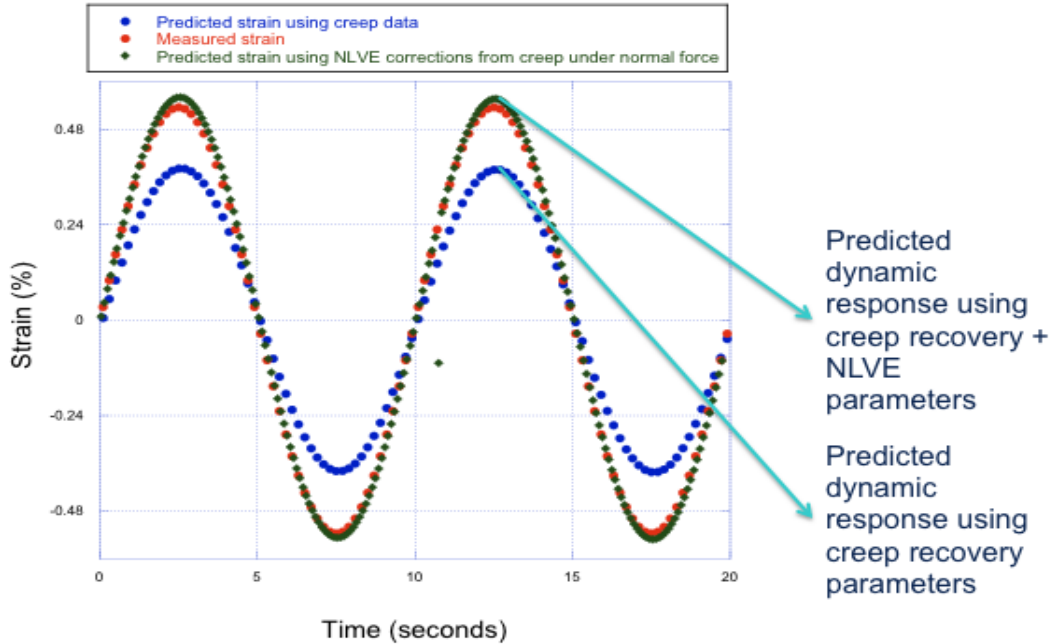


Figure F1b-1.5. Predicted versus measured shear strain under cyclic loading.

Significant Problems, Issues and Potential Impact on Progress

None.

Work Planned Next Quarter

In the next quarter we plan to finalize the procedure to calibrate the model that accounts for interaction nonlinearity. The expectation is that the findings from this subtask will result in a more robust constitutive model for the time and stress state dependent response for asphalt materials that can significantly improve the accuracy of micromechanical models.

Subtask F1b-2: Separation of Nonlinear Viscoelastic Deformation from Fracture Energy under Repeated and Monotonic Loading (TAMU)

Work Done This Quarter

A technical presentation, entitled “Characterization of Engineered Properties of Asphalt Mixtures as Inputs to PANDA”, was made in the Fundamental Properties and Advanced Models Expert Task Group of the Federal Highway Administration (FHWA) in Madison, Wisconsin, September 2010. This presentation summarized the characterization of engineered properties of undamaged and damaged asphalt mixtures under tensile loading and compressive loading, separately. The characterized material properties included the fatigue, healing, plasticity, aging and moisture susceptibility properties, all of which can serve as inputs to the 3-D finite element program “Pavement Analysis using a Nonlinear Damage Approach (PANDA)”.

In this quarter, the characterization of the engineered properties was continued within the expanded Engineered Properties Testing Plan that was made last quarter. Three different asphalt mixtures have been fabricated with the designed experimental variables shown in table F1b-2.1. The fabrication of Mixture No. 1 was finished in this quarter.

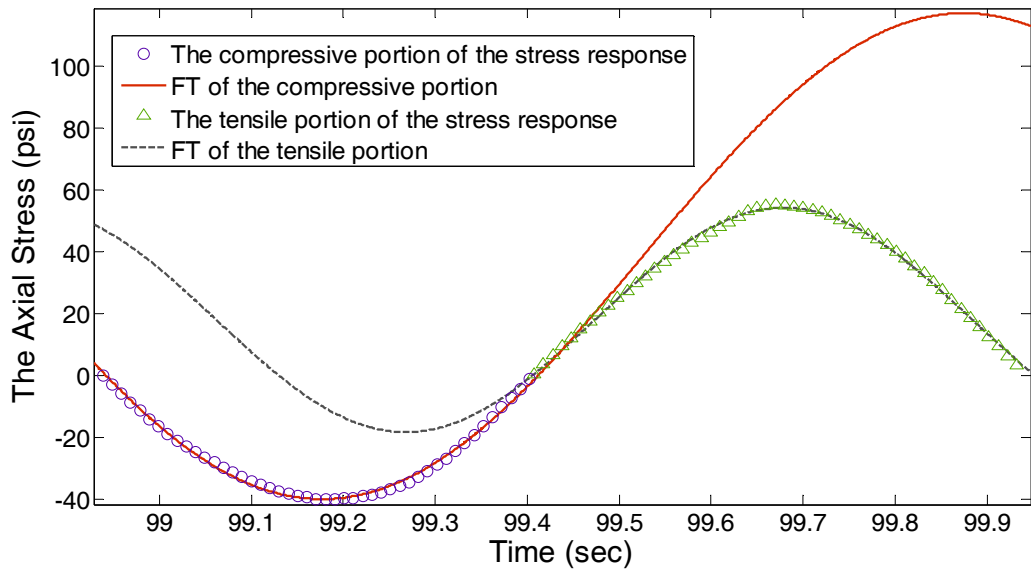
Table F1b-2.1. Types of asphalt mixtures and variables of mixture design.

Mixture No.	Materials	
	Asphalt Binder	Aggregate
1	NuStar Binder (Binder #1)	Hanson Limestone (Aggregate #1)
2	Valero Binder (Binder #2)	Hanson Limestone (Aggregate #1)
3	NuStar or Valero Binder (Binder #1 or #2)	Wyoming Siliceous (Aggregate #2)
Category of Mixture	Variable	Levels of Variable
Full mixture	Percent air (2)	4%, 7%
	Aging period (3)	0, 3, 6 month
	Loading mode (2)	Tension, compression
Fine mixture	Percent air (2)	To be calculated based on percent air and asphalt of the fine aggregate portion of full mixtures
	Aging period (3)	0, 3, 6 month
	Relative humidity (5)	0, 25, 50, 75, 100%

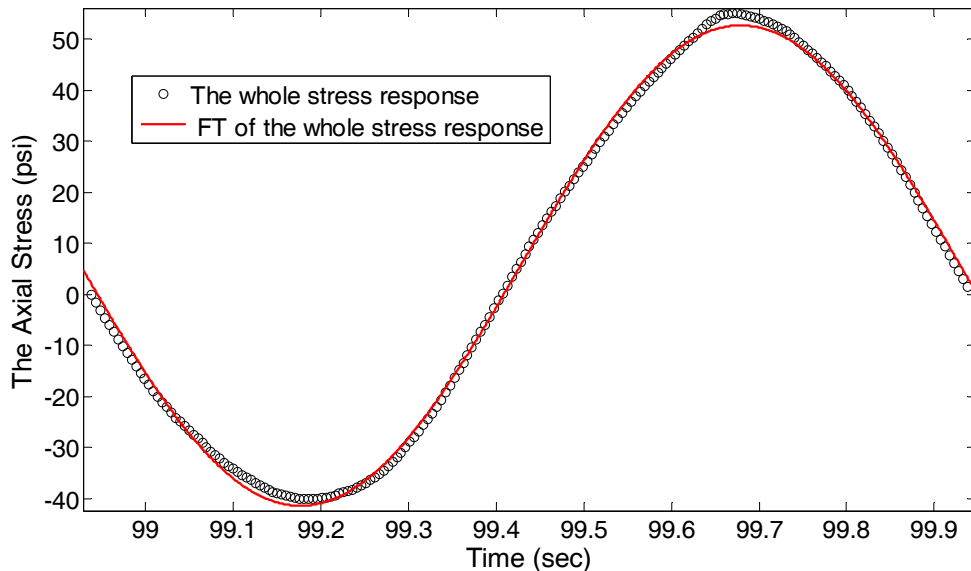
The testing protocols of the expanded testing plan include the tension test protocol of full mixtures, the compression test protocol of full mixtures, Dynamic Mechanical Analyzer (DMA) test protocol of fine mixtures, and extended healing and aging testing plan. Details of some test protocols were documented in previous quarterly reports. More development work was accomplished in this quarter in order to refine the analysis and extend the ability of the current analytical method to characterize the damage of the asphalt mixture under repeated load. With respect to the tension test protocol for full mixtures, the accomplishments included: (1) refinement on data analysis using the Fourier Transformation (FT), and (2) characterization of the healing properties of asphalt mixtures using the destructive repeated direct tension (RDT) test.

The FT was proposed in previous quarters to reduce the error in the measurement of the RDT test so as to obtain accurate complex moduli of asphalt mixtures. Originally the FT was applied to the entire stress response, which consisted of the tensile stress portion and the compressive stress portion. In this quarter, the difference between these two stress portions were taken into consideration, and the FT was applied to the tensile and compressive stress portions separately. A comparison of the new FT method and the original one is given in figure F1b-2.1. Figure F1b-2.1(a) shows the new FT method, which suggests that the transformed data better fit the raw data

when applying the FT to the tensile and compressive stress portions separately. Figure F1b-2.1(b) presents the original FT of the entire stress curve, which has a minor mismatch at the peak and valley of the stress curve. In addition, as observed from figure F1b-2.1 (a), when using the tensile stress portion to perform the FT for the entire loading cycle, the transformed compressive stress portion did not well match the measured data; similarly, if using the compressive stress portion to perform the FT for the entire loading cycle, the transformed tensile stress portion does not well match the measured tensile stress portion.



• **FT of Tensile Stress Portion and Compressive Stress Portion Separately**



• **FT of Entire Stress Curve Simultaneously**

Figure F1b-2.1. The raw data and Fourier transformed data of the stress response of an asphalt mixture in destructive RDT test.

The second achievement made in this quarter was the measurement of the healing speed. Healing is counter fracture and proven to significantly affect the fatigue process. The measure of healing, h , should represent the actual crack closure happening in the damaged asphalt mixture and can be quantified by the reduction of damage density, ϕ , during the healing period, as shown in equation F1b-2.1. The damage density, ϕ , was formulated in terms of the crack radius and the number of cracks, which was documented in previous quarterly reports.

$$h = \frac{\phi_{\text{after healing}} - \phi_{\text{original}}}{\phi_{\text{before healing}} - \phi_{\text{original}}} \quad (\text{F1b-2.1})$$

where $\phi_{\text{after healing}}$ is the damage density after healing; $\phi_{\text{before healing}}$ is the damage density before healing; and ϕ_{original} is the original damage density (i.e. the content of air voids). Figure F1b-2.2 shows the test protocol designed to obtain h , in which a sequence of 8 continuous 1000-cycle haversine tensile load were applied to the specimen. The rest periods between two sequential 1000 load cycles were 500 sec, 250 sec, 120 sec, 60 sec, 30 sec, 15 sec, 8 sec and 4 sec, respectively. The maximum rest period (500 sec) was chosen during which approximately 80% to 90% of healing would occur based on the analytical result.

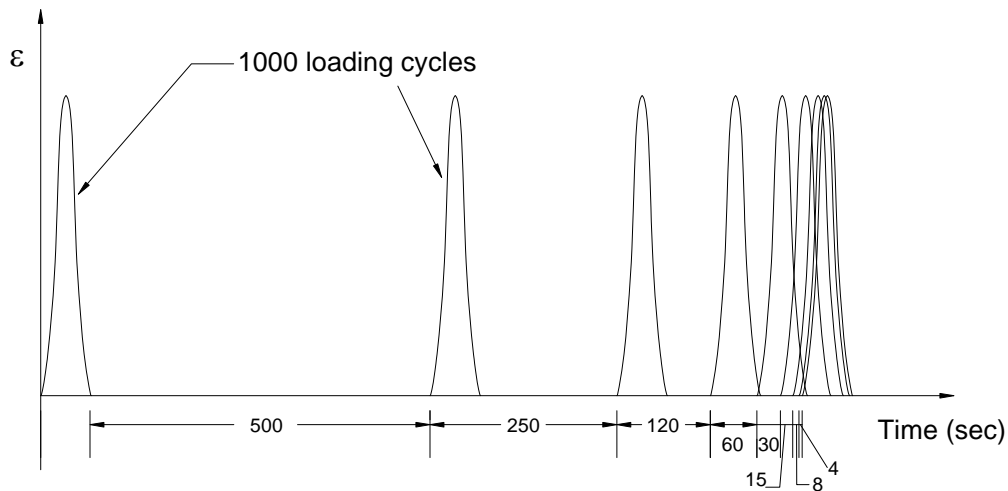


Figure F1b-2.2. Loading configuration to measure healing.

The measured h was plotted against the rest period, as shown in blue diamonds in figure F1b-2.3, in which the healing rate (the slope of the healing curve) varied with the length of rest period. The short-term healing rate (\dot{h}_1) was found to be larger than the long-term healing rate (\dot{h}_2) (see figure F1b-2.3). Both healing rates (\dot{h}_1 and \dot{h}_2) were used together with the healing scale parameter (h_β) in the healing speed model shown in equation F1b-2.2 (Lytton et al. 2001) to model the measured healing curve. The red squares in figure F1b-2.3 are the fitted h .

$$h = \left[\dot{h}_2 + \frac{\dot{h}_1 - \dot{h}_2}{1 + \frac{(\dot{h}_1 - \dot{h}_2)\Delta t}{h_\beta}} \right] \Delta t \quad (\text{F1b-2.2})$$

where \dot{h}_1 is the short term healing rate; \dot{h}_2 is the long term healing rate; h_β is the healing scale parameter; and Δt is the length of the rest period between loads during which healing takes place. As can be seen from figure F1b-2.3, the fitted healing curve well matches the measured healing curve.

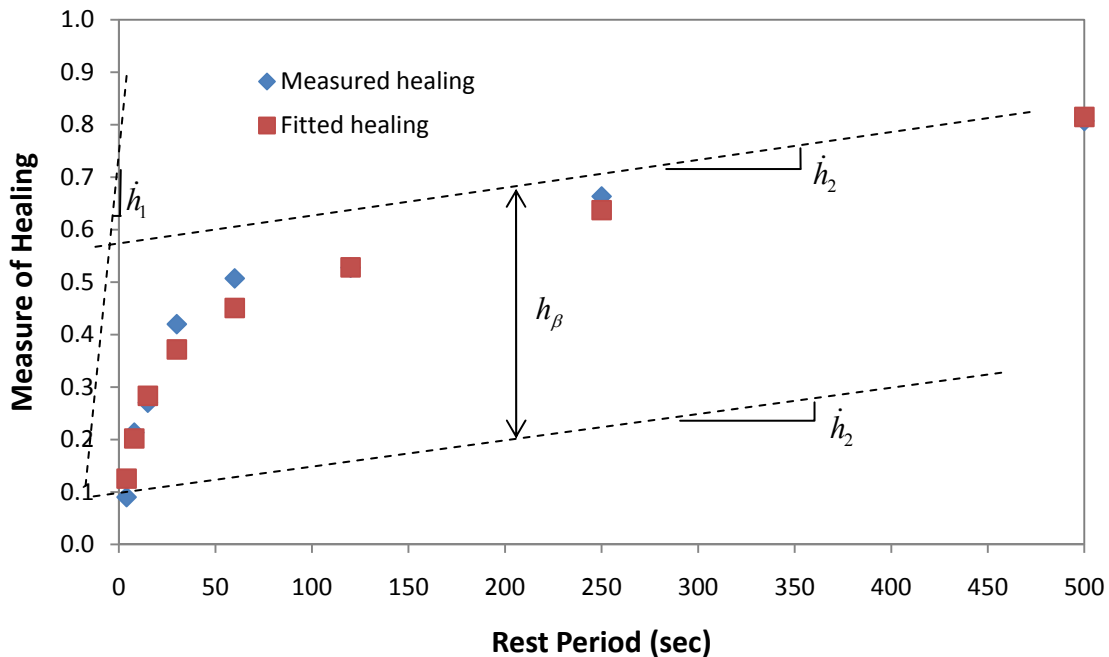


Figure F1b-2.3. Measure of healing versus rest periods.

Significant Results

The expanded experiment was started to further characterize the engineered properties of asphalt mixtures and to investigate the various types of damage developed in asphalt mixtures under destructive loading. The material properties of asphalt mixtures were characterized using efficient and economical tests and fundamental mechanistic data analysis. It is believed that the test protocol and data analysis can be applied to any type of asphalt mixtures because of the mechanistic nature of the test and analysis methods.

When analyzing the test data, the tensile stress portion and the compressive stress portion of the stress response in the controlled-strain RDT test were filtered separately using the FT in order to reduce the machine errors. By applying the FT to the stress curve, more accurate values of the magnitude and phase angle of the complex modulus were obtained.

The designed healing test was conducted on asphalt mixture specimens. The short-term healing rate was found to be significantly different from the long-term healing rate. The healing speed model reported in the literature was found to be able to successfully model the measured healing curve.

Significant Problems, Issues and Potential Impact on Progress

Nonuniform distribution of coarse aggregates was observed on the side surface of asphalt mixture specimens. Figure F1b-2.4 is a scanned image of the side surface of a cylindrical asphalt mixture specimen. A larger amount of coarse aggregates were observed in Zone A in this figure, while less coarse aggregates were found in Zone B. Because of the nonuniform distribution of coarse aggregates in the asphalt mixture, the stiffness varies along the perimeter of the cylindrical specimen. This problem will be fixed by making corrections to certain steps of the specimen fabrication process.

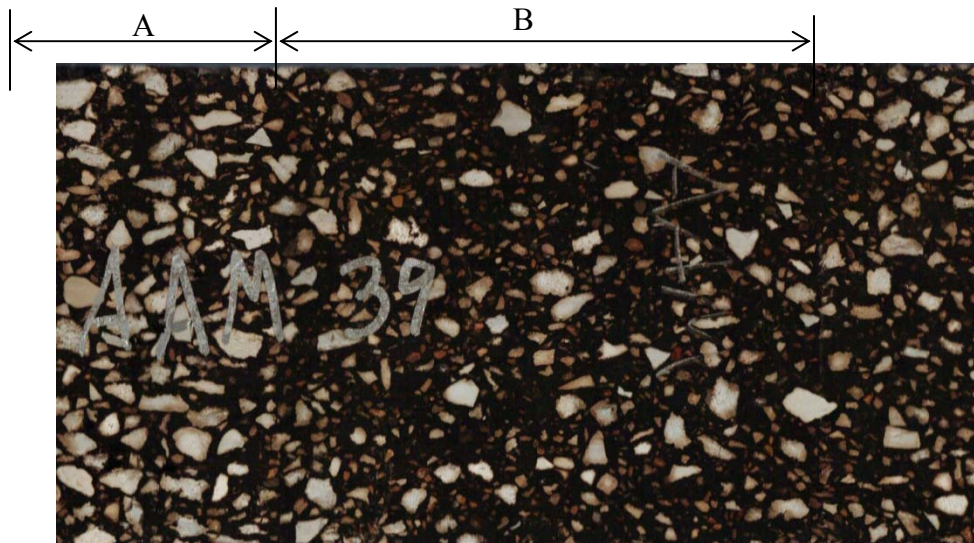


Figure F1b-2.4. Scanning of surface of cylindrical asphalt mixture specimen.

Work Planned Next Quarter

The asphalt mixture No. 2 and No. 3 in table F1b-2.1 will be fabricated when the corresponding asphalt binder and aggregates arrive at the McNew Laboratory of Texas A&M University. The characterization of asphalt mixtures will continue with addressing the effects of air void content, binder type, aggregate type, aging period and relative humidity.

The healing properties of asphalt mixtures will be further investigated using the fundamental mechanistic approach.

Cited Reference

Lytton, R. L., C. W. Chen, and D. N. Little, 2001, Fundamental Properties of Asphalts and Modified Asphalts, Vol. III: A Micromechanics Fracture and Healing Model for Asphalt Concrete. Federal Highway Administration Final Report No. FHWA-RD-98-143, Washington, D.C.

Work Element F1c: Aging

Subtask F1c-1: Critical Review of Binder Oxidative Aging and Its Impact on Mixtures (TAMU)

Work Done This Quarter

During this quarter a review of the literature on asphalt oxidation reactions was conducted with a focus specifically on fast-rate and constant rate mechanisms. An improved understanding of these mechanisms likely will provide an improved description of asphalt reaction kinetics and thus improved pavement oxidation and durability models.

Significant Results

Literature on asphalt oxidation mechanisms generally falls into three groups: the free radical chain reaction (FRCR) mechanism (including recent studies on antioxidants), Beaver's electron transfer initiated oxidation (ETIO) mechanism (to explain diesel fuel sedimentation), and Herrington's research on oxidation of asphalt components.

The free radical chain reaction (FRCR) mechanism was proposed and supported by several research studies. The presence of stable free radicals in asphalt-solvent solutions was detected, and various antioxidants that worked as free radical scavengers were reported to hinder oxidation (Knotnerus, 1972). However, no generically effective antioxidant was found, possibly for three reasons. First, the effectiveness of antioxidant is structurally dependent. For example, phenolic compounds of different chemical structure show different anti-radical power (Dizhbite et al. 2004). Second, the complex and source-dependent composition of asphalt makes the search for antioxidants very challenging. For instance, an additive (antioxidant or metal deactivator) might slow oxidation in some cases, but accelerate oxidation in other cases, and in some cases have no effect (Knotnerus 1972). Last but not the least, a second reaction pathway that is not affected by antioxidant might exist which complicates the evaluation of antioxidant effectiveness. For those three reasons, the search for generic antioxidants is extremely difficult. Nonetheless, FRCR as an oxidation reaction pathway is well established in the literature.

The second reaction pathway, electron transfer initiated oxidation (ETIO), was originally proposed for sediment formation in diesel fuel (Beaver and Gilmore 1991). The major oxidative

reactants studied were pyrroles and indoles. In the ETIO mechanism, the triplet oxygen reacts with electron-rich compounds (e.g. pyrroles) to form a charge-transfer complex. The oxygen molecule in the charge-transfer complex then attracts one electron from the electron-rich compound, forming the electron-transfer complex. This complex then rapidly forms peroxide that leads to oxidation products and sediments. King applied the ETIO mechanism later to asphalt oxidation, and proposed a catalyzed oxycyclic oxidation mechanism (Kin 1993). This mechanism is uncontrollable and is not affected by antioxidants. King's theory rationalized the formation of various oxidation products including ketones from benzylic carbon. Due to the presence of pyrrolic types and benzylic carbon in asphalt, this reaction pathway is also very likely important in binder oxidation.

These two reaction pathways were used to rationalize the "fast-rate plus constant-rate" scheme of carbonyl area growth observed in experiments. Petersen (2009) suggests that pyrrolic types are present in asphalt. Because pyrrole very likely oxidizes via ETIO, FTIR spectra for pyrrole were examined. Unfortunately, the IR spectra show that little pyrrole is present in asphalt. In terms of kinetics data, both FRCR and ETIO are capable of explaining the zero order constant-rate reaction assuming abundant benzylic carbon as the reactant. However, no clue was found of what reactants (except sulfide) are involved during the fast-rate period. Although Petersen (2009) proposed that dihydroaromatics are responsible for the initiation of fast-rate oxidation, Herrington's study (2001) clearly shows that dihydroaromatics are not important. To this point, it's very difficult to propose a mechanism that includes specific reactants.

Herrington (2004) proposed another mechanism called inhibited free radical autoxidation. It is used to explain the oxidation of asphaltenes in solution, which show similar trend as asphalt. The advantage of this mechanism is that it might provide a way to explain the kinetics of carbonyl area formation that is observed without getting into details of specific reactants.

Significant Problems, Issues and Potential Impact on Progress

There are no problems or issues.

Work Planned Next Quarter

Review of the literature and work on other research projects is ongoing.

Cited References

Beaver, B. D., and C. Gilmore, 1991, Oxidative Degradation of Petroleum Products Via A Non-peroxyl Radical Chain Pathway. Electron Transfer Initiated Oxidation (ETIO) Revisited. *Petroleum Science and Technology*, 9 (7), 811-823.

Dizhbite, T., G. Telysheva, V. Jurkjane, and U. Viesturs, 2004, Characterization of the Radical Scavenging Activity of Lignins – Natural Antioxidants. *Bioresource Technology*, 95 (3): 309-317.

Herrington, P. R., 2001, The Role of Hydroaromatic Species in the Oxidation of Petroleum Bitumens. *Energy Fuels*, 15 (2): 444-448.

Herrington, P.R., 2004, Effect of Oxygen Concentration on the Rate of Reaction of Asphaltenes with Oxygen. *Energy Fuels*, 18 (5): 1573-1577.

King, G. N., 1993, Oxycyclics: understanding catalyzed oxidation mechanisms in bitumen and other petroleum products. *Petroleum Science and Technology*, 11 (1): 201-238.

Knotnerus, J., 1972, Bitumen Durability – Measurement by Oxygen Absorption. *Ind. Eng. Chem. Prod. Res. Develop.*, 11 (4): 411-422.

Petersen, J. C., 2009, A Review of the Fundamentals of Asphalt Oxidation Chemical, Physicochemical, Physical Property, and Durability Relationships. *Transportation Research Circular, Number E-C140*. Transportation Research Board of the National Academies, Washington, DC.

Subtask F1c-2: Develop Experimental Design (TAMU)

Work Done This Quarter

No work this quarter.

Significant Results

None.

Significant Problems, Issues and Potential Impact on Progress

Conducting the planned experiments using ARC core binders is awaiting the arrival of ARC binders. Measurements on mixtures fabricated using other binders are underway.

Work Planned Next Quarter

Measurements of mixture rheology and fatigue continue. Also, rheological measurements of binders extracted and recovered from these mixtures will be made as part of the effort to link binder oxidation to changes in mixture properties.

Subtask F1c-3: Develop a Transport Model of Binder Oxidation in Pavements (TAMU)

Work Done This Quarter

Measurements of Recovered Binder Properties

Additional measurements of the pavement sites awaiting delivery of cores for testing.

Improved Modeling of Oxygen Transport and Reaction in Pavements

A more detailed model of oxygen transport and reaction in pavements is being developed to account for pavement air void features. In this model, oxygen transport and reaction in pavement is described as two interlinked steps (as demonstrated in figure F1c-3.1): 1) Diffusion and/or flow of oxygen from the atmosphere above the pavement into the interconnected air voids in the pavement; and 2) diffusion of oxygen from those air voids into the adjoining asphalt-aggregate matrix where it reacts with the asphalt. Because oxygen concentration in pavements likely is highly dependent on the pavement air void structure (air void size and distribution), characterization of air voids is important to developing and validating an accurate model for calculations. The previous model assumed atmospheric air throughout the air voids and assumed a single air void channel diameter for all voids, so these improvements are directed at providing a significantly more realistic representation of actual pavement structures. Further details of the developing enhanced model are described below including transport through the air voids, transport within the asphalt-aggregate matrix, air void characterization, and use of these elements to calculate a layer-by-layer bulk average asphalt oxidation rate. This work is still fairly early in the development stage so the discussions are largely conceptual and without example calculations.

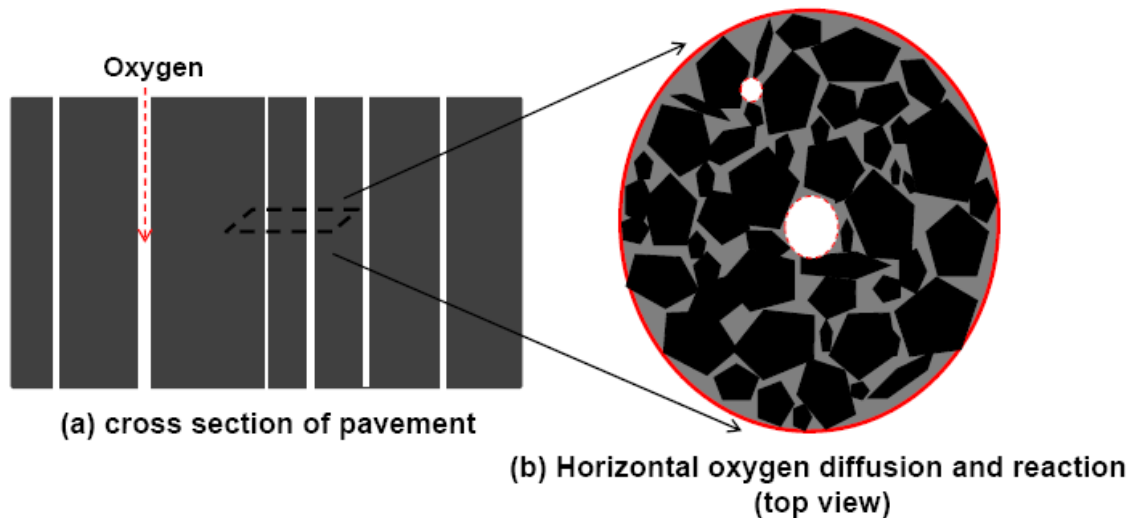


Figure F1c-3.1. Schematic of two idealized steps involved in oxygen transport and reaction in pavement: (a) vertical diffusion and/or flow of oxygen into air voids, and (b) horizontal diffusion into and reaction within the surrounding asphalt-aggregate matrix.

Transport through the Air Voids. In pavements, diffusion and/or convective flow of oxygen must occur in order to supply oxygen to interconnected air channels. From these channels, oxygen diffuses into and reacts within an asphalt-aggregate matrix. Oxygen concentration in those interconnected air channels is extremely important to model binder oxidation in pavements. This vertical oxygen transport process could occur by diffusion, when there is an oxygen concentration gradient between ambient air at the surface of the pavement and the oxygen concentration in the interconnected air voids, and/or by convective flow (for example,

when air undergoes expansion or contraction with pavement temperature fluctuations); however, there are no direct measurements of such convective flow in pavements. In this work, instead of assuming instantaneous convective flow (1 atm air in the interconnected channels at all times), two extreme oxygen concentration profiles in the air voids will be used; then these two cases will be used in calculations to give a range (upper and lower limits) of binder oxidation rates and corresponding oxidation levels over time in the pavement. The two extreme oxygen concentration profiles arise from 1) transport of oxygen through the air voids by diffusion only, and 2) instantaneous convective flow to provide atmospheric air concentrations throughout the interconnected air voids (0.2 atm oxygen in the voids). These two extreme conditions provide a range, instead of a single air void boundary value for binder oxidation in the asphalt-aggregate matrix. The constant and uniform oxygen partial pressure at 0.2 atm in interconnected air void gives the highest possible oxidation rate throughout the asphalt-aggregate matrix, while the oxygen diffusion extreme leads to the lowest oxidation rate.

Transport and Reaction within the Asphalt-Aggregate Matrix. This portion of the model is largely the same as that used previously but will allow for a pore size distribution rather than a single air void pore radius. Considering oxygen diffusion from an air void channel at a certain depth to react with the surrounding asphalt-aggregate matrix (a layer of finite thickness), a mathematical equation accounting for oxygen diffusion and reaction in a differential volume is:

$$\left(\frac{\partial C_{O_2}}{\partial t} \right) = -\nabla \cdot N_{O_2} - r_{O_2} \quad (\text{F1c-3.1})$$

With Fick's first law of diffusion, a governing equation with boundary conditions will be used to calculate estimates of oxygen partial pressure throughout a pavement layer. The PDE system will be solved for the oxygen partial pressure as a function of time and distance away from the air void-binder interface in a cylindrical coordinate system. Then this oxygen partial pressure profile can be used to calculate binder oxidation rates in the pavement (with oxidation measured by carbonyl content) and the hardening rate of binders (indicated by log viscosity, e.g.), which then can be combined with an appropriate performance model to estimate pavement durability and performance. The primary equation for the transport and reaction of oxygen in the asphalt-aggregate matrix is

$$\left(\frac{\partial P}{\partial t} \right) = \frac{1}{r} \frac{\partial}{\partial r} \left(r D_{O_2} \frac{\partial P}{\partial r} \right) - \left(\frac{cRT}{h} \right) r_{CA} \quad (\text{F1c-3.2})$$

$$\left(\frac{\partial P}{\partial r} \right) = 0 \quad \text{at} \quad r = r_{NFB} \quad \text{No Flux Boundary}$$

$$P = P_{av} \quad \text{at} \quad r = r_{PS} \quad \text{Air Void Surface}$$

$$P = 0 \quad \text{at} \quad t = 0 \quad \text{Initial Condition}$$

where c is an experimental constant and h is the Henry's law constant. r_{NFB} is an average distance between two nearby air voids, and P_{av} is the oxygen partial pressure in the air voids, a function of

distance in the air void channel from the atmospheric end and is calculated using the vertical diffusion or convective flow model, as appropriate.

This model can be solved numerically for oxygen concentration and oxidation rate in a surrounding asphalt-aggregate matrix for which diffusivity and binder oxidation kinetics parameters are known from separate materials properties experiments.

Air Void Characterization. The model described above is being developed to calculate air void oxygen concentrations and asphalt oxidation rates near a single air void channel at a specific pavement layer of finite thickness. Because air voids in pavements have a wide distribution (size distribution in each finite pavement layer, and, in principle, distributions that are different from pavement layer to layer), characterization of air void size and distribution properties are essential in order to estimate the bulk oxidation properties of binders in pavements.

Air Voids Distribution Measurement. X-ray CT scanning can be used to investigate the air void characteristics and structure of pavement cores. An X-ray source emits a beam of known intensity through the specimen, and a detector on the opposite side of the specimen measures the attenuated beam intensity. The specimen rotates 360° with respect to its center and moves at a specific fixed vertical interval to enable evaluation of the entire specimen volume. Each slice reveals the interior of the object on a plane, and if stacked together, the slices provide a three dimensional image of the object. These slices are generally about 1 mm in thickness with an overlap of 0.2 mm.

The original images obtained from x-ray CT can be converted to black and white by an image processing macro, where black areas represent the voids and white areas represent the aggregates and the mastic. By calibrating the air void content (from the Corelok method, for example), to the air void content obtained from experimental measurement, an appropriate threshold to generate the black-and-white images can be obtained, which may be used to generate a more accurate air void distribution in specimen slices.

The term interconnected air voids refers to the air void channels that connect together from the top to the bottom of specimens. To determine the interconnected AV content and distribution, stacks of black and white images at different depth increments of the specimen can be converted to binary bit files by macros developed by Masad et al., which can be further analyzed to determine the connected paths from top to bottom of the specimen by using an appropriate algorithm.

Mathematical Characterization of pavement air voids. The resolution of X-ray CT is affected by several factors such as the type and size of the X-ray source and detectors, the distance between the source, the solid and the detector, and the method used for image reconstruction. The image reconstruction consists of representing the object in a grid of picture elements (pixels) if using two dimensions, or volume elements (voxels) if using three dimensions. The images typically vary in resolution with a clear cut-off size near 0.02 mm; below this size, there are no air voids detected even if they are present.

A log-normal function may be used to estimate a complete air void size distribution from the X-ray CT images. The probability density function for a log-normal distribution is:

$$f(x; \mu, \sigma) = \frac{1}{x\sigma\sqrt{2\pi}} e^{-\frac{(\ln x - \mu)^2}{2\sigma^2}}, \quad x > 0 \quad (\text{F1c-3.3})$$

where μ and σ are the mean and standard deviation of the variable's natural logarithm (by definition, the variable's logarithm is assumed to be normally distributed).

It has been shown that air voids in pavements follow such a distribution, and measured distributions, although incomplete, provide enough data to allow estimates of the lognormal distribution parameters. Then with those parameters, an entire distribution can be calculated.

Bulk oxidation rate calculation: With estimates for the air void size distribution and the number of air voids in each finite pavement layer (slice), oxidation rates for the asphalt-aggregate matrix near each air void can be estimated from equation F1c-3.2. An overall oxidation rate for this entire finite pavement layer also can be calculated as a volume-weighted average of the oxidation rates for each asphalt volume element associated with each air void. Furthermore, a similar volume weighted average oxidation and hardening rate can be calculated for the entire pavement layer, if desired. These layer-by-layer calculations to give binder oxidation rates as a function of pavement depth and the overall pavement oxidation rate can be compared to measured values from pavement cores to obtain calibration and validation of the oxidation model.

Significant Results

The paper submitted to the Journal of Materials in Civil Engineering to document the improved pavement temperature model has been accepted for publication and is *in press*.

Significant Problems, Issues and Potential Impact on Progress

The effort to obtain cores from pavement sites in different climate zones continues. Cores from such sites will provide 1) data on binder oxidation as a function of time and depth in pavements and 2) data on changes to mixture rheology and fatigue resistance that occur in response to binder oxidation.

Work Planned Next Quarter

Field cores from sites as available from WRI will be tested to provide data on binder oxidation as a function of time and depth in pavements in different climate zones.

Density Measurements on asphalt binders continue, with a focus on improving measurement precision and accuracy.

Subtask F1c-4: The Effects of Binder Aging on Mixture Viscoelastic, Fracture, and Permanent Deformation Properties (TAMU)

Work Done This Quarter

The reader is referred to Work Elements F1b-2 and F2c.

Work Planned Next Quarter

The reader is referred to Work Elements F1b-2 and F2c.

Subtask F1c-5: Polymer Modified Asphalt Materials (TAMU)

Work Done This Quarter

None.

Work Planned Next Quarter

None at this time.

Work Element F1d: Healing (TAMU)

Subtask F1d-1: Critical review of the literature

Subtask F1d-2: Material selection

Subtask F1d-3: Experiment design

Subtask F1d-4: Test methods to measure properties related to healing

Subtask F1d-5a: Testing of materials and validating healing model

Subtask F1d-5b: Thermodynamic model for healing in asphalt binders

Work Done This Quarter

In the previous quarters we reported the influence of aging and temperature on the intrinsic healing properties of asphalt binders. We also reported the measurement of total healing in fine aggregate matrix specimens after 50% damage (based on G^*). The damage evolution after the first rest period was very different as compared to the damage evolution of the intact material (based on the complex modulus). The damage evolution of the fine aggregate matrix after each subsequent rest period was very similar as compared to the damage evolution following the first rest period (figure F1d.1). Similarly, the healing curves (based on the complex modulus) for each rest period following similar level of damage (based on complex modulus) were also very consistent (figure F1d.2.).

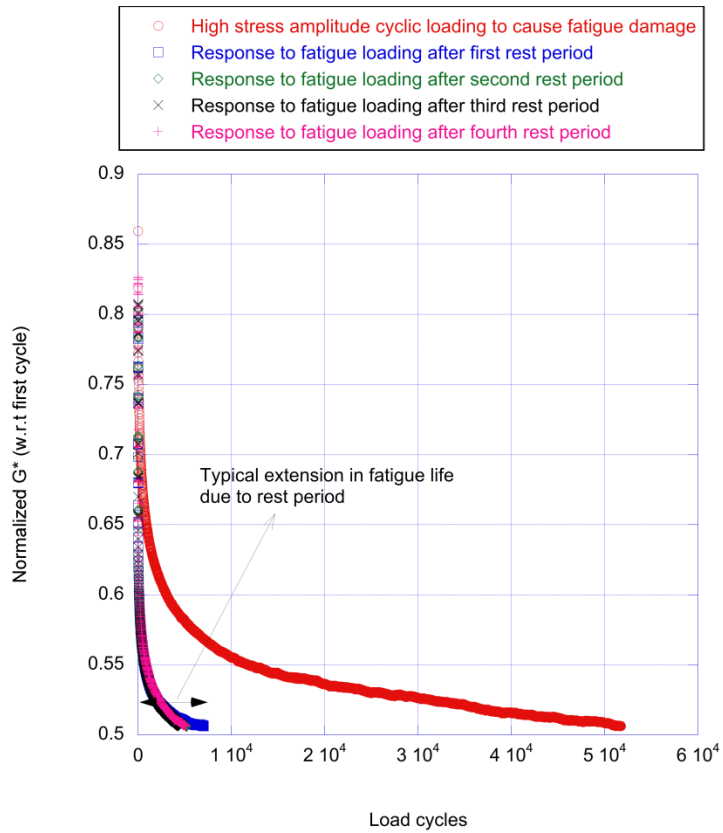


Figure F1d.1. Response to cyclic loading to induce fatigue for the original specimen and after rest periods.

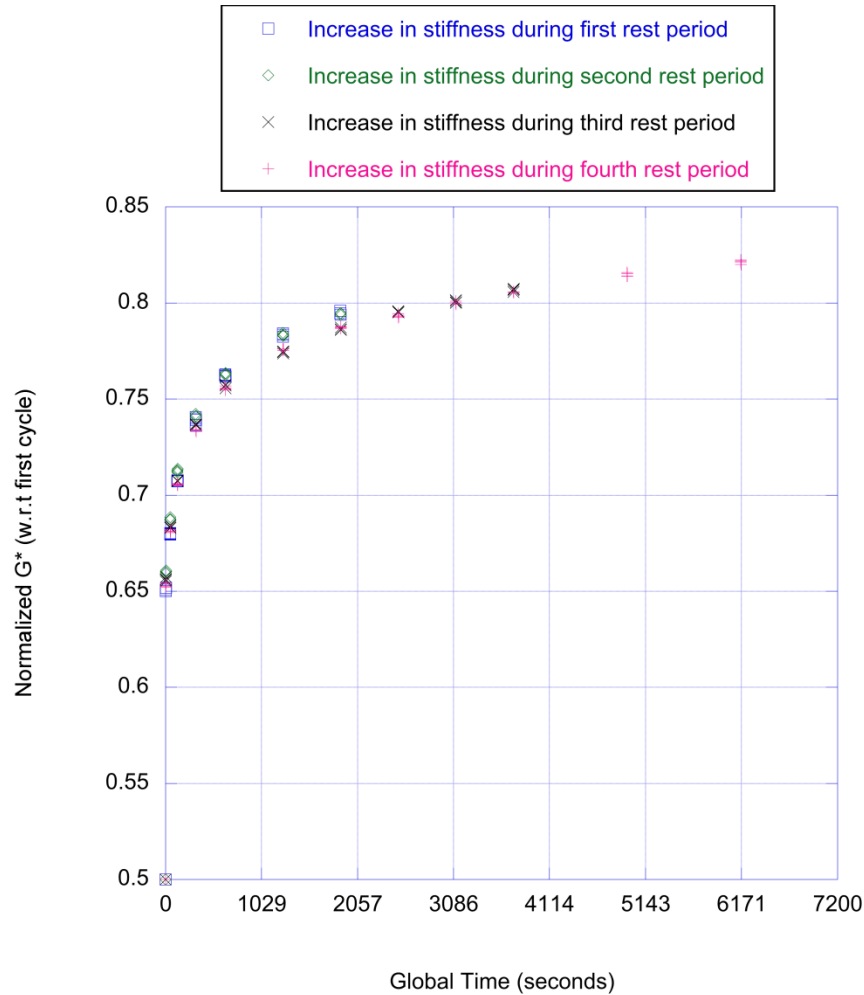


Figure F1d.2. Rate of stiffness gain during rest periods (each rest period was started when the specimen reached 50% of its linear viscoelastic complex modulus).

In this quarter, we have designed an experiment to measure the total healing (intrinsic and overall) of fine aggregate matrix specimens after different levels of damage. Since stiffness does not truly reflect the amount of damage in the specimen, we are also using the VECD model to quantify the amount of damage and healing in the specimen. On the binder side (intrinsic healing), we are measuring the rate of intrinsic healing as quantified based on the strength in addition to the stiffness. Based on preliminary results, it appears that yield strength may be a better indicator of intrinsic healing as compared to stiffness. Figure F1d.3. illustrates a typical healing curve of a short-term aged binder based on the gain in the complex modulus of a two-piece specimen over time. Figure F1d.4 illustrates the typical healing curve of a short-term aged binder (comparable binder and temperature) based on the gain in the yield strength of two-piece specimens. Since the latter is a destructive test, different specimens were used with each healing time.

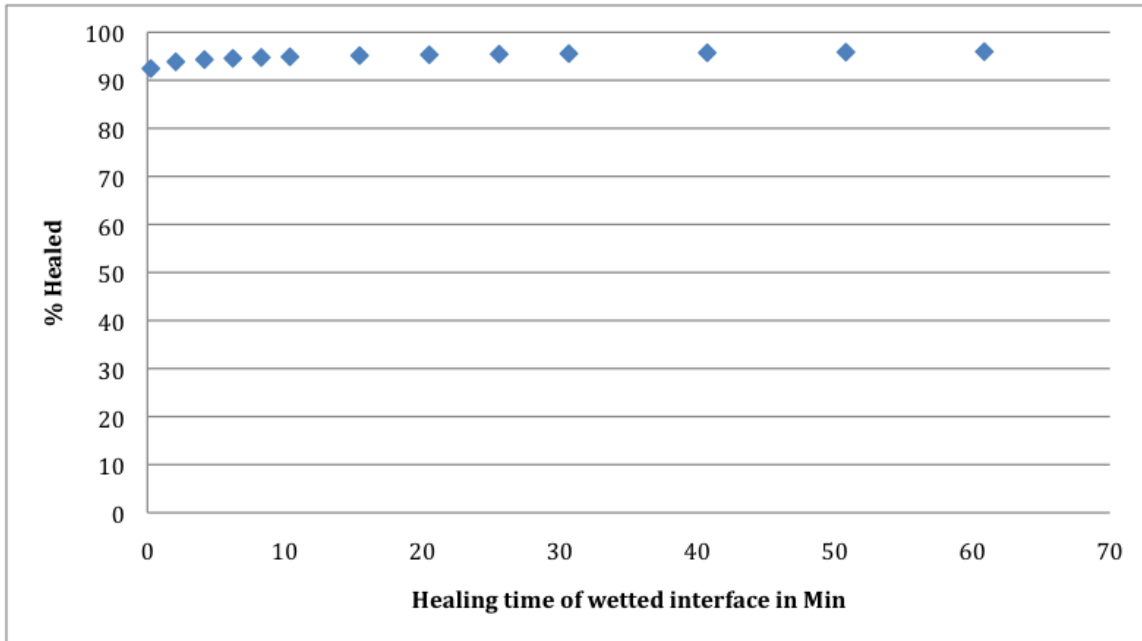


Figure F1d.3. Typical rate of intrinsic healing of an RTFO aged binder based on gain in complex shear modulus of a two piece specimen proportional to a single piece specimen.

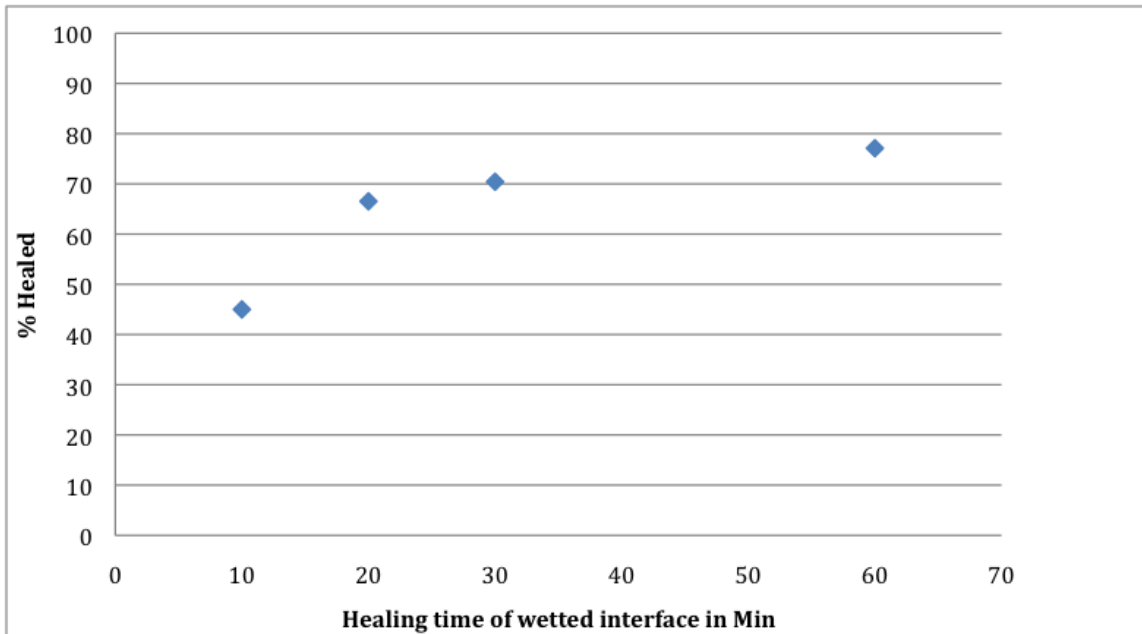


Figure F1d.4. Typical rate of intrinsic healing of an RTFO aged binder based on gain in yield strength of a two piece specimen proportional to a single piece specimen.

Significant Problems, Issues and Potential Impact on Progress

None.

Work Planned Next Quarter

We will continue to measure intrinsic healing as well as prepare FAM specimens to measure overall healing.

Subtask F1d-6: Evaluate Relationship Between Healing and Endurance Limit of Asphalt Binders (UWM)

Work Done This Quarter

Work this quarter included limited testing using a modified time sweep with intermittent loading. The proposed modified time sweep with rest periods consists of an oscillatory linear ramp to the target strain amplitude. Then, cyclic loading is applied at this strain amplitude followed by a rest period.

The Dynamic Shear Rheometer (DSR) used for the healing tests was not working properly for much of the past quarter. The DSR is incapable of making instantaneous changes in loading; therefore, the loading ramp is used in the healing test procedure to accommodate for the limitations of the machine. The results of tests conducted using this modified time sweep with rest periods are compared to a no-rest case, which consists of a single cyclic ramp to the target strain amplitude followed by cyclic loading at single strain amplitude. Currently, a five-second ramp is being employed for both the rest and no-rest case. In the rest-period case, following each ramping step 100 cycles of loading are applied at constant strain amplitude followed by 30 seconds of rest. All tests are conducted using a frequency of 10 Hz. Figure F1d-6.1 shows the loading sequence for both the no-rest and rest cases.

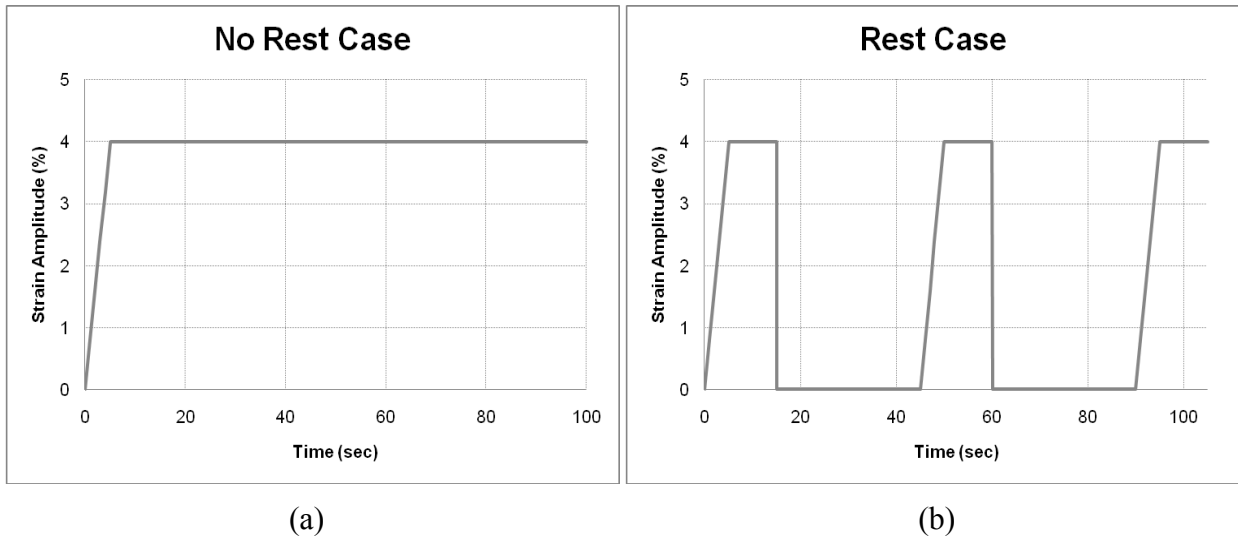


Figure F1d-6.1. Graphs. Loading schematic for healing testing for: (a) no-rest case; and (b) rest case.

Two un-aged asphalt binders have been tested using this testing procedure. The first binder is a PG 64-22 binder modified with linear styrene-butadiene-styrene (LSBS). The second is a PG 76-22 LTPP binder coded 37-0964. The strain amplitude used in all testing was 4%. The LSBS-modified binder exhibited a significant increase in fatigue life with inclusion of rest periods, while the LTPP binder exhibited insignificant healing effect, as shown in figures F1d-6.2 and F1d-6.3, respectively.

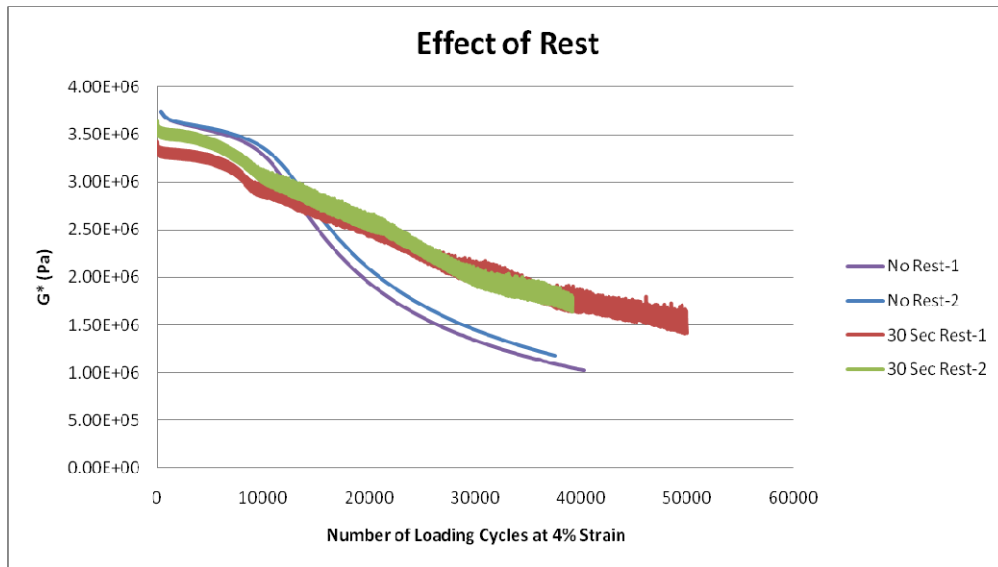


Figure F1d-6.2. Graph. PG 64-22 + LSBS healing testing results.

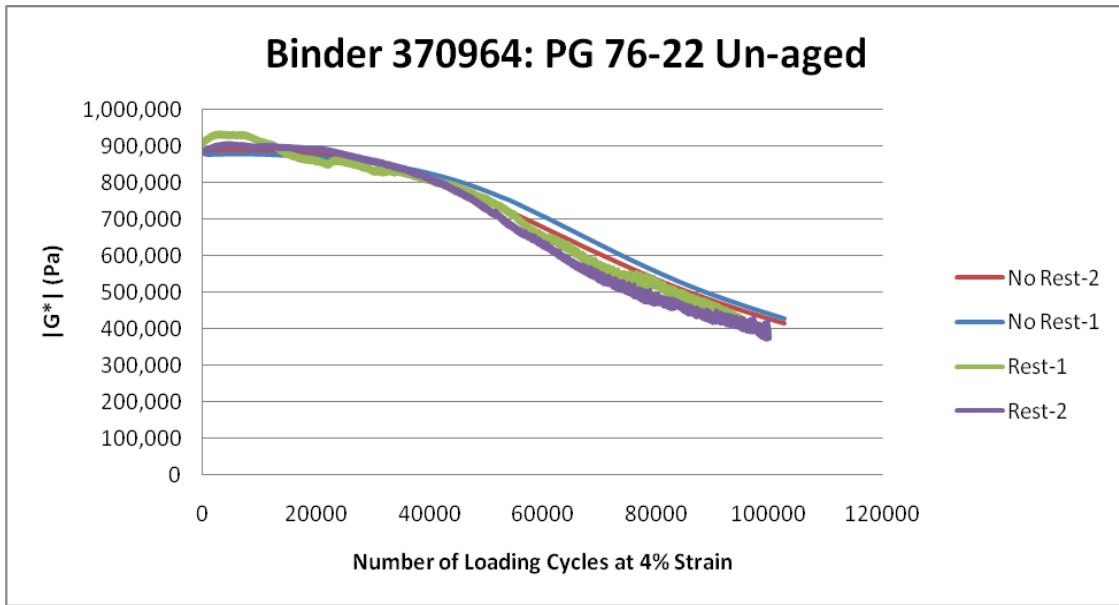


Figure F1d-6.3. Graph. LTPP 37-0964 binder healing results.

Experimental results were analyzed using the ratio of dissipated energy (RDEC) approach as recommended by Shen (Shen et al. 2010). The RDEC was defined in previous quarterly reports. In a strain-controlled time sweep test, the RDEC is nearly constant while the most rapid failure is occurring, (i.e., around 20000 cycles, as shown in figure F1d-6.2). This nearly constant RDEC is called the plateau value (PV). The PV was used as an indicator of fatigue resistance. A higher PV corresponds to a shorter fatigue life. Note that the loading cycles during the ramping steps were not considered in analysis. Thus, only the loading cycles at 4% strain were used in the estimation of RDEC and PV.

PV results for the two binders tested are presented in table F1d-6.1. The results indicate that the PVs are very similar for the rest and no-rest cases of the LTPP binder, while the magnitude of the PV decreases when rest periods are included for the LSBS-modified binder. The reduction of the PV due to rest periods is an indication of healing.

Table F1d-6.1. Plateau value results.

	PG 64-22 + LSBS	PG 76-22 LTPP 370964
No Rest	6.79E-05	1.51E-05
Rest	2.67E-05	1.50E-05

Significant Results

The research team noted that a modified time sweep with ramp and intermittent loading exhibits potential to serve as test to evaluate healing.

Significant Problems, Issues and Potential Impact on Progress

The DSR had many maintenance issues during much of the past quarter; therefore, delays in completing testing matrix for healing are expected. The research team is planning to double efforts in this work element in the next quarter to reduce the potential impact of these delays on the progress and final deliverables.

Work Planned Next Quarter

The research team will continue evaluating the modified time sweep with rest period procedure using LTPP binders. Also, the LTPP binders will be tested at different age levels to evaluate the effect of oxidative aging on healing.

Cited References

Shen, S., H. Chiu, and H. Huang, 2010, Characterization of Fatigue and Healing in Asphalt Binders. *ASCE Journal of Materials in Civil Engineering*, 22(9): 846-852.

Subtask F1d-7: Coordinate with Atomic Force Microscopic (AFM) Analysis (WRI)

Work Done This Quarter

Nothing to report.

Significant Problems, Issues and Potential Impact on Progress

None

Work Planned Next Quarter

Continuation: Analysis of existing data will continue in the next quarter. In these analyses, morphological features observed in asphalt and asphalt chromatographic fraction thin films prepared from validation site asphalts will be compared to performance data of the field site pavements. Image analysis of AFM scans will be developed to define a roughness “lumpiness” index.

Subtask F1d-8: Coordinate Form of Healing Parameter with Micromechanics and Continuum Damage Models (TAMU)

Work Done This Quarter

The focus of this quarter is on the development and validation of a micro-damage healing model that improves the ability of an integrated nonlinear viscoelastic, viscoplastic, and viscodamage constitutive model based on continuum damage mechanics for predicting the fatigue life of asphalt paving mixtures. The model parameters of the continuum-based healing model are related to fundamental material properties such as the surface energy, bond strength, and the size of the healing process zone. The micro-damage healing model is coupled to the viscoelastic, viscoplastic, and continuum damage mechanics constitutive models in the unified continuum damage mechanics code PANDA. Moreover, the model is validated by comparing its predictions with experimental data from the Nottingham database on an asphalt mix. These tests include repeated creep-recovery tests for different loading times and rest periods in both tension and compression. The significant enhancement of the ability of the constitutive model to predict fatigue life due to inclusion of the micro-damage healing is clearly demonstrated.

The essentials of this continuum micro-damage healing model are briefly summarized here and detailed in Abu Al-Rub et al. (2010). The effective (undamaged) stress in classical continuum damage mechanics is modified to read:

$$\bar{\sigma} = \frac{\sigma}{1 - \phi(1 - h)} \quad (\text{F1d-8.1})$$

where $0 \leq \phi \leq 1$ is the damage density (i.e., density of micro-cracks and micro-voids), and $0 \leq h \leq 1$ is the micro-damage healing density (i.e., density of healed micro-cracks and micro-voids). The evolution law for h is derived based on the laws of thermodynamics and is given as:

$$\frac{dh}{dt} = \Gamma_0^h (1 - \phi[1 - h])^{b_1} (1 - h)^{b_2} \exp \left[-b_3 \left(1 - \frac{T}{T_0} \right) \right] \quad (\text{F1d-8.2})$$

where Γ_0^h is the healing viscosity parameter at reference temperature T_0 , b_1 , b_2 , and b_3 are material parameters. It is noteworthy that Γ_0^h controls the rate at which healing occurs and is expressed in terms of fundamental material properties as:

$$\Gamma_0^h = \left[\frac{1}{D_1 k_m} \left(\frac{\pi W_c}{4(1 - \nu^2) \sigma_b^2 \Delta} - D_0 \right) \right]^{-\frac{1}{m}} \quad (\text{F1d-8.3})$$

where D_0 , D_1 , and m are obtained by assuming a power law function for the transient creep compliance (i.e., $D = D_0 + D_1 t^m$), and k_m is a material constant expressed in terms of m , $W_c = 2G$ is the work of cohesion and is related to the material's surface energy G , σ_b is the

bond strength along in the healing process zone, Δ , and ν is the Poisson's ratio. More details about the evolution law for the damage density ϕ can be found in Darabi et al. (2010).

The above micro-damage healing model is already implemented into the unified continuum damage code PANDA and can be used for now to conduct fairly complex micro and macro simulations on asphalt mixtures and pavements.

Significant Results

For example, figures F1d-8.1 and F1d-8.2 show the experimental data and the model predictions without and with the healing model for different loading time (LT) and unloading times (UT) in compression and tension, respectively. These figures clearly show that the model predictions when healing is included are significantly improved as compared to the experimental data and the predictions when healing is not included.

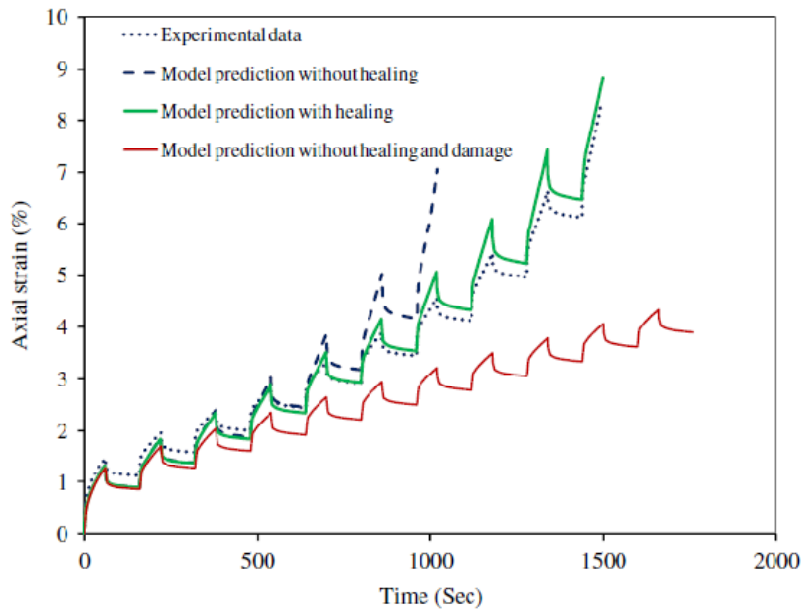


Figure F1d-8.1. Strain response for the repeated creep-recovery tests in compression when the applied stress is 1500 kPa where LT=120 s and UT= 100 s.

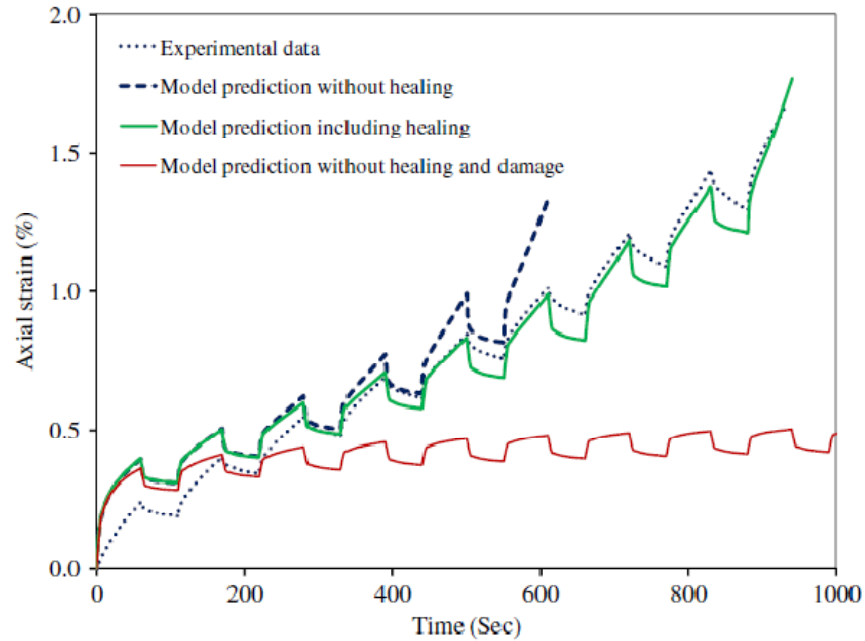


Figure F1d-8.2. Strain response for the repeated creep-recovery tests in tension when the applied stress is 300 kPa for LT=60 s and UT= 50 s.

Significant Problems, Issues and Potential Impact on Progress

None

Work Planned Next Quarter

In the coming quarter the formulated micro-damage healing model will be validated against ALF experimental data and other existing data on another asphalt mixture in the Nottingham database.

Cited References

Abu Al-Rub, R.K., M. K. Darabi, D. Little, and E. A. Masad, 2010, A micro-damage healing model that improves prediction of fatigue life of asphalt mixes. *International Journal of Engineering Science* DOI: [10.1016/j.ijengsci.2010.09.016](https://doi.org/10.1016/j.ijengsci.2010.09.016).

Darabi, M. K., R. K. Abu Al-Rub, E. A. Masad, C.-W. Huang, and D. N. Little, 2010, A thermo-viscoelastic-viscoplastic-viscodamage constitutive model for asphaltic materials. *International Journal of Solids and Structures* DOI: [10.1016/j.ijsolstr.2010.09.019](https://doi.org/10.1016/j.ijsolstr.2010.09.019).

CATEGORY F2: TEST METHOD DEVELOPMENT

Work Element F2a: Binder Tests and Effect of Composition (UWM)

Work Done This Quarter

This quarter the research team investigated the relationship that exists between Binder Yield Energy Test (BYET), time sweep and Linear Amplitude Sweep (LAS) tests. As indicated in a previous quarterly report, new parameters were selected to characterize the binder yield energy: BYE20 (BYET energy at 20 strain), BYEpeak/G* (BYET energy/G*) and BYE20/G* (BYET energy at 20 strain/G*). The selected parameter to define failure in the time sweep test is the number of cycles (N_p) corresponding to the maximum dissipated energy ratio. Plotting the initial dissipated energy against the number of cycles to failure in a logarithmic scale and fitting a power law equation, the slope (K_1) and intercept (K_2) were determined. These two parameters (K_1 and K_2) were used to determine the fatigue life at different energy levels. The fatigue life was determined at 10 kPa and 30 kPa. The number of cycles to failure for the LAS was calculated using the following equation:

$$N_f = A_{35} (\gamma_{max})^{-B} \quad (F2a.1)$$

where A and B were calculated using viscoelastic continuum damage (VECD) theory.

Significant Results

The selected parameter from the BYET for comparison purposes was BYE20/G*. This parameter was compared with the number of cycles to failure at 10 kPa (N_f at 10 kPa). The results shown in figure F2a.1 illustrate that some relation exists between these two parameters ($R^2 = 0.67$).

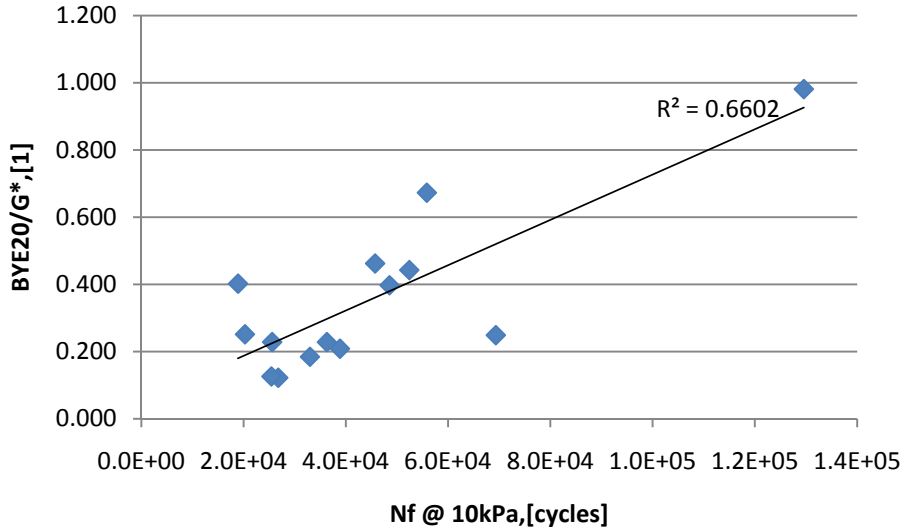


Figure F2a.1. Graph. Relation between BYE20/G* and number of cycles to failure at 10 kPa from time sweep. (Nf = fatigue life.)

The BYE20/G* results were also compared with the number of cycles to failure from the LAS test at 2.5% strain (N_f at 2.5%) and 5% strain (N_f at 5%). The results of the comparison are shown in figure F2a.2. A weak relation exists between BYE20/G* and N_f at 2.5% (R²=0.39). Note that poor correlation was also observed for other strain levels.

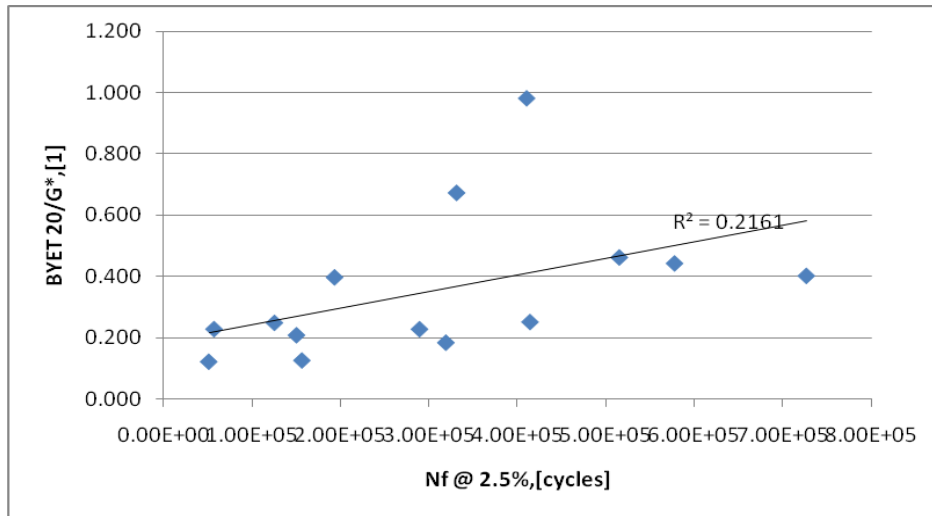


Figure F2a.2. Graph. Relation between BYE20/G* and number of cycles to failure at 2.5% strain from LAS.

The relation between the N_f at 10 kPa and N_f at 2.5% strain is shown in figure F2a.3. It can be seen that there is no correlation between results from these tests. The comparison at other strain and energy levels showed insignificant correlation between LAS and time sweep results.

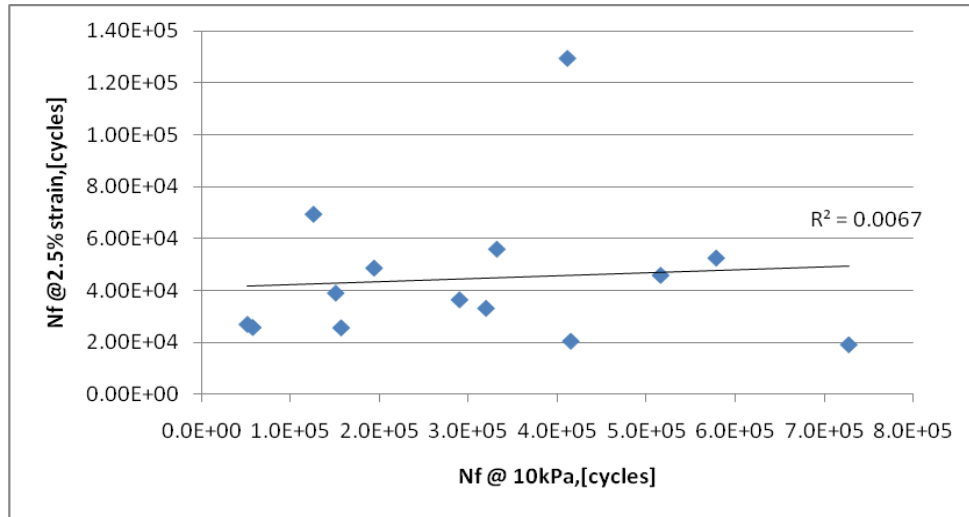
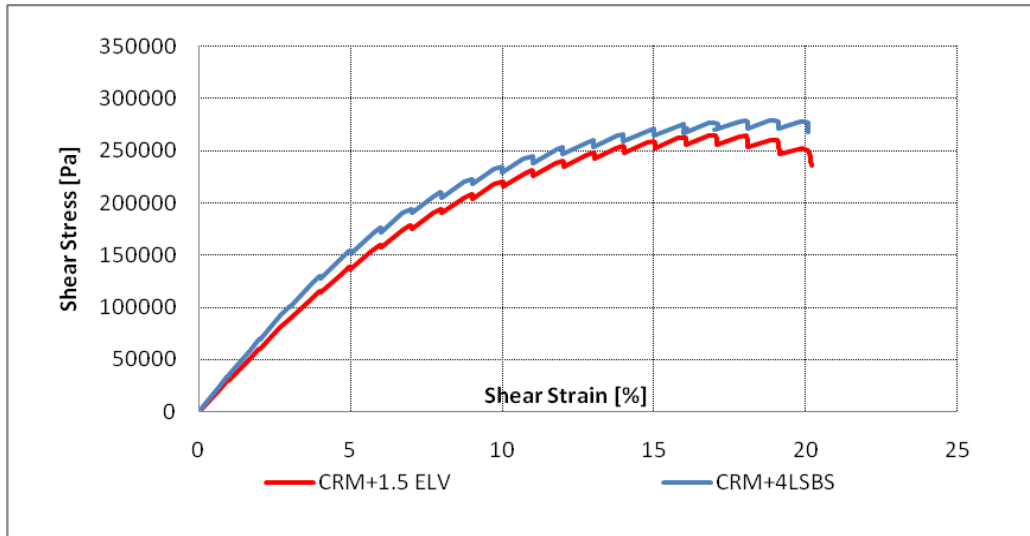
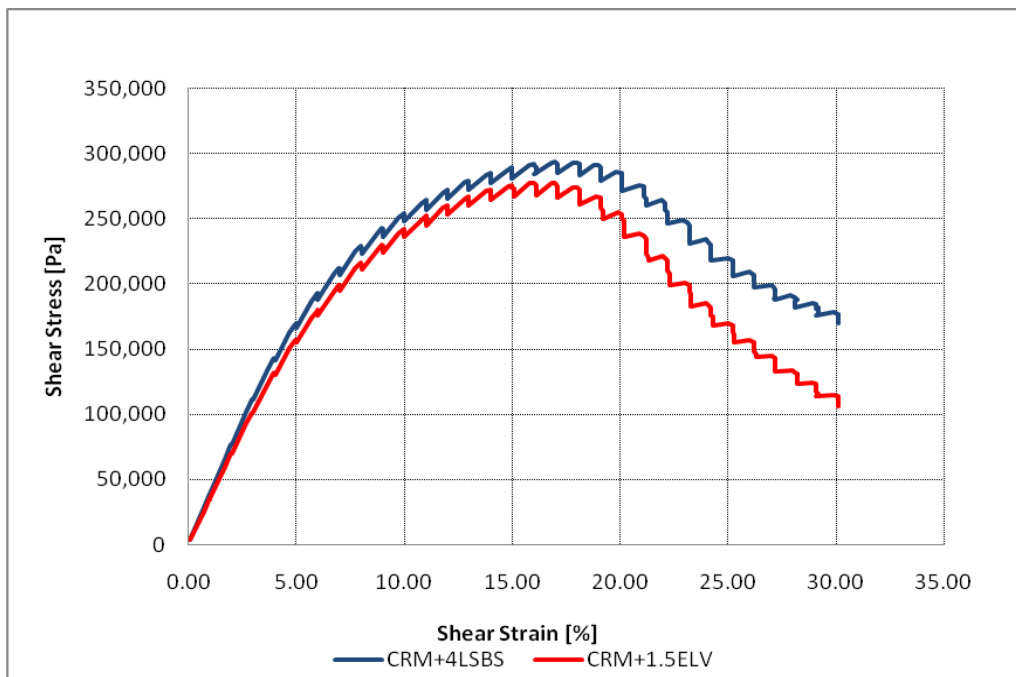


Figure F2a.3. Graph. Relation between N_f at 10 kPa from time sweep and N_f at 2.5% strain from LAS.

The poor correlation observed can be attributed to different factors. First, according to the current protocol the shear strain is increased from 0.1% to 20%. Examining the stress versus strain curve, it was observed that for some binders the 20% strain level did not cause significant damage to the material. This behavior is shown in figure F2a.4(a) for two binders. As it can be seen, these binders did not accumulate significant amount of damage at 20% strain. Therefore, it was decided to increase the maximum strain level to 30%. An example of a test conducted at these additional strain levels is shown in figure F2a.4(b).



(a)



(b)

Figure F2a.4. Graphs. LAS stress versus strain curve to: (a) maximum strain level of 20%; and (b) maximum strain level of 30%. (LSBS = linear styrene-butadiene-styrene. ELV = Elvaloy.)

Different fatigue law parameters will be obtained if the analysis is conducted using LAS data up to 30% of strain instead of the proposed 20% strain level. An analysis of variance (ANOVA) confirmed that the N_f at 2.5% calculated at 20% strain is statistically different than N_f at 2.5% at 30% strain (p-value=0.037).

The second explanation for the lack of correlation between the time sweep tests and LAS tests can be attributed to the way α is measured. Current protocol measures the relaxation modulus at 0.1% strain. Selected materials were tested at different strain levels: 0.1%, 0.3%, 0.9%, 2.7%, 5.4% and 8.1%. The results for the α at different strain levels are shown in table F2a. 1. The results indicate that α values are sensitive to the strain level at which this property is measured.

Table F2a.1 Effect of the strain level on α .

Material	α @					
	0.10%	0.30%	0.90%	2.70%	5.40%	8.10%
FH+4LSBS	2.55	2.56	2.57	2.68	2.82	3.01
FH+1.5ELV	2.38	2.38	2.39	2.43	2.53	2.60
FH+1.5PPA	2.63	2.64	2.66	2.75	2.92	3.05
CRM+4LSBS	2.45	2.45	2.46	2.52	2.65	2.80
CRM+1.5ELV	2.38	2.38	2.38	2.43	2.54	2.64

PPA = polyphosphoric acid.

The Gantt chart for this work element was updated to reflect the August 2010 submission of a journal paper to the 90th TRB Annual Meeting in January 2011 on the topic of modification of the elastic recovery test and its relationship to performance-related properties of modified asphalt binders.

Significant Problems, Issues and Potential Impact on Progress

None.

Work Planned Next Quarter

Work in the next quarter will focus on preparing mastics and conducting the mechanical tests proposed in the Year 4 work plan. The issue of α value changes with strain, and how to consider it in the analysis, will be studied in detail.

Work Element F2b: Mastic Testing Protocol (TAMU)

Work Done This Quarter

The reader is referred to work element M1c where the procedure for preparing FAM specimens and software development is presented.

Work planned next Quarter

Work will be conducted and presented in work element M1c.

Work Element F2c: Mixture Testing Protocol (TAMU)

Work Done This Quarter

A technical presentation, entitled “Characterization of Engineered Properties of Asphalt Mixtures as Inputs to PANDA”, has been made in the Fundamental Properties and Advanced Models Expert Task Group of the Federal Highway Administration (FHWA) in Madison, Wisconsin, September 2010. This presentation summarizes the progress made in this quarter on the master curve models of the asphalt mixture and the data analysis of the stress-controlled test on the lab-mixed-lab-compacted (LMLC) asphalt mixture specimens. Specifically, the progress made in this quarter includes:

- An “inverse S” model has been proposed to construct the master curve of the magnitude of the complex Poisson’s ratio, and a “ β -model” has been developed to establish the master curve of the phase angle of both complex modulus and complex Poisson’s ratio for the asphalt mixtures;
- Dynamic modulus tests have been conducted on LMLC specimens to validate the proposed master curve models and to verify the nondestructive anisotropic testing protocols for the undamaged asphalt mixtures.
- An analytical method has been developed based on the Dissipated Pseudo Strain Energy (DPSE) theory to analyze the data of the controlled-stress repeated loading test so as to investigate the stress and energy redistribution with damage and predict the crack growth and the plastic deformation accumulation.

Details of the achievements made in this quarter are presented as follows:

1) Master Curve Models of Complex Modulus and Complex Poisson’s Ratio

To characterize the viscoelastic properties of asphalt mixtures in a broad range of temperature and frequency, it is necessary to construct the master curves for the magnitude and phase angle of the complex modulus and the complex Poisson’s ratio. When constructing the master curves, the undamaged asphalt mixture is considered as a linearly viscoelastic material so that the time-temperature superposition principle can be employed. Therefore, the master curves are constructed by conducting tests at multiple temperatures and shifting the data to the reference temperature.

The CAM model (Marasteanu and Anderson 1999) shown in equation F2c.1 has proved to be able to successfully construct the master curve of the magnitude of the complex modulus (Luo and Lytton 2010). The CAM model is used in this study to formulate the master curves of the magnitudes of both compressive complex modulus and the tensile complex modulus.

$$|E^*(\omega)| = \frac{E_g}{\left[1 + \left(\frac{\omega_{cE}}{\omega \cdot 10^{C_E(T-T_r)}} \right)^{\frac{\log 2}{R_E}} \right]^{\frac{R_E}{\log 2}}} \quad (\text{F2c.1})$$

where E_g = glassy modulus of the asphalt mixture, MPa; ω_{cE} = crossover frequency of the asphalt mixture for modulus, rad/sec; R_E = rheological index of the asphalt mixture for modulus; and C_E = slope of temperature shift factor for modulus. The CAM model in equation F2c.1 yields a rising “S-shaped” curve for the magnitude of the complex modulus that approaches an asymptote of the horizontal glassy modulus, E_g .

It is found that the magnitude of the complex Poisson’s ratio decreases as the frequency increases, which has an “inverse S” shape. Therefore, a formula in the similar form of the CAM model is developed to construct the master curve of the magnitude of the complex Poisson’s ratio, as shown in equation F2c.2. The model presents a falling S-shaped curve in the frequency domain and is named as the Inverse S Model.

$$|v^*(\omega)| = \frac{v_g}{\left[1 + \left(\frac{\omega \cdot 10^{C_v(T-T_r)}}{\omega_{cv}} \right)^{\frac{\log 2}{R_v}} \right]^{\frac{R_v}{\log 2}}} \quad (\text{F2c.2})$$

where v_g = glassy Poisson’s ratio of the asphalt mixture, MPa; ω_{cv} = crossover frequency of the asphalt mixture for Poisson’s ratio, rad/sec; R_v = rheological index for Poisson’s ratio; and C_v = slope of temperature shift factor for Poisson’s ratio.

For the master curve of the phase angle of the complex modulus, Bahia et al. (2001) developed a model shown in equation F2c.3 that presents a bell-shaped curve which is symmetric on a log-log plot of phase angle versus frequency. The Williams-Landel-Ferry (WLF) function is recommended to calculate the time-temperature shift factor (Luo and Lytton 2010).

$$\varphi_E = \frac{\varphi_{mE}}{\left\{ 1 + \left[\frac{\log \left(\frac{\omega_{mE}}{\omega \cdot 10^{\frac{C_1(T-T_r)}{C_2+(T-T_r)}}}} \right)}{R_{\varphi E}} \right]^2 \right\}^{\frac{m}{2}}} \quad (\text{F2c.3})$$

where φ_{mE} = the maximum phase angle for modulus, degrees; ω_{mE} = the frequency when φ_{mE} occurs, rad/sec; $m, R_{\varphi E}$ = fitting parameters for modulus phase angle; T_r = reference temperature; and C_1 and C_2 = regression constants in WLF function.

It is reasonable to use a bell-shaped curve to model the master curve of the phase angle of the complex modulus because the phase angle approaches zero at a frequency of zero or infinity. In other words, a viscoelastic solid, such as the asphalt mixture, behaves as an elastic solid at extremely low or high frequencies. However, for an asphalt mixture, the master curve of the phase angle may not be symmetric on a log-log plot of the phase angle versus the frequency. As a result, a more general model as presented in equation F2c.4 is developed and named as the β -model for the phase angle master curve of both complex modulus and complex Poisson's ratio. This model also produces a bell-shaped curve but the curve is not constrained to be symmetric on the plot of phase angle versus the logarithm of frequency.

$$\varphi = \frac{\varphi_{max}}{\text{Exp} \left\{ \left(\frac{\beta + 1}{\beta} \right) \left[\left(\frac{\omega_R}{\omega \cdot \alpha_T} \right)^\beta - 1 \right] \right\} \left(\frac{\omega \cdot \alpha_T}{\omega_R} \right)^{\beta + 1}} \quad (\text{F2c.4})$$

where φ_{max} = the maximum phase angle, degrees; ω_R = the reference frequency where φ_{mE} occurs, rad/sec; β = fitting parameter that determine the curvature of the phase angle master curve; α_T = time-temperature shift factor, e.g. $\log \alpha_T = C_1 (T - T_r) / [C_2 + (T - T_r)]$ if the WLF model is used. When $\varphi_{max} > 0$, equation (F2c.4) produces a bell-shaped curve that is applicable for the master curve of the phase angle of the complex modulus; when $\varphi_{max} < 0$, equation (F2c.4) yields an inverted bell-shaped curve that is applicable for the master curve of the phase angle of the complex Poisson's ratio.

2) Validation of Master Curve Models and Anisotropic Testing Protocols

In the previous quarters, a test protocol with three nondestructive test scenarios was developed to determine the six independent variables: $E_{11}^{C*}(\omega)$, $\nu_{12}^{C*}(\omega)$, $E_{22}^{C*}(\omega)$, $\nu_{23}^{C*}(\omega)$, $E_{11}^{T*}(\omega)$, and $\nu_{12}^{T*}(\omega)$, which were employed to characterize the anisotropy of asphalt mixtures. The test protocol includes the uniaxial compressive creep test, uniaxial tensile creep test and indirect tensile creep test. To validate this test protocol and the master curve models, the three test scenarios were conducted at three temperatures (10°C, 20°C and 30°C) on the asphalt mixture specimens that vary in asphalt binder (AAD and AAM), air void content (4% and 7%) and aging period (non-aging and 6-month continuous aging at 60°C). Then the nondestructive dynamic modulus test was conducted at frequencies of 0.5Hz and 1Hz, respectively, on the same asphalt mixture specimens. The magnitudes and phase angles of the compressive complex modulus in vertical direction determined by the dynamic test were compared to the predicted values using the master curves constructed based on the test data of the developed test protocol. More details of the findings are discussed as follows.

Figure F2c.1 and figure F2c.2 show the $|E_{11}^{C*}|$ and $\varphi_{E_{11}^{C*}}$, respectively, that are measured using the dynamic test at the two frequencies and that are determined by the constructed master curves. Even though the volumetric composition of the asphalt mixture varied, both $|E_{11}^{C*}|$ and $\varphi_{E_{11}^{C*}}$ predicted by the master curves match those measured by the dynamic test very well. This demonstrates that the proposed test protocol effectively determines the complex modulus including the magnitude and phase angle. In addition, $\varphi_{E_{11}^{C*}}$ measured by the dynamic test at the two frequencies are also plotted as black circles in figure F2c.3. The two black circles are close to the master curve constructed using equation F2c.4, but they do not well match the master curve constructed using equation F2c.3. Consequently, the asymmetric β -model in equation F2c.4 is a more appropriate model of constructing the master curve of the phase angle of the complex modulus.

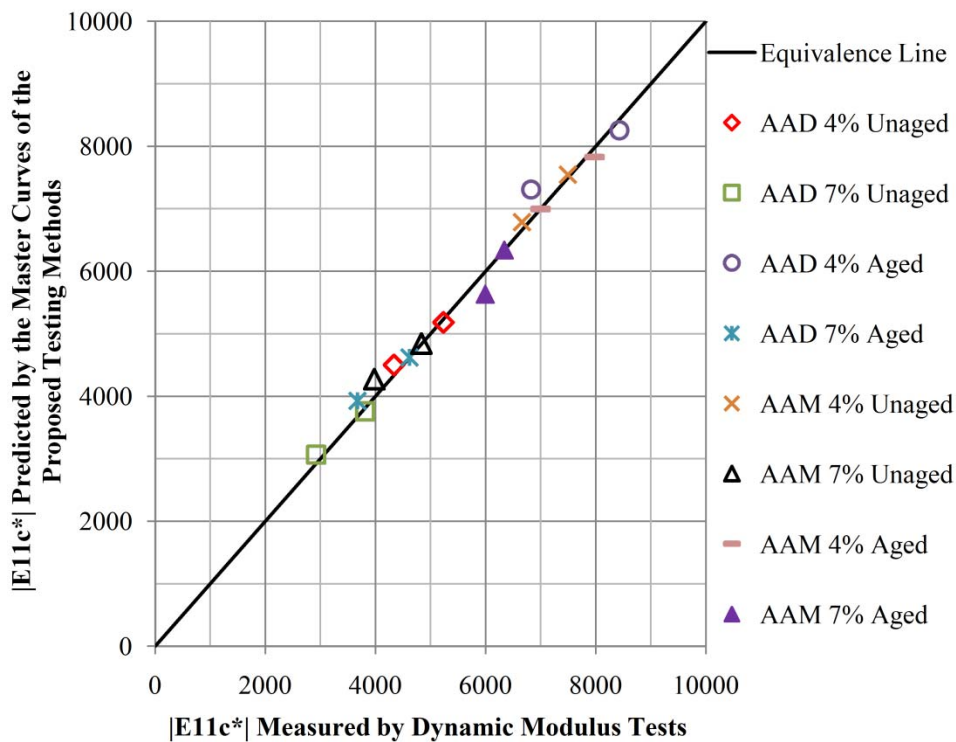


Figure F2c.1. Comparison of magnitudes of E_{11}^{C*} from master curves with dynamic modulus tests.

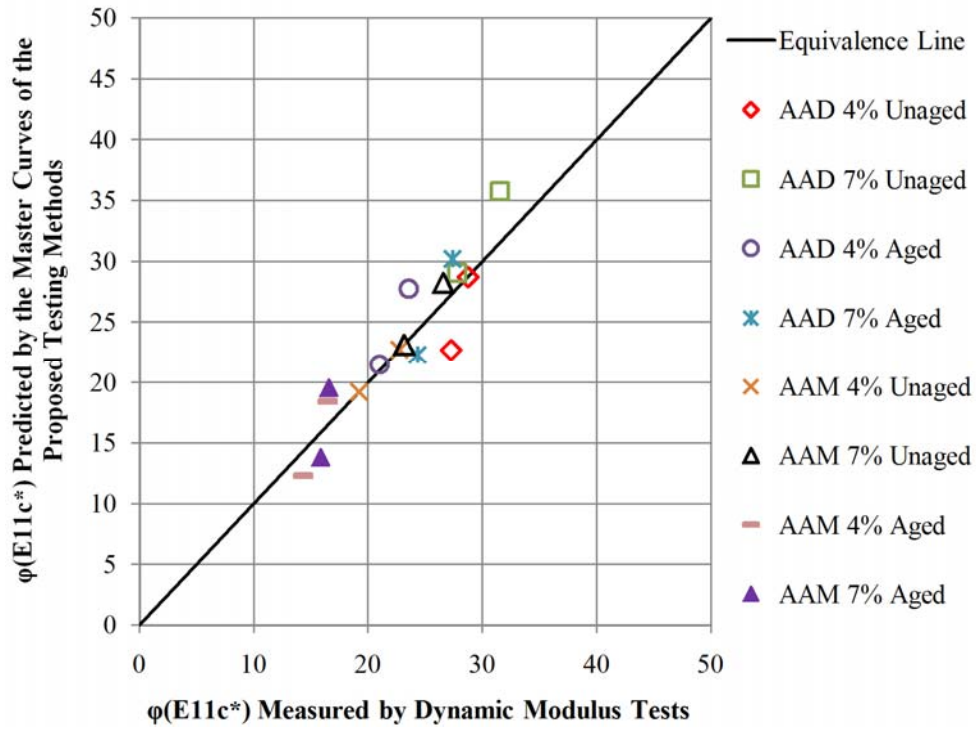


Figure F2c.2. Comparison of phase angles of E_{11}^{C*} from master curves with dynamic modulus tests.

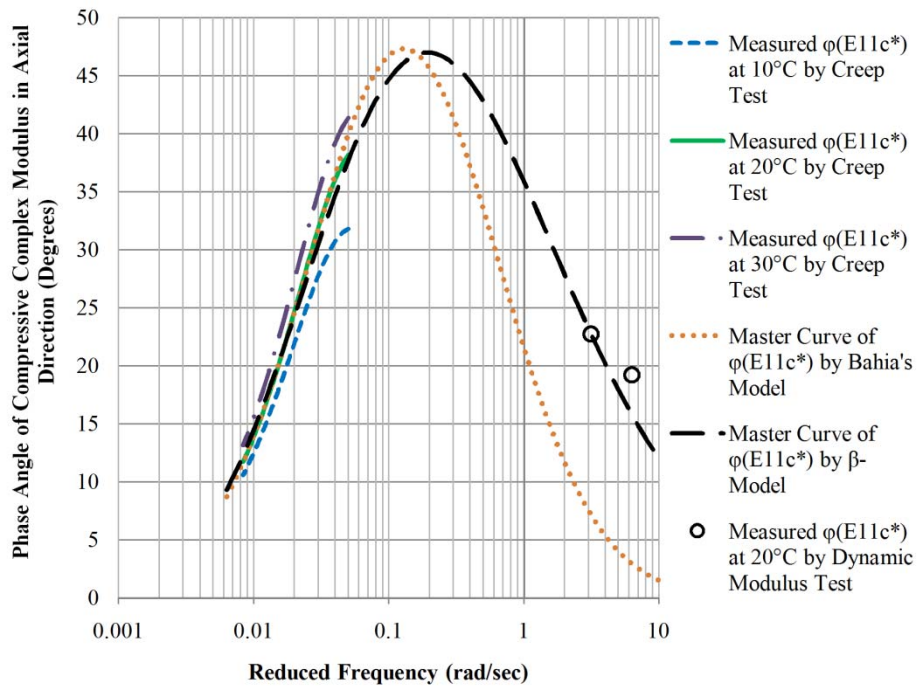


Figure F2c.3. Phase angle of the E_{11}^{C*} at different temperatures and master curve at 20°C.

The master curves of $|\nu_{12}^{C*}|$, $|\nu_{12}^{T*}|$ and $|\nu_{23}^{C*}|$ at the reference temperature of 20°C are also constructed with respect to frequency. Each magnitude master curve of the Poisson's ratio has an inverse S shape on the log scale of the frequency, which decreases as the frequency increases. Therefore the inverse S model in equation F2c.2 is appropriate to construct the magnitude of the master curve of the complex Poisson's ratio. The master curves of $\varphi_{\nu_{12}^{C*}}$, $\varphi_{\nu_{12}^{T*}}$ and $\varphi_{\nu_{23}^{C*}}$ have a reversed bell-shaped curve on the log scale of the frequency, which can be modeled by using the β -model in equation F2c.4.

To evaluate the effects of the binder type, air void content and aging period on $|E_{11}^{C*}|$, $|E_{11}^{T*}|$ and $|E_{22}^{C*}|$, the values of $|E_{11}^{C*}|$, $|E_{11}^{T*}|$ and $|E_{22}^{C*}|$ at a frequency of 0.1 rad/sec on the master curves are selected as the representative modulus magnitudes. Figure F2c.4 plots the average and standard deviation of the representative modulus magnitude of each combination of the binder type, air void content and aging period. This figure shows that the specimens with the AAM binder are stiffer than the specimens with the AAD binder. When the air void content increases from 4% to 7%, $|E_{11}^{C*}|$, $|E_{11}^{T*}|$ and $|E_{22}^{C*}|$ all decrease. The aged asphalt mixtures have higher moduli than the unaged specimens. All of these findings are consistent with the common understandings of the asphalt mixture properties. For any combination of the binder type, air void content and aging period, $|E_{11}^{C*}|$ is always larger than $|E_{22}^{C*}|$; the ratio of $|E_{11}^{C*}|$ to $|E_{22}^{C*}|$ ranges from 1.2 to 2, which proves that asphalt mixtures have significant anisotropy under a compressive load. Figure F2c.5 plots the average and standard deviation of the peak phase angles. It can be seen that the peak values of $\varphi_{E_{11}^{C*}}$ and $\varphi_{E_{22}^{C*}}$ are close to each other, which are in a range of 35 to 55 degrees, while $\varphi_{E_{11}^{T*}}$ always has a higher peak value ranging from 65 to 85 degrees. These findings can be explained by the stronger viscoelasticity of asphalt mixtures in tension but less viscoelasticity of mixtures in compression.

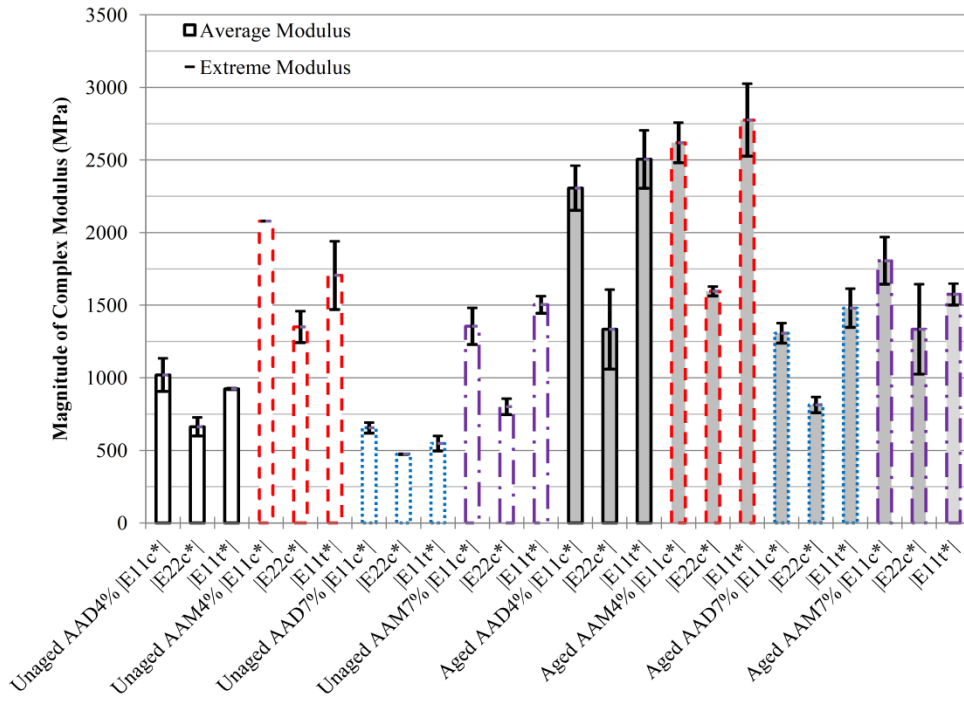


Figure F2c.4. Magnitude of the E_{11}^{C*} , E_{11}^{T*} and E_{22}^{C*} at 0.1 Hz on the master curves at 20°C.

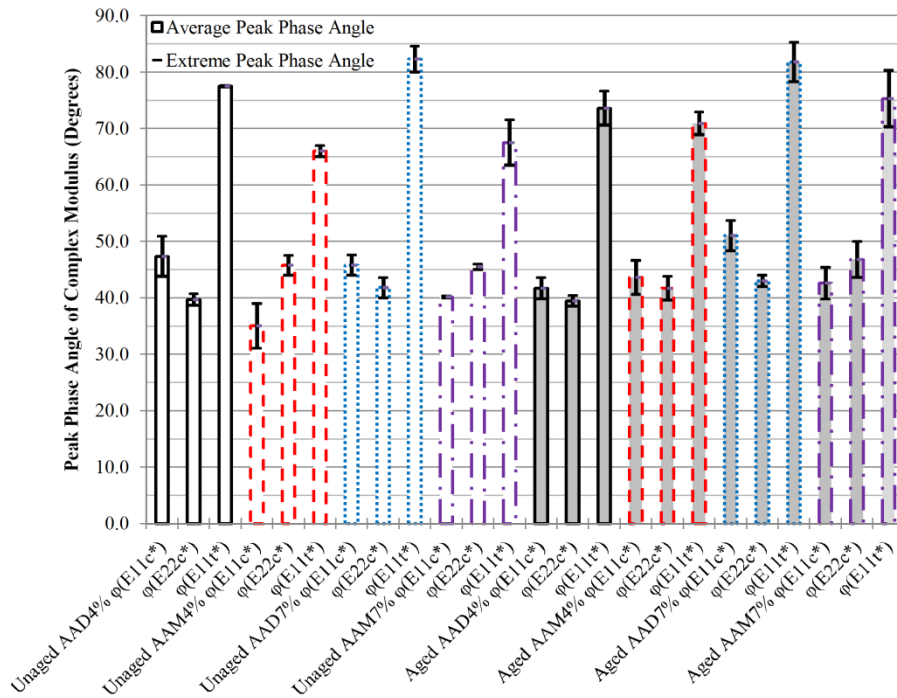


Figure F2c.5. Peak phase angle of the E_{11}^{C*} , E_{11}^{T*} and E_{22}^{C*} on the master curves at 20°C.

3) Crack and Plasticity Analysis in Controlled-Stress Test using DPSE Method

The Dissipated Pseudo Strain Energy (DPSE) method has been proved to be an effective way to analyze the damage evolution of the asphalt mixture. The pseudo strain is defined as the calculated linear viscoelastic stress divided by a reference modulus and shown in equation F2c.5. The advantage of introducing pseudo strain is that it can be related to the stress through Hooke's law, and eventually the viscoelasticity of the material can be eliminated. The DPSE is calculated as the area of a hysteresis loop on the plot of the measured stress versus the pseudo strain and is shown in equation F2c.6. For the undamaged material, the plot of the measured stress with the pseudo strain is a straight line and the DPSE equals zero because no energy is dissipated for damage. For the damaged material, a hysteresis loop appears and the DPSE is greater than zero because the pseudo strain energy is dissipated to develop the damages including cracks and the plastic deformation.

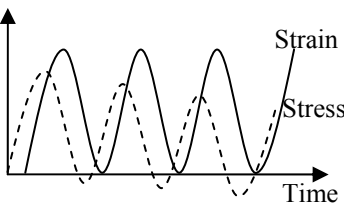
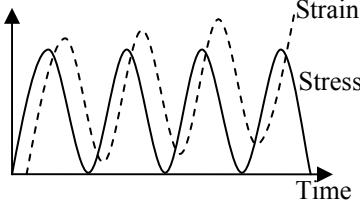
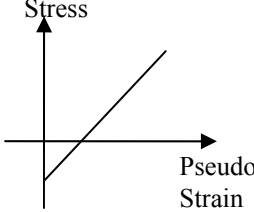
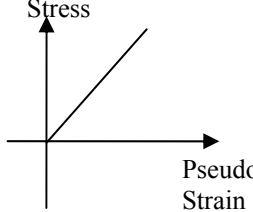
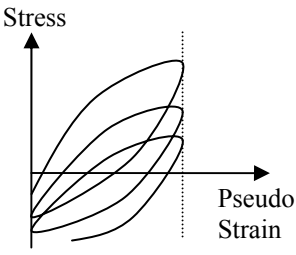
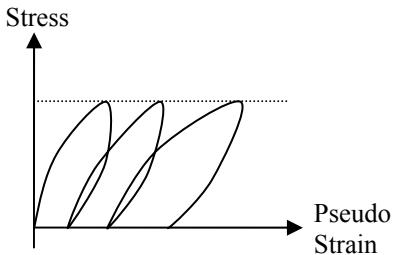
$$\varepsilon^R = \frac{\sigma_{LVE}}{E_R} = \frac{1}{E_R} \int_0^t E_u(t-\tau) \frac{d\varepsilon(\tau)}{d\tau} d\tau \quad (F2c.5)$$

$$DPSE = \int_0^{\frac{2\pi}{\omega}} \sigma(t) \frac{d\varepsilon^R(t)}{dt} dt \quad (F2c.6)$$

where ε^R = pseudo strain; σ_{LVE} = linear viscoelastic stress; E_R = reference modulus; $E_u(t)$ = undamaged relaxation modulus; $\varepsilon(t)$ = measured strain; t = current time; τ = previous time at which strain is measured; $\sigma(t)$ = measured stress; and ω = frequency in the repeated loading test.

The DPSE method are successfully employed to predict the crack initiation and propagation in the controlled-strain repeated loading test, during which three balance equations including the stress balance, DPSE balance and the Recoverable Pseudo Pseudo Strain Energy (RPSE) balance equation are established between the nominal configuration and the true configuration to solve for the true stress, the mean crack length and the damage density changing with load cycles. In the controlled-strain test, the pseudo strain energy mainly contributes to the formulation of the crack surfaces and the plastic deformation in the plastic zone near the tips of the cracks, both of which leads to the viscoelastic fracture in the asphalt mixtures. In contrast, in the controlled-stress test, the pseudo strain energy dissipates to develop not only the viscoelastic fracture but also the plastic deformation within the intact material far away from the crack tips. Thus the formulation of using the DPSE method in the controlled-stress test is significantly different from that in the controlled-strain test. Both formulations of the two testing modes are established based on the basic definitions in equations F2c.5 and F2c.6 and summarized in table F2c. 1.

Table F2c.1. DPSE analysis method in controlled-strain test and controlled-stress test.

Comparison	Strain-controlled Test	Stress-controlled Test
Input	$\varepsilon = \varepsilon_0 [1 - \cos(\omega t - \varphi)]$	$\sigma = \sigma_0 [1 - \cos(\omega t)]$
Output	$\sigma = \sigma_0 [1 - \cos(\omega t)] - \sigma_i(t)$	$\varepsilon = \varepsilon_0 [1 - \cos(\omega t - \varphi)] + \varepsilon_c(t)$
Stress, Strain vs. Time		
Pseudo Strain (undamaged)	$\varepsilon_u^R = \varepsilon_0 \left[\frac{E_u(t)}{ E^* _u} - \cos(\omega t) \right]$	$\varepsilon_u^R = \varepsilon_0 [1 - \cos(\omega t)]$
Stress vs. Pseudo strain (undamaged)		
Pseudo Strain (damaged)	$\varepsilon_d^R = \varepsilon_0 \left[\frac{E_u(t)}{ E^* _d} - \cos(\omega t - \varphi + \phi_{LVE}) \right]$	$\varepsilon_d^R = \sigma_0 \dot{D}_d \cdot t - \frac{\sigma_0}{ E^* _d} \cos(\omega t - \varphi + \phi_{LVE})$
Stress vs. Pseudo strain (damaged)		
DPSE	$DPSE = \pi \frac{\sigma_0^2}{ E^* _d} \sin(\varphi - \phi_{LVE})$	$DPSE = \sigma_0^2 \Delta D_d + \pi \frac{\sigma_0^2}{ E^* _d} \sin(\varphi - \phi_{LVE})$
True Stress	$\sigma_T = \sigma_0 \sqrt{\frac{ E^* _u \sin(\varphi - \phi_{LVE})}{ E^* _d \sin(\varphi_{NLVE} - \phi_{LVE})}}$	$\sigma_T = \sigma_0 \sqrt{\frac{\Delta D_d + \pi E^* _d^{-1} \sin(\varphi - \phi_{LVE})}{\Delta D_u + \pi E^* _u^{-1} \sin(\varphi_{NLVE} - \phi_{LVE})}}$

Significant Results

Progress has been made in this quarter to develop the master curve models for the magnitude and phase angle of the complex modulus and complex Poisson's ratio of the asphalt mixture. The

widely used CAM model is introduced to form the magnitude master curve of the complex modulus. An “inverse S” model that has an inverse form of the CAM model is proposed to construct the magnitude of the master curve of the complex Poisson’s ratio. For the phase angle master curve of both the complex modulus and complex Poisson’s ratio, a general model named the “ β -model” is developed to construct the asymmetric bell-shaped phase angle master curves.

The anisotropic test protocols including uniaxial compressive creep test, uniaxial tensile creep test and indirect tensile creep test are conducted on the asphalt mixture specimens that vary in the binder type, air void content and the aging period to validate the proposed master curve models. The dynamic modulus tests are conducted on the same specimens to validate the nondestructive anisotropic testing protocols for the undamaged asphalt mixtures.

The Dissipated Pseudo Strain Energy (DPSE) method is employed in analyzing the controlled-stress repeated loading test, in which the formulations of the pseudo strain and DPSE are established. The true stress is calculated based on the DPSE balance equation and it can be used to predict the crack growth and the plastic deformation accumulation in the controlled-stress mode.

Significant Problems, Issues and Potential Impact on Progress

Several assumptions are made in the data analysis by using the DPSE method for both controlled-strain mode and controlled-stress mode. For example, the drifting stress $\sigma_t(t)$ changes with time in the controlled-strain test, it is assumed to be constant within one loading cycle and only change with loading cycles. Therefore, the undamaged relaxation modulus $E_u(t)$ is unchanged within one loading cycle. In the controlled-stress test, the creep part of the strain $\varepsilon_c(t)$ is assumed to have a linear relationship with time in one loading cycle, that is, the slope of creep strain is assumed to be constant within one cycle and to decrease with loading cycles. All of the assumptions need to be validated by analyzing the test data of the asphalt mixture.

Work Planned Next Quarter

- More controlled-stress repeated loading tests will be conducted on asphalt mixture specimens to verify the assumptions made in the calculations of the pseudo strain and DPSE;
- The RPSE balance equation needs to be formulated to solve for the mean crack length and the damage density that changes with loading cycles;
- The DPSE for developing viscoelastic fracture (cracks) needs to be separated from the DPSE for developing the plasticity in the intact materials (permanent deformation) in the asphalt mixture under the controlled-stress loading mode.

Cited References

Bahia, H. U., D. I. Hason, M. Zeng, H. Zhai, M. A. HKhatri, and R. M. Anderson, 2001, "Characterization of Modified Asphalt Binders in Suprepave Mix Design, Report 459." National

Cooperative Highway Research Program (NCHRP), Transportation Research Board, National Research Council, Washington, D.C.

Luo, R., and R. L. Lytton, 2010, Characterization of the Tensile Viscoelastic Properties of an Undamaged Asphalt Mixture. *Journal of Transportation Engineering*, 136 (3): 173-180.

Marasteanu, M. O., and D. A. Anderson, 1999, Improved Model for Bitumen Rheological Characterization. Eurobitume Workshop on Performance Related Properties for Bituminous Binders, Luxembourg, paper no. 133.

Work Element F2d: Structural Characterization of Micromechanical Properties in Bitumen using Atomic Force Microscopy (TAMU)

Work Done This Quarter

Tomography is carried out as needed on specimens that are used in developments of aging, healing and unified models. The reader is referred to work element F1c-3.

Significant Results

None.

Significant Problems, Issues and Potential Impact on Progress

None.

Work Planned Next Quarter

Tomography will be carried out as needed for the models development.

Work Element F2e: Verification of the Relationship between DSR Binder Fatigue Tests and Mixture Fatigue Performance (UWM)

Work Done This Quarter

In the past quarter, the research team investigated the use of higher strain levels in the Linear Amplitude Sweep (LAS) test. A range of polymer-modified binders do not accumulate significant damage in the current testing protocol that includes 20% maximum strain. In the original test protocol, loading began with 100 cycles of sinusoidal loading at 0.1% strain to obtain an undamaged response. Next, each load step consisted of 100 cycles at a rate of increase of 1% applied strain up to a maximum of 20% strain. The modified LAS test procedure extends the applied strain to 30%. The new testing protocol was evaluated using eight LTPP asphalt binders. The shear stress response for these tests is shown in figure F2e.1. While some binders did not exhibit a significant decrease in stress response at 20% applied strain, all binders show substantial material degradation when additional strain loading levels are applied.

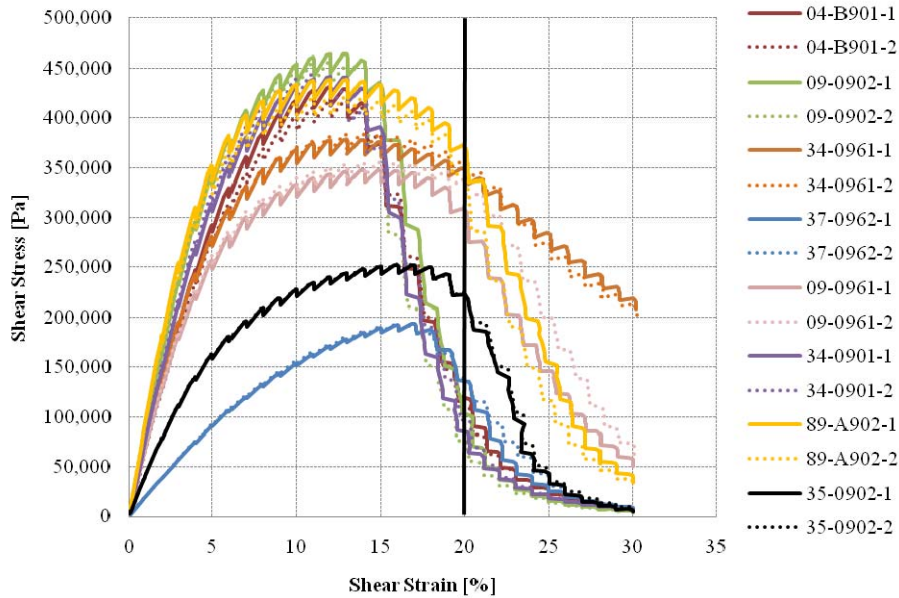


Figure F2e.1. Graph. LAS results using a maximum strain of 30%.

A comparison between results using maximum strain amplitudes of 20% and 30% was performed. This was conducted by comparing the fatigue law parameter A_{35} described in previous quarterly reports. In figure F2e.2, the A_{35} values computed using strains levels up to 30% were compared with the values computed using only the strains up to 20%. Note that the “35” in A_{35} implies that the fatigue life calculation is based on the damage intensity corresponding to a 35% reduction in $|G^*| \cdot \sin \delta$, and also that the computation of A_{35} using a maximum strain of 20% was accomplished using the test data excluding strains above 20%.

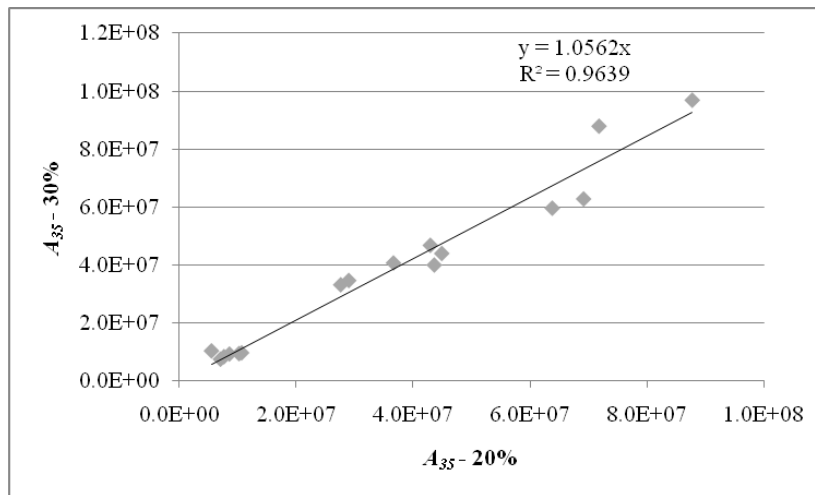


Figure F2e.2. Graph. Correlation between A_{35} derived using different maximum strains.

Figure F2e.2 indicates that there is no significant difference between A_{35} calculated from the different strain levels. This can be explained by the fact that fatigue life is based on a 35% reduction in $|G^*| \cdot \sin \delta$, which is reached by all binders by the end of the 20% strain step. Therefore, future work will focus on identifying if the 35% reduction in $|G^*| \cdot \sin \delta$ is acceptable failure criteria or if a higher decrease in material integrity should be used to define failure.

Significant Results

A sensitivity analysis of LAS model parameters was conducted using three binders with varying LAS performance. The shear stress response for the three binders used in this sensitivity analysis is shown in figure F2e.3. The sensitivity analysis was accomplished by changing the independent fatigue law parameters while holding the others constant. These parameters include C_0 , C_1 , C_2 , α and I_D . The effect of increasing each parameter by 1%, 2%, 5% and 10% in magnitude on N_f (fatigue life) predictions at 2.5% strain was evaluated and is shown in figure F2e.4.

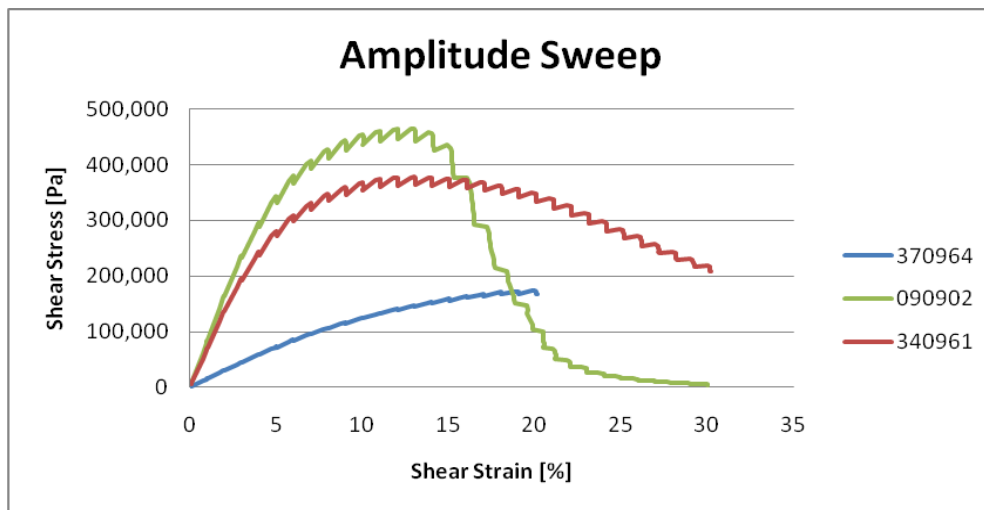


Figure F2e.3. Graph. LAS results of binders used in sensitivity analysis.

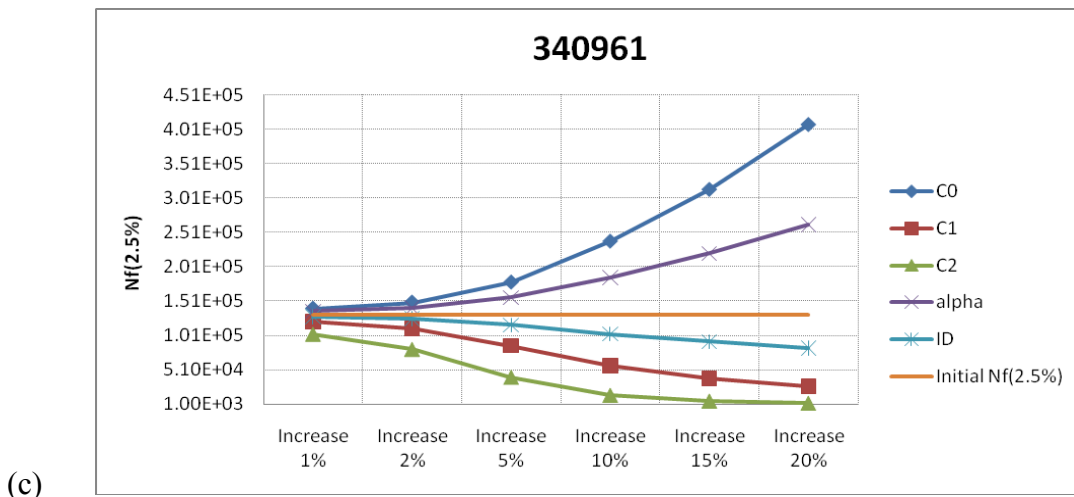
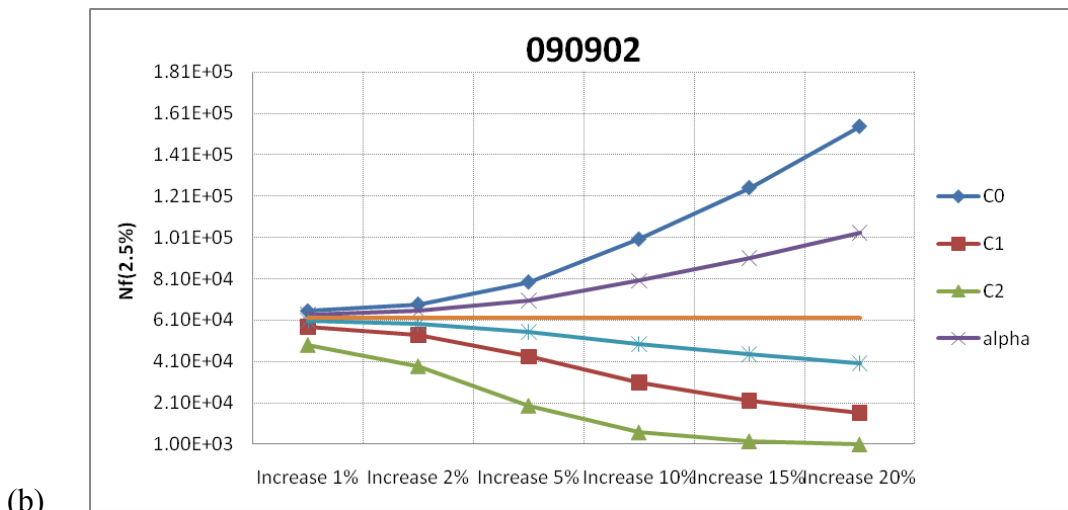
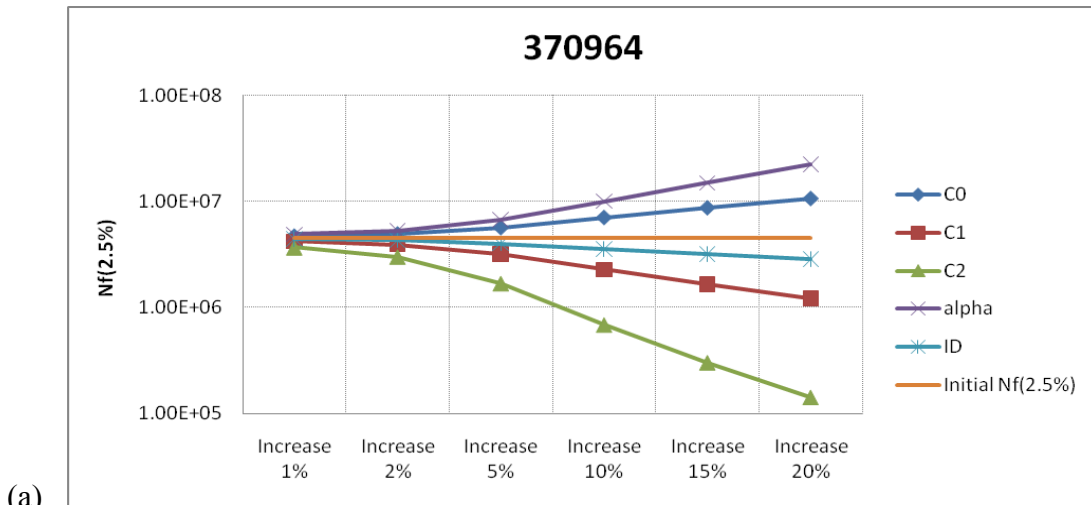


Figure F2e.4. Graphs. Sensitivity analysis results for binders: (a) 370964; (b) 090902; and (c) 340961.

As evident by the sensitivity analysis results, changes in all parameters lead to significant changes in N_f . The results presented in figure F2e.4 show that fatigue life calculated by the viscoelastic continuum damage (VECD) model is most sensitive to C_0 , α and C_2 . Note that C_0 and α are based on the undamaged linear viscoelastic response and that C_2 is the only damage parameter calculated from the slope of a log-log plot of $|G^*| \cdot \sin\delta$ versus damage.

Significant Problems, Issues and Potential Impact on Progress

None.

Work Planned Next Quarter

An investigation of using different damage levels on LAS results will be conducted. Also, binder and mixture fatigue testing data will be compared. The team will start fatigue testing of mixtures using the Indirect Tensile Test (IDT) setup. A typical mix design with locally available aggregates will be used for the mixture testing. The binders used for the asphalt mixtures will be tested using LAS and their performance will be compared to mixture fatigue results.

CATEGORY F3: MODELING

Work Element F3a: Asphalt Microstructural Model

Work Done This Quarter

Subtask F3a-1. ab initio Theories, Molecular Mechanics/Dynamics and Density Functional Theory Simulations of Asphalt Molecular Structure Interactions (URI)

Research results were presented at the Petersen Asphalt Research Conference and at the American Chemical Society (Petroleum Chemistry division). The latter helped to alert oil companies to this project.

Quantum mechanics calculations continued to test asphaltene molecular structures. Higher levels of theory required for accurate results have extended the computational time requirements.

Initial compositions have been identified for next-generation molecular models of AAA-1 (Canadian), AAK-1 (Venezuelan), and AAM-1 (W Texas) asphalts. Hansen solubility parameter estimates using molecular correlation software have been made for the compounds that make up the model asphalts. The accuracy of the solubility parameter results are being considered at the end of the quarter and the start of the next quarter. Achieving a sufficiently high heteroatom concentration while maintaining high enough molecular weight and low enough aromatic-to-aliphatic carbon ratio is proving to be quite challenging.

Analysis continued of DSR data to model distributions of relaxation times for assorted asphalts (including Venezuelan and Canadian sources) in the presence and absence of waxes. These

relaxation time results provide a target for interpreting later temperature-dependent dynamics calculations.

Subtask F3a-2. Develop algorithms and methods for directly linking molecular simulation outputs and phase field inputs (URI, NIST, VT)

During last quarter, the Virginia Tech team including its subcontractor NIST focused on Phase-Field Modeling of Asphalt Microstructure. For the initial phase of this part, literature review, concept refinement and development of specific plans were the main focus during the last quarter. The goal of this subtask is to develop a phase-field model to simulate the asphalt microstructure evolution. The concept of diffuse interfaces, the phase-field variables, the thermodynamic driving force for microstructure evolution, and the kinetic phase-field equations will be employed in follow-up research. Furthermore, techniques for parameter determination and numerical solution of the equations will be addressed.

The proposed phase-field modeling of the asphalt microstructure evolution focus on fulfilling the following major objectives; prove the proposed idea regarding its technological feasibility in asphalt, and to collect useful information for the modeling and characterization to be conducted. This sub-task is divided into 6 sub-subtasks organized in a logical way for scientific exploration. A brief description of each subtask is stated as following:

Sub-subtask F3a-2.1. Collect information on available models and numerical methods suitable for phase field modeling

The research team will conduct a comprehensive internet search, literature review, and personal communications to collect, screen, and recommend phase field models, potentials, and parameters. Information relevant to the application will also be collected for potential use in order to refine the concept of phase field modeling.

Sub-subtask F3a-2.2. Phase-field parameter determination

For all mesoscale modeling techniques, the phase-field equations contain a large number of parameters that need be defined in order to introduce the material specific properties for asphalt. The parameters in the homogeneous free energy density determine the equilibrium composition of the bulk domains and the gradient energy coefficients. The double-well (Takezawa et al. 2010) coefficient is related to the interfacial energy and width. The kinetic parameter in the Cahn-Hilliard equation (Bo et al. 2010) is related to diffusion properties and the kinetic parameter in the Ginzburg-Landau equation (Yang 2010) describes mobility of the interfaces. For solid-state phase transformations, the micro-elasticity theory requires also the elastic modulus of all coexisting phases.

The parameters may also show directional, compositional, and temperature dependence. In particular, the orientation dependence of the properties is important for the morphological evolution. Due to the difficulty in determining the large number of parameters experimentally, obtaining parameters for phase field models is not straightforward. To reduce the dependence on experimental input, the phase-field technique was used to be combined with the Computer

Coupling of Phase Diagrams and Thermo-chemistry (CALPHAD) (Kaufman and Bernstein 1970, Lukas et al. 2007) approach for multi-component alloys. In this study, CALPHAD method will be used as an effective way to determine the asphalt binder phase field parameters.

Sub-subtask F3a-2.3. Numerical solution of the phase-field equations

The numerical implementation of phase-field equations is relatively simple and straightforward because there is no need to track the interfaces. However, the resolution of the numerical technique needs to be refined to account for the steep transitions of the phase-field variables at interfaces. Simulations for real system sizes and time scales may not be feasible in using the regular numerical techniques due to the excessive computational cost. The finite element analysis that utilizes an adaptive mesh is usually applied for simulating crystal growth. The finer mesh is implemented at the solid-liquid interface while coarser mesh is taken within the bulk domains. For asphalt phase transformations, in order to increase the system size, the width of the diffuse interface need be taken artificially large. Therefore, it is important to develop phase-field formulations that will change the interface width without affecting the interfacial energy and mobility. In this study, we will make progress in controlling the interfacial profiles of the phase-field variables and suppressing non-equilibrium effects. In order to accommodate the high computational demand, high performance algorithms and computing technology will be employed.

Sub-subtask F3a-2.4. Application of diffuse interface modeling to asphalt microstructure evolution

There are many phase-field models, but most of them are based on a diffuse-interface description. The interfaces between domains are identified by a continuous variation of the properties within a narrow region. The diffuse-interface approach allows us to study the evolution of arbitrary complex grain morphologies without any assumption of their shape or mutual distribution. It is also straightforward to account for different thermodynamic driving forces for microstructure evolution, such as bulk and interfacial energy, and elastic energy. The effect of different transport processes, such as mass diffusion, heat conduction, and asphalt aging process, are also addressed by various thermodynamics driving forces. As a result of its versatile capability, diffuse-interface modeling will be employed to simulate inter-phases diffusion during the asphalt microstructure evolution.

Sub-subtask F3a-2.5. Develop phase field models for characterizing asphalt emulsion and phase separation processes

Phase-field models will also be used to simulate the stability and time-dependent mesoscale structure of colloidal asphalt binder emulsions (Sabbagh and Lesser 1998, Martinez-Boza *et al.* 2001), which is a colloidal structure system. By formulating the bulk and gradient energy in terms of the system's constitutive variables (e.g. order parameters), we can obtain predictions of phase separation and phase morphology in emulsions as a function of temperature and composition. This study will start with deriving the general form for the free energy density. This form includes the number and type of relevant order parameters that are required to provide a

detailed description of the structural evolution of asphalt emulsions. Then, computational algorithms for phase-field models will be employed to solve the evolution equations.

Sub-subtask F3a-2.6. Phase-field modeling for fatigue cracking and self-healing processes

Micro fatigue cracking and self-healing are mesoscale phenomena of the macroscale fatigue effects. Available experimental evidence (Soltani and Anderson 2005, Qiu et al. 2009) indicates the beneficial effects of rest periods in restoring the stiffness and strength characteristics of asphalt subject to fatigue loading. In this study, the phase-field model will be employed to simulate fatigue cracking and self-healing processes within asphalt. Experimental and numerical approaches can be carried out to investigate the mesoscale mechanisms leading to the initiation, propagation, and healing of damage in asphalt concrete pavements. Then, by proposing a decomposition of the deformation mode, one useful equation will be obtained for the viscoplastic responses of asphalt binder. Consequently, the fatigue and self-healing properties of the bituminous material can be simulated by this phase-field model.

Technically, the healing of the asphalt binder will be simulated by a phase field model, utilizing a modified version of the Cahn Hilliard (Matsumoto and Takada 2010) and Flory-Huggins equations (Kim *et al.* 2010). The model will be implemented in the finite element code ABAQUS. Results from ABAQUS analysis will be integrated in the simulation of asphalt concrete cracking and the self-healing capability under the appropriate environmental and mechanical conditions.

Subtask F3a-3. Obtain temperature-dependent dynamics results for model asphalts that represent asphalts of different crude oil sources (URI)

Nothing to report.

Subtask F3a-4. Simulate changes in asphalt dynamics after inducing representations of chemical and/or physical changes to a model asphalt (URI)

Nothing to report.

Subtask F3a-5. Molecular mechanics simulations of asphalt-aggregate interfaces (VT)

Nothing to report.

Subtask F3a-6. Modeling of fatigue behavior at atomic scale (VT, NIST)

Based on the developments and refining additional to the NSF project by VT and NIST, we will perform nano-scale simulations to understand the mechanism of fatigue and healing. Although tremendous research efforts have been devoted to the investigation of fatigue behavior of asphalt concrete the understanding of fatigue at microscopic and nano scale is very much limited. Fatigue life of a specimen is currently determined at 50% reduction of the modulus. A scientific basis is needed for better understanding the fatigue and healing mechanism and interpretation of the currently experimental data.

Subtask F3a-7. Modeling of moisture damage (VT)

Moisture damage has several mechanisms including excess pore water pressure, and chemical-mechanical coupling. When water penetrates into the micro pores at the interfaces between binder and aggregates, the excess pore water pressure mechanism and the chemical-mechanical coupling mechanism may have to be considered together. Nano mechanics simulations will present a basis for understanding the mechanisms of moisture damage and the coupled phenomena of moisture damage and fatigue.

Subtask F3a-8. ab initio Calculations of Asphalt Molecular Structures and Correlation to Experimental Physico-Chemical Properties of SHRP Asphalts (WRI-TU Delft)

Nothing to report.

Significant Problems, Issues and Potential Impact on Progress

Normally, quantitative validation of the different phase-field models is based on simulations for pure Ni alloys, since it is a simple system and its physical properties are known. In the case of solid-state phase transformations, especially those involving elastic strains or sharp-interface models are not well established. Materials showing a non-ordered transformation (e.g. asphalt binder) are complicated and difficult to characterize. Therefore, quantitative validation in sub-subtask F3a-2.3 is a challenge for our phase field model.

We will make efforts to demonstrate the mentioned research in detail for the case of asphalt emulsion, fatigue cracking, and microstructure evaluation. We will also contribute to the relationship between physical variables and numerical parameters, then determine how to choose the model parameters, and compare the computational efficiency of different phase-field models depending on the choice of the thermodynamic potential. Finally, we will incorporate values for the thermo-dynamic properties (e.g. enthalpy of mixing, interface free energy, and temperature dependence) that determine the exact form of the free energy function for the asphalt binder system under consideration. By doing so, the phase field model could be validated.

Work Planned Next Quarter

Composition work will be finalized for new model asphalts that reflect speciation of asphalts from Venezuelan and Canadian crude oil sources. Characterization data for new asphaltenes, resins, aromatics, and saturates will be near to experimental values to the greatest extent possible. Monte Carlo and molecular dynamics simulations will be used to relax molecule arrangements toward equilibrium configurations.

Data analysis and manuscripts will be completed on a spontaneous wax formation event in a molecular simulation and on unique attributes of asphaltene chemistry that have been recognized through quantum mechanics calculations and molecular simulations.

The experimental characterization of the asphalt phase separation, emulsion, and self-healing will be performed by multiscale CT (Computerized Tomography), Atomic Force Microscopy, and Nano-Indentation experiments; a) the use of multiscale CT technology to characterize the asphalt microstructure from nanoscale to millimeter scale; b) the use of Atomic Force Microscopy and Nano-Indentation experiments on meso-scale samples to characterize the mechanical properties of materials at nano and micro scales will be performed so that modeling and simulation can be integrated.

References

Bo, L. J., K. H. Shi, and Y. J. Wang, 2010, Support theorem for a stochastic cahn-hilliard equation. *Electronic Journal of Probability*, 15: 484-525.

Kaufman, L., and H. Bernstein, 1970, *Computer calculation of phase diagrams with special reference to refractory metals*, Academic Press, New York.

Kim, S. D., S. Chakravarti, J. Tian, and P. Bell, 2010, The phase behavior and the flory-huggins interaction parameter of blends containing amorphous poly(resorcinol phthalate-block-carbonate), poly(bisphenol-a carbonate) and poly(ethylene terephthalate). *Polymer*, 51 (10): 2199-2206.

Lukas, H. L., S. G. Fries, and B. Sundman, 2007, *Computational thermodynamics : The calphad method*, Cambridge University Press, Cambridge.

Martinez-Boza, F., P. Partal, F. J. Navarro, and C. Gallegos, 2001, Rheology and microstructure of asphalt binders. *Rheologica Acta*, 40 (2): 135-141.

Matsumoto, J., and N. Takada, 2010, Numerical simulations for gas-liquid two-phase flow. *Journal of Japanese Society of Tribologists*, 55 (6): 387-393.

Qiu, J., M. F. C. Van De Ven, S. Wu, J. Yu, and A. A. A. Molenaar, 2009, Investigating the self healing capability of bituminous binders. *Road Materials and Pavement Design*, 10: 81-94.

Sabbagh, A. B. and A. J. Lesser, 1998, Effect of particle morphology on the emulsion stability and mechanical performance of polyolefin modified asphalts. *Polymer Engineering and Science*, 38 (5): 707-715.

Soltani, A., and D. A. Anderson, 2005, New test protocol to measure fatigue damage in asphalt mixtures. *Road Materials and Pavement Design*, 6 (4): 485-514.

Takezawa, A., S. Nishiwaki, and M. Kitamura, 2010, Shape and topology optimization based on the phase field method and sensitivity analysis. *Journal of Computational Physics*, 229 (7): 2697-2718.

Yang, D. S., 2010, On the generalized 2-d stochastic ginzburg-landau equation. *Acta Mathematica Sinica-English Series*, 26 (8): 1601-1612.

Work Element F3b: Micromechanics Model (TAMU)

Subtask F3b-1: Model Development

Cohesive Zone Micromechanical Model (UNL)

Work Done This Quarter

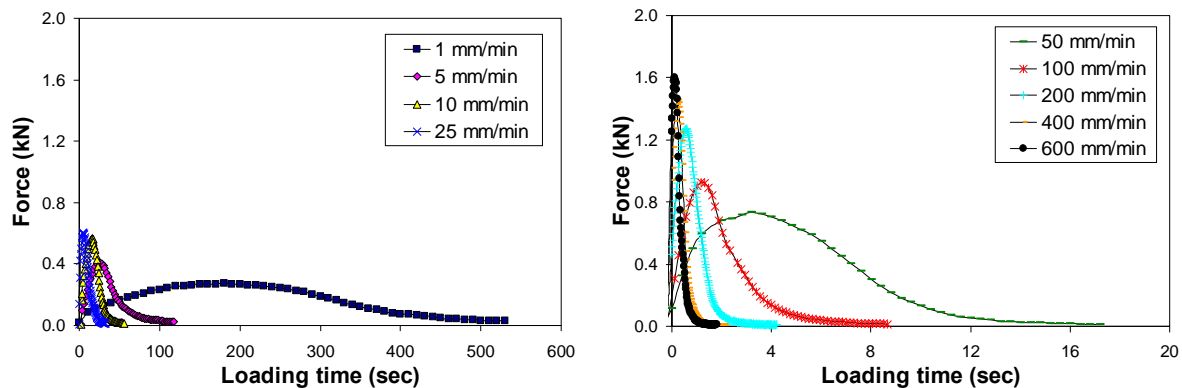
During this quarter we have mainly progressed towards two activities:

- We performed semi-circular bend (SCB) fracture tests of fine aggregate matrix (FAM) specimens within a wide range of loading rates (i.e., 1, 5, 10, 25, 50, 100, 200, 400, and 600 mm/min) and their cohesive zone modeling to identify the rate-dependent fracture characteristics of FAM phase in asphalt concrete mixtures.
- We have also progressed on the extension of the rate-independent ABAQUS User Element (UEL) cohesive zone code to incorporate the rate-dependent characteristics of the cohesive zone fracture parameters.

Work progress and significance of each activity can be summarized as follows:

SCB Fracture Tests and Modeling of FAM Mixtures

As presented in the previous report, several loading displacement rates were applied to the top center line of SCB specimens, following the testing protocol developed to obtain cohesive zone fracture parameters. During this quarter, we performed fracture tests with SCB specimens to investigate fracture characteristics of the FAM mixture within a wide range of loading rates. Nine different rates (1, 5, 10, 25, 50, 100, 200, 400, and 600 mm/min) were attempted in this quarter. Figure F3b-1.1 presents the SCB test results by plotting the average reaction forces at the line of load application as the loading time increased.

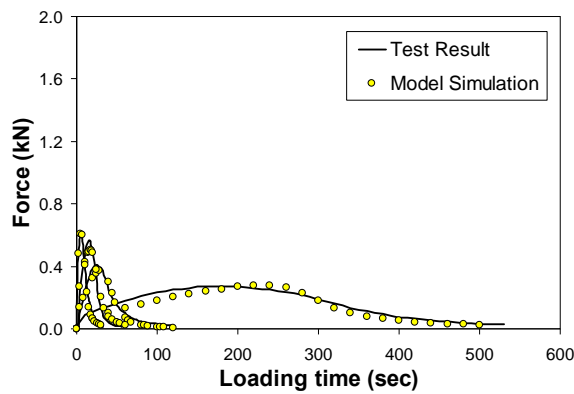


(a) test results (at 1, 5, 10, and 25 mm/min.) (b) test results (at 50, 100, 200, 400, and 600 mm/min.)

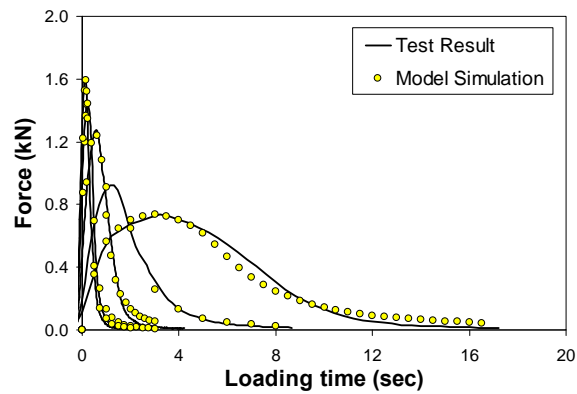
Figure F3b-1.1. SCB fracture test results at the nine different loading rates.

Slower loading speeds produced more compliant responses than faster cases. The rate-dependent mechanical response is related to several effects, such as the viscoelasticity of the bulk FAM and the fracture characteristics throughout the fracture process zone (or cohesive zone). As attempted in the previous quarter, test results were incorporated with numerical simulations that account for both the material viscoelasticity and the cohesive zone fracture process. This is done to separately identify the sources of rate dependency so as to better determine if the rate-dependent mechanical response is related to the fracture process. Cohesive zone fracture parameters determined through this experimental-numerical integrated approach can provide the rate-related fracture process, if it exists.

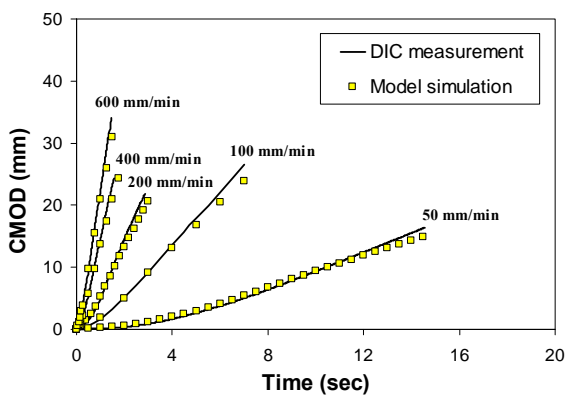
As described in the previous quarterly report, cohesive zone fracture parameters were then determined for each loading rate via an inverse approach by matching simulation results with test results. A strong agreement between experimental test results and numerical simulations of reaction force, crack mouth opening displacement (CMOD) and crack tip opening displacement (CTOD) is observed as demonstrated in figure F3b-1.2. The figure indicates that the model parameters were accurately obtained, with no major discrepancies between experimental and numerical simulation results.



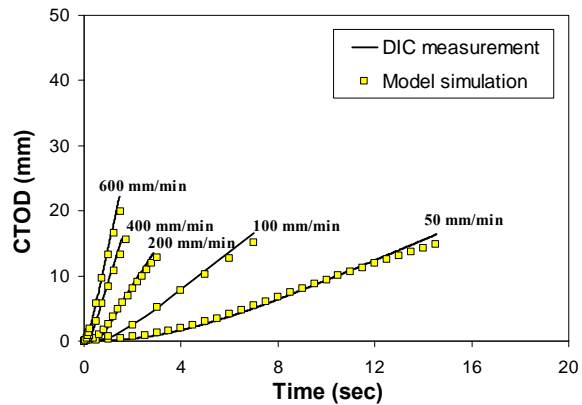
(a) force vs. loading time



(b) force vs. loading time



(c) CMOD vs. loading time



(d) CTOD vs. loading time

Figure F3b-1.2. Test results vs. numerical simulations.

The two fracture parameters (i.e., cohesive zone strength and cohesive zone fracture energy) identified at the local fracture process zone are plotted in figure F3b-1.3 as the applied loading rates varied. It appears that cohesive strength is fairly rate-independent until the loading rates are less than 50 mm/min, while the cohesive zone fracture energy generally increases as the loading rates become higher. The trends presented in figure F3b-1.3 infer that the rate-related nature of the fracture characteristics needs to be considered accordingly when modeling the mechanical performance of typical asphalt concrete mixtures and pavements in which a wide range of strain rates is usually associated due to the mixture's significant heterogeneity and the various loading conditions.

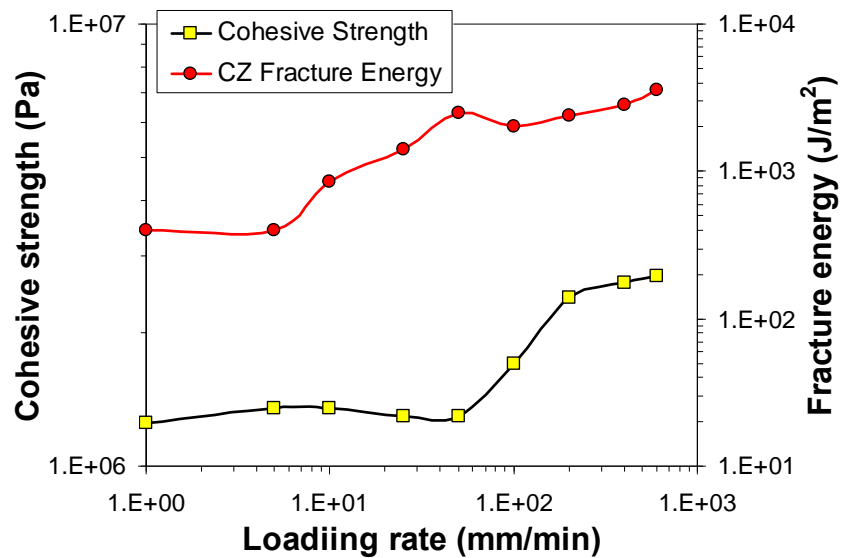


Figure F3b-1.3. Cohesive zone fracture parameters at different loading rates.

Figure F3b-1.4 compares the fracture energy characterized at the local fracture process zone (FPZ) based on the cohesive zone model with the fracture energy traditionally characterized by calculating an area under the load-CMOD (or load-CTOD) curve that is normalized by the area of the fractured surface, i.e., initial ligament length multiplied by the specimen thickness. As presented in the figure, the fracture energies obtained from the area under the load-CMOD (or load-CTOD) curve were larger than the fracture energy obtained at the local FPZ with the same trend. Furthermore, it is clear that fracture energy values obtained from the load-CTOD curve were closer to the values characterized at the local FPZ than those obtained from the load-CMOD curve. This observation seems reasonable since the energy obtained from CMOD measurements may overestimate the true fracture toughness, as it includes other sources of energy dissipation such as material viscoelasticity, which is not related to the fracture process.

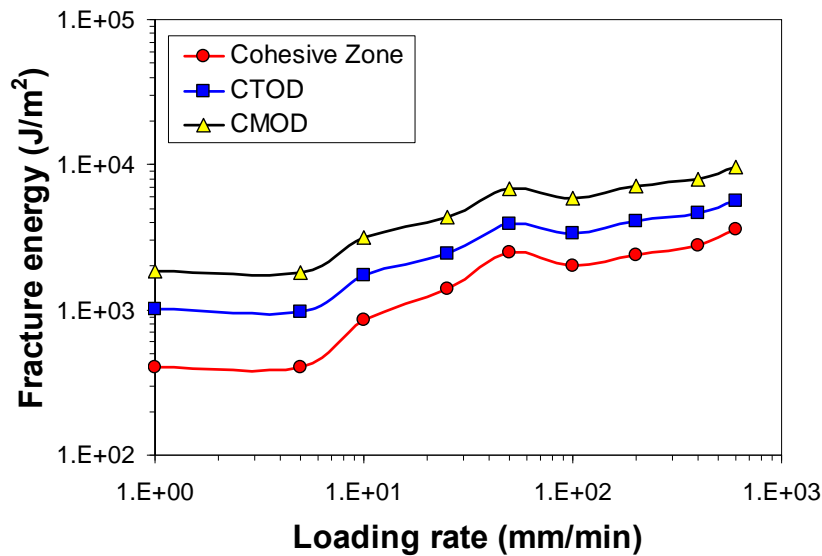
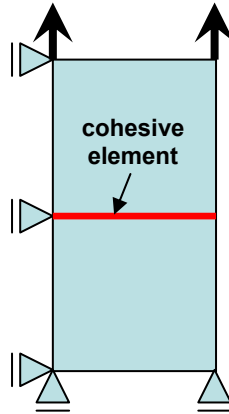


Figure F3b-1.4. Fracture energy characterized based on local FPZ, CTOD, and CMOD.

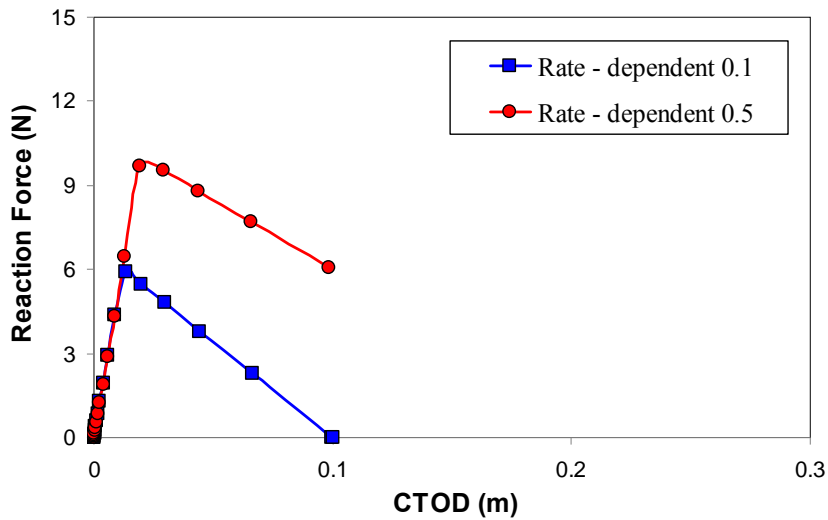
Implementation of the Rate-Dependent Cohesive Zone Fracture into ABAQUS UEL

Another key element of our modeling efforts is the development and implementation of a rate-dependent cohesive zone fracture model. During this quarter, we extended the rate-independent intrinsic bilinear cohesive zone model previously implemented by other researchers to a rate-dependent cohesive zone model in the form of an ABAQUS UEL subroutine.

To demonstrate the ability of the UEL code to model rate-dependent fracture behavior, model simulations of a simple uniaxial bar containing a cohesive element between two bulk elastic elements were conducted by applying two different tensile load rates (0.1 and 0.5 m/sec), as illustrated in figure F3b-1.5(a). The UEL code assigns different cohesive zone fracture parameters according to the rate of relative displacements between the top and bottom faces of the cohesive zone element. Figure F3b-1.5(b) shows simulation results which clearly demonstrate the rate-dependent mechanical behavior due to different fracture properties involved.



(a) simple uniaxial bar with a cohesive zone element



(b) simulation results with rate-dependent fracture

Figure F3b-1.5. Simulation of a simple uniaxial bar using the rate-dependent UEL.

Cohesive Zone Micromechanical Model (TAMU)

During this quarter we have mainly progressed towards two activities:

- We have worked on the implementation of a cohesive zone model that is capable of accounting for the rate-dependent fracture process in asphaltic materials. More specifically, we have implemented two different UEL codes (customized *ABAQUS* USER ELEMENT subroutines) available in the open literature into the *ABAQUS* main frame and have tested one UEL (four-node bilinear cohesive zone model) by comparing model simulation results obtained from the newly implemented UEL with simulation results from the customary bilinear model that exists in the original *ABAQUS*. The idea is to extend the UEL subroutine, after successful implementation, for predicting the rate-

dependent fracture characteristics, since none of cohesive zone models featured in the current *ABAQUS* can be applied to the rate-dependent fracture problems.

- Another primary task we focused on during this quarter was the development of a proper mixing-compaction-production practice of the fine aggregate matrix (FAM) phase in asphalt concrete mixtures. This effort is to provide more accurate mechanical properties (viscoelastic properties and cohesive zone properties of matrix phase) of the FAM phase to accomplish the finite element-based micromechanics modeling. Some significant findings obtained during this quarter are presented in this report.

The research outcomes were presented in two recent conferences: the 2010 TRB annual meeting and the ASCE GeoFlorida conference and at the Advanced Models ETG meeting held in Irvine CA. In addition, one paper was written and submitted for the ASCE Engineering Mechanics Special Publication (EMSP), and two journal papers under review process have finally been accepted for publication. Work progress and significance of each activity can be summarized as follows.

- UEL implementation into *ABAQUS* main frame

During this quarter we started working on the development of a rate-dependent cohesive zone model. This is an essential part of our work as it will allow us to simulate fracture in asphalt mixtures in a more realistic way by accounting for the rate-dependent fracture characteristics. Towards this challenging task, the first step we took was to implement rate-independent cohesive zone models in a form of UEL (USER ELEMENT) subroutine into the *ABAQUS* main frame. The cohesive zone models implemented are the ones that have already been featured in the current version of *ABAQUS*; therefore, simulation results between two can be compared to check if the UEL implementation is correctly accomplished. Then, as mentioned earlier, the newly implemented UEL will be extended to address the rate-dependent fracture characteristics.

Among many available models, we have implemented two UEL codes (i.e., an exponential model provided by Gao and Bower (2004) and a bilinear model provided by Song (2006)) into the main frame of *ABAQUS*. To check if the implementation is made correctly, a uniaxial bar in tension (shown in figure F3b-1.6) was simulated. The bar is elastic with a four-node cohesive zone element in the middle of the bar. Simulation results were compared, and as clearly seen in figure F3b-1.6, both results were identical, which indicates that the new UEL model has been successfully implemented into *ABAQUS*. The UEL is now being expanded to allow the prediction of rate-dependent fracture process.

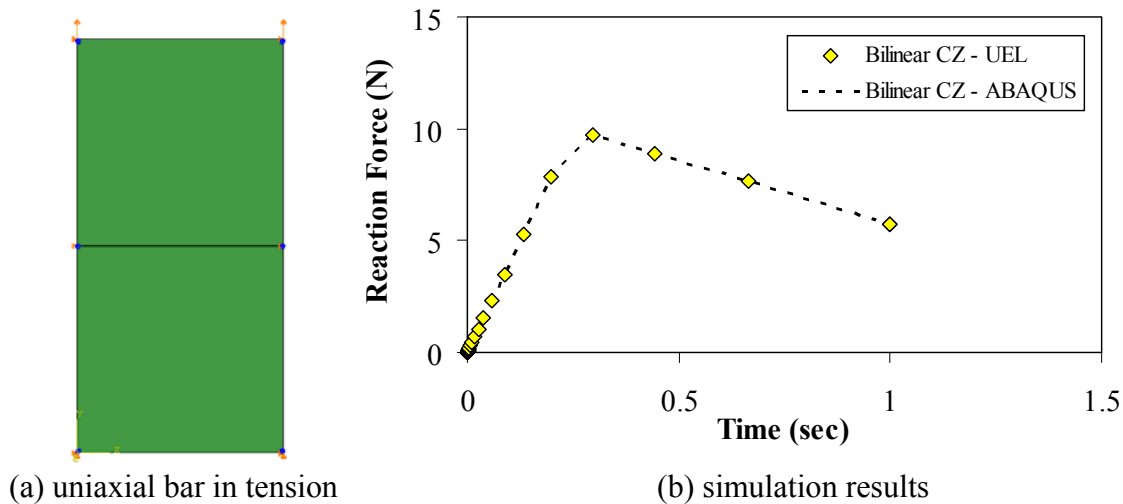


Figure F3b-1.6.. A uniaxial bar problem to check the accuracy of UEL implementation.

- Development of a protocol for mixing, compaction, and production of FAM phase to provide mechanical properties for the micromechanical modeling

To accomplish our computational micromechanics modeling based on the finite element method, individual phases in asphalt mixtures need to be characterized for their mechanical properties as model inputs. The more accurate characterization of phase properties will guarantee the more accurate predictions of mixture behavior. FAM is considered one of primary phases constituting the asphalt concrete mixture as shown in figure F3b-1.7; however, the characterization of mechanical properties of the FAM phase has been performed somewhat carelessly because of many unknowns such as the volumetric characteristics of the FAM. For example, accurate estimation of binder content, air voids, aggregate particle sizes and distributions in the FAM phase is not easy to make; probably it is impossible. Nevertheless, in order to improve model accuracy based on the more accurate characterization of constituent properties (model inputs), we have attempted to develop an approach that is more articulate and scientific than pre-existing approaches (Kim et al. 2003, 2006; Song et al. 2005; Masad et al. 2006; Castelo et al. 2008) in the process of mixing-compaction-production of the FAM specimen.

Unlike conventional asphalt concrete volumetric systems, we assumed that the asphalt concrete mixtures consist of two primary material phases – the elastic phase of aggregates and the viscoelastic phase of FAM, which is composed of asphalt binder, fine aggregates passing sieve No. 16 (mesh size of 1.19 mm), and entrained air voids. The maximum fine aggregate size of 1.19 mm in the FAM mixture was determined based on two-dimensional digital image analyses of cross sections obtained from various compacted asphalt concrete samples. The digital images could not properly capture aggregates approximately less than 1.0 mm, which is close to the mesh size of sieve No. 16. The mix design of the FAM phase has been postulated on the basis of the sharing of binder by the coarse and fine aggregates in the asphalt concrete mixture. The mix design considered binder content that is absorbed into aggregates and that covers aggregates with a fixed binder film thickness. Algebraically, the required binder content to produce the FAM

specimen was proposed as the one remaining after excluding binder absorbed in the coarse aggregates and the thin film (12 micron for the current approach) of binder covering coarse aggregates from the total binder in the bulk asphalt concrete mixtures.



Figure F3b-1.7. Typical microstructure of asphalt concrete mixtures.

The new protocol also incorporated the extraction of small DMA specimens out of Superpave gyratory bulk samples that were compacted with different amounts of FAM mixtures to represent different levels of air voids. Each DMA specimen produced was tested to characterize linear viscoelastic properties (in a form of dynamic modulus master curve) at each different level of air voids. The aggregate phase was considered an elastic material of which property (Young's modulus) was obtained by performing the nano-indentation tests using a Berkovich diamond indenter. Test results (DMA tests for the FAM and nano-indentation tests for the coarse aggregates) were then incorporated with the micromechanical finite element simulations to predict linear viscoelastic dynamic moduli of the corresponding bulk asphalt concrete mixture. Simulated dynamic moduli from the micromechanical model were finally compared to dynamic moduli obtained from laboratory tests, so that the appropriate level of FAM density (i.e., the amount of air voids) can be determined. Figure F3b-1.8 briefly illustrates the process employed for this study.

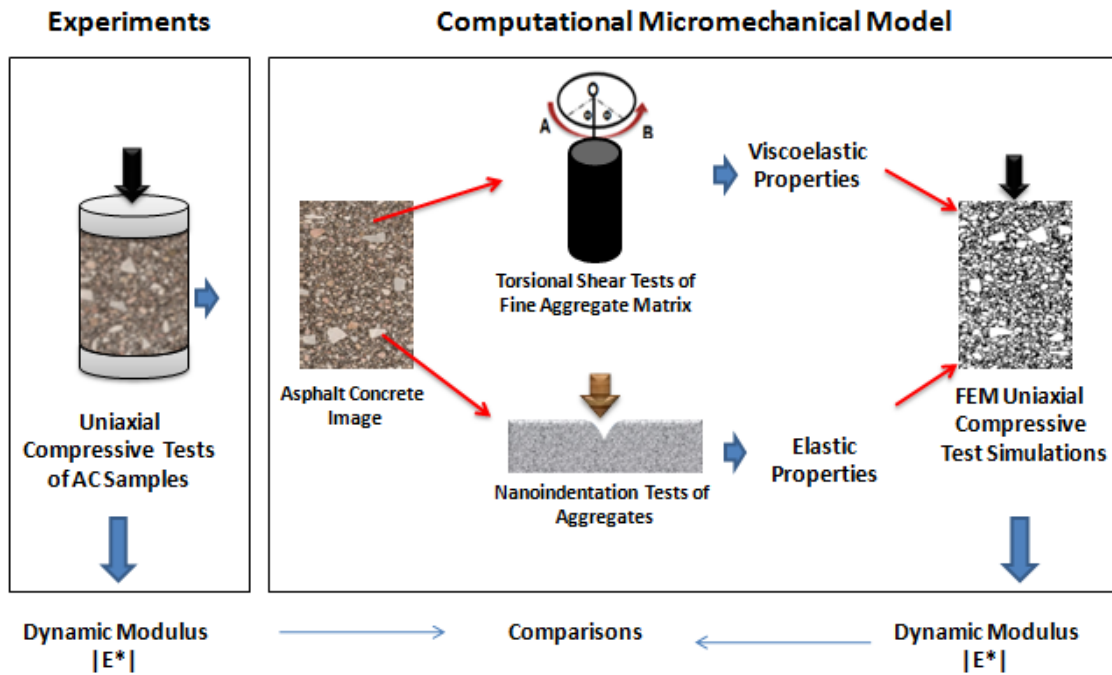


Figure F3b-1.8. Research method employed for the characterization of FAM phase.

DMA test results for the viscoelastic properties of the FAM phase and the nano-indentation test results for the elastic property of coarse aggregates are presented in figure F3b-1.9 and figure F3b-1.10, respectively. Five different air voids (from 0.00 % to 1.75 %) were attempted for the production of FAM specimens. Clearly, as shown in figure F3b-1.9, FAM mixtures with lower air voids presented stiffer behavior than the mixtures with higher air voids. Twenty nano-indentation measurements were made for the elastic property (Young's modulus) of coarse aggregates and it resulted in a mean value of 60.9 GPa, as presented in figure F3b-1.10.

With the treated digital image of asphalt concrete mixture microstructure and the properties of each phase, computational micromechanics modeling was then conducted. Figure F3b-1.11 shows the digital image of the mixture used to construct finite element meshes. For this study, a two-dimensional approximation of the three-dimensional mixtures was adopted because of the significant geometric complexity. Furthermore, as mentioned earlier, air voids were not explicitly considered in the microstructure, but were considered an entrained form in the matrix phase. Figure F3b-1.11 also presents boundary conditions applied to the sample. Vertical displacements (U_y) were constrained at the bottom face of the sample, and a compressive haversine traction (T_y) was evenly applied to the top nodes. To construct a dynamic modulus master curve, a wide spectrum of loading frequencies was simulated (10^{-4} to 10^3 Hz).

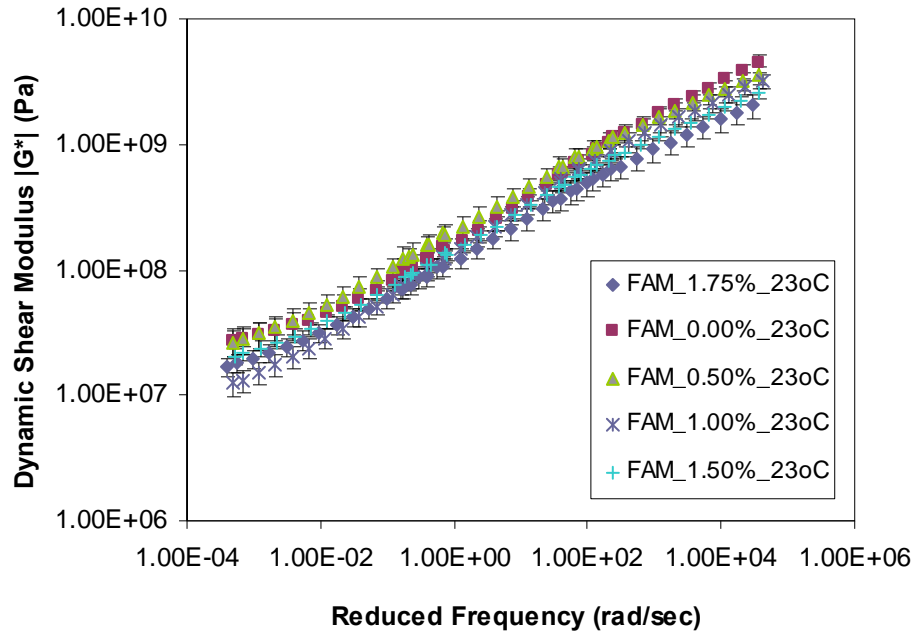


Figure F3b-1.9. DMA test results of FAM mixtures with different air voids.

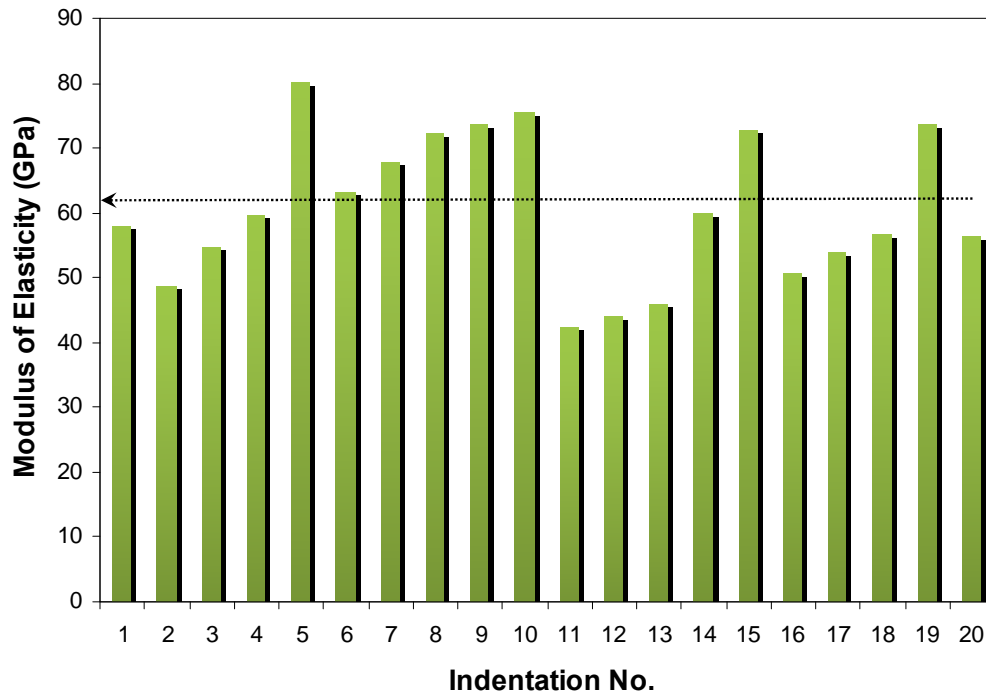


Figure F3b-1.10. Nano-indentation test results (modulus of elasticity) of coarse aggregates.

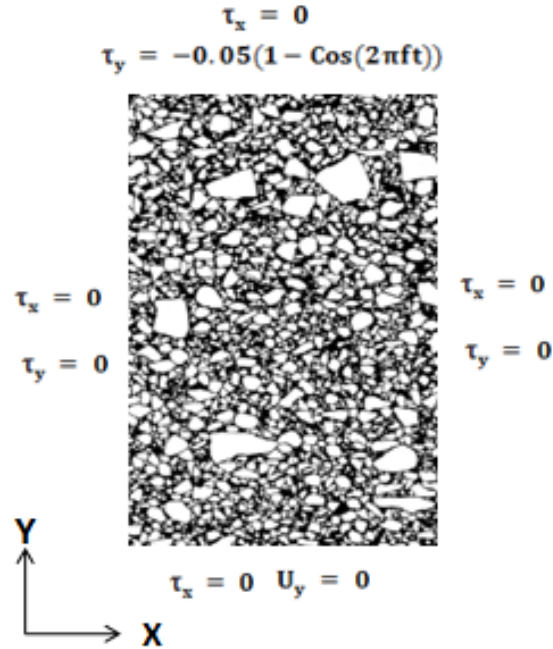


Figure F3b-1.11. Finite element mesh of the digital image treated and boundary conditions imposed.

As presented in figure F3b-1.8, dynamic modulus tests were also performed on the cylindrical asphalt concrete specimens in the uniaxial cyclic compressive testing mode. The loading levels were carefully adjusted until the strain levels were within the range of 0.00005-0.000075. Three linear variable differential transformers (LVDTs) were mounted onto the surface of the specimen at 120° radial intervals with a 100-mm gauge length. Vertical deformations averaged from the three LVDTs were used to calculate the dynamic modulus, defined simply as the ratio of the sinusoidal stress amplitude to the sinusoidal strain amplitude. Three temperatures (4, 20, and 40°C) with varying frequencies were used. The frequency-temperature superposition concept was then applied in order to develop the master curve at 23°C. Three replicates were tested and test results are presented in figure F3b-1.12. As error bars embedded in the master curve show, test results between replicates were fairly consistent at high loading frequencies, whereas greater variations of the moduli were observed at lower loading frequencies (high testing temperatures).

Figure F3b-1.13 shows dynamic modulus comparisons between model simulations from each different FAM cases and the experimental results. In general, all predictions at the different levels of air voids were in fair agreement with the test results. Comparison between experimental results and the model simulations presented a relatively higher deviation at lower loading frequencies but better agreement when the loading frequency was larger.

Figure F3b-1.14 plots the upper and lower limits of experimental tests along with the two extreme cases of FEM simulations that are placed within the limits. As shown, the dynamic modulus master curves predicted by FEM simulations were within the range of experimental variations for the samples with those FAM phase which had 1.00 to 1.75 % of air voids. The

master curves of asphalt mixtures containing the FAM of 0.00 % and 0.50% air voids were not within the upper-lower limits. This implies that the FAM phase must contain air voids to certain extent for representing mixture properties more accurately.

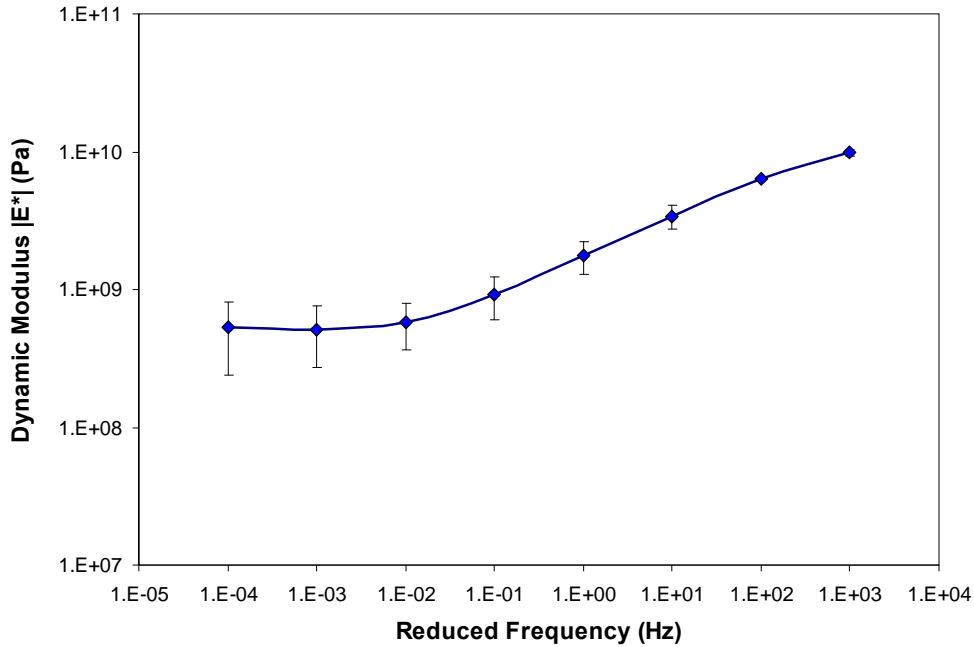


Figure F3b-1.12. Dynamic modulus test results of asphalt concrete cylinders (three replicates).

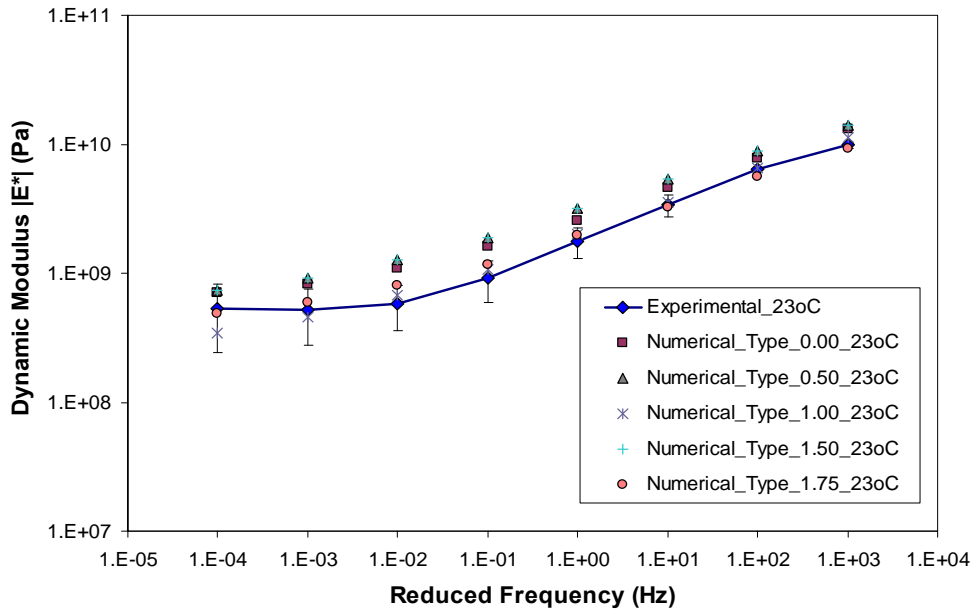


Figure F3b-1.13. Dynamic modulus comparisons between model simulations and test results.

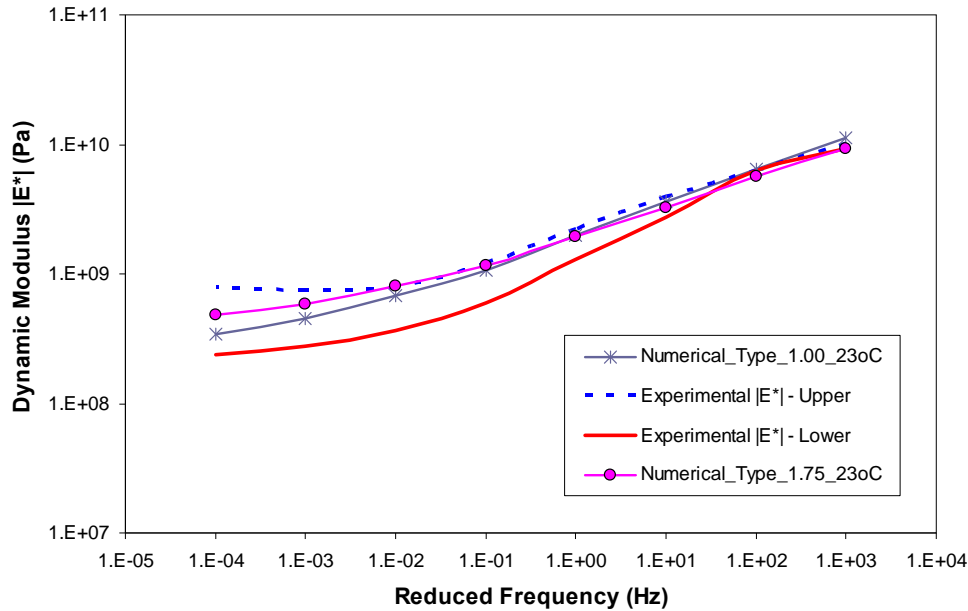


Figure F3b-1.14. Dynamic modulus comparisons: upper-lower limits of experimental data vs. simulation placed within the upper-lower limits.

Lattice Micromechanical Model (NCSU)

The efforts in the previous quarter focused on including the effect of air voids in the lattice model. Among the many possible ways to include the effects of air voids, the research team decided to incorporate air voids as a separate phase in the model. That is, the geometry of each air void that is present in each scale is generated and included in the specimen as a separate phase. The effect of such an approach on the various parameters has been checked. For example, the team has found that including air voids as a separate phase in the model does not change the representative volume element (RVE) size significantly.

Experimental observations show that air voids vary in size and may exist in multiple scales. Accordingly, the ultimate goal is to use the proposed procedure for multiple scales. Therefore, the team needed to discern ways that including air voids at multiple scales can function in the context of the multiscale modeling used in this research. This issue has been investigated during the current quarter. The effect of the shape of air voids has been reviewed as another parameter.

Before using specimens with air voids in the multiscale lattice framework, the accuracy of the scaling up process must be checked. In other words, the team needed to determine if the scaling up process yields the same results as the single-scale solution. Single-scale specimens are those that contain the aggregate particles of the entire range of sizes. Such specimens require high resolution (i.e., a small lattice size) so that all the particles can be generated, no matter how small they are. These specimens are very large with respect to size and almost impossible to simulate within a realistic time.

However, for verification purposes it is not necessary to include all the different sizes of aggregates in one specimen. Only a part of the whole gradation may be used. Then, this part can be analyzed once using the multiscale procedure and once directly. Because of the availability of experimental data, FAM has been chosen as part of the gradation. FAM itself has been divided into two scales. Therefore, results from the small scale have been used as an input for the coarse scale. As the alternative method, the whole FAM gradation has been used to generate specimens. A comparison between the results of each of these two methods can verify the accuracy of the multiscale modeling procedure. The initial stiffness value of the FAM has been selected as the representative parameter for comparison. A sufficient number of replicates has been generated to consider the effects of specimen-to-specimen variability. The air void content (percentage) has been chosen to be the same for both procedures. Different air void levels have been analyzed and compared (figure F3b-1.15).

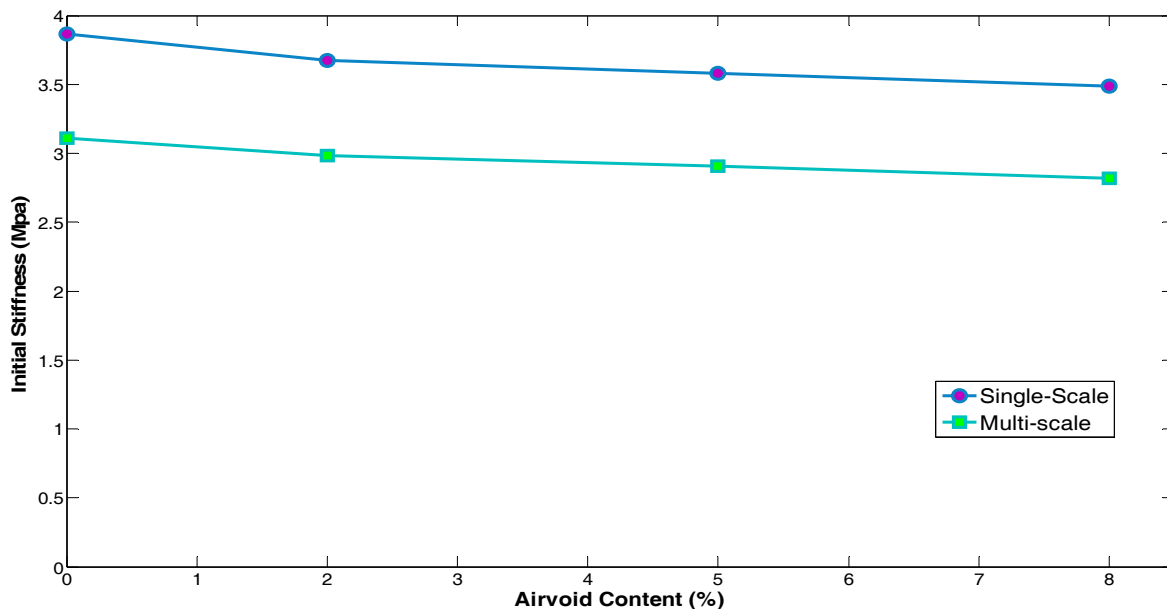


Figure F3b-1.15. Scaling procedure verification: single-scale vs. multi-scale.

In order to obtain the initial stiffness values for the whole FAM from the multiscale modeling, the initial stiffness values obtained from both subscales must be multiplied. Because multiple specimens have been tested for each subscale, the most probable case must be found in which enough repetitions have been completed. To do so, the probability density functions of all the possible multiplication cases have been found, and the most probable case has been selected as the final initial stiffness. The obtained probability density functions are compared with the single-scale results in figure F3b-1.16.

Figure F3b-1.15 shows that the multiscale modeling always under-predicts the actual initial stiffness values measured by single-scale analysis. According to parametric studies performed on the resolution of the lattice and RVE size, the amount of error can be reduced significantly. However, such accuracy can significantly increase the simulation costs as well. Because the

amount of error for all the air void contents is almost the same, an adjustment factor can be introduced instead of changing the mesh parameters, thus significantly reducing the computational costs. For the current resolution and RVE size, an adjustment factor of 1.24 is recommended.

Further verification can be achieved by comparing the actual results with the experimental results. FAM material has been tested for different air void content levels, and initial stiffness values of the corresponding FAM have been found for different frequencies, temperatures and strain rates. The same tests can be reproduced virtually using the explained multiscale modeling for different mix design data and air void contents.

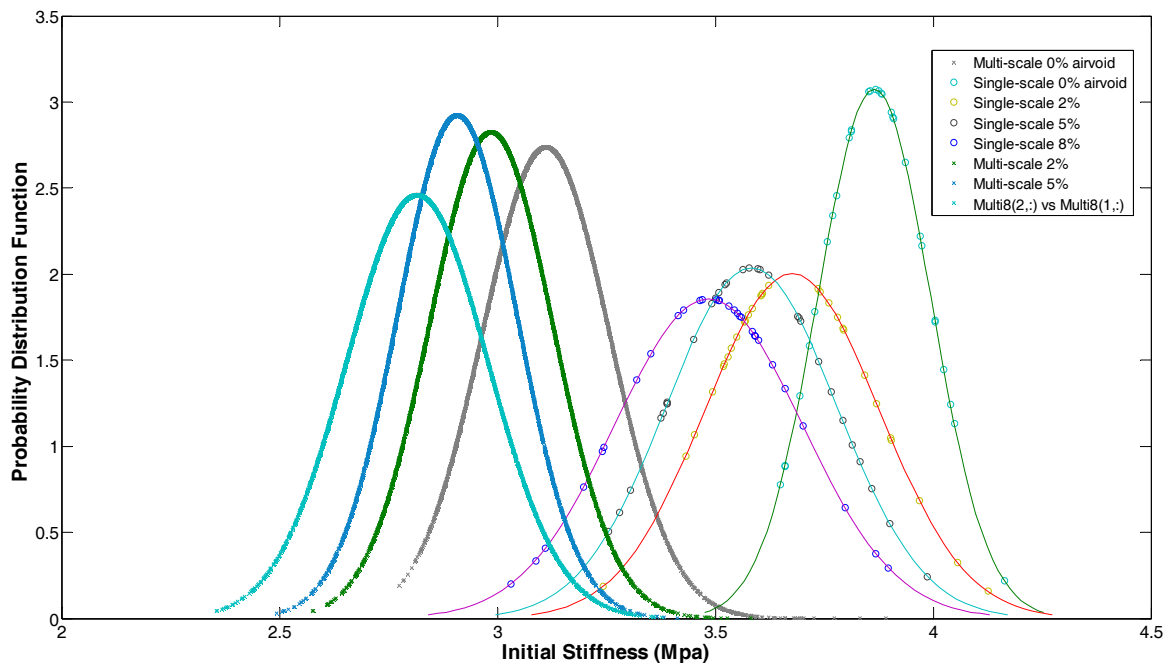


Figure F3b-1.16. Probability density functions of the results for single-scale and multi-scale procedures.

The normalized initial stiffness values for the different air void contents are compared with the experimental results in figure F3b-1.17. The analysis shows that the multiscale modeling yields acceptable results within the range of data obtained from the experiments. However, it can be seen that the simulations are not sensitive to mix design. In figure F3b-1.17, no significant differences in the slopes of the different mix designs are evident. It should be noted that the simulations yield different results for different mix designs, but the normalized values do not seem to show any change in slope. The reasons for this discrepancy will be investigated in the following quarter.

All of the above specimens include air voids of different sizes, but all have a circular shape. The shape of the air voids was then changed to a random octagonal shape, and the tests were repeated. Figure F3b-1.18 shows a specimen virtually generated using the new air void shape.

Results show that the slope of the line changes considerably when the shape of the air voids is changed (figure F3b-1.17). However, with the random shape, the same slopes emerge for the different mix designs. Further investigation regarding this issue is the subject of future work.

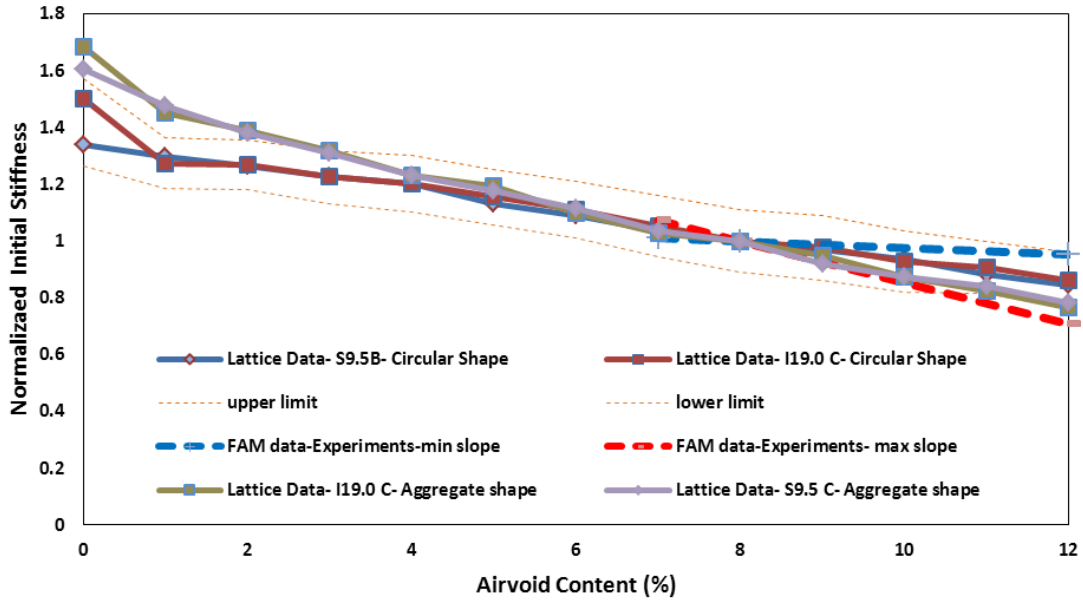


Figure F3b-1.17. Effect of air void content on initial slope.

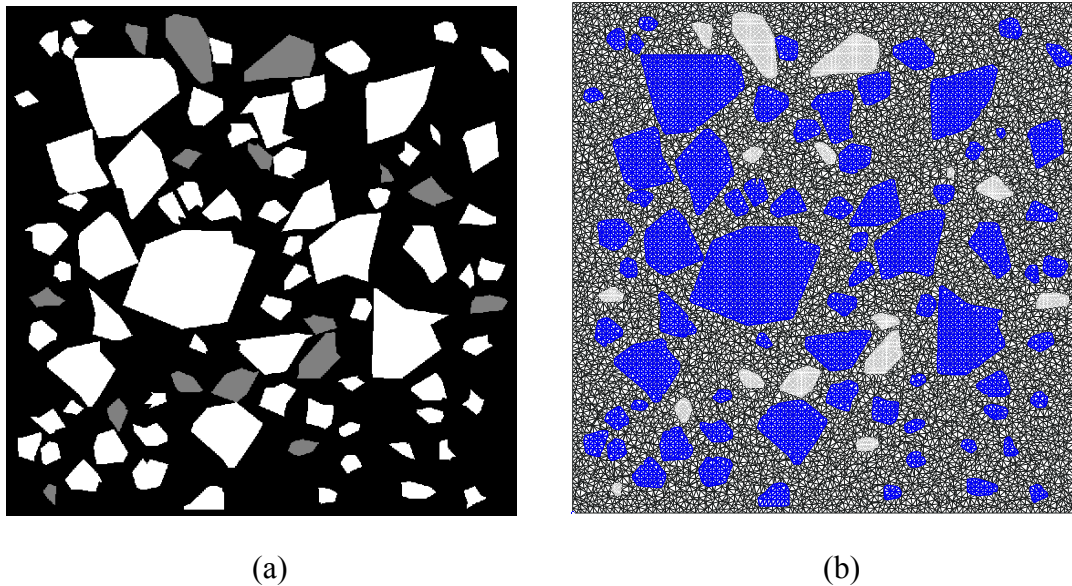


Figure F3b-1.18. New shapes for air voids: (a) virtually fabricated image; (b) mesh associated with the image of the virtually fabricated image, (a).

The rest of the time in the current quarter has been spent trying to better understand the behavior of asphalt concrete as it is subjected to cyclic loads. It is well known that the dominant type of load applied to pavements in service has a repeating nature, which is often simplified as cyclic loading. Cyclic loading is simulated in lattice modeling using the viscoelastic continuum damage (VECD) model, coupled with extrapolation models developed as part of the in-house finite element code, FEP++. Further refinement and testing is underway to ensure the accuracy of the resulting procedure.

Continuum Damage to Fracture (NCSU)

Computational implementation of the nonlocal damage modeling framework has been initiated this quarter. The implementation into a higher dimensional finite element model and the development of a specific nonlocal damage model through experimental observations are subjects of future efforts.

Significant Results

None

Significant Problems, Issues and Potential Impact on Progress

None

Work Planned Next Quarter

Cohesive Zone Micromechanical Model (UNL)

In the next quarter we will work on the following activities:

- Model validation and calibration: performance tests of asphalt concrete mixtures, modeling of the asphalt concrete mixture tests, and comparisons between model simulation results and experimental test results.
- Material characterization and fracture testing of fine aggregate matrix mixtures using ARC core materials.

Cohesive Zone Micromechanical Model (TAMU)

In the next quarter we will work on the following activities:

- Extension of the current rate-independent UEL code to incorporate the rate-dependence of the cohesive zone fracture parameters;
- Analysis of the SCB (Semi-Circular Bending) fracture test results (presented in the previous quarters) to more accurately identify rate-dependent fracture characteristics of FAM materials; and

- Development of the mixing-compact-production practice of the FAM phase with more test data and simulation results to reach more conclusive findings.

Lattice Micromechanical Model (NCSU)

- Refinement and quantitative verification of the proposed model for cyclic loads
- Evaluation of the effect of air voids as a function of mixture type

Continuum Damage to Fracture (NCSU)

- Continuation of computational implementation of nonlocal framework in higher dimensional finite element code

Cited References

Castelo, B. V., E. Masad, A. Bhasin, and D. N. Little, 2008, Fatigue analysis of asphalt mixtures independent of mode of loading. *Transportation Research Record*, 2507: 149-156.

Gao, Y. F. and A. F. Bower, 2004, A Simple Technique for Avoiding Convergence Problems in Finite Element Simulations of Crack Nucleation and Growth on Cohesive Interfaces. *Modeling and Simulation in Materials Science and Engineering*, 12: 453-463.

Kim, Y, D. N. Little, and R. L. Lytton, 2003, Fatigue and healing characterization of asphalt mixtures. *Journal of Materials in Civil Engineering*, 15(1): 75-83.

Kim, Y., H. J. Lee, D. N. Little, and Y. R. Kim, 2006, A simple testing method to evaluate fatigue fracture and damage performance of asphalt mixtures. *Journal of the Association of Asphalt Paving Technologists*, 755-787.

Masad, E, C. Zollinger, R. Bulut, D. N. Little, and R. L. Lytton, 2006, Characterization of HMA moisture damage using surface energy and fracture properties. *Journal of the Association of Asphalt Paving Technologists*, 75: 713-754.

Song, I, D. N. Little, E. Masad, and R. L. Lytton, 2005, Comprehensive evaluation of damage in asphalt mastics using X-ray CT, continuum mechanics, and micromechanics. *Journal of the Association of Asphalt Paving Technologists*, 74: 885-920.

Song, S. H., 2006, Fracture of Asphalt Concrete: A Cohesive Zone Modeling Approach Considering Viscoelastic Effects. Ph.D. dissertation at University of Illinois at Urbana-Champaign.

Subtask F3b-2: Account for Material Microstructure and Fundamental Material Properties

The reader is referred to work elements F1c and F1d.

Work Element F3c: Development of Unified Continuum Model (TAMU)

Work Done This Quarter

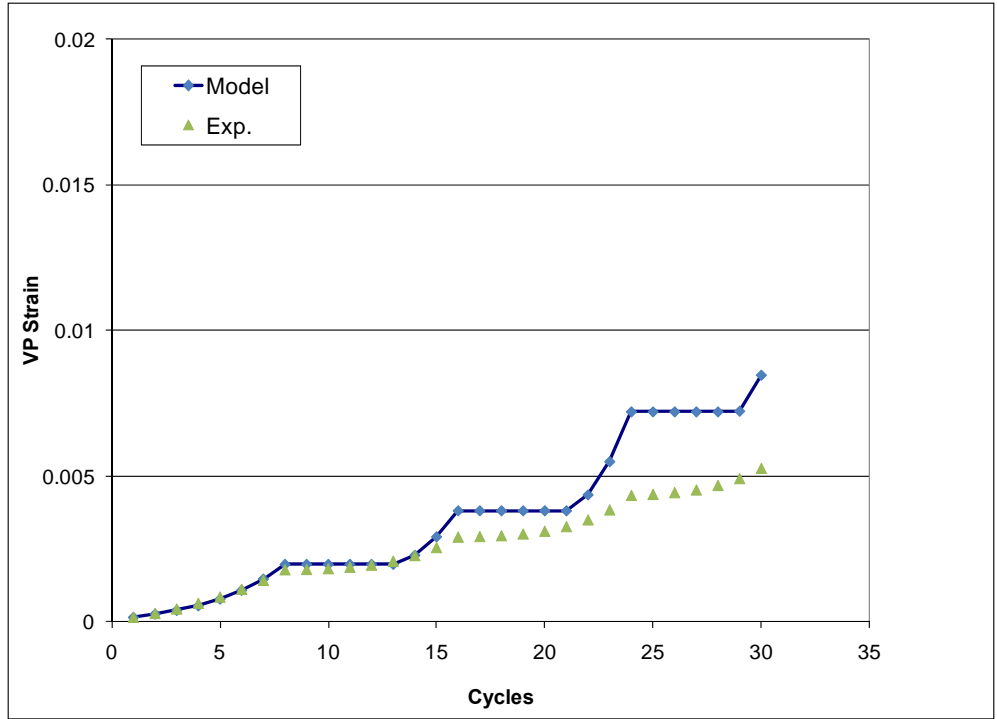
See M4c for details on the progress in the development of the continuum-based moisture-induced damage mode. Also see F1d-8 on the development of the continuum-based micro-damage healing model. The focus of this quarter was on the calibration and validation of the unified continuum damage model based on the ALF data. Detailed description of the ALF data is available in the final report of project DTFH61.05.RA.00108, which was submitted by North Carolina State University to the Federal Highway Administration on May 2008. Also, special emphasis was placed on formulating a continuum-based aging model based on oxidation hardening. Therefore, Pavement Analysis using a Nonlinear Damage Approach (PANDA) at this stage includes the following modeling capabilities: (1) nonlinear thermo-viscoelasticity; (2) thermo-viscoplasticity; (3) thermo-viscodamage (i.e. rate- and temperature-dependent damage) for modeling fatigue damage; (4) moisture-induced damage distinguishing between adhesive and cohesive moisture damages; (5) micro-damage healing; and (6) aging.

A systematic procedure was developed and validated for determining the viscoelastic (VE) and viscoplastic (VP) parameters of the model. This procedure utilizes the repeated creep and recovery test with various loading levels (VL) of the ALF tests. The first step in this analysis procedure is to determine the VE material parameters and Schapery's nonlinear parameters from the analysis of the response during the recovery periods of creep test conducted at different stress levels. The second step is to use the loading part of the creep tests to decouple the VP response from the nonlinear viscoelastic response. This VP response at multiple stress levels is then analyzed to determine the VP model parameters.

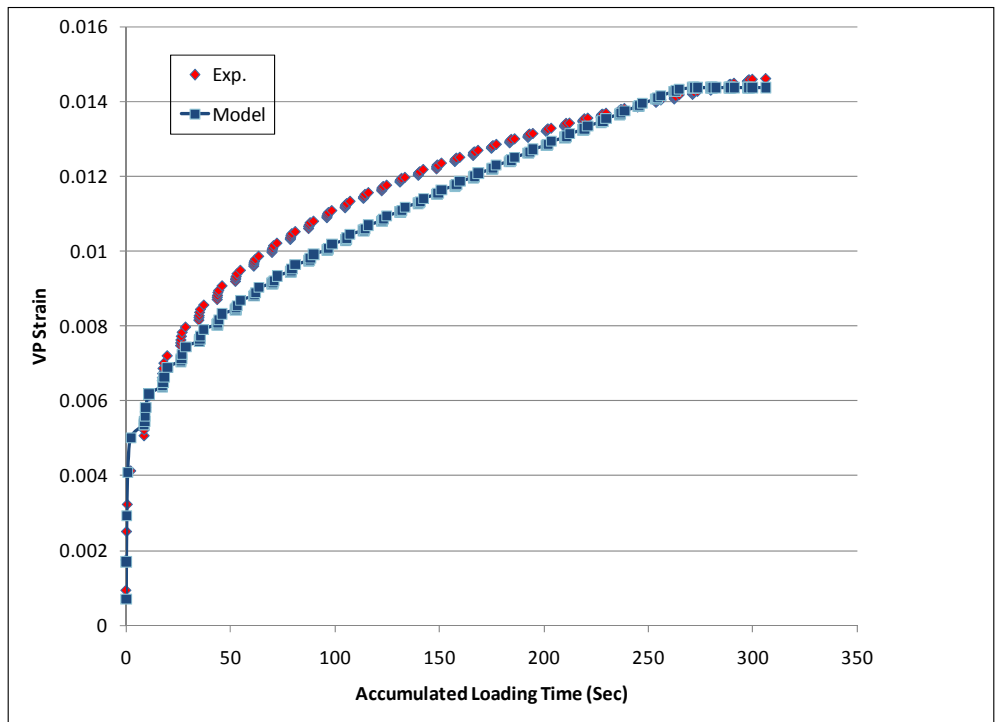
Significant Results

One of the significant outcomes of this task is the validation of the method for determining the model parameters using the comprehensive ALF database. Another significant finding is that it was found during the analysis that the material experiences softening (or loss of hardening) during the unloading stage of the creep test.

Figure F3c.1 shows the relationship between the VP response of the model and the results of the VL and VT tests. The validation of model is also achieved by comparing the model predictions of the repeated creep and recovery tests with constant loading level and time (CLT), variable loading level and time (VLT) and reversed variable loading time (RVT) as shown in figure F3c.2.

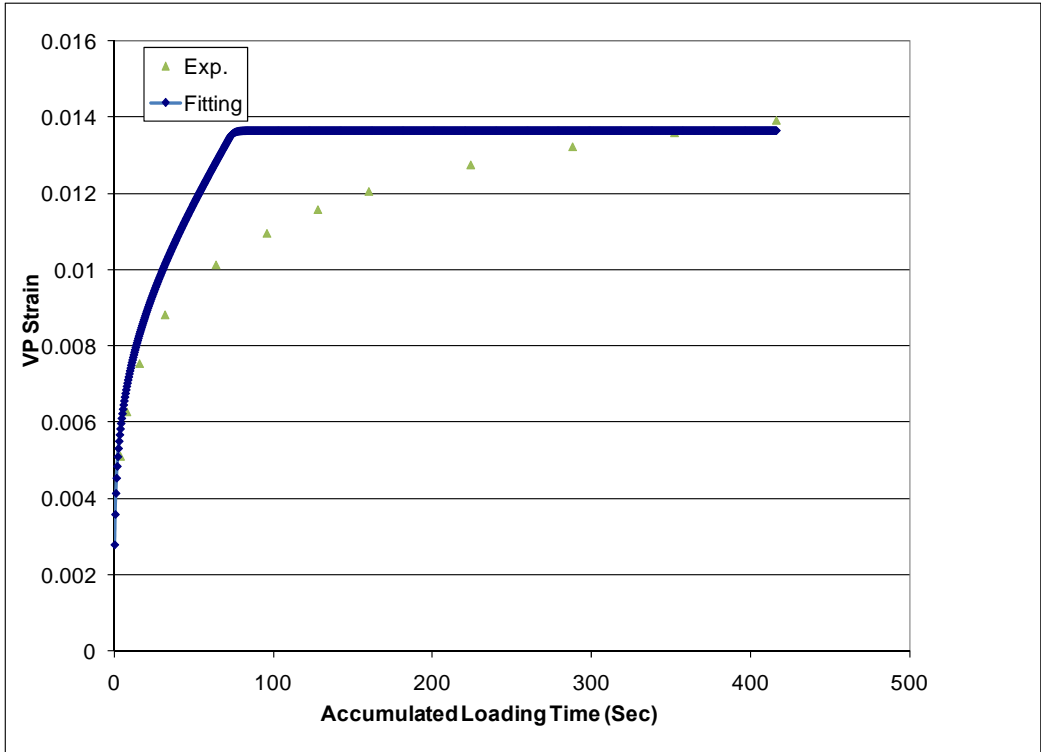


(a) VL test

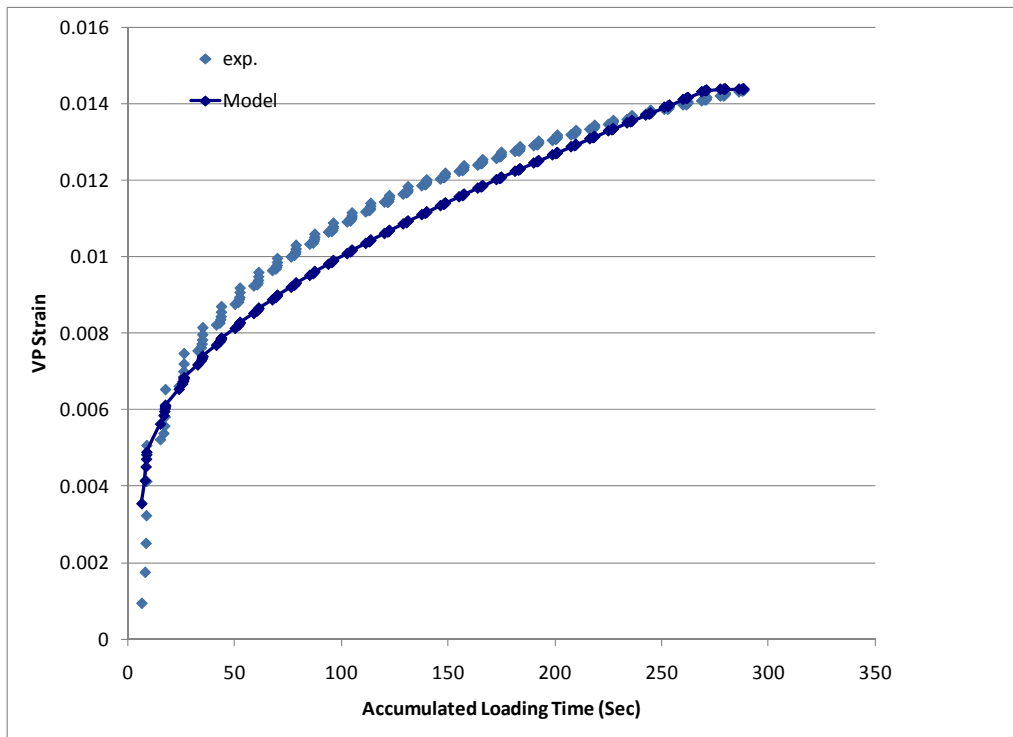


(b) VT test

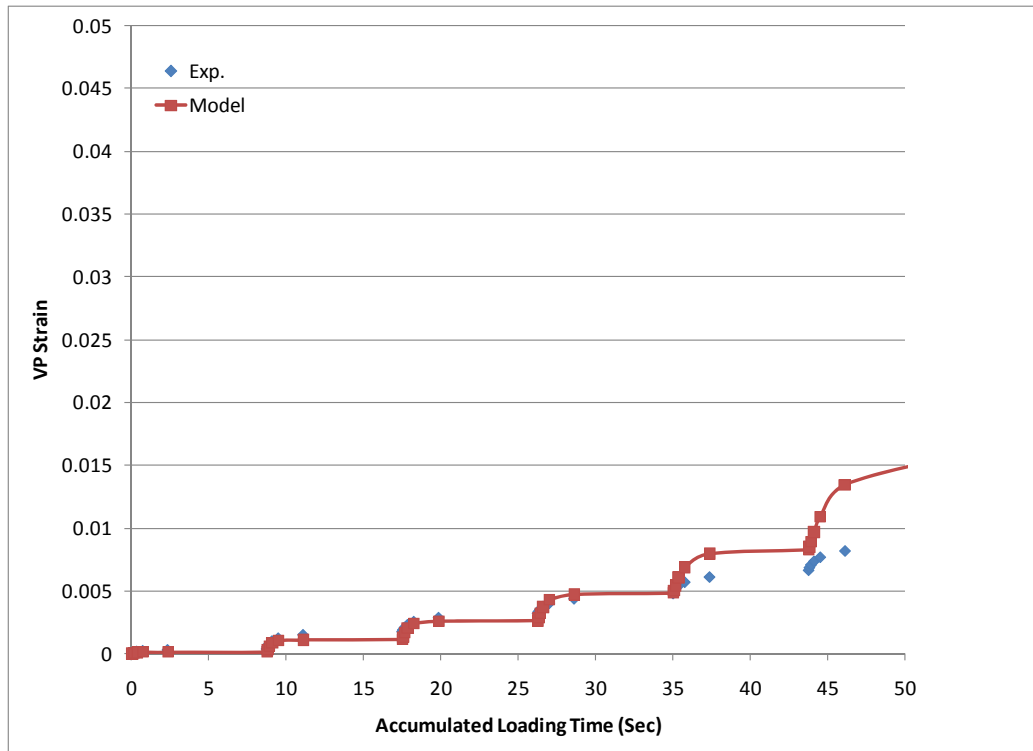
Figure F3c.1. The model simulation results of viscoplastic strain for (a) VL and (b) VT tests.



(a) CLT test



(b) RVT test



(c) VLT test

Figure F3c.2. The model predictions for (a) CLT test, (b) RVT test and (c) VLT test.

Significant Problems, Issues and Potential Impact on Progress

This is the first time that the researchers use a comprehensive database with various tests to evaluate the model. Several changes in the model were necessary based on the findings and knowledge gained from the analysis of the ALF database.

Work Planned Next Quarter

We will finalize the analysis of the ALF database using the damage and healing functions of the model. We will also conduct simulations to validate the model against the structural response of the various sections of the ALF experiment.

Continuum-based Model for Aging

Work Done This Quarter

In this quarter, the phenomenological aging model for asphaltic mixtures that has been developed during the previous quarter has been numerically implement into PANDA and verified qualitatively against a wide range of experimental trends that include single creep, creep-recovery, repeated creep-recovery, monotonic tension, monotonic compression, cyclic tension,

cyclic compression, relaxation, cyclic relaxation, and rutting performance. Also, as emphasized before the developed aging model incorporates micromechanical effects such as the amount of oxygen that has been diffused and the rate of carbonyl formation. Furthermore, how these micromechanical aspects affect the viscoelastic, viscoplastic, damage, and healing properties has been investigated. It is shown that the aging model predicts well the effect of oxidation hardening on the various mechanical properties of the asphalt mixture.

Initial attempts have been made to calibrate and validate the aging model against existing experimental data from previous FHWA projects; mainly the experimental results documented in report FHWA/TX-05/0-4468.

Significant Results

For example, the effect of the aging internal state variable A on the tensile and compressive stress-strain responses are shown in figure F3c.3. The aging variable A physically indicates the percentage of carbonyl area formation due to oxidation. Figure F3c.3 clearly shows the ability of the model in predicting the increase in the initial stiffness, increase in the ultimate strength, and decrease in ductility due to aging. Also, the model clearly distinguishes between the asphalt mix behavior in tension and compression loading conditions. In figure F3c.3 the evolution of the damage density as a function of the imposed strain is shown up to failure. Figure F3c.4 shows the variation of the aging variable with the depth of an asphalt layer and the rutting predictions for various aging periods.

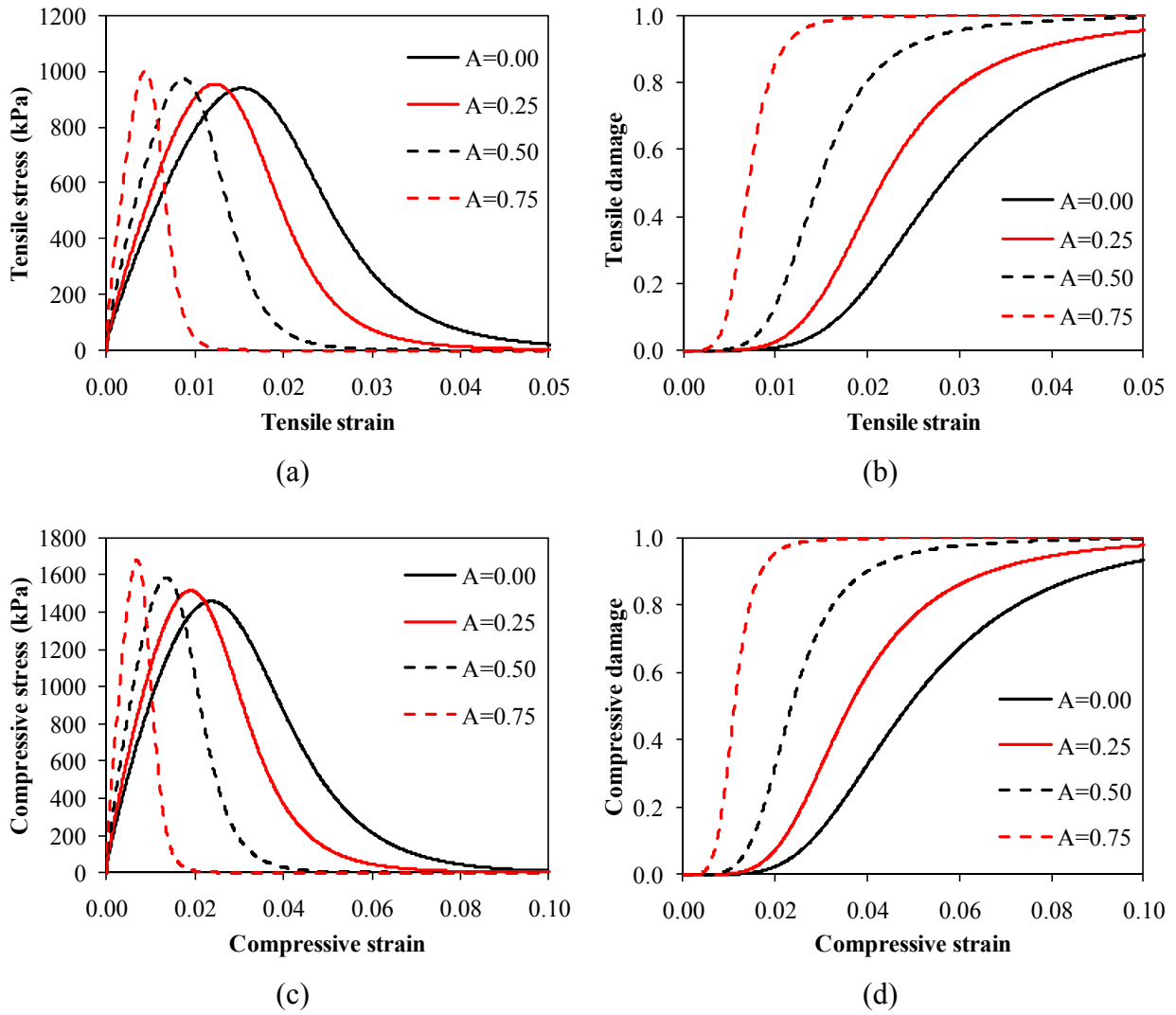


Figure F3c.3. Monotonic uniaxial tensile and compressive loading response of asphalt mixture with different aging levels: (a) tensile stress, (b) tensile damage density, (c) compressive stress, and (d) compressive damage density.

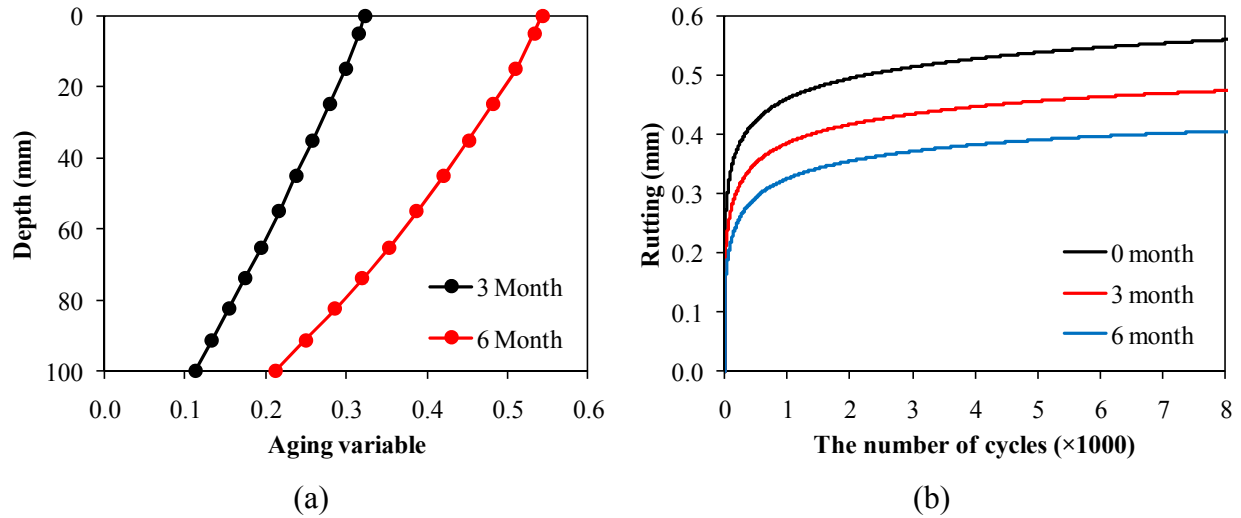


Figure F3c.4. Rutting simulation results. (a) Variation of the aging variable through the asphalt layer thickness and (b) rutting depth variation for various aging periods.

Significant Problems, Issues and Potential Impact on Progress

None

Work Planned Next Quarter

Currently, oxygen transport is simulated using Fick's second law. However, attempts to employ a more accurate transport equation and its coupling with temperature will be made in the following quarter. Moreover, the focus in the coming quarter is on validating the model against existing experimental data from previous FHWA projects.

Fatigue Year 4		Year 4 (4/10-3/11)											Team	
		4	5	6	7	8	9	10	11	12	1	2		3
Material Properties														
F1a	Cohesive and Adhesive Properties													
F1a-1	Critical review of literature													TAMU
F1a-2	Develop experiment design													
F1a-3	Thermodynamic work of adhesion and cohesion													
F1a-4	Mechanical work of adhesion and cohesion				D			F						
F1a-5	Evaluate acid-base scale for surface energy calculations													
F1b	Viscoelastic Properties													
F1b-1	Separation of nonlinear viscoelastic deformation from fracture energy under cyclic loading				M&A, F, JP			JP						TAMU
F1b-2	Separation of nonlinear viscoelastic deformation from fracture energy under monotonic loading												JP	
F1c	Aging													
F1c-1	Critical review of binder oxidative aging and its impact on mixtures													TAMU
F1c-2	Develop experiment design													
F1c-3	Develop transport model for binder oxidation in pavements						P					P, JP		
F1c-4	Effect of binder aging on properties and performance											P, JP		
F1c-5	Polymer modified asphalt materials						P							
F1d	Healing													
F1d-1	Critical review of literature													TAMU
F1d-2	Select materials with targeted properties													TAMU
F1d-3	Develop experiment design													TAMU
F1d-4	Test methods to determine properties relevant to healing					D			F					TAMU
F1d-5	Testing of materials								JP					TAMU
F1d-6	Evaluate relationship between healing and endurance limit of asphalt binders								JP			P		UWM
F1d-7	Coordinate with AFM analysis													WRI
F1d-8	Coordinate form of healing parameter with micromechanics and continuum damage models													TAMU
Test Methods														
F2a	Binder tests and effect of composition													
F2a-1	Analyze Existing Fatigue Data on PMA													UWM
F2a-2	Select Virgin Binders and Modifiers and Prepare Modified Binder													
F2a-3	Laboratory Aging Procedures													
F2a-4	Collect Fatigue Test Data											DP, P	JP	
F2a-5	Analyze data and propose mechanisms											P		
F2b	Mastic testing protocol													
F2b-1	Develop specimen preparation procedures							F						TAMU
F2b-2	Document test and analysis procedures in AASHTO format							F						
F2c	Mixture testing protocol													
F2d	Tomography and microstructural characterization													
F2d-1	Micro scale physicochemical and morphological changes in asphalt binders										JP			TAMU
F2e	Verify relationship between DSR binder fatigue tests and mixture fatigue performance													
F2e-1	Evaluate Binder Fatigue Correlation to Mixture Fatigue Data													UWM
F2e-2	Selection of Testing Protocols				D			F						
F2e-3	Binder and Mixture Fatigue Testing													
F2e-4	Verification of Surrogate Fatigue Test									D		F, DP		
F2e-5	Interpretation and Modeling of Data							JP					M&A	
F2e-6	Recommendations for Use in Unified Fatigue Damage Model											P		
Models														
F3a	Asphalt microstructural model													WRI
F3b	Micromechanics model													
F3b-1	Model development							JP				P		TAMU
F3b-2	Account for material microstructure and fundamental material properties													
F3c	Develop unified continuum model													
F3c-1	Analytical fatigue model for mixture design													TAMU
F3c-2	Unified continuum model										JP		M&A	
F3c-3	Multi-scale modeling										JP		M&A	
	Lattice Model				DP		DP, JP							NCSU
	Continuum Damage to Fracture									JP				

LEGEND

Deliverable codes

- D: Draft Report
- F: Final Report
- M&A: Model and algorithm
- SW: Software
- JP: Journal paper
- P: Presentation
- DP: Decision Point
- [x]

- Work planned
- Work completed
- Parallel topic

Deliverable Description

- Report delivered to FHWA for 3 week review period.
- Final report delivered in compliance with FHWA publication standards
- Mathematical model and sample code
- Executable software, code and user manual
- Paper submitted to conference or journal
- Presentation for symposium, conference or other
- Time to make a decision on two parallel paths as to which is most promising to follow through
- Indicates completion of deliverable x

Fatigue Year 2 - 5		Year 2 (4/08-3/09)				Year 3 (4/09-3/10)				Year 4 (04/10-03/11)				Year 5 (04/11-03/12)				Team
		Q1	Q2	Q3	Q4	Q1	Q2	Q3	Q4	Q1	Q2	Q3	Q4	Q1	Q2	Q3	Q4	
Material Properties																		
F1a	Cohesive and Adhesive Properties																	
F1a-1	Critical review of literature			JP													TAMU	
F1a-2	Develop experiment design																	
F1a-3	Thermodynamic work of adhesion and cohesion																	
F1a-4	Mechanical work of adhesion and cohesion					JP				D	F							
F1a-5	Evaluate acid-base scale for surface energy calculations														JP			
F1b	Viscoelastic Properties																	
F1b-1	Separation of nonlinear viscoelastic deformation from fracture energy under cyclic loading			D,JP	M&A				JP	(M&A,F,J)	JP		P		JP,M&A,D	F	TAMU	
F1b-2	Separation of nonlinear viscoelastic deformation from fracture energy under monotonic loading			JP	M&A				JP				JP		JP,M&A,D	F		
F1c	Aging																	
F1c-1	Critical review of binder oxidative aging and its impact on mixtures																TAMU	
F1c-2	Develop experiment design			D		F												
F1c-3	Develop transport model for binder oxidation in pavements		P		P,JP		P		P,JP		P		P,JP		D,M&A	F		
F1c-4	Effect of binder aging on properties and performance				JP,P		JP	D	F			P,JP		JP	D	F		
F1c-5	Polymer modified asphalt materials						P				P					D	F	
F1d	Healing																	
F1d-1	Critical review of literature																TAMU	
F1d-2	Select materials with targeted properties																TAMU	
F1d-3	Develop experiment design																TAMU	
F1d-4	Test methods to determine properties relevant to healing				JP				JP	D	F						TAMU	
F1d-5	Testing of materials							JP			JP			M&A,D	JP,F		TAMU	
F1d-6	Evaluate relationship between healing and endurance limit of asphalt binders	DP				DP	JP	DP			JP		P		JP	D	F	UWM
F1d-7	Coordinate with AFM analysis									JP								WRI
F1d-8	Coordinate form of healing parameter with micromechanics and continuum damage models															JP,D	F	TAMU
Test Methods																		
F2a	Binder tests and effect of composition																	
F2a-1	Analyze Existing Fatigue Data on PMA		DP															UWM
F2a-2	Select Virgin Binders and Modifiers and Prepare Modified Binder		DP															
F2a-3	Laboratory Aging Procedures																	
F2a-4	Collect Fatigue Test Data		P		JP		P		P				P,DP,JP					
F2a-5	Analyze data and propose mechanisms				P		P					P			P	D	F	
F2b	Mastic testing protocol																	
F2b-1	Develop specimen preparation procedures		D								F						TAMU	
F2b-2	Document test and analysis procedures in AASHTO format		D								F							
F2c	Mixture testing protocol																	
F2c-1	Evaluate Binder Fatigue Correlation to Mixture Fatigue Data		D,JP	F														
F2d	Tomography and microstructural characterization																	
F2d-1	Micro scale physicochemical and morphological changes in asphalt binders						JP					JP					TAMU	
F2e	Verify relationship between DSR binder fatigue tests and mixture fatigue performance																	
F2e-1	Evaluate Binder Fatigue Correlation to Mixture Fatigue Data						DP,D	F			D	F					UWM	
F2e-2	Selection of Testing Protocols																	
F2e-3	Binder and Mixture Fatigue Testing																	
F2e-4	Verification of Surrogate Fatigue Test												D	F,DP				
F2e-5	Interpretation and Modeling of Data		JP		P		JP		P		JP		M&A					
F2e-6	Recommendations for Use in Unified Fatigue Damage Model												P			D	F	
Models																		
F3a	Asphalt microstructural model							JP								M&A	F	WRI
F3b	Micromechanics model																	
F3b-1	Model development				JP				JP		JP		P	D	DP	F,SW	TAMU	
F3b-2	Account for material microstructure and fundamental material properties													D		F		
F3c	Develop unified continuum model																	
F3c-1	Analytical fatigue model for mixture design														M&A,D	F	TAMU	
F3c-2	Unified continuum model			JP				JP				JP	M&A	D	DP	F,SW		
F3c-3	Multi-scale modeling											JP	M&A	D		F		
	Lattice Model										DP	DP,JP					NCSU	
	Continuum Damage to Fracture										DP	JP						

LEGEND

Deliverable codes

- D: Draft Report
- F: Final Report
- M&A: Model and algorithm
- SW: Software
- JP: Journal paper
- P: Presentation
- DP: Decision Point
- [x]

- Work planned
- Work completed
- Parallel topic

Deliverable Description

- Report delivered to FHWA for 3 week review period.
- Final report delivered in compliance with FHWA publication standards
- Mathematical model and sample code
- Executable software, code and user manual
- Paper submitted to conference or journal
- Presentation for symposium, conference or other
- Time to make a decision on two parallel paths as to which is most promising to follow through
- Indicates completion of deliverable x

PROGRAM AREA: ENGINEERED MATERIALS

CATEGORY E1: MODELING

Work element E1a: Analytical and Micro-mechanics Models for Mechanical Behavior of Mixtures (TAMU)

Work Done This Quarter

A technical presentation, entitled “Characterization of Engineered Properties of Asphalt Mixtures as Inputs to PANDA”, was made in the Fundamental Properties and Advanced Models Expert Task Group of the Federal Highway Administration (FHWA) in Madison, Wisconsin, September 2010.

In this quarter, master curve models were developed for the phase angle of the asphalt binder and asphalt mastic. Equation E1a.1 shows the developed master curve model for the phase angle of the asphalt binder, and equation E1a.2 presents the proposed master curve model for the phase angle of the asphalt mastic.

$$\varphi(\omega a_T) = \varphi_{\max} - \varphi_{\text{diff}} e^{-\left(\frac{\beta+1}{\beta}\right)\left(\frac{\omega_r}{\omega a_T}\right)^\beta} \quad (\text{E1a.1})$$

where φ_{\max} = maximum binder phase angle; φ_{diff} = phase angle difference; ω_r = reference frequency; β = regression parameter; and a_T = time-temperature shift factor.

$$\varphi(\omega a_T) = \varphi_{\min} + \frac{\varphi_{\text{diff}} \left[\frac{\beta+1}{\omega_r} \right] e^{-\left(\frac{\beta+1}{\beta}\right)\left(\frac{\omega_r}{\omega a_T}\right)^\beta}}{\left[\frac{\omega a_T}{\omega_r} \right]^{\beta+1}} \quad (\text{E1a.2})$$

where φ_{\min} = minimum mastic phase angle; φ_{diff} = phase angle difference; ω_r = reference frequency; β = regression parameter; and a_T = time-temperature shift factor. These two models were applied to the data of the sweep frequency tests performed on a 64 UM-FH asphalt binder and the corresponding mastic with a filler to binder ratio of 1. The sweep frequency test data were provided by Dr. Bahia at University of Wisconsin at Madison. The fitting parameters were determined using the System Identification Model followed by the Gauss-Newton iteration method. The System Identification Model was programmed in Excel to determine the fitting parameters in equations E1a.1 and E1a.2. Figure E1a.1 illustrates the construction of the master curve of the asphalt binder phase angle. Figure E1a.2 compares the phase angle master curve of the asphalt binder to that of the corresponding asphalt mastic.

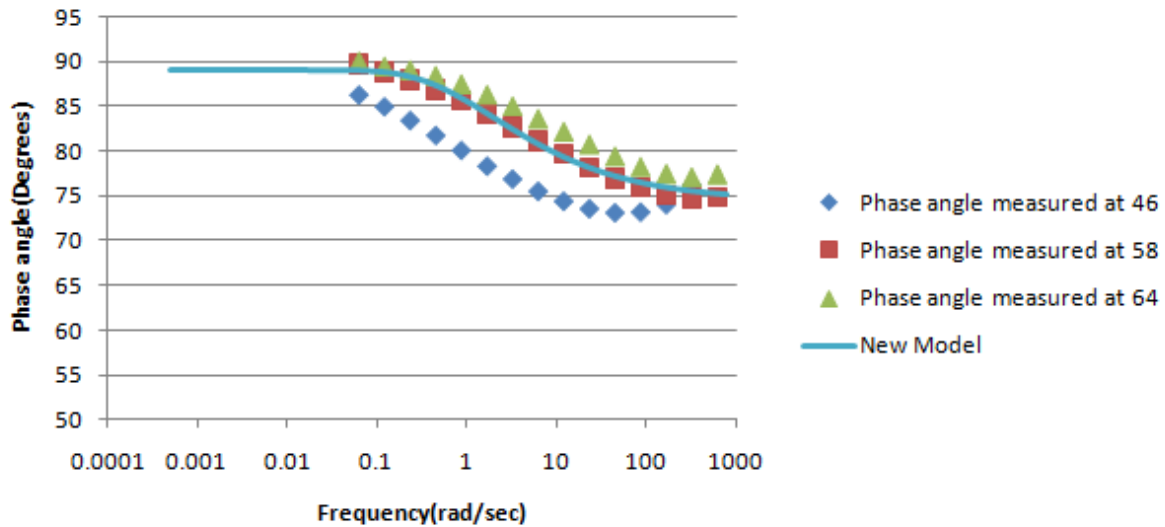


Figure E1a.1. Construction of phase angle master curve of asphalt binder.

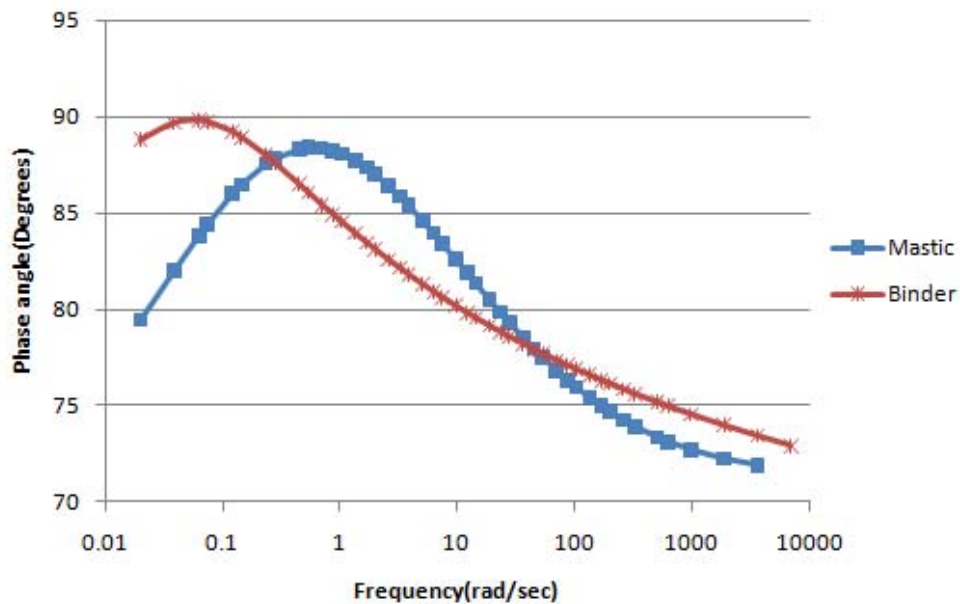


Figure E1a.2. Comparison between phase angle master curves of asphalt binder and corresponding asphalt mastic

Another accomplishment made in this quarter was the modeling of fatigue cracks in the fine asphalt mixtures (FAM) at various levels of relative humidity, which was formulated based on the Strain Energy Equivalence Principle (SEEP). The SEEP assumed that the material with local damage had the same strain energy, including dissipated strain energy, stored strain energy and the total of both, as the equivalent continuum material when they were subjected to repeated

loading. When evaluating the fatigue cracking of the FAM, the controlled-stress repeated direct tension (RDT) test was conducted on the FAM specimens using the Dynamic Mechanical Analyzer (DMA). Figure E1a.3 shows an example of the applied tensile stress and the corresponding strain response in a destructive controlled-stress RDT test.

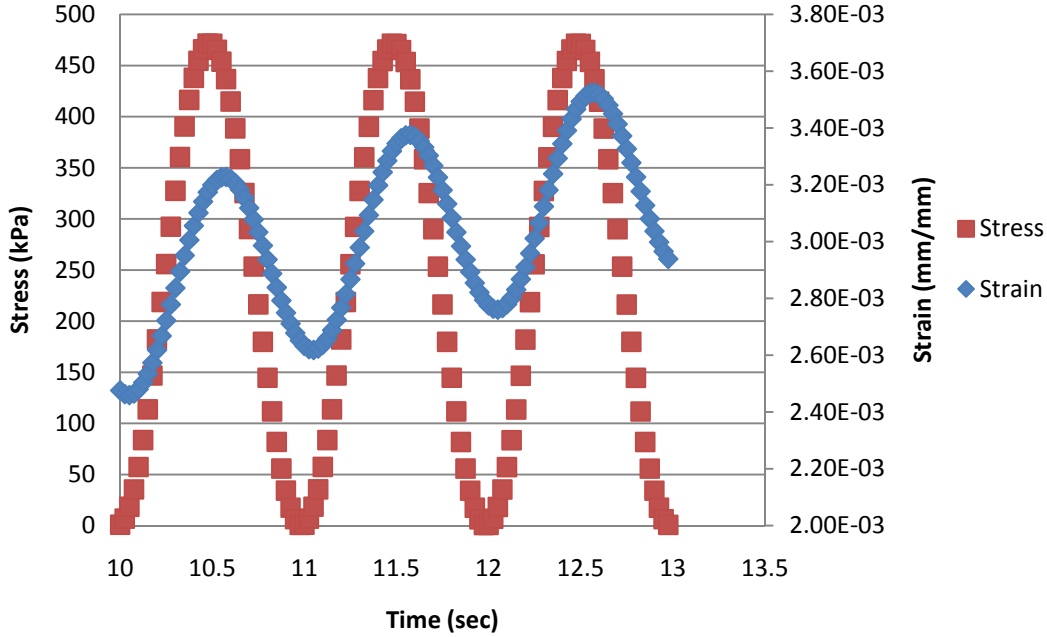


Figure E1a.3. Stress and strain of FAM specimen in controlled-stress test.

Based on the test data, the strain energy equivalence equations were formulated in equations E1a.3 and E1a.4.

$$DPSE^A = \pi \frac{(\sigma^T)^2}{E_{LVE}} \sin(\varphi_0 - \varphi_{NLVE}) + (\sigma^T)^2 \Delta D \quad (E1a.3)$$

$$RPSE^A * A_{AM} \bar{t} = \frac{(\sigma^T)^2}{2E_{LVE}} A_{AM} \bar{t} - \frac{(\sigma^T)^2}{2E_{LVE}} \left(\frac{2M\pi^2\bar{c}^3}{3} \right) + 2M\pi\bar{c}^2 G_f^a \quad (E1a.4)$$

where σ = tensile stress; \bar{t} = asphalt film thickness; E_{LVE} = linear viscoelastic modulus of FAM specimen that is measured from the undamaged RDT test; φ_0 = phase angle of FAM specimen at zero loading cycle (intercept from the phase angle curve fitting of damaged FAM specimen); A_{AM} = total area of damaged asphalt mastic; φ_d = phase angle measured from the destructive RDT; \bar{c} = mean crack radius; M = number of cracks; ΔD = creep compliance slope with one loading cycle of undamaged FAM specimen; G_f^a = FAM adhesive bond energy; and the

superscript A and T represents “Apparent” and “True” respectively. Equation E1a.3 was used to determine the true stress of the intact material, and equation E1a.4 was employed to estimate the mean crack radius at various numbers of loading cycles.

Prior to performing the controlled-stress RDT test and data analysis on the real FAM specimens, pilot tests were conducted on dummy specimens. At a low stress level with a stress amplitude of 88 kPa, the modulus magnitude of the test specimen was found to increase with the number of load cycles, and the phase angle of the complex modulus decreased with number of load cycles, as illustrated in figures E1a.4 and E1a.5. The possible reason of these findings was that the aggregate were being drawn together during the repeated loading since the asphalt mastic was pulled by the tensile stress that led to the reduction of the cross-sectional area and a thinner film thickness (Lytton 2004; Marek 1994). Figure E1a.6 illustrates the densification of the aggregates during the RDT test. When the stress amplitude increased to approximately 471 kPa, the modulus decreased with the number of load cycles, which indicates the FAM specimen became softer, and the phase angle remained approximately the same with the number of load cycles, as illustrated in figure E1a.7. The reason for this finding is under investigation.

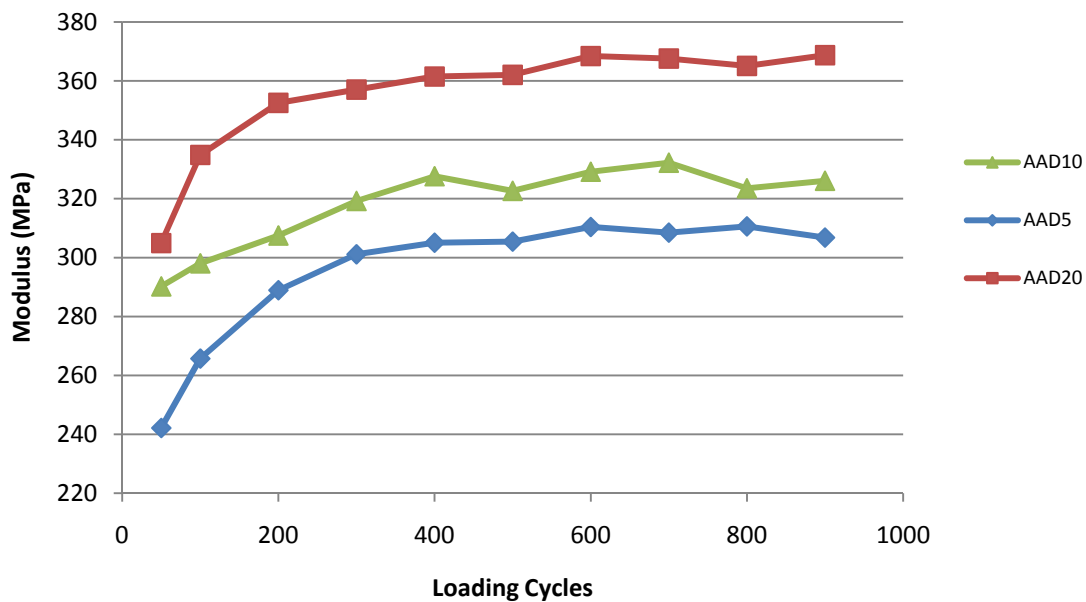


Figure E1a.4. Modulus magnitude of FAM specimen in controlled-stress RDT test with stress amplitude of 88 kPa.

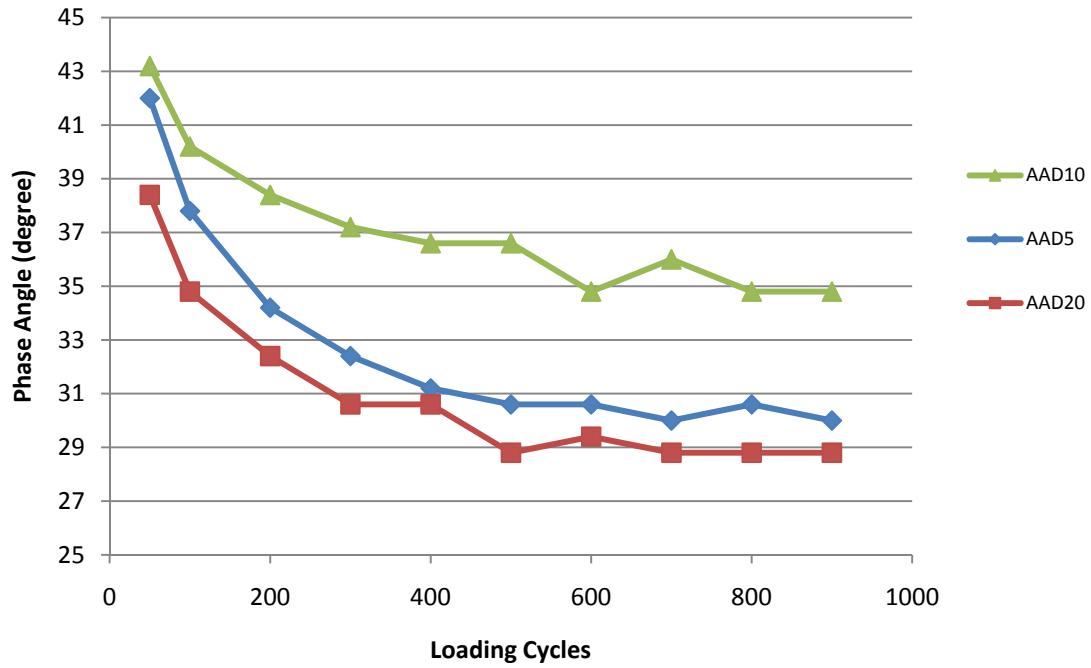


Figure E1a.5. Modulus phase angle of FAM specimen in controlled-stress RDT test with stress amplitude of 88 kPa.

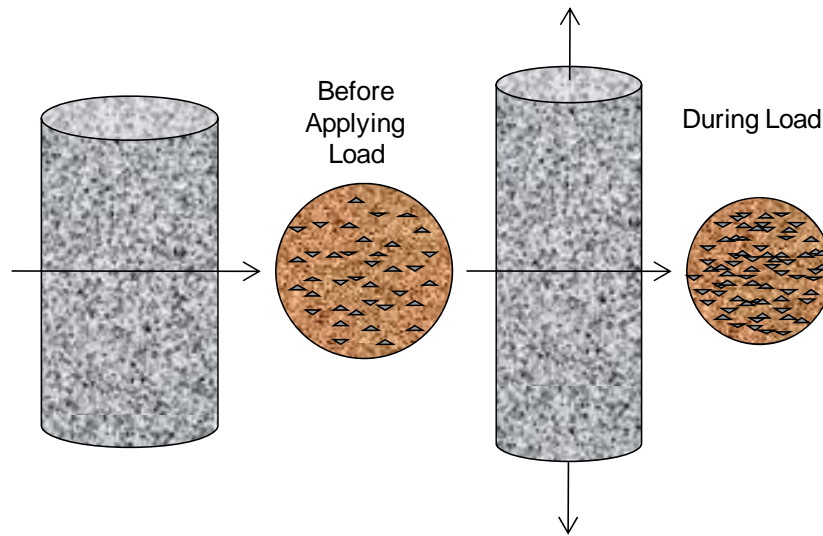


Figure E1a.6. Assembly of aggregates in FAM specimen in RDT test.

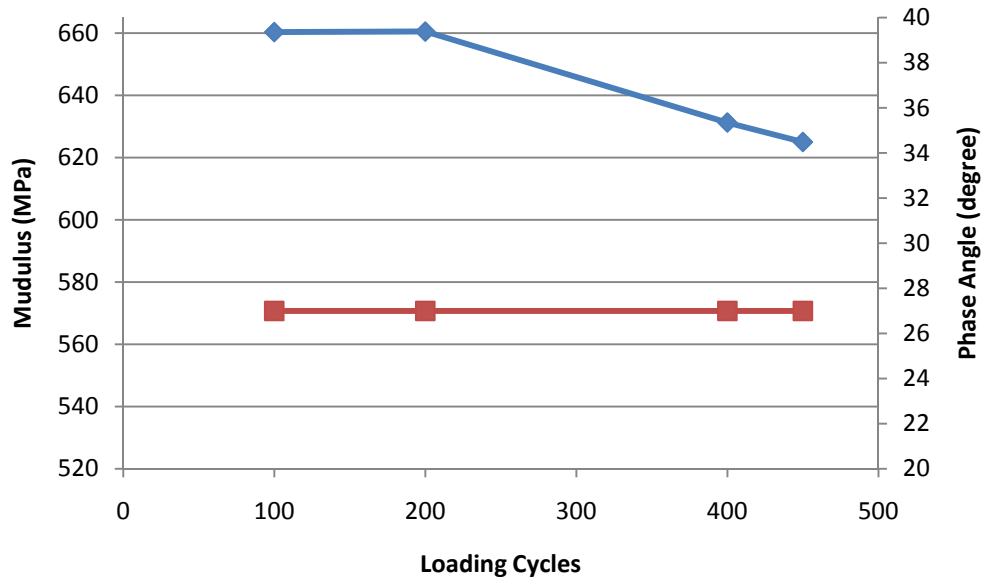


Figure E1a.7. Magnitude and phase angle of complex modulus of FAM specimen in controlled-stress RDT test with stress amplitude of 471 kPa.

Significant Results

Phase angle models were developed for the asphalt binder and the asphalt mastic. The proposed models were applied to the binder and mastic data provided by Dr. Bahia at University of Wisconsin and proved to be able to successfully construct the master curves of the asphalt binder and the corresponding mastic.

The fatigue crack model was formulated based on the Strain Energy Equivalence Principle for the FAM specimen under the controlled-stress RDT test. A number of dummy FAM specimens were tested using the newly purchased DMA. Different stress levels were used in the controlled-stress tests.

Work Planned Next Quarter

The newly developed phase angle models will be applied to more sets of data of asphalt binders and corresponding asphalt mastics provided by Dr. Bahia's group. The constructed master curve will serve as inputs to the self-consistent micromechanics models that were developed in previous quarters.

More FAM specimens with different levels of relative humidity will be tested using the controlled-stress RDT test. The crack growth in each specimen will be evaluated using the developed fatigue crack model.

References

- Lytton, R. L., 2004, "Adhesive Fracture in Asphalt Concrete Mixtures." Unpublished work.
- Marek, C. R., 1994, Tensile Behavior and Failure Characteristics of Asphalt Cements in Thin Films. *Proc.*, Association of Asphalt Paving Technologists, 37 (1968): 386-421.

Work element E1b: Binder Damage Resistance Characterization (DRC) (UWM)

Subtask E1b-1: Rutting of Asphalt Binders

Work Done This Quarter

Work completed during this quarter included estimation of modifier concentration for preparing modified binders with similar high-temperature PG. The research team also completed Repeated Creep and Recovery (RCR) and Multiple Stress Creep and Recovery (MSCR) testing of neat and plastomer-modified binder. The testing matrix included two replicates for each test type at 46 °C, 58 °C and 70 °C, and at stress levels of 100, 3200 and 10000 Pa. Also in this quarter, four binders (one neat and three modified) were used to prepare coarse and fine asphalt mixtures with limestone aggregates according to the gradations presented in previous quarterly reports. Duplicate mixtures were prepared to allow for replicates to be used for mechanical testing and imaging techniques to determine internal aggregate structure.

Significant Results

Significant results include the percent modifier required to produce binders with similar PG grades. After several trial blends to determine the nonlinear relationship between percent modifier and high-temperature grade, blends were identified to exhibit grades within ± 0.25 °C target high-temperature grade. The required percentage of each modifier and resulting grade can be seen in table E1b-1.1.

Table E1b-1.1. Percent modifier used and resulting high-temperature grade.

Modifier	Percent	True Grade (°C)
Elastomer	3.2	77.88
Plastomer	4.7	78.08
Ground Tire Rubber (GTR)	7.1	77.87

A helium pycnometer was used to determine the specific gravity (Gs) of each modifier to allow for the effective specific gravity of each modified binder to be determined and used in volumetric calculations for compacting to a targeted density. The specific gravity of each modifier is shown in table E1b-1.2.

Table E1b-1.2. Specific gravity of modifiers as determined by helium pycnometer.

Modifier	Specific Gravity				
	Rep. 1	Rep. 2	Rep. 3	Average	COV (%)
GTR	1.196	1.251	1.216	1.221	2.28
Elastomer	0.977	0.974	0.983	0.978	0.47
Plastomer	1.031	1.024	1.013	1.023	0.89

COV = coefficient of variation.

Initial analysis of RCR and MSCR test results appear reasonable and present noticeable trends that also match expectation. A partial representation of the results is shown in table E1b-1.3.

Table E1b-1.3. MSCR test result for unmodified binder.

T=46 °C				T=58 °C				T=70 °C			
Jnr (1/kPa)		%R		Jnr (1/kPa)		%R		Jnr (1/kPa)		%R	
R100	R3200	R100	R3200	R100	R3200	R100	R3200	R100	R3200	R100	R3200
0.088	0.087	23.449	22.997	0.749	0.779	8.651	5.319	4.281	4.572	1.636	0.258

Jnr = nonrecoverable creep compliance. %R = percent recovery.

To ensure accurate results and reliability of the Dynamic Shear Rheometer (DSR) machine intended to be used for the duration of this task, additional MSCR tests were conducted using two alternate machines. The results are very similar between equipment and ensure proper functioning of testing equipment. Table E1b-1.4 shows the summary of the results from three machines.

Table E1b-1.4. MSCR test results for neat binder with different machine.

MSCR	T=46 °C				T=58 °C				T=70 °C			
	Jnr (1/kPa)		%R		Jnr (1/kPa)		%R		Jnr (1/kPa)		%R	
	R100	R3200	R100	R3200	R100	R3200	R100	R3200	R100	R3200	R100	R3200
Bohlin	0.088	0.087	23.449	22.997	0.749	0.779	8.651	5.319	4.281	4.572	1.636	0.258
TA Instruments	0.094	0.093	25.947	24.999	0.757	0.814	12.540	5.944	4.434	4.752	3.264	0.545
Paar Physica	0.092	0.097	23.363	21.237	0.756	0.824	6.222	2.695	4.566	4.937	2.062	0.357

Flow number (FN) testing was conducted for both fine and coarse gradations of limestone using each of the four binders at stress levels of 344 and 1034 kPa. Mixture testing was conducted at a temperature of 46 °C. A summary of the test results for limestone mixtures is shown in table E1b-1.5.

Table E1b-1.5. Summary of FN results for limestone mixtures compacted to 7% air voids.

Sample	Stress (kPa)	
	344	1034
Neat-Coarse	450	100
Neat-Fine	730	150
GTR-Coarse	690	160
GTR-Fine	1575	240
Plastomer-Coarse	3000	210
Plastomer-Fine	50000	400
Elastomer-Coarse	1050	260
Elastomer-Fine	3150	430

Results show consistently that the fine gradation had a greater FN value than the coarse gradation for each of the binder types and at both stress levels. It should be noted that the coarse gradation was intentionally made to fit the extreme control point of the Superpave allowable gradation limits. Also, the FN values show consistent reduction when the stress level was increased. Contrary to what it is expected, the mixtures with plastomer modification exhibited higher FN values than those with elastomeric modification for all combinations of stress levels and gradations. These results suggest that the effect of plastomeric modification is the increase in total strain per cycle. In fact, the fine gradation with plastomeric binder did not exhibit tertiary flow within a 50000-cycle loading duration. The research team investigated the use of the creep rate in the secondary zone of the creep versus number of cycles curve as a parameter that better explains the differences observed between plastomeric and elastomeric binders.

An example of the results obtained from FN testing at 344 kPa is shown in figure E1b-1.1. As shown in the plots, the plastomer with coarse gradation is performing better than the elastomer with fine gradation. The plastomer with fine gradation lasted more than 50000 cycles without showing tertiary flow and is thus not shown in the plot.

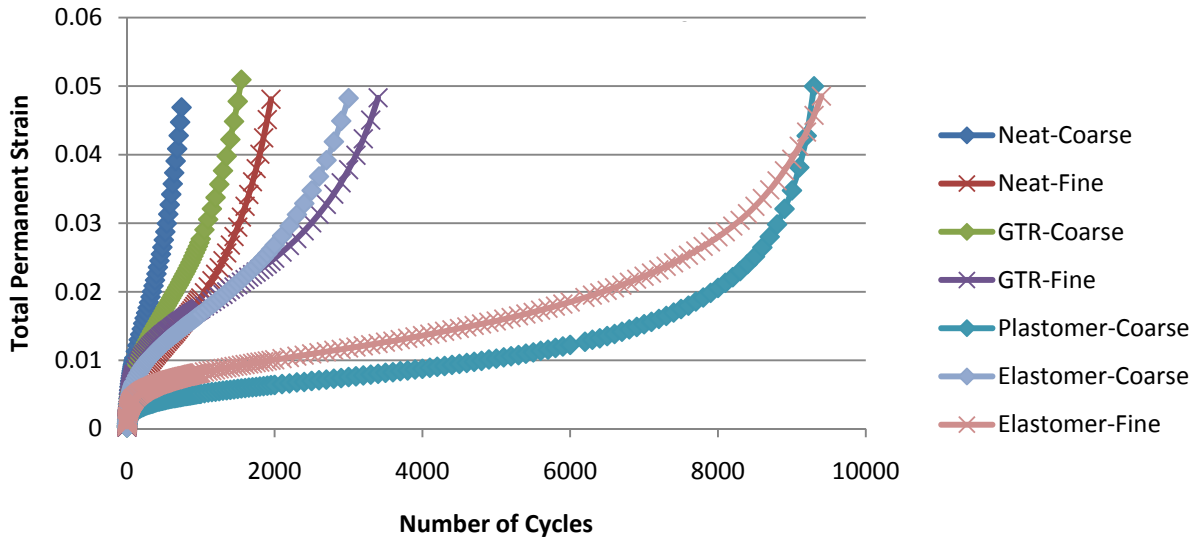


Figure E1b-1.1. Graph. FN results for limestone mixtures at 344 kPa.

It is also important to note that this work element is being conducted in collaboration with the Recycled Materials Resource Center on the University of Wisconsin–Madison campus. The GTR is included in this study as a recycled product that could have equal beneficial impact to the virgin polymers of an elastomeric and plastomeric nature. As shown in figure E1b-1.1, the GTR is not showing equivalent performance and thus new formulations will be considered.

Significant Problems, Issues and Potential Impact on Progress

Targeting a consistent air void content in preparation of limestone mixtures was difficult. More specifically, mixtures containing the GTR-modified binder resulted in samples with significantly low density and high air voids. The research team repeated the preparation of the GTR-modified samples; however, the low density and high air voids was still observed. Any mixtures tested at increased air voids would result in a falsely low FN. To account for this, additional GTR mixtures were prepared and compacted to an increased targeted density and checked. The target versus actual percent air voids did not appear entirely predictable and is thought to be caused by continued swelling of the rubber particles while the sample is at elevated temperatures from mixing and compacting. After several additional trial compactions, a corrected targeted density for both the fine and coarse gradation was determined and specimens resulting in the same overall air voids were compacted and tested. This has not significantly delayed progress, but required additional time spent on limestone mixes prior to preparation of granite mixtures.

Work Planned Next Quarter

Work for next quarter will focus on the following tasks:

- Complete RCR and MSCR testing of elastomeric and GTR-modified binders.
- Continued analysis of all binder results.

- Begin preparation of mastics with the neat and modified binders and conduct mechanical testing.
- Preparation of granite aggregates for mixture preparation (i.e., washing, sieving, batching) and mixing and compaction of granite mixes, along with cutting and coring for mechanical testing.

Subtask E1b-2: Feasibility of Determining Rheological and Fracture Properties of Asphalt Binders and Mastics using Simple Indentation Tests

Work Done This Quarter

The research team finished the modification of the new indentation test. Two new components were added to the previous system: a counterbalance system to improve contact and flexibility of loading, and an automatic data acquisition system to improve resolution of measurements. The new indentation/penetration device is shown in figure E1b-2.1.

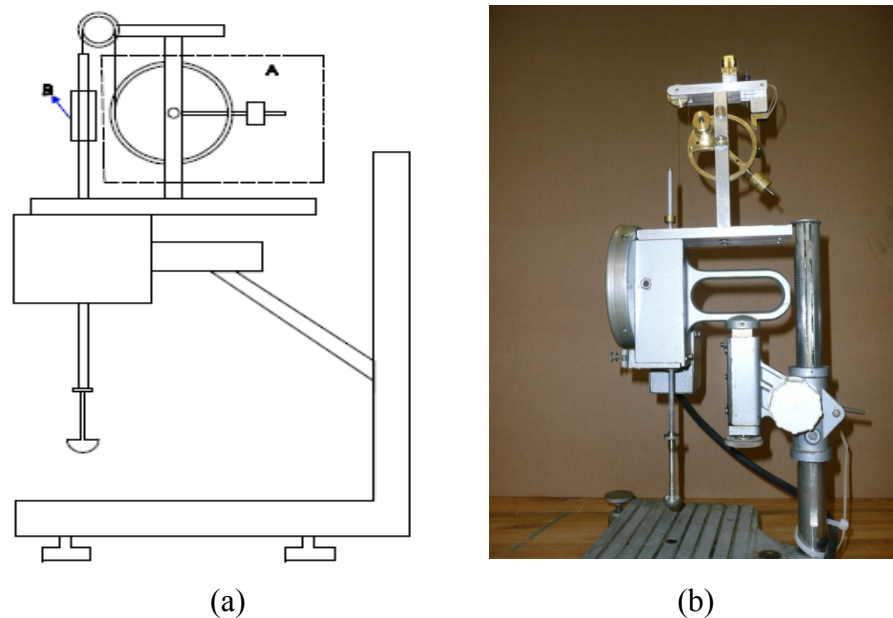


Figure E1b-2.1. Illustration and photograph. Modified indentation/penetration test components: (a) counterbalance system; and (b) magnetic encoder to measure displacements.

In the device, the indenter shaft is attached to a pulley system with counterweights, as shown in figure E1b-2.1(a), to allow the shaft with the indenter to float freely. Note that the preloading or initial contact issue is minimized with the addition of the pulley system.

The research team also continued efforts on developing a procedure to estimate the nonrecoverable creep compliance (J_{nr}) based on two approaches: fitting Burgers viscoelastic model and using multistep loading during the indentation test.

The finite element model for the penetration test with the needle was implemented in Abaqus to show the difficulties in estimating actual material properties from the complex stress field develop during the standard penetration test.

Significant Results

The pulley-counterweight system seems to improve the initial contact problem observed previously in indentation tests. Preliminary results for a typical set of asphalt binders indicate that the J_{nr} can be estimated from indentation measurements.

Significant Problems, Issues and Potential Impact on Progress

The delivery of the modified penetration device, which includes the pulley system and automated penetration sensors, was delayed due to availability issues of the electronic components. The research team is not expecting that this delay will impact the overall progress of the work element. The team will double efforts to test and implement the new penetration system to measure both rheological properties and J_{nr} of asphalt binders.

Work Planned Next Quarter

Work next quarter will focus on the following tasks:

- Test the repeatability and accuracy of the modified indentation/penetration device to measure rheological properties and J_{nr} of asphalt binders.
- Use the counterbalance system to test whether the initial contact of the indentation test is improved.
- Continue the collaborative effort with the University of Minnesota on the estimation of fracture properties of asphalt binders with indentation tests at low temperatures.

Work Element E1c: Warm and Cold Mixes

Subtask E1c-1: Warm Mixes

Work Done This Quarter

The asphalt lubricity test was further developed and applied by evaluation of the sensitivity of the asphalt binder coefficient of friction to testing conditions and changes in materials. The relevance of the asphalt lubricity test to overall mixture workability was also evaluated through statistical comparison between mixture workability models and measurements at compaction temperatures ranging from 90 °C to 135 °C. Results, which were summarized in a paper submitted for publication by TRB, indicate that asphalt binder lubricity significantly impacts mixture workability at lower compaction temperatures.

The potential performance implications due to both reduced production temperatures was also investigated through evaluating the impacts of reduced short-term aging temperatures on asphalt binder performance properties. Results indicate that aging temperature has the most significant impact on high-temperature binder PG. Flow number (FN) testing conducted at various mixture short-term aging temperatures confirmed that the reduced performance realized in the asphalt binder testing corresponds to a reduction in mixture rutting resistance indicators. Furthermore, strong correlations were observed between mixture performance and both the standard Superpave binder performance parameter ($G^*/\sin\delta$) and the nonrecoverable creep compliance (J_{nr}) from the Multiple Stress Creep and Recovery (MSCR) test. Results were summarized in a paper that was submitted to the Association of Asphalt Pavement Technologists (AAPT) for possible publication.

Coordination efforts continue with University of Nevada, Reno and the Wisconsin Department of Transportation (WisDOT). Work with UNR is focused on assessing the impact of warm mix asphalt (WMA) on moisture damage using mixture performance testing conducted at UNR and Bitumen Bond Strength (BBS) testing at UW–Madison. To date, 50% of the BBS testing is complete and mixture performance of the control HMA mixes has been completed. A work plan for field evaluation of WMA has been established with WisDOT; however, no WMA field projects were constructed in the third quarter of 2010. The research team continues to work with WisDOT to identify potential WMA projects and opportunities for ARC support.

Significant Results

To further develop the asphalt lubricity test procedure, sensitivity analysis of the controlled testing variables—testing temperature and speed—was conducted using conventional and WMA-modified asphalts. Specifically, the surfactant-based WMA additive was used in combination with both PG 64-22 and PG 76-22 asphalt binders for the study. Three testing temperatures (90 °C, 110 °C and 135 °C) and three testing speeds (10 rpm, 20 rpm and 40 rpm) were used in the study. Statistically significant differences in coefficient of friction were observed between testing temperatures of 90 °C and 110 °C. The effect of testing speed was deemed statistically insignificant. Based on these findings, the test procedure was finalized to include two testing temperatures (90 °C and 110 °C) and a testing speed of 20 rpm. The testing speed was selected because it provided the most consistent control of normal force. The sensitivity of the test to binder type and the presence of WMA additive are provided in figure E1c-1.1.

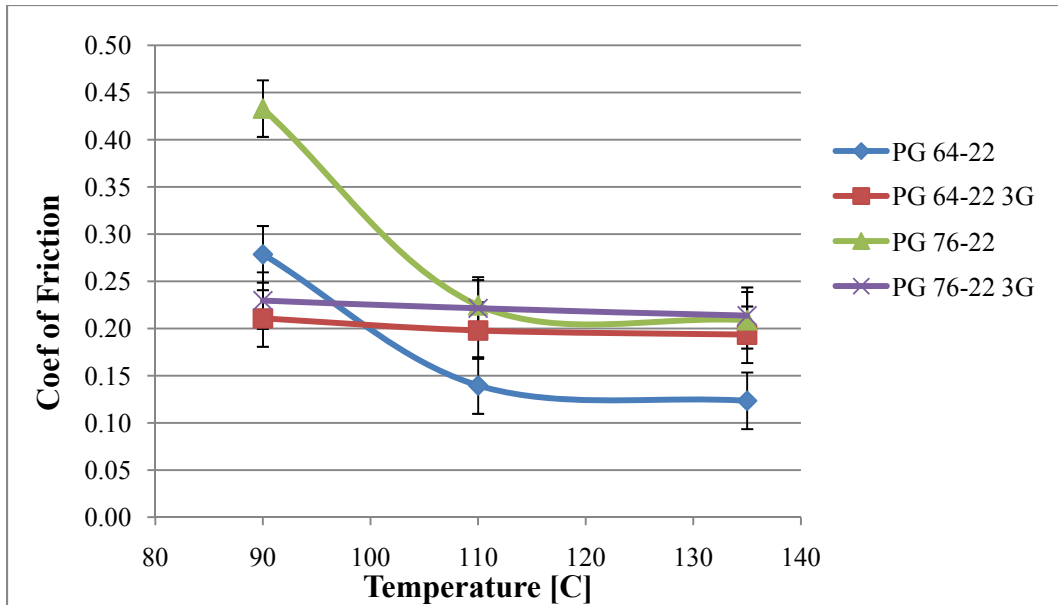


Figure E1c-1.1. Graph. Sensitivity of the asphalt lubricity test to testing temperature and material type.

Results are consistent with expectations, demonstrating logical relationships for both the effects of asphalt binder modification and the presence of WMA additives on asphalt binder workability. The use of a styrene-butadiene-styrene (SBS)-modified binder reduces binder workability across all temperatures, as evident by the higher values of coefficient of friction. The use of WMA additives reduces the temperature sensitivity of asphalt binder coefficient to friction. This finding is consistent with measurements presented using the torque measured by the Asphalt Workability Device (AWD), which found that negligible differences between HMA and WMA were not observed until lower temperatures (Austerman et al. 2009). Results are also consistent with data presenting the effects of WMA additives on mixture workability and its relationship with compaction temperature (Hanz et al. 2010).

The relationship between mixture workability and the coefficient of friction measured by the asphalt lubricity tests indicates that viscosity alone is inadequate to characterize the asphalt binder affect on mixture workability. This hypothesis was investigated through use of a regression model, including the lubricity parameter in conjunction with asphalt binder viscosity and mixture gradation in a regression model to predict measured mixture workability at the aforementioned compaction temperatures. Data were separated into two temperature ranges—90 °C to 110 °C and 110 °C to 135 °C—to represent WMA and HMA temperature regimes, respectively. Results of the regression analysis are presented in table E1c-1.1. Results indicate that across all temperatures, mixture gradation most significantly affects mixture workability. With respect to binder properties, viscosity is relevant in the HMA temperature regime, with coefficient of friction statistically significant as compaction temperatures are reduced to the WMA range.

Table E1c-1.1. Results of regression analysis predicting mix workability based on asphalt binder and mixture properties using separate temperature ranges.

Model CFI 90 -110					Model CFI 110-135			
Parameter	Coef	SE Coef	T	P	Coef	SE Coef	T	P
Constant	-639.3	97.9	-6.53	0.000	-401.9	63.0	-6.38	0.000
Friction	620.9	274.8	2.26	0.043	-62.9	236.8	-0.27	0.795
Viscosity	0.002	0.001	1.50	0.159	0.009	0.004	2.47	0.037
Beta	160.1	16.8	9.45	0.000	134.4	11.0	12.23	0.000
R²	91.8%				93.9%			

CFI = Construction Force Index.

Performance implications of the reduced short-term aging temperatures were investigated based on the recommendations of NCHRP 9-43 to estimate allowable reductions in production temperature associated with half and full reductions in the high-temperature PG (Bonaquist 2008). In developing these estimates, asphalt binder sensitivity to aging temperature and aging susceptibility were identified as relevant to performance. Experimental results demonstrate that both of these parameters are sensitive to asphalt binder source and the presence of WMA additives. Further work is needed to refine this relationship. The detrimental effect of reduced aging temperature to high-temperature binder performance grade is also observed in mixture resistance to permanent deformation.

Values of FN at different aging temperatures obtained using the repeated load deformation test are provided in figure E1c-1.2. Preliminary results indicate that short-term aging temperatures significantly impact mixture performance, necessitating the consideration of establishing a minimum production temperature to ensure adequate performance of WMA.

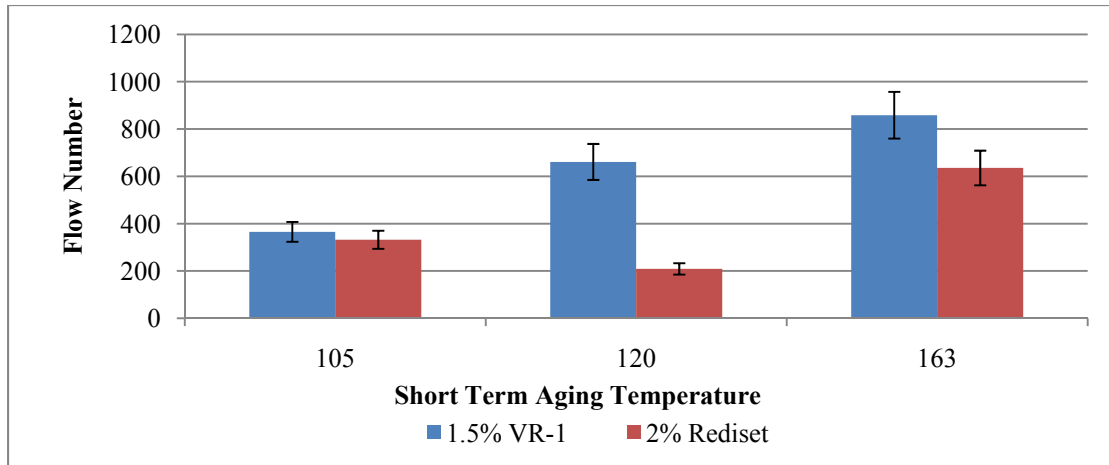


Figure E1c-1.2. Graph. Impacts of reduced aging temperatures on mixture FN.

Significant Problems, Issues and Potential Impact on Progress

The asphalt binder lubricity testing fixture was unavailable for 66% of the quarter because the mixture needed to be remachined due to failure of the threads in the testing cup. The fixture is also being redesigned to ensure that no eccentricity exists when the normal force is applied for testing. The research team will proceed with testing to get back on schedule in the next quarter.

Field validation has been delayed due to lack of WisDOT WMA projects. The research team hopes that two to three projects will be constructed in the 2010 construction season.

The original Gantt chart has been revised to reflect continued work on both tasks focused on capturing the impacts of WMA on asphalt binder performance and binder/mixture workability. These extensions represent efforts to develop a standard test method for the lubricity test and incorporation of aging considerations into evaluation of the impacts of WMA on asphalt binder performance.

Work Planned Next Quarter

The following activities are planned for next quarter:

- *Asphalt binder/mixture workability.* Continue development of the asphalt lubricity test, including establishment of precision/bias and investigating the effect of rolling thin film oven (RTFO) aging on response of the test. Test will be expanded to other classes of WMA additives.
- *Impacts of WMA on performance.* Work will continue in investigating the impacts of reduced aging temperatures on both asphalt binder and mixture performance. Aging temperatures and material types used will be expanded to refine aging models used to estimate minimum production temperatures. UW–Madison will continue to work with UNR to quantify the impacts of WMA additives and reduced production temperatures on moisture damage.

- *Field validation.* The research team will continue to pursue field projects to implement the field validation plan developed in 2010 Q2.

Cited References

Austerman, A. J., W. S. Mogawer, and R. Bonaquist, 2009, “Evaluating the Effects of Warm Mix Asphalt Technology Additive Dosages on the Workability and Durability of Asphalt.” Presented at 88th Annual Meeting of the Transportation Research Board, Washington, D.C.

Bonaquist, R., October 31, 2008, NCHRP 9-43: Mix Design Practices for Warm Mix Asphalt. Interim Report, National Research Council, Washington, D.C.

Hanz, A., A. Faheem, E. Mahmoud, and H. U. Bahia, 2010, “Measuring Effects of Warm Mix Additives Using a Newly Developed Binder Lubricity Test for the DSR.” Presented at 89th Annual Meeting of the Transportation Research Board, Washington, D.C.

Subtask E1c-2: Improvement of Emulsions’ Characterization and Mixture Design for Cold Bitumen Applications

Work Done This Quarter

Work this quarter focused on evaluating construction properties of emulsions and laboratory measurement of chip seal performance. Emulsion procedures and tests included the ASTM D7000 sweep test, viscosity and residue recovery. A study of the sweep test focused on identifying test conditions and material properties that significantly affect aggregate retention. Variables considered in the experiment included aggregate gradation, aggregate mineralogy, emulsion application rate, emulsion type and curing time.

Emulsion viscosity was evaluated using the Brookfield rotational viscometer (RV) fitted with a No. 21 spindle to evaluate the effects of temperature, time and shear rate on emulsion viscosity. Six emulsion types commonly used in Wisconsin for sprayed surface seals were tested at 50 °C and 80 °C at five shear rates ranging from 4.65/sec to 97.65/sec, corresponding to rotational speeds between 5 rpm and 105 rpm. The effect of modification on emulsion viscosity was also analyzed at each temperature.

Researchers recovered the residue for all six emulsion samples collected from the field using a thin film evaporative recovery method, specifically “Standard Practice for Recovering Residue from Emulsified Asphalt Using a Low Temperature Evaporative Technique: Method B” (ASTM 2010). Performance properties of these residues will be evaluated according to specification framework developed in conjunction with the Emulsion Task Force. The research team continues to actively participate with this working group and made two presentations at the most recent meeting held on July 26-27 in Boston, Mass. The research team also helped with finalizing a draft AASHTO standard that was approved by the AASHTO Subcommittee on Materials for balloting in their August meeting.

Significant Results

Researchers used the sweep test to investigate which factors affect early chip seal performance in terms of aggregate retention. The significance of the experimental variables was determined using analysis of variance (ANOVA) at an alpha value of 0.05. The variables included curing time, aggregate type, emulsion type and aggregate gradation. Emulsion application rate was not deemed a significant factor. Results and analysis indicate that if correlations between sweep test results and field performance can be identified, early aggregate loss could be reduced by considering these options:

- Following the work in NCHRP 14-17, establishing a relationship between curing time and moisture loss to provide a link to the field to define appropriate timing for opening to traffic.
- Implementation of design procedures that allow for selection of project aggregates and emulsions based on compatibility and selection of aggregate gradations based on anticipated emulsion application rates.

The effects of aggregate mineralogy and emulsion type on aggregate retention are demonstrated in figure E1c-2.1. Results show that limestone aggregates perform better than granite with all three emulsions tested. Granite performs well with the CRS-2 emulsion compared to HFRS-2 and HFRS-2L emulsions. Furthermore, modification of the HFRS-2 binder with latex does not appear to improve the performance of granite. With respect to curing time, CRS-2 performs better than HFRS-2 and HFRS-2L at 2 and 6 hours curing time. The HFRS-2L emulsion demonstrated a lower aggregate loss compared to HFRS-2 at 6 hours curing time. This improvement in aggregate retention can be attributed to the latex modification.

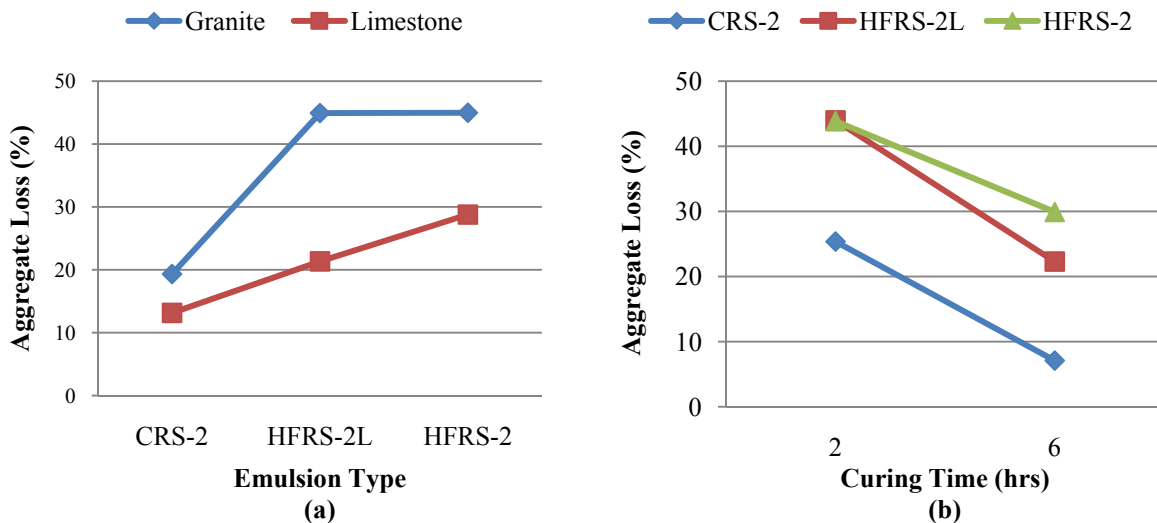


Figure E1c-2.1. Graphs. Effect on aggregate loss of: (a) aggregate type; and (b) curing time.

Emulsions and testing conditions for viscosity measurements are provided in table E1c-2.1. To ensure that a steady-state viscosity has been achieved prior to testing, the material is subjected to a constant shear rate of 46.5/sec for 20 to 30 minutes to allow a steady-state viscosity to be reached. The lower equilibration time was required for the 80 °C testing temperature.

Table E1c-2.1. Experimental factors and levels for RV testing.

Factors	Levels
Emulsion Type	HFRS-2, HFRS-2P, HFRS-2L, CRS-2, CRS-2P, CRS-2L
Temperature (°C)	50, 80
Shear Rate (1/second)	4.7, 27.9, 51.2, 74.4, 97.7
Spindle	No. 21

Testing temperatures were selected to represent temperatures during storage (80 °C) and after spraying (50 °C). In evaluating emulsion viscosity, the research team has identified shear sensitivity and viscosity at high and low shear rates as potentially relevant parameters. In the field, shear sensitivity relates to the possibility that emulsion viscosity could drop significantly during handling and spraying, leading to drain-down upon application to the pavement surface. Experimental results show that all emulsions exhibit non-Newtonian behavior at 50 °C and 80 °C. The results for the shear susceptibility of the six emulsions tested at both temperatures are given in figure E1c-2.2. Shear susceptibility is defined as the ratio of viscosity at a low shear rate to the viscosity at a high shear rate.

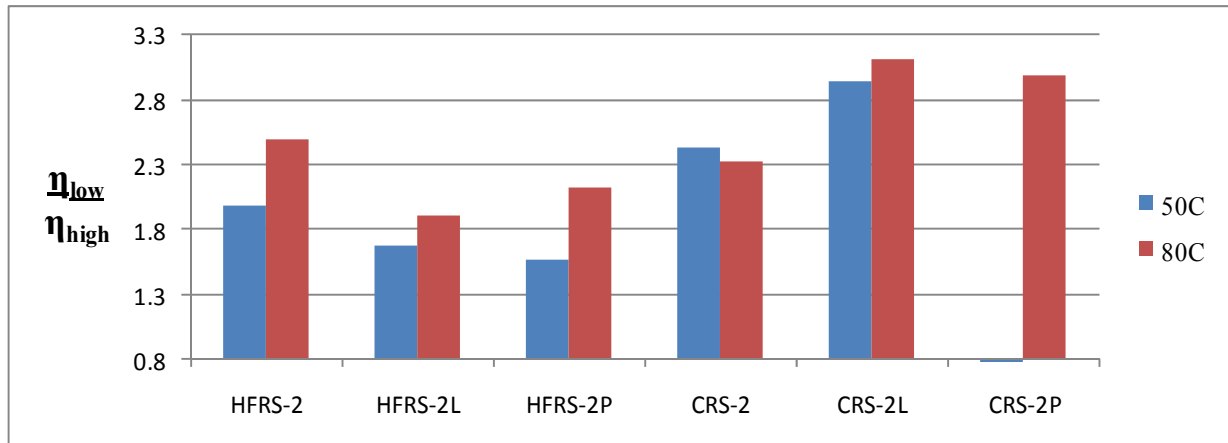


Figure E1c-2.2. Chart. Shear susceptibility at temperatures of 50 °C and 80 °C for six emulsions.

For the anionic emulsions, higher shear susceptibility was observed at the 80 °C testing temperature, especially for the HFRS-2 and HFRS-2P systems. This result indicates there is potential for the HFRS series emulsions to experience decreases in viscosity during pumping or

handling. No effect of temperature was observed for the cationic emulsions. However, these materials displayed differing shear sensitivities. The CRS-2 exhibits shear susceptibility similar to the HFRS series products, with modification causing an increase in shear sensitivity. Small chunks of polymer were observed in the CRS-2P system; as a result, testing at 50 °C consistently exceeded the torque capability of the machine. The comparison of values of viscosity at a shear rate of 4.6/sec (5 rpm) and 74.4/sec (80 rpm) for 50 °C and 80 °C testing temperatures is provided in figure E1c-2.3.



Figure E1c-2.3. Chart. Viscosity at a shear rate of 4.65/sec at temperatures of 50 °C and 80 °C for six emulsions.

In field application, it is hypothesized at high temperatures and high shear rates that low viscosity is desired for more uniform spraying. Conversely, the low-temperature/low-shear-rate properties represent the material at rest after spraying; under these conditions, high emulsion viscosity is desired because it allows for the material to maintain a uniform film thickness during curing. Results presented in figure E1c-2.3 demonstrate significantly differing results for both conditions, with the cationic emulsions demonstrating more favorable properties.

Investigation of the relationship between viscosity and shear rate revealed differing effects of temperature for the HFRS and CRS series emulsions. The anionic emulsions followed a logical trend, with an increase in testing temperature leading to a slight decrease in viscosity. Conversely, viscosity values of cationic emulsions are significantly higher at 80 °C than at 50 °C, indicating that there is potential that the emulsion is breaking. This finding was substantiated earlier in a study by Salomon and Palasch, who found that at testing temperatures higher than 60 °C the viscosity of cationic emulsions increases because the emulsion begins to break (Salomon and Palasch 2002). Preliminary results are promising in demonstrating sensitivity of emulsions to both temperature and shear susceptibility; however, the results for the cationic emulsions indicate that further development of the testing procedure is needed.

Three replicates at each testing condition were collected. In general, results exhibit both reproducibility and repeatability. Measurements of steady-state viscosity generally exhibit low variability, with a coefficient of variation (COV) of 5% or less observed for each replicate. The reproducibility of the steady-state condition is also acceptable, with COVs typically less than 15% percent. Of 36 samples tested, 30 samples demonstrate a COV less than 15%. High variability (COV > 15%) is observed for the three cationic emulsion samples at a variety of shear rates. This higher variation confirms that modification to the testing or sample handling procedures for CRS-2 emulsions may be necessary. Data were collected at the end of the quarter; further analysis is needed to draw conclusions.

Significant Problems, Issues and Potential Impact on Progress

Components used in the Bitumen Bond Strength (BBS) test malfunctioned during the quarter, which limited adhesion testing. The issue has since been resolved and BBS testing is expected to continue in the next quarter.

Preliminary results of viscosity testing indicate that, for cationic emulsions, modification to the procedure is needed to obtain repeatable results. Also, there is a potential that a smaller spindle size is required for evaluation of emulsions containing small polymer particles in the fluid.

To date work has focused on development of selection of appropriate performance tests for chip seals. The research team plans to implement the test matrix developed in the next quarter. As a result, delays have occurred in selecting and validating performance guidelines. Emulsion characterization for chip seals has been identified as a research need by the Emulsion Task Force, causing minor delays in developing design methods for cold mix applications. It is expected effort expended on cold mixes will increase in upcoming quarters.

Work Planned Next Quarter

Work next quarter will focus on the following tasks:

- *Emulsion construction properties.* BBS testing will continue on all emulsions received from the field. Analysis will continue on collected viscosity data.
- *Emulsion residue properties.* Testing will be conducted on the residues of the six emulsions evaluated for viscosity.
- *Field testing.* The research team will attempt to work with a local contractor to evaluate chip seal field performance.
- *Cold mix asphalt.* The research team will coordinate testing activities with UNR.
- *ARC Project Advisory Group and Emulsion Task Force activities.* The research team will continue to hold advisory group meetings and support Emulsion Task Force activities.

Cited References

ASTM, 2010, Standard Practice for Recovering Residue from Emulsified Asphalt Using a Low Temperature Evaporative Technique. American Society of Testing and Materials. West Conshohocken, PA. Draft procedure currently under review.

Salomon, D., and M. Palasch, 2002, "Kinetic Properties of Emulsified Asphalts." Technical Bulletin, Idaho Asphalt Supply Inc. Accessed 6/28/2010, <http://www.technopave.com/publications/Kinetic-Properties-of-Emulsified-Asphalts-May-2002.pdf>.

CATEGORY E2: DESIGN GUIDANCE

Work element E2a: Comparison of Modification Techniques (UWM)

Work Done This Quarter

The research team continued testing the binders included in the material library developed for this work element. This library includes 17 binders from six sources, five base binder grades and 12 modified binder grades. Tests performed to date include rheological measurements using the Dynamic Shear Rheometer (DSR) according to AASHTO TP5, Multiple Stress Creep and Recovery (MSCR) tests according to ASTM D7405-08a, Binder Yield Energy Test (BYET), frequency sweep testing, Single-Edge Notched Bending (SENB) testing, and Bending Beam Rheometer (BBR) testing. The collected binders were also tested after aging according to laboratory aging techniques such as rolling thin film oven (RTFO) (AASHTO T240) and pressure aging vessel (PAV) (AASHTO R28).

Table E2a.1 shows the progress in testing the binders included in the material library. As shown in table E2a.1, no work was performed on the binders marked D1 and D2 due to the fact that the research team had difficulties in obtaining this material. The manufacturer did not reply to several requests from the team regarding this binder. The research team decided to replace this material with a binder having the same PG grade.

Significant Results

An example of the SENB test results tested at -12 °C is shown in figure E2a.1. The results shown reveal that the SENB test can discriminate between different binders and between different modification types. The low-temperature parameters obtained from SENB testing are:

- Energy at fracture (i.e., defined as the area under the force-displacement curve at maximum force (mNmm).
- Maximum load (mN).
- Displacement at maximum load (mm).

Table E2a.1. Testing matrix update.

Binder Label	BYET		MSCR		Frequency Sweep		SENB @ 2 temp		BBR @ 2 temp	
	RUN1	RUN2	RUN1	RUN2	RUN1	RUN2	RUN1	RUN2	RUN1	RUN2
A0	X	X	X	X	X	X	X	X		X
A1	X	X	X	X	X	X	X	X	X	X
A2	X	X	X	X	X	X	X	X	X	X
A3	X	X	X	X	X	X	X	X	X	X
A4	X	X	X	X	X	X	X	X	X	X
B0	X	X	X	X	X	X	X	X	X	X
B1	X	X	X	X	X	X	X	X	X	X
B2	X	X	X	X	X	X	X	X	X	X
C0	X	X	X	X	X	X	X	X	X	X
C1	X	X	X	X	X	X	X	X	X	X
C2	X	X	X	X	X	X	X	X	X	X
D0	X	X	X	X	X	X	X	X	X	X
D1										
D2										
E0	X	X	X	X	X	X	X	X	X	X
E1	X	X	X	X	X	X	X	X	X	X
E2	X	X	X	X	X	X	X	X	X	X

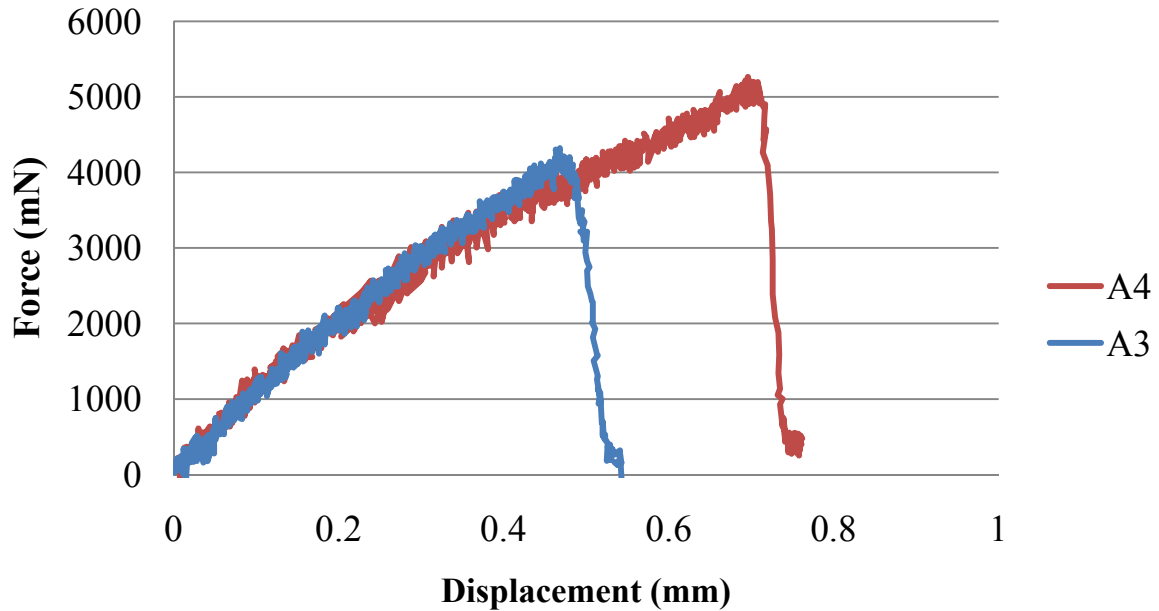


Figure E2a.1. Graph. Typical results from SENB testing.

Fracture energies at -12 °C and the error bars for the base binder A are shown in figure E2a.2. As revealed by the error bars, good repeatability between replicates is obtained for all binders.

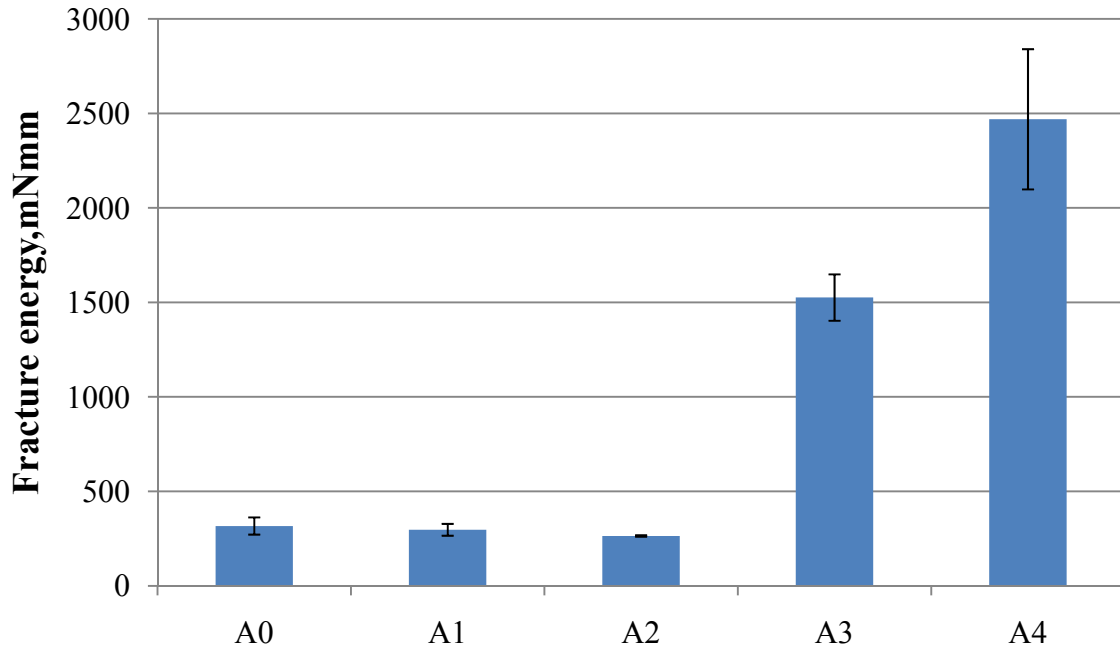


Figure E2a.2. Chart. Fracture energy for A-based binder at -12 °C.

Figure E2a.3 shows the normalized values for the fracture energy at different temperatures for the tested binders. The normalized values correspond to the energy of fracture of the modified binder divided by that for the corresponding neat binder at a specific temperature.

The results presented in figure E2a.3 indicate that modification has different effects on the low-temperature fracture properties of the binder. For example, the A1 and A2 binders show a decrease in the fracture energy compared with the A0 binder at -12 °C. For this case, the polymer used for modification has a negative effect on the fracture properties. Another important observation is that the amount of modifier affects the fracture properties of the binder. Note that the polymer used in A3 and A4 binders increases the fracture energy significantly in comparison to the fracture energy of the neat binder. With the exception of A1, all the modified binder performs better than the unmodified binder at -18 °C.

The asphalt source seems to significantly affect the fracture properties. For example, A3 and A4 binders have the same PG grade as E1 and E2 binders. The unmodified binder in both cases was graded as a PG 64-22 and the same polymer was used for modification. But as can be seen in figure E2a.3, different fracture energies are obtained for the binders are modified with same additives.

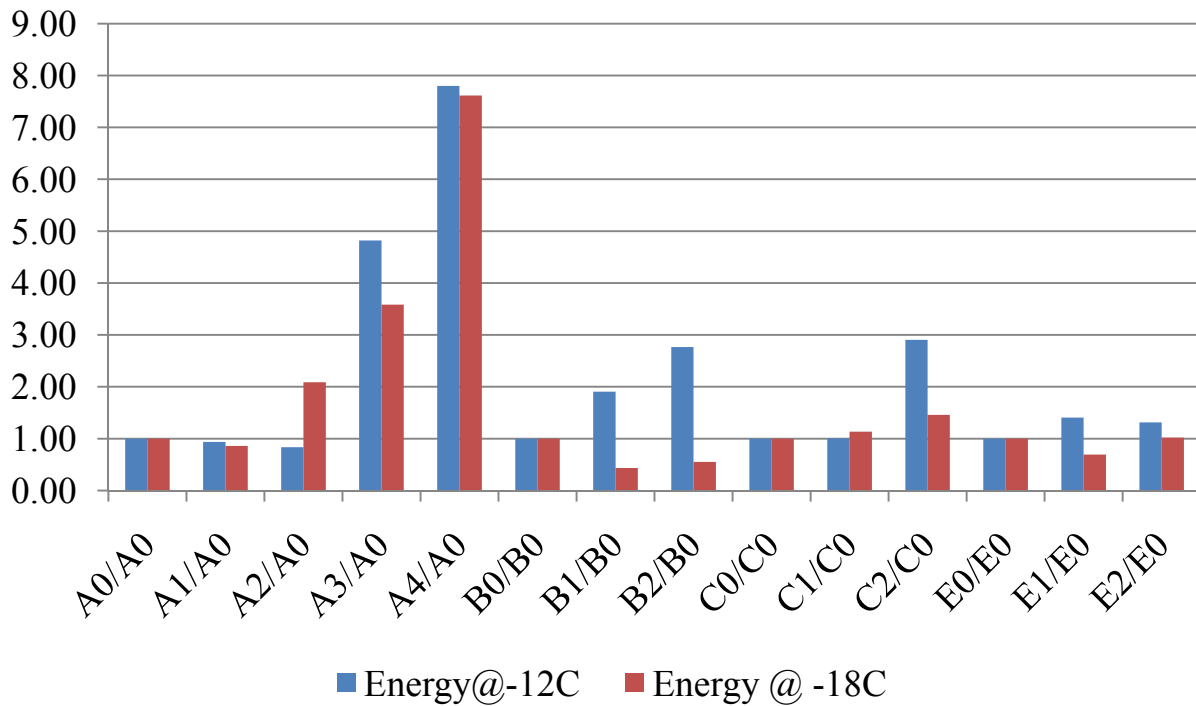


Figure E2a.3. Chart. Normalized values of fracture energy at different temperatures from SENB.

The relationship between the fracture energy and stiffness and (m) value measured with the BBR at -12 °C is shown in figures E2a.4 and E2a.5, respectively. As shown in these figures, poor relations between fracture energy and BBR results are observed. These trends clearly show that for modified binders the SENB is needed to measure failure properties that cannot be estimated from the BBR test.

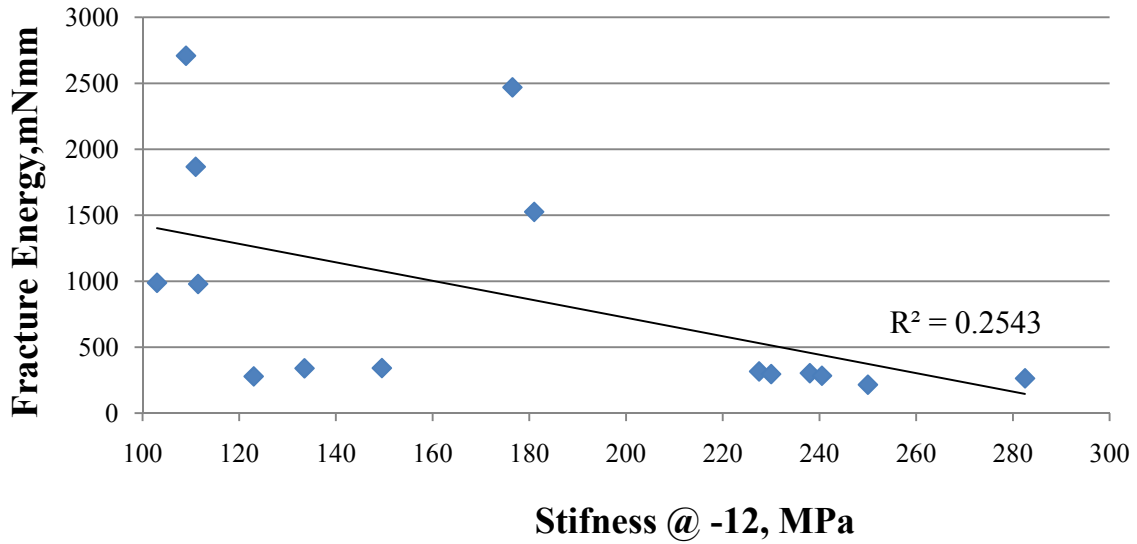


Figure E2a.4. Graph. Fracture energy versus stiffness at -12 °C.

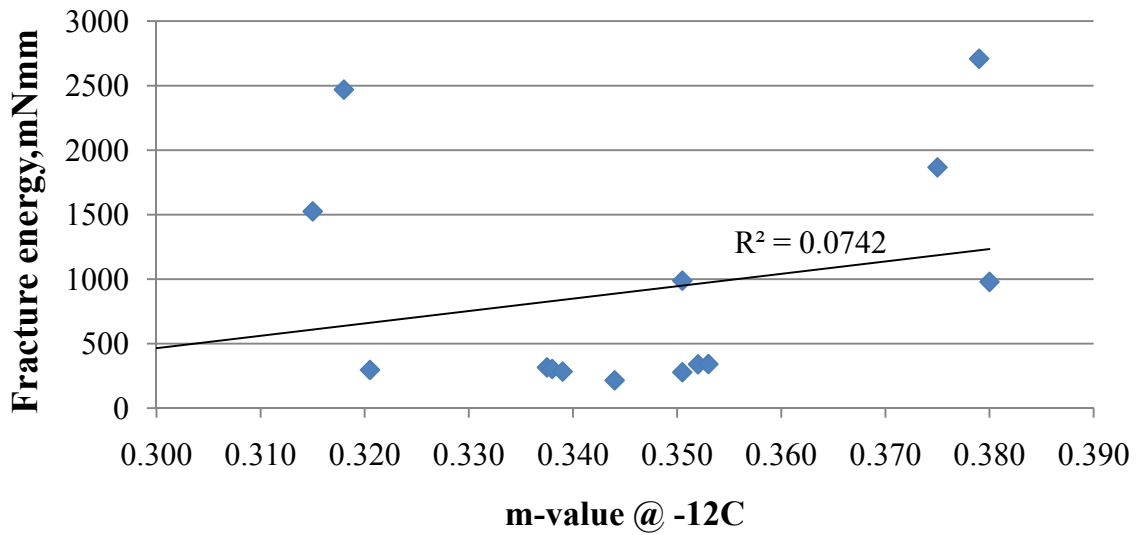


Figure E2a.5. Graph. Fracture energy versus m-value at -12 °C.

The Gantt chart for this work element was updated to reflect that a presentation on the research findings has been rescheduled from July 2010 to January 2011. It will be presented in conjunction with the 90th TRB Annual Meeting.

Significant Problems, Issues and Potential Impact on Progress

None.

Work Planned Next Quarter

Work for next quarter will focus on analyzing experimental data and on completing the test matrix presented in table E2a.1.

Work element E2b: Design System for HMA Containing a High Percentage of RAP Materials (UNR)

Work Done This Quarter

This work element is a joint project between University of Nevada, Reno and University of Wisconsin–Madison. The recycled asphaltic material (RAM) binder analysis procedure developed in previous quarters was further verified and applied to several new cases of recycled asphalt pavement (RAP), recycled asphalt shingles (RAS), and RAP/RAS combinations to demonstrate variability and impacts on binder properties. The verification procedure outlined in the ARC Q2 2010 quarterly report was used to evaluate the quality of the estimate of high-, intermediate-, and low-temperature true grade estimates using the RAM binder analysis procedure. Very good matches for low and intermediate true grade temperatures were obtained, but inconsistencies were observed for high-temperature measurements. As a result, sensitivity analysis was conducted to identify factors contributing to the discrepancies observed. In addition, the procedure was applied to differing RAP and base binder sources, including modified binders. To confirm that the procedure applies for RAP/RAS blends, multiple combinations of RAP and RAS blends were used to develop a chart for PG versus % RAP + % RAS binder profile.

Initial testing was started for fracture properties of the RAP mortars using the Single-Edge Notched Bending (SENB) test. Specifically, samples containing a defined percentage of RAP binder were tested at decreasing temperatures to establish effects of RAP binders on low-temperature fracture properties of fresh binders.

Under subtask E2b-5, extracted/recovered asphalt binders from the Manitoba PTH8 field-produced and lab-produced mixtures are being tested to determine their rheological properties. Additionally, all mixes were evaluated in terms of their dynamic modulus and their resistance to thermal cracking using the TSRST test. Additionally, the moisture resistance of the various mixtures was evaluated at multiple freeze-thaw cycles. The dynamic modulus data is being used to backcalculate the properties of the blend asphalt binders using the Hirsh model and the Huet-Sayegh model. Additionally, the developed recycled asphaltic material (RAM) binder analysis was applied to the RAP material from Manitoba. A paper summarizing the current findings was submitted to TRB for the 2011 annual meeting. The paper got accepted for presentation at the annual meeting and was recommended for publication in the journal of the TRB.

UNR has been working with Granite construction in Utah to collect material for the RAP mixing experiment.

Significant Results

The verification procedure outlined in the 2010 Q2 quarterly report for the developed RAM binder analysis procedure was applied using a higher percentage of RAP to allow for better validation. The validation procedure included comparing the measured continuous grade of the blended binder to the estimate from the analysis procedure involving artificial RAP mortars. The artificial RAP was produced by mixing the P₅₀/R₁₀₀ fraction (passing No. 50 sieve and retained on No. 100 sieve) aggregate material with binder aged for 40 hours in the pressure aging vessel (PAV) at an asphalt content of 10.5%. The asphalt content selected is similar to the observed values in the P₅₀/R₁₀₀ fraction of conventional RAP material. Estimates of high-, intermediate-, and low-temperature PG continuous grades for the twice PAV-aged “artificial” RAP binder-fresh binder blend were obtained using the test procedure detailed in the ARC Q2 2010 quarterly report. The artificial RAP and fresh binder sources used in this verification step is identical to the Case I scenario presented in the previous quarter:

Case I: *Artificial RAP_A + PG 64 – 22 fresh binder*

where

Artificial RAP_A = 40-hour PAV-aged PG 64-22 binder + R₁₀₀ aggregate from Reno, Nevada, mixed at a 10.5% total asphalt content

The accuracy of the estimate was evaluated through direct measurement of the continuous grade of a blend of fresh binder and a given concentration of twice PAV-aged binder. The aged binder concentration was increased from 15% to 25% for evaluation of intermediate- and low-temperature properties, while high-temperature properties were measured using a concentration of 20%. Results of the comparison of estimated values with the direct measurements collected using the physically blended binders are summarized in table E2b.1. Also shown in the table are the original verification values for Case I at 15% RAP binder for comparison purposes.

At low temperatures, the analysis procedure appears to predict the blended binder continuous grade with the same degree of accuracy independent of percent RAP binder present. The analysis procedure also tends to provide conservative estimates of the blended binder continuous grade. At intermediate temperatures, increasing the amount of RAP binder present in the mortars, and hence in the testing samples, appeared to increase the accuracy of continuous grade estimation in the analysis procedure. It is hypothesized this difference exists because of the relatively small binder sample used for testing in the 8-mm Dynamic Shear Rheometer (DSR) geometry (approximately 1 gram). With this small quantity, increasing the concentration of RAP binder present allows for a sample with properties more representative of those observed in an actual RAP binder. Additional testing is needed in the DSR to further establish this finding.

Table E2b.1. Low- and intermediate-temperature verification results.

Low Temperature					
	Test Temp. [°C]	Binder Replacement	Estimated Continuous Grade [°C]	Measured Continuous Grade [°C]	Difference [°C]
Case I	-6	15%	-18.87	-19.18	0.31
	-12				
Case I	-6	25%	-20.43	-21.05	0.62
	-12				
Intermediate Temperature					
	Test Temp. [°C]	Binder Replacement	Estimated Continuous Grade [°C]	Measured Continuous Grade [°C]	Difference [°C]
Case I	25	15%	19.72	21.62	1.90
	28				
Case I	25	25%	23.85	24.28	0.43
	28				

Verification results presented in the ARC Q2 2010 quarterly report demonstrated that high-temperature testing yielded poor approximations of the blended binder continuous grade; differences between the estimated and measured blended binder continuous grade were found to range from approximately 3.5 °C to 6 °C. As discussed previously, different geometries were tried to address this problem; as a result of these trials a geometry utilizing the 25-mm plate at a 2-mm gap was selected for further study. Results for Case I using 20% RAP binder using this geometry indicate that discrepancies between estimated and measured high-temperature continuous grade still exist. In addition to the gap setting, several other factors were tested in an attempt to resolve this issue, including: conditioning time of the blended mortar samples was increased to allow more complete blending of the RAP and fresh binders; the fresh binder source was changed to isolate potential blending chemistry problems; aggregate gradation was tested after the ignition oven to isolate potential aggregate effect; and total asphalt content was increased to assure no aggregate interlock was occurring. The results of the sensitivity analysis are presented in table E2b.2.

Table E2b.2. Sensitivity analysis for high-temperature verification.

Original Difference in Continuous Grade*:		3.84		
Difference in Continuous Grade*				
Gap Setting	Conditioning Time	Blend Chemistry	Asphalt Gradation	Content
3.12	3.12	3.72	Negligible	2.97

* Difference in measured and estimated (analysis procedure) blended binder continuous grade.

It was found that increasing the total asphalt content from about 35% to 50% produced a smaller difference between estimated and measured continuous grade values. Further testing at higher asphalt contents is currently underway to examine this trend further. However, increasing the total asphalt content causes the maximum RAP binder estimation value to decrease; very high asphalt content samples (approximately 45% to 50% or greater) allow for approximately 5% RAP binder estimation, limiting the practicality of the procedure. The research team continues to explore alternative procedures.

Testing was completed for multiple binders and RAP sources to help establish the sensitivity of the procedure to changes in materials. Four RAP sources were blended individually with each of two fresh binder grades—a PG 58-28 and PG 64-22. Individual RAP sources were blended with fresh binders at the same total RAP binder content in mortar for both binder grades. Since RAP sources vary in binder content, they were mixed at varying percentages with fresh binders, as shown in table E2b.3.

Table E2b.3. Sensitivity analysis of characterization procedure.

RAP Source	RAP Binder Percent [%]	Fresh Binder Grade	Continuous Grade (°C)		Grade Change Rate (Degree / % RAP)
			Fresh Binder	Blended Binder	
E.B.	25.17	58-28	-28.6	-17.6	0.44
		64-22	-22.0	-18.9	0.12
J.H.	19.75	58-28	-28.2	-24.0	0.21
		64-22	-19.8	-16.3	0.18
R.R.	15.00	58-28	-31.4	-22.8	0.57
		64-22	-25.4	-17.6	0.52
P.B.	15.28	58-28	-30.6	-25.8	0.31
		64-22	-21.4	-17.6	0.25

The analysis shows that binders in RAP sources have varying effects as evidenced by differing rates of change in PG grade per RAP within the same RAP source, as well as among different RAP sources. In other words, each RAP-fresh binder combination produces a unique grade change rate result. Based on these results, the traditional “tiered” approach to RAP mix design, which groups all RAP sources and binder performance grades together, may not accurately capture the effect of RAP binder on the final blended binder grade.

This analysis also confirms that the testing procedure is not dominated by RAP or fresh binder source. The output is sensitive to the properties of both the RAP binder and the fresh binder.

The analysis procedure was also applied to RAS and RAP blends to test linearity in the PG/% RAP binder profile. Only one RAS source and one RAP source were used to make two blends at varying proportions. The initial results indicated strong linearity in effect of RAS and RAP on blended binder.

Table E2b.4 summarizes the findings for the two RAP and RAS blends. The measured low-temperature continuous grade was calculated from actual Bending Beam Rheometer (BBR) testing, while the estimated continuous grade was determined by applying a linear relationship between the results of testing RAS alone (mixed with fresh binder) and RAP alone (mixed with a fresh binder). Both were tested using the standard analysis procedure for RAP described earlier. The differences in continuous grade values indicate a linear relationship exists; however, further testing on a wider range of materials is needed.

Table E2b.4 RAP and RAS blend testing.

Blend	% RAP Binder	% RAS Binder	% Fresh Binder	Low-Temperature Continuous Grade [°C]		Difference [°C]
				Measured	Calculated	
1	8.7	8.0	83.2	-26.8	-24.8	2.08
2	14.6	13.5	71.9	-21.8	-21.0	0.82

The analysis of the data for the RAP mixtures from Manitoba shows that mixtures with 50% RAP resulted in acceptable resistance to moisture damage with a better resistance for the mixture with PG52-34 (i.e., Pen 200-300) asphalt binder. The observed difference in the mixtures' resistance to moisture damage has to do more with the compatibility of the PG52-34 virgin asphalt binder with the RAP binder. The mixtures with 50% RAP exhibited an acceptable resistance to thermal cracking as measured with the TSRST with again a better resistance for the mixture with PG52-34 asphalt binder. The monitoring of the field performance will help validating the findings of this study and hopefully explain the difference between the TSRST fracture temperatures and the recovered asphalt binders' critical low temperatures of the 50% RAP mixes.

Regardless of the RAP content, the Superpave procedure of 4 hours at 275°F in a forced draft oven did not simulate the aging of the field-produced mixtures. Overall, all test results showed that laboratory-produced mixtures can be used to evaluate the relative resistance of the field-produced mixtures to moisture damage and thermal cracking. However, some differences in the measured values were observed between the field-produced and laboratory-produced mixtures which may require the adjustment to any criteria used.

Significant Problems, Issues and Potential Impact on Progress

Work continues to modify SENB test procedures to allow for more repeatable measure of fracture properties of RAP mortars. Delays in evaluation of high-temperature properties have occurred due to the inability of the estimation procedure to accurately predict measured results. Testing continues to improve this procedure.

The sampling of the material from Granite Construction in UTAH for subtask E2b-3 has been delayed because of no Production of Superpave mixes. It is anticipated that material will be received by UNR by the end of October 2010. The work progress is reflected on the Gantt chart.

Under subtask E2b-1.a, there has been some delay in the AIMS testing for the Alabama and Florida aggregates. NCAT is working on completing the testing.

Work Planned Next Quarter

A summary report for the PG analysis procedure will be completed and include concluding remarks regarding the verification procedure. A work plan will be developed for workability testing of high-percentage RAM mixes to further validate the analysis procedure. Other potential work areas include extraction testing on mixture samples for comparison with the current procedure, variability analysis (especially among RAS samples), and refining the fracture testing data and applying similar concepts to glass transition temperature testing.

Work will continue on the evaluation of the extracted/recovered asphalt binders from the virgin and the RAP-containing asphalt mixtures from Manitoba.

Collect the material for the experimental plan of subtask E2b-3 “Develop a Mix Design Procedure,” and start the testing.

Work element E2c: Critically Designed HMA Mixtures (UNR)

Work Done This Quarter

Work continued to evaluate the applicability of the recommended deviator and confining stresses for the flow number test. Evaluation of the permanent deformation characteristics of laboratory-produced mixtures under the testing conditions identified in Subtask E2c-1 was conducted. The impact of air-voids, and binder type on the asphalt mixture critical temperature was also evaluated.

The FN test was conducted using the determined stress conditions at each testing temperatures for 20,000 cycles or until the specimen reaches 5% strain, whichever occurs first. At each temperature, the corresponding deviator and confining stresses were determined using the testing conditions identified in Subtask E2c-1.

The preliminary results indicate that the HMA critical conditions determined in the FN test are affected by the density of the samples and the PG grade of the asphalt binder. The analysis will continue to determine the influence of the pulse time and rest period. A complete analysis of the results for the different HMA mixtures is being developed to determine the influence of the air-void level and the binder type on the asphalt mixture critical temperature.

The issue of converting the pulse duration in time domain for a given pavement response into frequency domain is being investigated. The Fast Fourier Transformation (FFT) is being used to convert the pavement responses from time domain to frequency domain. An investigation of the existence of predominant frequency(ies), f_p , and the ability to predict all components of the pavement response using those predominant frequencies is being developed. The study used an extensive database of computed pavement response histories of two different asphalt pavement

structures (thin and thick) at two temperatures (70 and 104°F) subjected to a tandem axle load at three different speeds (10, 40 and 60 mph) using 3D-Move. An example of the normal strains is presented in figure E2c.1. The predominant frequencies were obtained for all components of computed responses (stresses and strains) time histories, as illustrated in figure E2c.2. Based upon the results obtained this quarter, a paper was submitted to AAPT for the 2011 annual meeting.

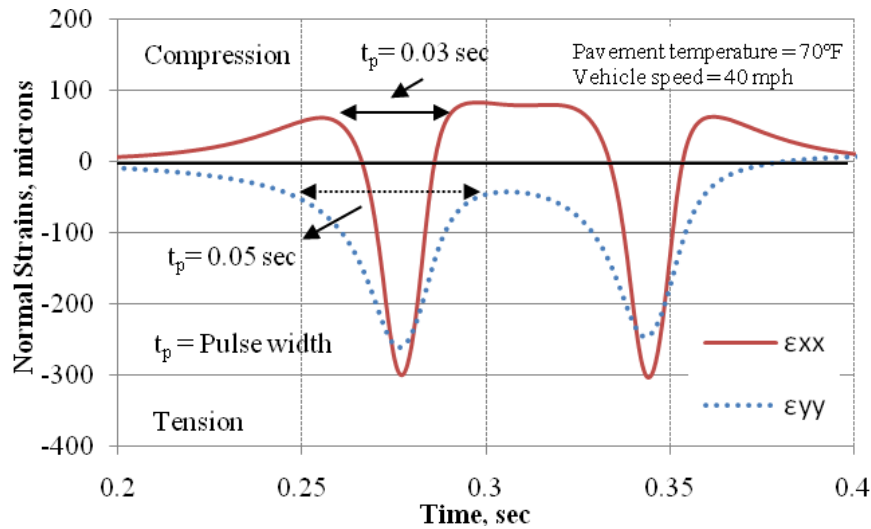


Figure E2c.1. Normal strain histories under the center of the tire at the bottom of the 4-inch HMA layer.

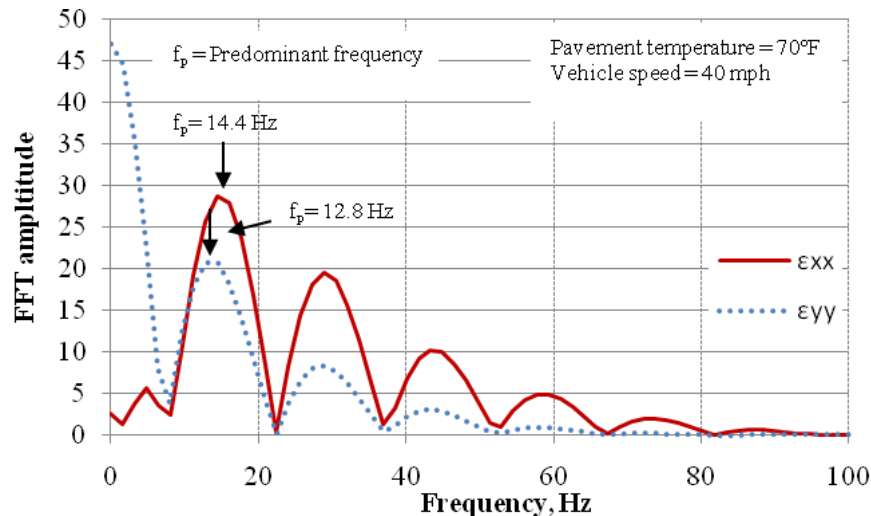


Figure E2c.2. Fast Fourier amplitudes of the normal strains under the center of the tire at the bottom of the 4-inch HMA layer.

Materials have been collected for the experimental plan developed by the Flow Number Task Force to develop criteria for asphalt concrete mixture design. UNR arranged for the shipping of aggregates and binders from Alabama, Florida, and Texas.

Significant Results

The FFT analysis of the various pavement responses showed promising results by having a consistent set of predominant frequencies for the asphalt layer. Additionally, it was found that the predominant frequencies strongly depend on the response component being considered. For example, except for thin pavement at intermediate temperatures (i.e. 70°F), the predominant frequencies of longitudinal strains are substantially different from those of vertical strains. This means that the use of one single set of predominant frequencies cannot be assigned to the asphalt layer to study all components of its response, as shown in figures E2c.3 and E2c.4.

A direct application of the predominant frequencies concept would be in the MEPDG analysis to improve the current approach for assigning loading frequencies to the various asphalt sublayers. However, additional work is needed to compare the frequencies as proposed by the MEPDG procedure with the predominant frequencies determined in this study.

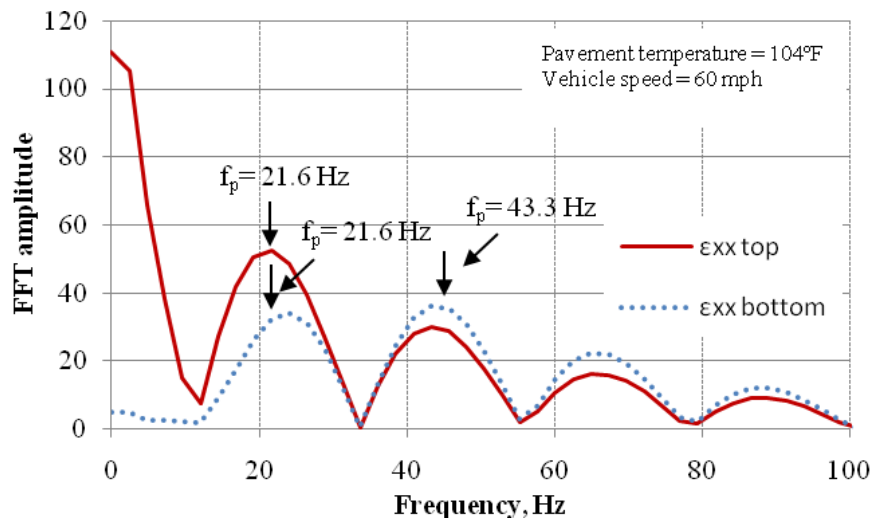


Figure E2c.3 Fourier amplitudes of the longitudinal strains under the center of the tire at the top and bottom of the 4-inch HMA layer.

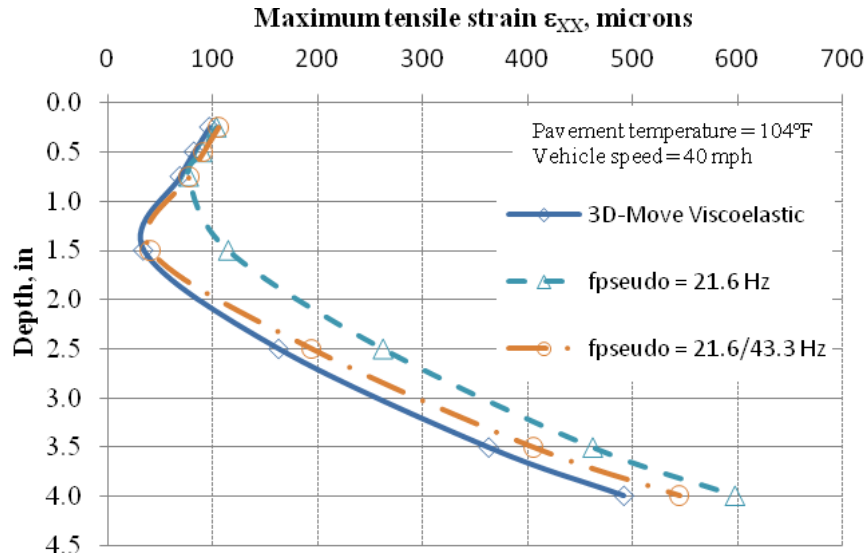


Figure E2c.4. Maximum tensile longitudinal strains at the center of the tire in the 4-inch HMA layer.

Significant Problems, Issues and Potential Impact on Progress

The write-ups for the figures and tables captions have delayed the submission of the subtask E2c.1 report for review.

The FN testing was delayed because of malfunction in the LVDTs. A new set of LVDTs was ordered which delayed testing by more than a month. Consequently, a paper summarizing the results of the FN testing experiment was not submitted for either TRB or AAPT annual meetings. This has been reflected on the Year 4 Gantt chart.

Work Planned for Next Quarter

Work will continue on the evaluation of the impact of air-voids, gradation, and binder type on mixtures' critical temperature.

Complete the tables and figures write-ups for the report.

Compare the frequencies as proposed by the MEPDG procedure with the predominant frequencies determined by the FFT analysis.

Collect the rest of the material for the experimental plan developed by the Flow Number Task Force and start the testing for the received materials.

Work element E2d: Thermal Cracking Resistant Mixes for Intermountain States (UNR & UWM)

Work Done This Quarter

This work element is a joint project between University of Nevada Reno and University of Wisconsin–Madison.

The long-term oven aging process is still on-going for the binders as described in the experimental plan for this work element. Additionally, the completed aged binders are under testing for their rheological properties.

Efforts this quarter focused on testing asphalt mixtures for glass transition temperature (T_g) using the recently developed T_g -Thermal Stress Restrained Specimen Test (TSRST) testing device. The samples tested were gyratory-compacted at target air voids of 7%. The loose mixes used for sample preparation come from different MnROAD test sections that are being monitored for cracking as part of a pooled fund project.

Previously, the research team conducted glass transition tests of asphalt mixtures using beam samples cut from slab-compacted mixtures. However, since slab compactors are not readily available in many agencies and laboratories, the usefulness of a test requiring such a compactor would be limited. Therefore, the research team focused on developing a method to produce a sample from the Superpave gyratory sample. The gyratory compactor is accessible in most laboratories.

The team worked on producing samples from gyratory-compacted samples. Three possible geometries were investigated before selecting the optimal solution. The first two are based on coring the samples and gluing three cored pieces that are 1 inch and 2.5 inches in diameter. After gluing, the specimens are approximately 12 inches long. This minimal length is required in T_g measurements of mixtures to allow measurable changes in length of the sample during cooling. Taking into account the usual height of a gyratory-compacted sample, three cores are required for such a sample. In a previous quarterly report, the effect of the thin layers of glue in the sample on the T_g was investigated and preliminary results indicated that the effect is minimal.

Results of glass transition tests run on the samples with different diameters, as shown in figure E2d.1, show that the core diameter did not significantly affect the glass transition measurements. It is observed in figure E2d.1 that both specimen sizes yielded similar T_g . The main drawback to the 2.5-inch specimen is the difficulty in extracting more than one core from each gyratory-compacted sample. Furthermore, for the 1-inch specimen, concerns about size effects (e.g., specimen smaller than the representative volume element (RVE)) prevented the research team from moving forward with these geometries. Therefore, a third geometry that includes a prismatic geometry was considered.

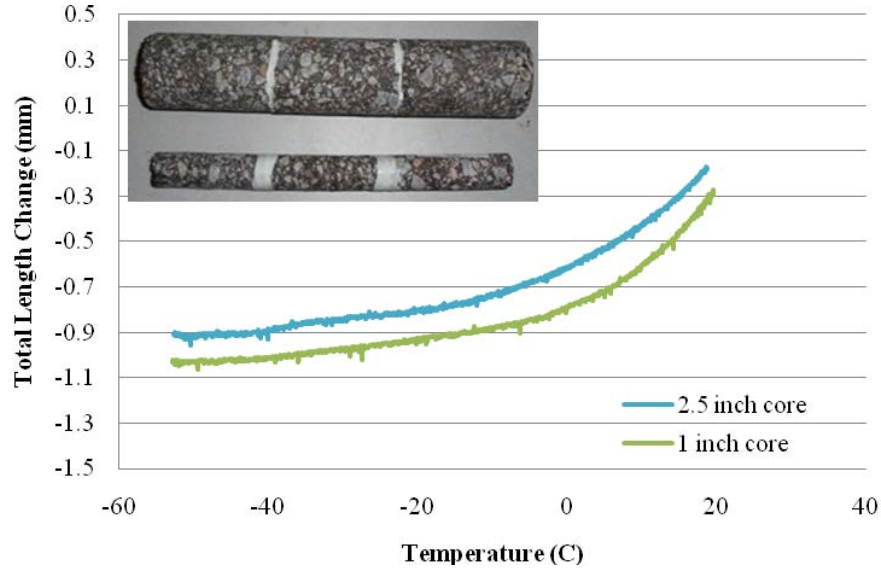


Figure E2d.1. Graph. Comparison of T_g results from samples with $\phi = 1$ inch and 2.5 inches.

In the third method, instead of coring, a few cuts were made in the gyratory-compacted sample using a masonry saw such that four prismatic beams of about 2-inch by 2-inch in cross section and about 4 inches long were produced. Three of these beams were glued to each other using epoxy resin to produce a 12-inch-long prismatic beam, as shown in figure E2d.2. It was observed that this method was less time and labor intensive than the coring methods, and the samples were easier to glue to each other. Furthermore, positioning the sample on the rollers and between the two linear variable differential transformers (LVDTs) was much easier, as the sample geometry prevented it from moving laterally, which was the case with cylindrical samples produced from coring.



Figure E2d.2. Illustration and photograph. Prismatic beams made from gluing blocks cut out of gyratory-compacted samples.

Figure E2d.3 shows the final setup used for the glass transition tests of asphalt mixtures. The LVDTs used in the T_g device were tested for linearity and accuracy using a micrometer. The setup was also checked by testing a nickel rod with known coefficient of thermal

contraction/expansion. The results of tests with cooling and heating cycles confirmed that the setup is not introducing any bias in the results.

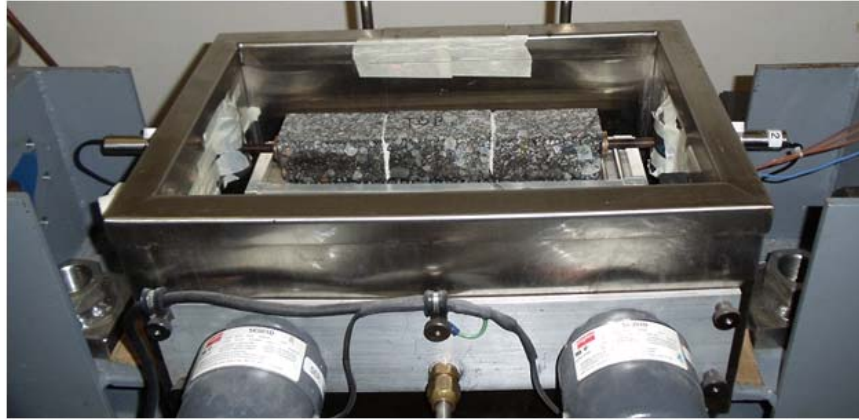


Figure E2d.3. Photograph. Test setup used for the T_g of beams made from gyratory-compacted samples.

Also in this quarter, the research team continued efforts in implementing the Single-Edge Notched Bending (SENB) test for low-temperature characterization of asphalt binders and mastics. Three binders—PG 64-22, PG 64-22 + Polyphosphoric Acid (PPA) and PG 64-22 + Sasobit—were tested to assess the effect of these modifiers on the fracture properties of the neat binder. The results from SENB testing of these asphalt binders are shown in figure E2d.4.

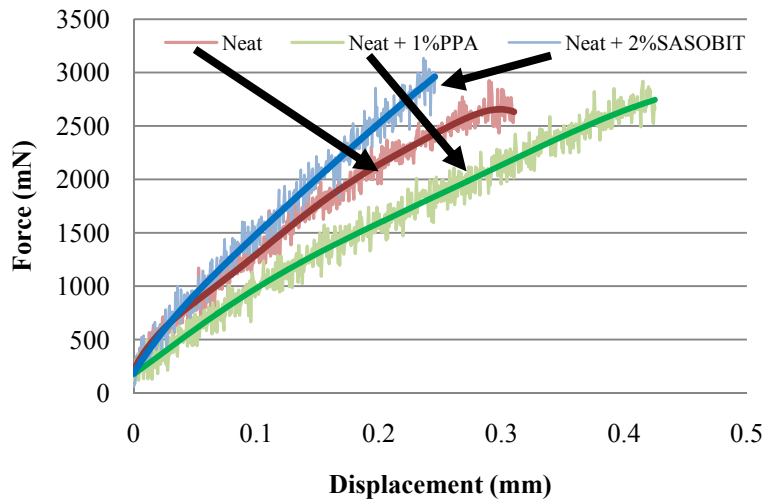


Figure E2d.4. Graph. SENB force-displacement graph for PG 64-22 binder plus modification at 12 °C.

It can be seen in figure E2d.4 that adding PPA to this binder decreased low-temperature stiffness and increased ductility. On the other hand, Sasobit stiffened the binder and fracture occurred after a smaller deformation. Fracture load (i.e., maximum load) did not change significantly with modification. This behavior indicates an improvement in low-temperature performance by adding PPA, as opposed to a deterioration of low-temperature performance caused by adding Sasobit to the base binder.

On the other hand, the research team evaluated the effect of specimen geometry and compaction method on low-temperature properties of asphalt mixtures using the TSRST test. Also, the fracture temperatures obtained from the TSRST test were checked against the true low temperature performance grade (PG) of the recovered binders from tested specimens.

Rectangular TSRST specimens (254×51×51 mm) were prepared by trimming 305×76×76 mm beam compacted samples as shown in figure E2d.5. The rectangular TSRST samples were named “Beam.” Three methods were used to prepare cylindrical TSRST specimens from SGC samples. The first method involved coring one specimen (152×57 mm) vertically from one 150-mm SGC sample as shown in figure E2d.5b. These specimens were named “1-in-1 Cylinder.” The second method involved coring three specimens (152×57 mm) vertically from one 150-mm SGC sample as shown in figure E2d.5c. These specimens were named “3-in-1 Cylinder.” The third method involved coring two specimens (140×57 mm) horizontally from the side of one 150-mm gyratory compacted sample as shown in figure E2d.5d which was named “Side Cylinder.” It should be noted that beam specimens and side coring provided cylindrical specimens that were compacted in the direction perpendicular to that of testing in TSRST.

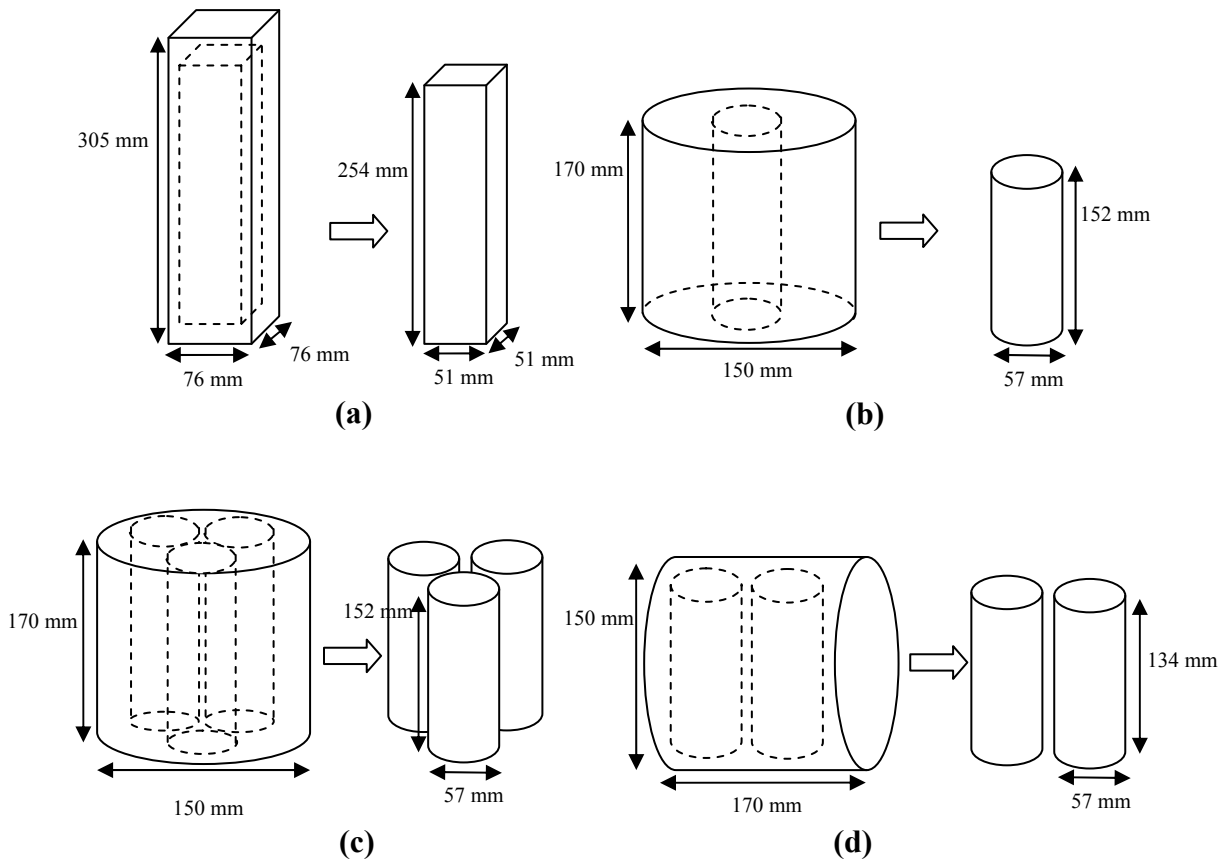


Figure E2d.5. Graph. Different TSRST specimen geometries (a) Beam, (b) 1-in-1 Cylinder, (c) 3-in-1 Cylinder, (d) Side Cylinder.

Table E2d.1 presents the test matrix. The initial phase involved comparing TSRST results of beam specimens to cylindrical specimens from Superpave gyratory compacted (SGC) samples. A PG64-22 mix was used for this phase. A total of 24 specimens (4 specimen types×6 replicates) were prepared and tested in the TSRST. Then, the repeatability as well as the validity of the test results were evaluated to determine if cylindrical samples produced by the Superpave gyratory compactor compare or are better than specimens prepared from beams. The TSRST fracture temperature was compared to the true low PG of the virgin and recovered asphalt binder from the corresponding tested specimens. As a preliminary study, the number of aggregate contact points for each specimen type was investigated using 2-D image analysis to see if it had an effect on any TSRST test results.

The cylindrical specimen that deemed to have promising results was then selected to determine whether findings for the PG64-22 unmodified mixture would also be present for a PG64-28 polymer-modified mixture. In this phase, only beam specimens and the selected cylindrical specimen were tested in the TSRST. Similarly, six replicates for each specimen type were prepared.

Based upon the obtained results, papers on TSRST findings as well as cooling/warming rates in the intermountain regions of the US findings were submitted to TRB and AAPT for the 2011 annual meetings.

Table E2d.1. Test matrix for TSRST experiment.

Binder	Nominal Maximum Aggregate Size	Test	Beam Specimens	1-in-1 Cylinder	3-in-1 Cylinder	Side Cylinder
PG 64-22	12.5 mm	TSRST @ cooling rate of 10°C/hr	x	x	x	x
		2-D image analysis	x	x	x	x
		Extraction/recovery	x	x	x	x
PG 64-28NV	19.0 mm	TSRST @ cooling rate of 10°C/hr	x			x
		2-D image analysis	x			x
		Extraction/recovery	x			x

Under subtasks E2d.3.b and E2d.3.c, nearly all the E*-compression testing with only a few samples still undergoing oven aging. All of the E*-compression samples are scheduled to complete their aging durations before the end of the calendar year.

Upon completion of the E* testing the samples are being extracted and the binder recovered for further testing. Just under 40% of the samples have been extracted and recovered to date. A change in the location of the Fourier Transform Infrared Spectroscopy (FT-IR) testing for Carbonyl Area (CA) to Texas A&M University has improved the efficiency of that testing with approximately 20% of the CA measurements being complete. Further samples are in the process of being tested.

The Thermally Stressed Restrained Specimen Test (TSRST) specimens are all mixed and compacted and are currently going through their aging durations. Since this was recently added to the work plan, few samples have been tested, however, all of the 0 and some 3 month aged samples have been cut and prepared for testing. Along with the TSRST preparation, samples for the coefficient of thermal expansion, α , have also been prepared and are undergoing their respective aging.

Under subtask E2d-4, UNR is working with TTI for the possibility of modifying the viscoelastic finite element tool (VE2D) developed by TTI to incorporate the findings of this work element. The “VE2D” is used for pavement low temperature cracking analysis and is based on viscoelastic two-dimensional (2D) finite element (FE) method. The “VE2D” is being evaluated for possible incorporation of the following general features:

1. Account for different coefficient of thermal expansions as a function of temperature and time (aging effect)
2. Account for the effect of aging on the asphalt layer property
3. Use the developed temperature model

Significant Results

The research team made some important observations while developing the glass transition temperature (T_g) test setup. Most noteworthy was the significant effect of not maintaining a completely constant rate of temperature change with time. Initial tests showed a highly variable volume-temperature slope at the two extreme ends of the testing temperatures, to the point of becoming nearly horizontal and vertical at the low and high test temperatures, respectively.

To investigate the cause of this phenomenon, the temperature change rate during the test was analyzed. It was observed that when testing using the initial hold time settings—20 minutes at 30 °C and 10 minutes at -60 °C—the temperature inside the sample was unable to reach the desired temperature within the holding time, and thus did not stabilize before the temperature change rate was reversed toward the high temperature. This resulted in a continuous nonlinear temperature change rate at the two extremes of the test. New tests were performed on the samples in which the holding times at the two extremes were increased to 40 minutes, which allowed the sample to reach the target temperature. After implementing this modification of the procedure, reasonable values of the slope of the volume-temperature curves at the two extremes of the testing temperatures were observed. This analysis highlights the extreme importance of monitoring the temperature change rate within the sample during testing and maintaining a constant rate through the test.

Volumetric stability at isothermal conditions was also tested using the T_g test setup by decreasing the sample temperature to -25 °C and then keeping the temperature constant for conditioning. The results of preliminary tests conducted using this procedure show a decreasing length over time clearly visible over the course of the isothermal conditioning. The isothermal reduction in length of the asphalt mixture tested was of a magnitude of about 7% of the total length change when the temperature is reduced from 30 °C to -25 °C. The results are important, as the observed behavior is of the same order of magnitude as the change in stiffness resulting from physical hardening observed in binders, a phenomenon that has been extremely difficult to study and detect in asphalt mixtures in previous studies. Further tests and analysis of results is required to investigate the exact nature of the observed behavior.

Based on the TSRST test results, it was found that cylindrical specimens prepared from SGC samples may provide a better alternative to beam specimens for TSRST testing. Particularly, side cylinders which are cored perpendicular to the compaction direction seem promising. The repeatability of the test results improved when side cylinders instead of beams were tested in the TSRST. Furthermore, TSRST values for beam specimens were not significantly different from TSRST values for side cylinders. Also, the aging procedure described in AASHTO R30 seems to simulate long-term aging reasonably for the side cylinders.

There are a few benefits of having the option to use the SGC to prepare TSRST specimens. The equipment is readily available for most laboratories since the SGC is increasingly becoming the compaction method of choice in the United States. Therefore, additional equipment would not be needed to prepare cylindrical specimens as opposed to beams.

Side cylinders can also be easily obtained from field samples. Cylindrical specimens can be cored from different lifts within the asphalt layer in pavements parallel to the traffic direction. The orientation of the specimens will be preserved and can be tested to simulate actual thermal loading conditions in the lab by subjecting tensile stresses parallel to traffic direction.

Under subtasks E2d.3.b and E2d.3.c, with a significant portion of the E*-compression testing being completed, some results and conclusions can be made. However, preliminary results seem to indicate additional information may be needed to help differentiate the observed results. Based upon the results obtained this quarter, the following results are a summary of those submitted to TRB for the 2011 annual meeting.

The overall subject of the paper was to present the results of the E*-compression testing and the Carbonyl Area measurements as an indicator of the binder aging. Based upon the mixes utilized, differences in the aging rate among the two binders (neat PG64-22 and SBS modified PG64-28) as well as the differences between the ageing rates between the two aggregate sources (Nevada and Colorado) were considered. The submitted manuscript included only part of the overall test matrix which included the following mixtures found in table E2d.2.

Table E2d.2. Mixture summary.

Source	Location	Mineralogy	Aggregate Absorption (%)	Binder Grade	Binder Content (% TWM)	Apparent Film Thickness (µm)
Nevada	Sparks, NV	Rhyolite, Silica Sand	2.7	PG64-22	5.4	9.0
				PG64-28	5.2	9.0
Colorado	Morrison, CO	Mica Gneiss, Mica Schist, Quartz Sand	0.9	PG64-22	4.5	11.7
				PG64-28	4.5	11.7

As previously noted the E*-compression results indicate the aging protocol being used does age and thus stiffen the mixture as indicated by the typical E*-compression masters curves noted in figure E2d.6. These curves follow the typical response and happen to be one of the mixtures utilized in the submitted manuscript.

Utilizing the extracted and recovered binder noted in table E2d.2, the aging was quantified utilizing the carbonyl area (CA) of the respective binders as measured by the Fourier Transform Infrared Spectroscopy (FT-IR) testing. The following figure E2d.7 presents a summary of the CA measurements as a function of the oven aging for each respective mixture.

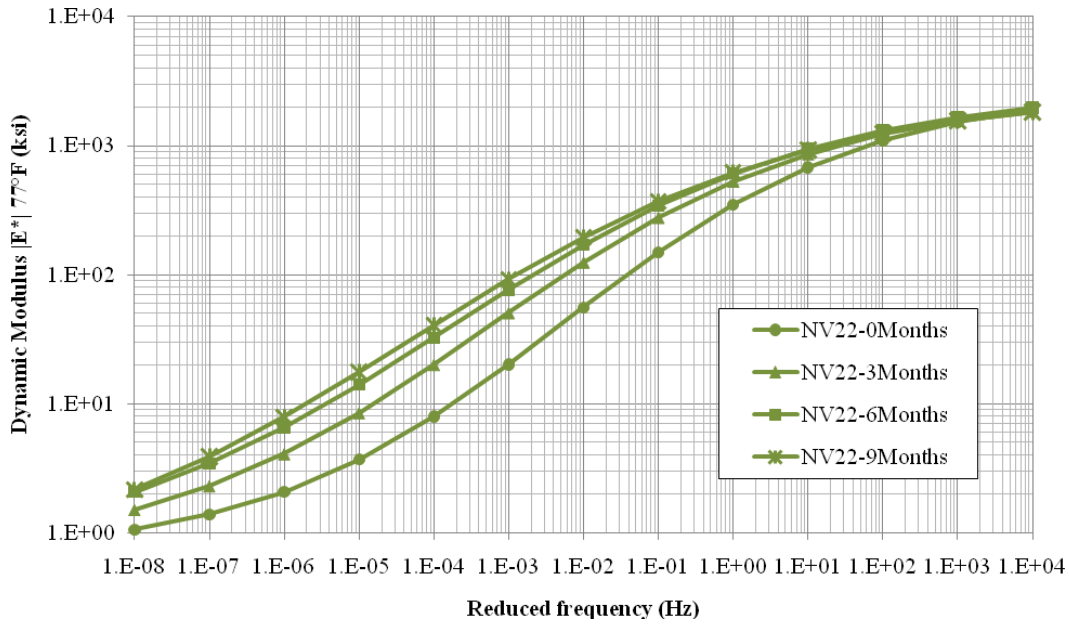


Figure E2d.6. Typical E*-compression master curves with oven aging.

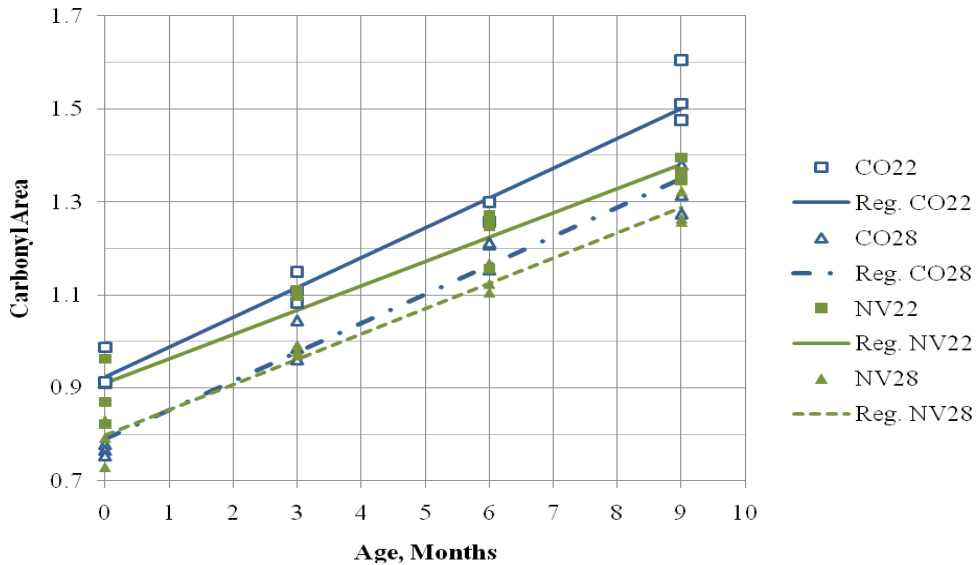


Figure E2d.7. Carbonyl measurement as a function of oven aging.

To adequately examine the aging of the binder itself within the mixture, consideration of the mixture stiffness, E^* , is needed in terms of oxidation, measured as CA, rather than aging time. This is required in order to single out the aging effects rather than having the differences in stiffness or other mixture characteristic compounded by differences in oxidation level, which do not necessarily progress at the same rate with respect to time.

To accomplish these comparisons, E^* must be simplified down to a few useable values rather than a full curve or large data matrix as is often produced during testing. To appropriately reduce the data, the fundamentals of viscoelastic theory are referenced. It is generally accepted that HMA mixtures are most appropriately characterized as a viscoelastic solid. Specifically, this means that the material will not exhibit purely viscous behavior, most directly indicated by a phase angle approaching 90° . Zeng et al. (2001) clearly show this to be the case for HMA mixtures subjected to shear loading. What makes HMA a viscoelastic solid is that the phase angle increases to a point then begins to decrease with decreasing loading frequency. The same principle applies to the axial loading conditions applied during E^* testing. In the same report, it is shown that asphalt binders, on the other hand, can be considered viscoelastic liquids. This is evidenced by the increasing phase angle with slower loading frequencies, essentially leading to the low or zero shear viscosity concept, LSV or ZSV, respectively. Similar to LSV theory, it is much preferred to conduct such analysis with actual measured data points rather than using responses from a fitted model, i.e. master curve. Therefore the E^* analysis is limited to the temperatures and frequencies mentioned previously.

Since this investigation is interested in the aging of the asphalt binders and corresponding changes to the mixture properties, it is desired to capture as much of the viscous response of the mixture as possible. The most direct evidence of the most viscous response in an E^* test is to locate the highest phase angle, which will not be at the lowest frequency and the highest temperature, as would be the case for binder testing. After much consideration into the measured phase angle at each of the E^* testing conditions, it was decided that the best overall option would be to consider E^* at both 70 and 100°F at 0.1 Hz. Explorations also considered the elastic, E' , and viscous, E'' , components of the measured E^* values, however their relationship to E^* through the phase angle, δ , resulted in very similar results as E^* . Even though this methodology was developed independently, it was later verified in the literature by AbWahab et al. (1993). Therefore, for the sake of simplicity E^* at 70 and 100°F at 0.1 Hz will be considered with respect to the measured CA from the previous section. Figures E2d.8 and E2d.9 present the plots for both 70 and 100°F at 0.1 Hz, respectively.

Based upon the findings of this portion of the study which included statistical considerations of the data not presented here, the following conclusions were made.

This study evaluated the effect of different aggregate sources, their corresponding change in mixture characteristics, namely the binder apparent film thickness (AFT), and their influence on both binder oxidation rates and changes in mixture stiffness at a constant mixture air void level of 7% when compacted mixtures were exposed to laboratory aging conditions. The two aggregate sources, Colorado and Nevada, had different gradations and different water absorption values which led to differences in the calculated AFT for each mixture (11.7 versus 9.0 μm). The two asphalt binders, a neat PG64-22 and an SBS modified PG64-28, were both made from the same base stock binder.

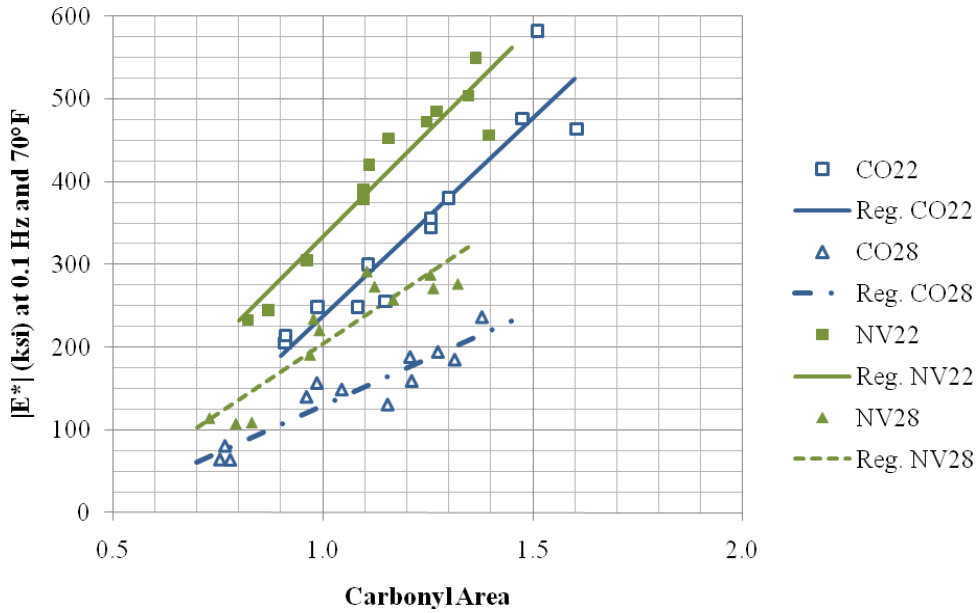


Figure E2d.8. Dynamic modulus at 70°F with respect to carbonyl area.

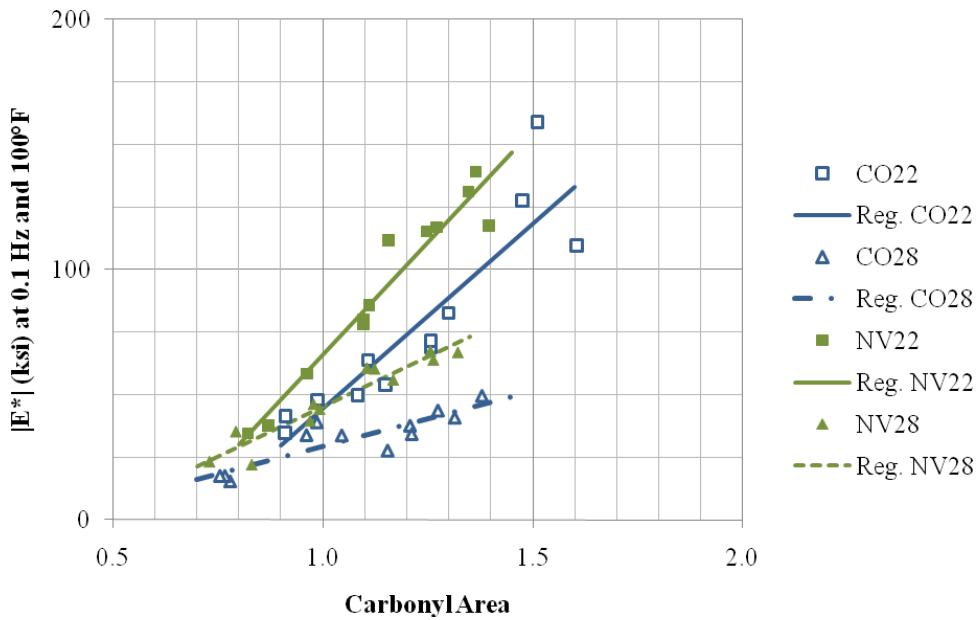


Figure E2d.9. Dynamic modulus at 100°F with respect to carbonyl area.

The overall findings of the study indicate that the mixture characteristics influence the oxidation rates of the binder, with the two binders oxidizing by similar amounts when aged in the same mixture characteristics (AFT and mixture air voids). It was further determined that the influence

of the oxidation changes in binder have differing effects on the stiffness of the mixture as a function of age, thus leading to the conclusion that not only are the mixture characteristics influential to the mixture stiffness and aging relationships, but the binder themselves, in particular polymer modification, influence the aging and stiffness relationships of mixtures with age.

Now that evidence is presented concluding that mixture characteristics potentially influence oxidative aging, further study is needed to specifically differentiate how each mix parameter influences both the binder aging and the mixtures response to such changes in the binder. At this point in the study, the most influential mix parameters are not fully understood nor what causes them. As an example, it appears that the aggregate properties may influence the mix characteristics and thus the oxidation of the binder, but this may only be to the extent that the aggregate absorption affects the AFT. Further studies are needed to solidify the meaning of these findings.

Significant Problems, Issues and Potential Impact on Progress

Further progress has been made in the E^* -tension area, with the previous control issues expected to be resolved just recently. A few preliminary tests have been conducted; however the data have not been thoroughly reviewed and are not yet ready for presentation.

With UNR's DSR still out of commission no binder master curves or LSV (low shear viscosity) testing has been conducted this quarter for Subtask E2d-3. Supposedly the DSR is repaired and should be arriving at any time allowing the testing to get back underway. This delayed the work under Subtask E2d-4 as the findings from Subtask E2d-3 are supposed to be incorporated in the modeling system.

Work Planned Next Quarter

Continue the experiment to evaluate the aging characteristics (oxidation and hardening kinetics) of asphalt binders when aged in forced convection (horizontal airflow) ovens.

The research team will evaluate the effect of cooling rate on TSRST results using the proposed cylindrical test geometry. Typical cooling rates obtained for the intermountain region of the United States obtained under Subtask E2d-1 will be used. A monotonic cooling rate and a binary cooling rate will be evaluated.

Tests have begun on the mixture glass transition setup. Final calibrations have been made to the TSRST system being developed using the same T_g setup. TSRST tests will be conducted after T_g measurements of the asphalt mixtures proposed in the Year 4 work plan are completed. Results will be studied closely to assess the suitability of the proposed beam geometry for performing TSRST tests, and whether a slab compactor is needed to prepare beams for this test.

Under subtasks E2d.3.b and E2d.3.c, the main focus early in the next quarter will be to significantly increase the amount of completed testing. All of the E^* -compression testing is expected to be completed as well as the final procedure for E^* in tension is expected to be

finalized and begin production testing. Once the DSR arrives, the development of the binder master curves and LSV measurements is expected to proceed with little difficulty once the DSR has been repaired. Testing on the TSRST will also get underway as samples are available from their respective aging cycles.

The research team will work with TTI to develop a plan on how to modify the viscoelastic finite element tool (VE2D) to incorporate the findings of this work element.

Cited References

AbWahab, Y., D. Sosnovske, C. A. Bell, and P. Ryus, 1993, "Evaluation of Asphalt-Aggregate Mixture Aging by Dynamic Mechanical Analysis," Transportation Research Record 1386, Transportation Research Board, Washington, D.C.

Zeng, M., H. Bahia, H., Zhai, and P. Turner, 2001, Rheological Modeling of Modified Asphalt Binders and Mixtures. *Journal of the Association of Asphalt Paving Technologists*, 70: 403.

Work element E2e: Design Guidance for Fatigue and Rut Resistance Mixtures (AAT)

Work Done This Quarter

Additional analyses of uniaxial fatigue data was done, using both the extended experiment performed earlier this year and data from NCHRP Projects 9-25/31. The objective of this analysis was to develop an empirical relationship that could be used to predict damage curves for HMA mixtures, using values for $|E^*|$, phase angle, binder properties, and/or volumetric properties. A relationship was developed that gives very accurate predictions for almost all mixes, including several that were not included in the database used to develop the equations. The basic equation for damage ratio C is

$$C = \frac{1}{1 + \left(\frac{N_R}{K_1}\right)^{K_2}} \quad (\text{E2e.1})$$

Where

- N_R = reduced cycles
- K_1 = location parameter for the damage function
- K_2 = shape parameter for the damage function

Reduced cycles are calculated from initial modulus, applied strain, the continuum damage parameter (and material property) α , the shift factor $a(T)$ and the number of loading cycles. The empirical equations for K_1 and K_2 are as follows:

$$\log K_1 = 29.71 - 4.369 \log |E^*|_0 - 101.1 \log \alpha + 17.6 \log |E^*|_0 \log \alpha \quad (\text{E2e.2})$$

$$\log K_2 = 1.601 - 1.601 \log |E^*|_0 - 1.163 \log \alpha \quad (\text{E2e.3})$$

The r-squared values for these equations are not impressive—47% and 38%, respectively (adjusted for degrees of freedom)—however, given that predictions made using this approach are very accurate the low r-squared values apparently are the result of the inherently highly variable nature of fatigue characterization. The two figures below give examples of typical damage curves predicted using equations E2e.2 and E2e.3 compared to experimentally determined damage curves. Figure E2e.1 is for a mixture tested during NCHRP Project 9-25, and figure E2e.2 is for a mixture recently tested in research being funded by the Federal Aviation Administration (FAA). It should be noted that the latter mixture was not included in the data set used to develop the predictive equations, and was gathered using a different test device (the asphalt mixture performance tester or AMPT) and protocol.

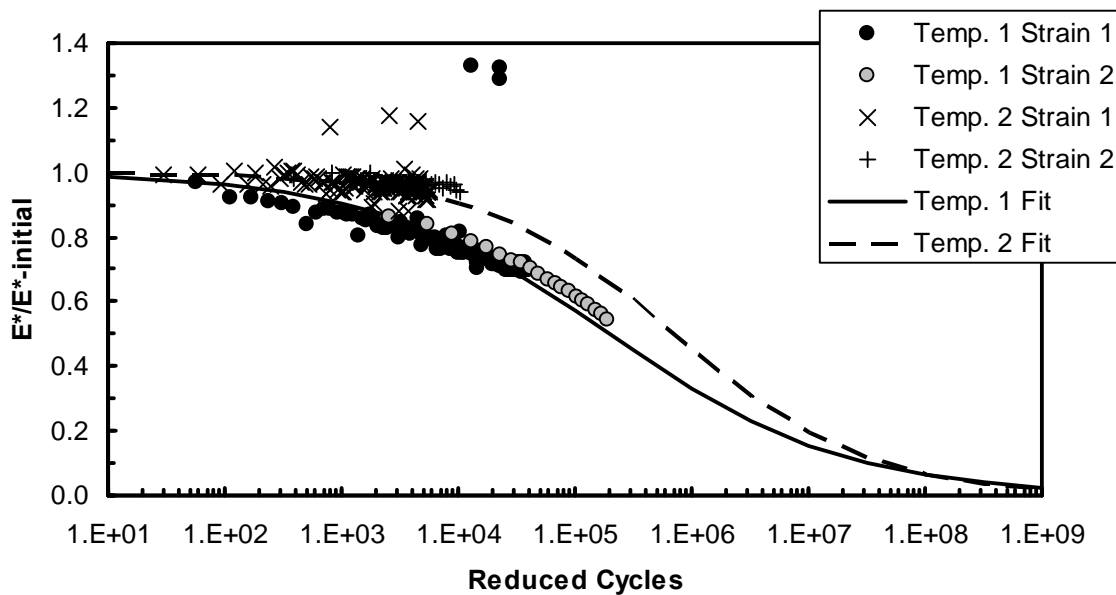


Figure E2e.1. Measured and predicted damage curves for and HMA tested as part of NCHRP Project 9-25/31.

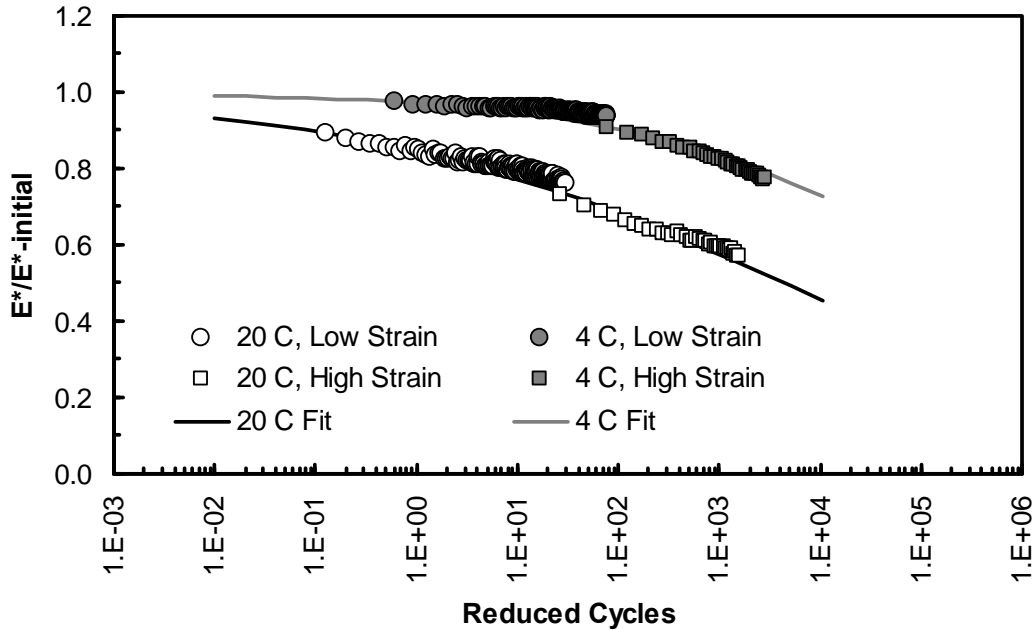


Figure E2e.2. Measured and predicted damage curves for HMA tested for FAA-sponsored research.

The ability to predict damage curves based on modulus and mixture composition is extremely useful, with many applications in both pavement engineering and research. Such predictions can be used to develop very effective fatigue testing protocols. In pavement design, this approach could potentially be used to develop relatively accurate fatigue damage predictions based only upon mixture composition and modulus values, determined either from measurements made with the AMPT or from predictive methods such as the Hirsch model.

Also during last quarter some limited work was done in refining the resistivity/rutting model. Data on recent test sections placed at the NCAT test track was compiled to determine if this model could accurately predict rutting for these sections. However, there was not enough data for enough sections to make any conclusions on the accuracy of the model.

Work Planned Next Quarter

The testing protocol for fatigue testing at AAT will be evaluated on the basis of the newly developed predictive model, to ensure optimum results. Additional efforts to refine the predictive models, using mixture composition data and binder information will be made.

Work on both the fatigue experiments and rutting experiments will accelerate during the next quarter.

Significant Problems, Issues and Potential Impact on Progress

None.

Engineered Materials Year 4	Year 4 (4/2010-3/2011)												Team
	4	5	6	7	8	9	10	11	12	1	2	3	
(1) High Performance Asphalt Materials													
E1a: Analytical and Micro-mechanics Models for Mechanical behavior of mixtures													TAMU
E1a-1: Analytical Micromechanical Models of Binder Properties				P							P		
E1a-2: Analytical Micromechanical Models of Modified Mastic Systems				P							P		
E1a-3: Analytical Models of Mechanical Properties of Asphalt Mixtures				P, JP					JP (2)		P		M&A
E1a-4: Analytical Model of Asphalt Mixture Response and Damage											P		
E1b: Binder Damage Resistance Characterization													UWM
E1b-1: Rutting of Asphalt Binders													
E1b-1-i: Literature review													
E1b-1-2: Select Materials & Develop Work Plan													
E1b-1-3: Conduct Testing		DP											
E1b-1-4: Analysis & Interpretation									JP				
E1b-1-5: Standard Testing Procedure and Recommendation for Specifications					P							DP	
E1b-2: Feasibility of determining rheological and fracture properties of asphalt binders and mastics using simple indentation tests (modified title)													UWM
E1b-2i: Literature Review													
E1b-2ii: Proposed SuperPave testing modifications													
E1b-2iii: Preliminary testing and correlation of results							JP						
E1b-2iv: Feasibility of using indentation tests for fracture and rheological properties											P		D
E2a: Comparison of Modification Techniques													UWM
E2a-1: Identify modification targets and material suppliers													
E2a-2: Test material properties											P		
E2a-3: Develop model to estimate level of modification needed and cost index													
E2a-4: Write asphalt modification guideline/report on modifier impact over binder properties							JP						
E2c: Critically Designed HMA Mixtures													UNR
E2c-1: Identify the Critical Conditions													
E2c-2: Conduct Mixtures Evaluations											JP		
E2c-3: Develop a Simple Test													
E2c-4: Develop Standard Test Procedure													
E2c-5: Evaluate the Impact of Mix Characteristics													
E2d: Thermal Cracking Resistant Mixes for Intermountain States													UWMUNR
E2d-1: Identify Field Sections													
E2d-2: Identify the Causes of the Thermal Cracking													
E2d-3: Identify an Evaluation and Testing System							JP				P		
E2d-4: Modeling and Validation of the Developed System							JP					P	
E2d-5: Develop a Standard													
E2e: Design Guidance for Fatigue and Rut Resistance Mixtures													AAT
E2e-1: Identify Model Improvements													
E2e-2: Design and Execute Laboratory Testing Program													
E2e-3: Perform Engineering and Statistical Analysis to Refine Models							JP						
E2e-4: Validate Refined Models													
E2e-5: Prepare Design Guidance													
(2) Green Asphalt Materials													
E2b: Design System for HMA Containing a High Percentage of RAP Material													UNR
E2b-1: Develop a System to Evaluate the Properties of RAP Materials		P				JP				P			
E2b-2: Compatibility of RAP and Virgin Binders													
E2b-3: Develop a Mix Design Procedure									D				
E2b-4: Impact of RAP Materials on Performance of Mixtures													
E2b-5: Field Trials							JP						
E1c: Warm and Cold Mixes													UWM
E1c-1: Warm Mixes													
E1c-1i: Effects of Warm Mix Additives on Rheological Properties of Binders													
E1c-1ii: Effects of Warm Mix Additives on Mixture Workability and Stability							JP						
E1c-1iii: Mixture Performance Testing													
E1c-1iv: Develop Revised Mix Design Procedures		DP, P											
E1c-1v: Field Evaluation of Mix Design Procedures and Performance Recommendations													
E1c-2: Improvement of Emulsions' Characterization and Mixture Design for Cold Bitumen Applications													UWMUNR
E1c-2i: Review of Literature and Standards									D				
E1c-2ii: Creation of Advisory Group													
E1c-2iii: Identify Tests and Develop Experimental Plan													
E1c-2iv: Develop Material Library and Collect Materials													
E1c-2v: Conduct Testing Plan							JP				P		
E1c-2-vi: Develop Performance Selection Guidelines							JP				P		F
E1c-2-vii: Validate Performance Guidelines													
E1c-2-viii: Develop CMA Mix Design Guidelines													
E1c-2-ix: Develop CMA Performance Guidelines													

Deliverable codes
D: Draft Report
F: Final Report
M&A: Model and algorithm
SW: Software
JP: Journal paper
P: Presentation
DP: Decision Point

Deliverable Description
Report delivered to FHWA for 3 week review period.
Final report delivered in compliance with FHWA publication standards
Mathematical model and sample code
Executable software, code and user manual
Paper submitted to conference or journal
Presentation for symposium, conference or other
Time to make a decision on two parallel paths as to which is most promising to follow through

Work planned
Work completed
Parallel topic

Engineered Materials Year 2 - 5	Year 2 (4/08-3/09)				Year 3 (4/09-3/10)				Year 4 (04/10-03/11)				Year 5 (04/11-03/12)				Team
	Q1	Q2	Q3	Q4	Q1	Q2	Q3	Q4	Q1	Q2	Q3	Q4	Q1	Q2	Q3	Q4	
(1) High Performance Asphalt Materials																	
E1a: Analytical and Micro-mechanics Models for Mechanical behavior of mixtures																	
E1a-1: Analytical Micromechanical Models of Binder Properties				P, JP	JP	P	P	JP		P		P	P	JP	D, JP	F	TAMU
E1a-2: Analytical Micromechanical Models of Modified Mastic Systems				P, JP	JP	P	P		P		P	P	JP	D	F, SW, M&A		
E1a-3: Analytical Models of Mechanical Properties of Asphalt Mixtures	P	P, JP		P, JP	JP	P	P	M&A		P, JP(2)	JP (2)	P, M&A	P	JP(2)	D, JP	F, SW, M&A	
E1a-4: Analytical Model of Asphalt Mixture Response and Damage				P, JP	JP	P	P					P	P		D	F, SW, M&A	
E1b: Binder Damage Resistance Characterization																	
E1b-1: Rutting of Asphalt Binders																	
E1b-1-1: Literature review																	
E1b-1-2: Select Materials & Develop Work Plan	DP, P		P														
E1b-1-3: Conduct Testing			P			JP		P	DP								
E1b-1-4: Analysis & Interpretation			JP	P	JP					JP							
E1b-1-5: Standard Testing Procedure and Recommendation for Specifications										P		DP	P	D	JP	F	
E1b-2: Feasibility of Determining rheological and fracture properties of asphalt binders and mastics using simple indentation tests (modified title)																	
E1b-2i: Literature Review						D											
E1b-2ii: Proposed SuperPave testing modifications or new testing devices						P											
E1b-2iii: Preliminary testing and correlation of results								D		JP							
E1b-2iv: Feasibility of using indentation tests for fracture and rheological properties						JP		P				P, D	F				
E2a: Comparison of Modification Techniques																	
E2a-1: Identify modification targets and material suppliers					DP		DP						P				
E2a-2: Test material properties								P									
E2a-3: Develop model to estimate level of modification needed and cost index																	
E2a-4: Write asphalt modification guideline/report on modifier impact over binder properties										JP							
E2a: Critically Designed HMA Mixtures																	
E2c-1: Identify the Critical Conditions			JP		D, F		JP	D	F				JP				
E2c-2: Conduct Mixtures Evaluations																	
E2c-3: Develop a Simple Test								D						D, F	JP		
E2c-4: Develop Standard Test Procedure																	
E2c-5: Evaluate the Impact of Mix Characteristics															D, F		
E2d: Thermal Cracking Resistant Mixes for Intermountain States																	
E2d-1: Identify Field Sections			D, F	D, F	D	F											
E2d-2: Identify the Causes of the Thermal Cracking																	
E2d-3: Identify an Evaluation and Testing System					DP	JP	DP, D			JP		P	JP				
E2d-4: Modeling and Validation of the Developed System										JP		P				D, F	
E2d-5: Develop a Standard																D, F	
E2e: Design Guidance for Fatigue and Rut Resistance Mixtures																	
E2e-1: Identify Model Improvements																	
E2e-2: Design and Execute Laboratory Testing Program																	
E2e-3: Perform Engineering and Statistical Analysis to Refine Models										JP				P, D, F			
E2e-4: Validate Refined Models														JP			
E2e-5: Prepare Design Guidance															M&A	P, D, F	
(2) Green Asphalt Materials																	
E2b: Design System for HMA Containing a High Percentage of RAP Material																	
E2b-1: Develop a System to Evaluate the Properties of RAP Materials			JP		P	D	D, F	D		P	JP	P					
E2b-2: Compatibility of RAP and Virgin Binders															D, F	JP	
E2b-3: Develop a Mix Design Procedure									D						D, F	JP	
E2b-4: Impact of RAP Materials on Performance of Mixtures																D, F	
E2b-5: Field Trials										JP						D, F	
E1c: Warm and Cold Mixes																	
E1c-1: Warm Mixes																	
E1c-1-i: Effects of Warm Mix Additives on Rheological Properties of Binders																	
E1c-1-ii: Effects of Warm Mix Additives on Mixture Workability and Stability			P	D	F, DP							JP					
E1c-1-iii: Mixture Performance Testing							JP		P, DP	DP, P							
E1c-1-iv: Develop Revised Mix Design Procedures																	
E1c-1-v: Field Evaluation of Mix Design Procedures and Performance Recommendations															JP	D, P, F	
E1c-2: Improvement of Emulsions' Characterization and Mixture Design for Cold Bitumen Applications																	
E1c-2-i: Review of Literature and Standards			JP, P, D	F		D1	D3		D6			D					
E1c-2-ii: Creation of Advisory Group																	
E1c-2-iii: Identify Tests and Develop Experimental Plan					P, DP	D1		D4									
E1c-2-iv: Develop Material Library and Collect Materials																	
E1c-2-v: Conduct Testing Plan							JP	D5	P		JP		P				
E1c-2-vi: Develop Performance Selection Guidelines											JP		P, F				
E1c-2-vii: Validate Guidelines								D2						JP		P, F	
E1c-2-viii: Develop CMA Mix Design Procedure																	
E1c-2-ix: Develop CMA Performance Guidelines															JP	D, P, F	

Deliverable codes
D: Draft Report
F: Final Report
M&A: Model and algorithm
SW: Software
JP: Journal paper
P: Presentation
DP: Decision Point

Deliverable Description
Report delivered to FHWA for 3 week review period
Final report delivered in compliance with FHWA publication standards
Mathematical model and sample code
Executable software, code and user manual
Paper submitted to conference or journal
Presentation for symposium, conference or other
Time to make a decision on two parallel paths as to which is most promising to follow through

Work planned
Work completed
Parallel topic
Delayed

PROGRAM AREA: VEHICLE-PAVEMENT INTERACTION

CATEGORY VP1: WORKSHOP

Work element VP1a: Workshop on Super-Single Tires

This work element is complete.

CATEGORY VP2: DESIGN GUIDANCE

Work element VP2a: Mixture Design to Enhance Safety and Reduce Noise of HMA (UWM)

Work Done This Quarter

Work this quarter focused on configuring the Kundt tube for noise evaluation, resolving issues related to mean profile depth (MPD) estimation using a laser profilometer (LP), and preparing test equipment for field evaluation. Configuring the Kundt tube has challenged the research team and delayed progress, but recent efforts have resulted in successful software configuration and system calibration. After working with technicians in Italy to configure the system, researchers used two foam samples to calibrate the device. Preliminary results are presented in subsequent sections of this report.

Additional issues have been identified regarding the LP and related analysis methods. The issue of greatest concern is that of the laser spot diameter. Samples analyzed at UW–Madison and the University of Pisa in Italy using two different lasers on identical samples produced different results. Discrepancies in MPD values suggest that both digital filter type and laser spot diameter affect MPD values. Filter types specified in International Organization for Standardization (ISO) standards and used for digital image processing, specifically the Butterworth filter and the moving average filter, appear to affect MPD values. Another issue related to laser scan rate also came under consideration. The research team believes that a constant scan rate is important to achieving consistent results in the laboratory, and also to align laboratory scan rates with field test speeds.

Field sections have been identified for comparison to laboratory samples and field cores. These sections, located throughout Wisconsin, will provide information needed to validate the assumption that experimental results collected on gyratory samples can be related to actual field measurements. The dynamic friction tester (DFT) and circular track meter (CTM) will be used in field sections to estimate friction number and slip speed, respectively. These parameters allow for calculation of the International Friction Index (IFI). In addition, laboratory evaluation methods including the British Pendulum Tester (BPT) and LP may be used in the field to compare field sections to corresponding laboratory samples.

Significant Results

Of the two analysis techniques considered for analyzing LP measurements, the moving average filter is being discarded in favor of the Butterworth filter within the European Union (Losa 2010). This finding is expected to manifest itself in future ISO standards related to MPD estimation methods. This resolution confirms data presented in figure VP2a.2 of the previous quarterly report that the Butterworth filter better models the relationship between field core MPD values and gyratory compactor sample MPD values.

Preliminary Kundt tube calibration results are presented in figure VP2a.1 for two foam samples. Once calibrated, the equipment can be used to determine the normal incidence sound absorption coefficient α (ASTM 2008). The frequency-alpha plot shows the highest frequencies between 50 Hz and 150 Hz. Alpha values peak around 0.4 for both types of foam and diminish below 0.1 at frequencies greater than 200 Hz. At the highest frequencies, alpha values are approximately 10% of peak amplitude.

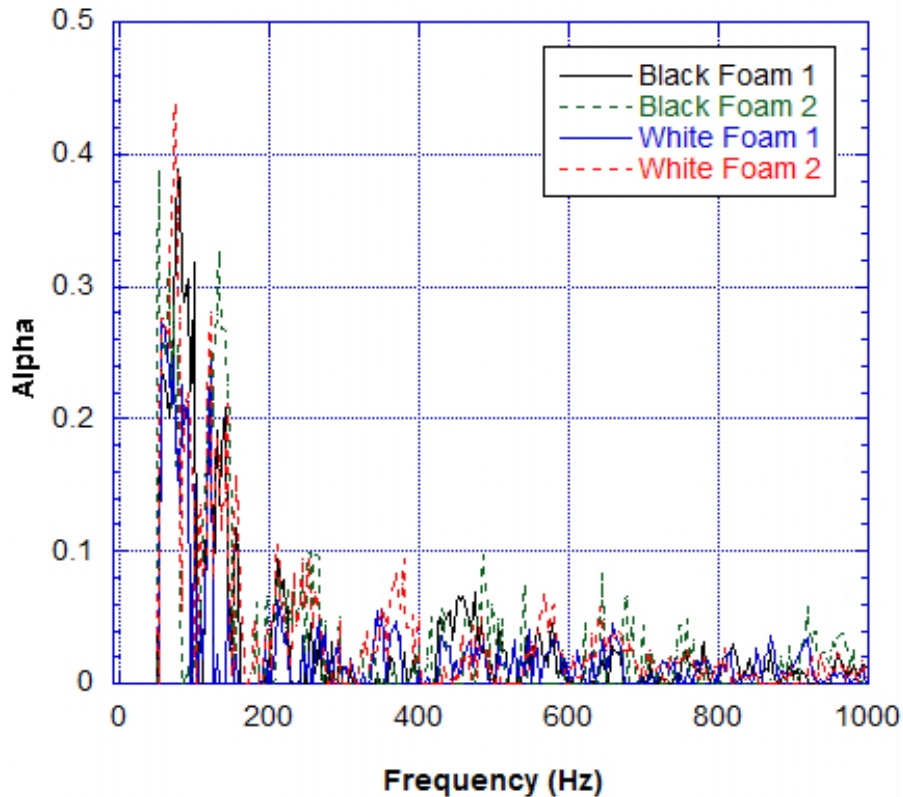


Figure VP2a.1. Graph. Preliminary calibration results for two foam materials.

Significant Problems, Issues and Potential Impact on Progress

Given that the Kundt tube has now been calibrated, there should be no further complications related to generating data with this device. Issues related to laser scan rate will be remedied with the installation of a small motor on the testing frame that will ensure that the laser passes over the sample at a constant rate.

Work Planned Next Quarter

Activities planned for the next quarter include:

- Contacting appropriate road controlling authorities seeking permission and support to conduct field evaluations.
- Using field results from the CTM and DFT to estimate slip speed and friction number in order to determine IFI.
- Comparing IFI values from field sections to IFI values calculated for one of two scenarios: from laboratory equipment (LP and BPT) used on gyratory compactor samples; and from the same laboratory equipment used on field sections tested concurrently with the CTM and DFT.
- Continuing to investigate the relationship between laser spot diameter and MPD.
- Testing cored gyratory compactor samples in the Kundt tube to begin modeling and correlating the acoustic responses of different mix types.

Cited References

ASTM, 2008, ASTM E1050 Standard Test Method for Impedance and Absorption of Acoustical Materials Using A Tube, Two Microphones and A Digital Frequency Analysis System, American Society for Testing and Materials, West Conshohocken, PA.

Losa, M., 2010. Personal correspondence.

CATEGORY VP3: MODELING

Work element VP3a: Pavement Response Model to Dynamic Loads (UNR)

Work Done This Quarter

Continued the work on the *3D-Move Analysis* software to make it a menu-driven software. The last beta-version of the 3D-Move Analysis (ver 1.1) was released on July, 2010. In 3D-Move, output is provided in formats: Text and Excel. An inconsistency has inadvertently occurred when these two formats were integrated. The inconsistency was present only in the Excel file, while the Text file output is correct. The origin of the slip-up was traced to the allocation of the columns when the data sharing between Text and Excel output files occurred. Further, there were concerns about the units of the 3D-Move responses being not prominently displayed. These

issues have been corrected and a modified beta-version of 3D-Move (ver 1.2) was released on August 2010.

Assisted user's with issues ranging from usage questions, concepts clarifications, and bugs.

Work is undergoing to integrate performance models in 3D-Move. Specifically, the following widely-used performance models of fatigue and rutting are to be incorporated within the software. The user will have the option to whether include or not the pavement performance analysis.

- MEPDG Models
 - AC Fatigue Cracking
 - AC Rutting
 - Base/Subbase Rutting
 - Subgrade Rutting
- VESYS Model
 - Fatigue Cracking
 - Layer Rutting
 - System Rutting

The effect of stress distributions and patterns as well as braking condition on pavement responses has been evaluated and the data are being analyzed. Pavement responses were evaluated under the following stress distributions and patterns. Table VP3a.1 shows the experimental matrix.

- Uniform pressure circular contact area
- Uniform pressure elliptical contact area
- Uniform pressure square contact area
- Non-uniform stress distribution

Table VP3a.1 Effect of stress distributions and patterns experimental program.

Pavement Structure	Mixture	Braking/ No-Braking	Analysis Temperature	Stress distributions and patterns			
				Non Uniform	Uniform Circle	Uniform Ellipse	Uniform Square
4" HMA/ 6" Base	Lockwood	Yes/Yes	70°F	X	X	X	X
			104°F	X	X	X	X
	Sloan	Yes/Yes	70°F	X	X	X	X
			104°F	X	X	X	X
6" HMA/ 8" Base	Lockwood	Yes/Yes	70°F	X	X	X	X
			104°F	X	X	X	X
	Sloan	Yes/Yes	70°F	X	X	X	X
			104°F	X	X	X	X
8" HMA/ 10" Base	Lockwood	Yes/Yes	70°F	X	X	X	X
			104°F	X	X	X	X
	Sloan	Yes/Yes	70°F	X	X	X	X
			104°F	X	X	X	X

Significant Results

One of the important inputs to 3D-Move is the material input for the layers. Our recent work on specifying properties for HMA has focused on adopting the different types of master curves. In existing 3D-Move ver 1.2, the following two types of master curves were included: (1) Symmetrical Sigmoidal Function (MEPDG), which requires dynamic modulus laboratory data and binder data, and (2) Witzak prediction equation which requires gradation of mixture and binder data. In the ver 1.3, which is under development, three additional types of master construction methods are being included.

Figure VP3a.1 shows the input window of HMA material properties. The top figure shows all types of master curves and they have been subdivided into two categories according to the approach used: (1) Laboratory Data and (2) Model Equation. While the first category requires laboratory-measured material data, the second category uses equations for which model constants need to be specified. The options available under these two categories are given below:

- Laboratory Data
 1. Symmetrical Sigmoidal Function (MEPDG):

$$\log|E^*| = \delta + \frac{\alpha}{1 + e^{\beta + \gamma(\log t - c(\log \eta - \log \eta_r))}}$$

2. Non-Symmetrical Sigmoidal Function:

$$\log|E^*| = \delta + \frac{\alpha}{[1 + \lambda e^{\beta + \gamma(\log \omega)}]^\lambda}$$

3. Symmetrical Sigmoidal Function (AMPT):

$$\log|E^*| = \delta + \frac{Max - \delta}{1 + e^{\beta + \gamma(\log f + \frac{\Delta E_a}{19.14714}[\frac{1}{T} - \frac{1}{T_r}])}}$$

4. Huet – Sayegh Model (Under Construction):

$$E^*(i\omega) = E_0 + \frac{E_\infty - E_0}{1 + \delta(i\omega\tau)^{-k} + (i\omega\tau)^{-h}}$$

5. User Input (Interpolation)

- Model Equation
 1. Witczak Model
 2. Huet – Sayegh

The bottom part of figure VP3a.1 shows the input window for the Symmetrical Sigmoidal Function (MEPDG) method. The bottom input window has been split into four sections. The first section requires input for the dynamic modulus laboratory data for a set of temperature and frequency, phase angle (or constant damping ratio) and Poisson's ratio. The second section requires input for the binder properties to calculate the A and VTS values. The third and fourth sections are to generate the master curve for reference temperature and analysis temperature, respectively. To generate the master curve for this method, 3D-Move uses principal axis optimization methods.

The option Non-Symmetrical Sigmoidal Function and Symmetrical Sigmoidal Function (AMPT), also requires similar type of input, however, binder properties are not needed. The 3D-Move uses Levenberg-Marquardt optimization method to develop the master curve.

The Huet – Sayegh model uses a different approach to establish the master curve. Work to incorporate this model in 3D-Move is underway. As shown in the figure VP3a.1, 3D-Move has capability to use model equation directly to establish the master curve. As explained above, at present Witczak and Huet-Sayegh models are included in the model equation category. Figure VP3a.2 shows the input window for the Witczak model and it requires inputs such as the gradation of mixture and binder properties to establish the master curve. Figure VP3a.3 shows the input window for Huet-Sayegh model. User has to input the model parameters which are already known to construct the master curve.

Pavement Layer Properties - Layer 1

Type of Material

Linear Elastic Material

Viscoelastic Material

Laboratory Data

Symmetrical Sigmoidal Function (MEPDG)

Non-Symmetrical Sigmoidal Function

Symmetrical Sigmoidal Function (AMPT)

Huet - Sayegh Model (Under Construction)

User Input (Interpolation)

Model Equation

Witczak Model

Huet - Sayegh

Layer Thickness in

Symmetrical Sigmoidal Function (MEPDG)

$$\log E^* = \delta + \frac{\alpha}{1 + e^{\beta + \gamma[\log(t) - c(\log(t) - \log(t_r))]}}$$

Asphalt Mixture Properties | Asphalt Binder Properties | **|E*| Master Curve** | Asphalt General

Dynamic Modulus, |E*| | Damping Ratio and Poisson's Ratio

No of Temperatures No of Frequencies Reference Temperature °F

Temperature (°F)	Dynamic Modulus E* , (psi)		
	0.1 Hz	0.5 Hz	1 Hz

Cancel Previous Next OK

Figure VP3a.1. Input window for the Symmetrical Sigmoidal Function (MEPDG).

Pavement Layer Properties - Layer 1

Type of Material
 Linear Elastic Material
 Viscoelastic Material

Layer Thickness in

Laboratory Data
 Symmetrical Sigmoidal Function (MEPDG)
 Non-Symmetrical Sigmoidal Function
 Symmetrical Sigmoidal Function (AMPT)
 Huet - Sayegh Model (Under Construction)
 User Input (Interpolation)

Model Equation
 Witzcak Model
 Huet - Sayegh

Witzcak's Model

$$\log E^* = 3.750063 + 0.02932\rho_{200} - 0.001767(\rho_{200})^2 - 0.002841\rho_4 - 0.058097V_a - 0.802208\left(\frac{V_{beff}}{V_{beff} + V_a}\right) + \frac{3.871977 - 0.0021\rho_4 + 0.003958\rho_{38} - 0.000017(\rho_{38})^2 + 0.005470\rho_{34}}{1 + e^{(-0.603313 - 0.313351\log(f) - 0.393532\log(\eta))}}$$

Asphalt Mix Properties | **Asphalt Binder Properties** | Asphalt General

Dynamic Modulus [E*] from Witzcak Equation

Aggregate Gradation
 Cumulative % Retained 3/4 inch Sieve:
 Cumulative % Retained 3/8 inch Sieve:
 Cumulative % Retained #4 Sieve:
 %Passing #200 Sieve:

Volumetric Properties
 Effective Binder content (By Volume): %
 Air Voids: %
 Unit Weight: lb/in³

Poisson's Ratio
 Constant Poisson's Ratio
 Poisson's Ratio from Model
 Parameter a Parameter b
 Note: a and b are constants. Typical Values : a = -1.63 and b = 3.84E-6

Frequency (Hz)			
Poisson's Ratio			

Damping Ratio %

Figure VP3a.2. Input window for the Witzcak model.

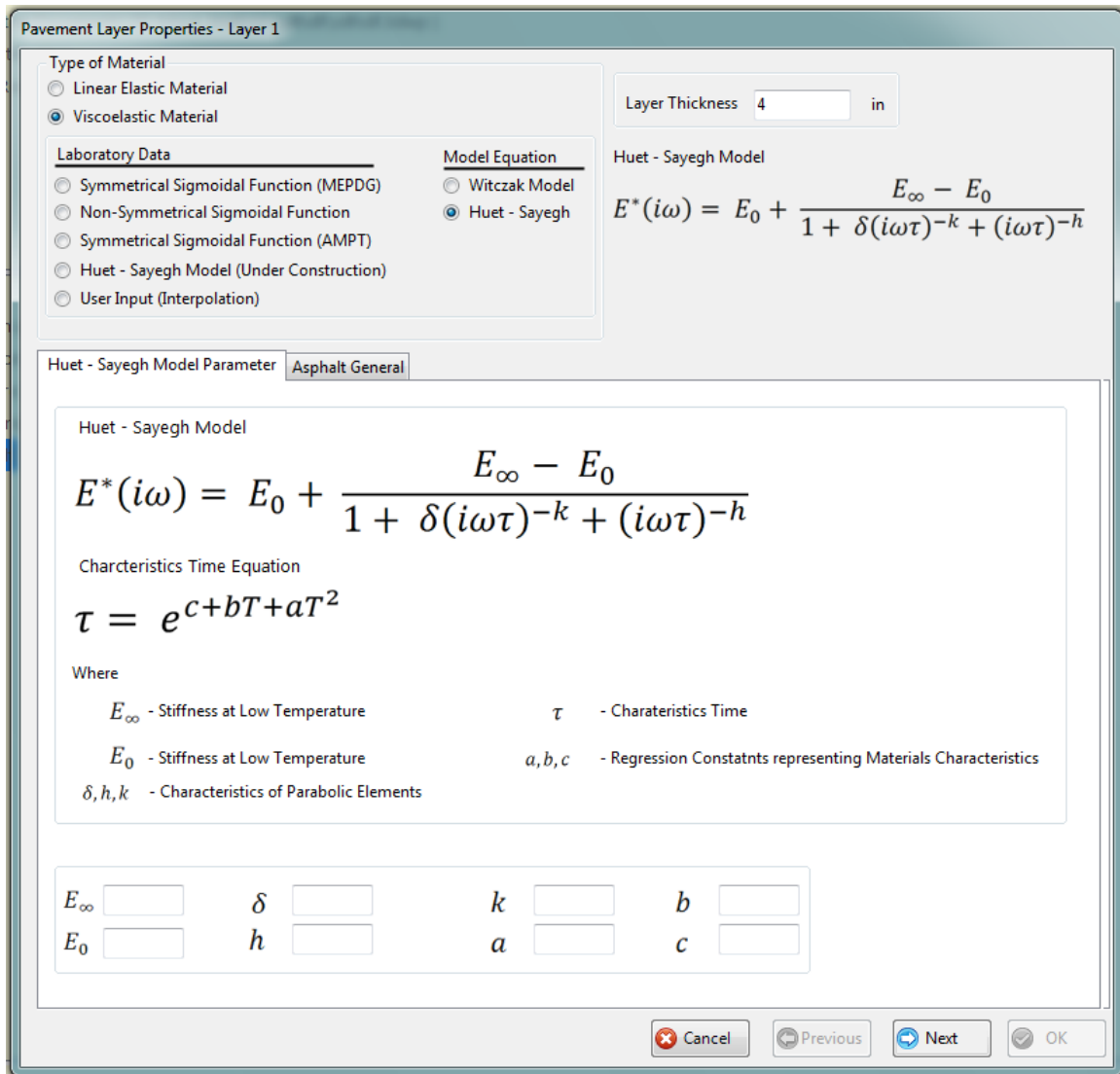


Figure VP3a.3. Input window for the Huet-Sayegh model.

Significant Problems, Issues and Potential Impact on Progress

The 3D-Move Analysis verification plan was postponed to solve the issues and bugs raised by the users, It is anticipated that a version 1.3 of the software be released in the next quarter that will address the various bugs.

Work Planned Next Quarter

Continue working on the 3D-Move model to make it a menu-driven software. Evaluate the beta version for 3D-Move.

Work will continue on the analysis of the effect of contact pressure distribution and braking condition on pavement response.

Work out the details for the *3D-Move Analysis* software verification plan in order to evaluate the potential for errors, bugs, and difficulties involved in using the software for pavement analysis purposes. UNR, with the help of FHWA, will solicit users to participate in the verification plan. It is anticipated that the list of participants will include:

- at least three representatives of public agencies,
- at least three representatives of academic researchers,
- at least three representatives of private industries, and
- at least one representative of FHWA.

Cited References

None

Vehicle-Pavement Interaction Year 4

	Year 4 (4/2010-3/2011)												Team	
	4	5	6	7	8	9	10	11	12	1	2	3		
(1) Workshop														
VP1a: Workshop on Super-Single Tires														UNR
(2) Design Guidance														
VP2a: Mixture Design to Enhance Safety and Reduce Noise of HMA														UWM
VP2a-1: Evaluate common physical and mechanical properties of asphalt mixtures with enhanced frictional skid characteristics														
VP2a-2: Evaluate pavement macro- and micro-textures and their relation to tire and pavement noise-generation mechanisms														
VP2a-3: Develop a laboratory testing protocol for the rapid evaluation of the macro and micro-texture of pavements														
VP2a-4: Run parametric studies on tire-pavement noise and skid response						JP								
VP2a-5: Establish collaboration with established national laboratories specialized in transportation noise measurements. Gather expertise on measurements and analysis														
VP2a-6: Model and correlate acoustic response of tested tire-pavement systems						JP	P							
VP2a-7: Proposed optimal guideline for design to include noise reduction, durability, safety and costs													P	
(3) Pavement Response Model Based on Dynamic Analyses														
VP3a: Pavement Response Model to Dynamic Loads														UNR
VP3a-1: Dynamic Loads														
VP3a-2: Stress Distribution at the Tire-Pavement Interface														
VP3a-3: Pavement Response Model										JP				
VP3a-4: Overall Model										SW				

Deliverable codes

- D: Draft Report
- F: Final Report
- M&A: Model and algorithm
- SW: Software
- JP: Journal paper
- P: Presentation
- DP: Decision Point

Deliverable Description

- Report delivered to FHWA for 3 week review period.
- Final report delivered in compliance with FHWA publication standards
- Mathematical model and sample code
- Executable software, code and user manual
- Paper submitted to conference or journal
- Presentation for symposium, conference or other
- Time to make a decision on two parallel paths as to which is most promising to follow through

	Work planned
	Work completed
	Parallel topic

Vehicle-Pavement Interaction Years 2 - 5

	Year 2 (4/08-3/09)				Year 3 (4/09-3/10)				Year 4 (04/10-03/11)				Year 5 (04/11-03/12)				Team
	Q1	Q2	Q3	Q4	Q1	Q2	Q3	Q4	Q1	Q2	Q3	Q4	Q1	Q2	Q3	Q4	
(1) Workshop																	
VP1a: Workshop on Super-Single Tires																	UNR
(2) Design Guidance																	
VP2a: Mixture Design to Enhance Safety and Reduce Noise of HMA																	
VP2a-1: Evaluate common physical and mechanical properties of asphalt mixtures with enhanced frictional skid characteristics				DP													UWM
VP2a-2: Evaluate pavement macro- and micro-textures and their relation to tire and pavement noise-generation mechanisms				DP													
VP2a-3: Develop a laboratory testing protocol for the rapid evaluation of the macro and micro-texture of pavements		M&A															
VP2a-4: Run parametric studies on tire-pavement noise and skid response						JP		D		JP							
VP2a-5: Establish collaboration with established national laboratories specialized in transportation noise measurements. Gather expertise on measurements and analysis																	
VP2a-6: Model and correlate acoustic response of tested tire-pavement systems										JP, P							
VP2a-7: Proposed optimal guideline for design to include noise reduction, durability, safety and costs													P				
(3) Pavement Response Model Based on Dynamic Analyses																	
VP3a: Pavement Response Model to Dynamic Loads																	
VP3a-1: Dynamic Loads			JP														UNR
VP3a-2: Stress Distribution at the Tire-Pavement Interface																	
VP3a-3: Pavement Response Model						SW, v. β					JP		SW, JP				
VP3a-4: Overall Model										SW			D	F			

Deliverable codes

- D: Draft Report
- F: Final Report
- M&A: Model and algorithm
- SW: Software
- JP: Journal paper
- P: Presentation
- DP: Decision Point

Deliverable Description

- Report delivered to FHWA for 3 week review period.
- Final report delivered in compliance with FHWA publication standards
- Mathematical model and sample code
- Executable software, code and user manual
- Paper submitted to conference or journal
- Presentation for symposium, conference or other
- Time to make a decision on two parallel paths as to which is most promising to follow through

	Work planned
	Work completed
	Parallel topic

PROGRAM AREA: VALIDATION

CATEGORY V1: FIELD VALIDATION

Work element V1a: Use and Monitoring of Warm Mix Asphalt Sections (WRI)

Work Done This Quarter

During the last quarter, construction of the WMA site in Manitoba was completed. The approximately 470 pails of samples were shipped from Canada to the ARC researchers at UNR, UWM, WRI, and also to the MRL in Sparks, Nevada.

The annual monitoring of the Yellowstone WMA sections, constructed by FHWA Western Federal Lands in 2007, was performed in early September. The Yellowstone sections are still performing excellent with no distress noted. Communication with the Park maintenance supervisor indicated that we will be able to obtain pavement core samples next year during the annual monitoring. Previously, the Park did not want to affect the visual quality of the pavement by removing core samples so this is an important change.

Significant Results

None.

Significant Problems, Issues and Potential Impact on Progress

None.

Work Planned Next Quarter

It is planned to establish the monitoring sections at the Manitoba WMA site and to conduct the initial monitoring. The first annual monitoring of the Manitoba RAP sections will also be conducted during the same trip.

Work element V1b: Construction and Monitoring of Additional Comparative Pavement Validation Sites (WRI)

Work Done This Quarter

The annual monitoring of the Minnesota site was performed during August. The distress noted at the Minnesota site continues to be transverse cracking but some other forms of distress have been noted. There continues to be significant differences between the amount of transverse cracking between the different asphalt source materials and between the RAP and no-RAP

sections. It was noted this year that there was not a large increase in distress in the sections from last year.

Significant Results

None.

Significant Problems, Issues and Potential Impact on Progress

None.

Work Planned Next Quarter

During the next quarter, it is planned to conduct the annual monitoring of the Arizona comparative pavement performance site.

CATEGORY V2: ACCELERATED PAVEMENT TESTING

Work element V2a: Accelerated Pavement Testing including Scale Model Load Simulation on Small Test Track (WRI)

Work Done This Quarter

No activity this quarter. This work element was included in order to accommodate any accelerated testing that may occur during the project.

Significant Results

None.

Significant Problems, Issues and Potential Impact on Progress

None.

Work Planned Next Quarter

No accelerated (field) testing is planned.

Work element V2b: Construction of Validation Sections at the Pecos Research & Testing Center (WRI)

This work element is included to indicate that this may be a possibility for accelerated pavement testing for ARC research because it is a facility in the TAMU system.

CATEGORY V3: R&D VALIDATION

Work element V3a: Continual Assessment of Specifications (UWM)

Work Done This Quarter

In this quarter the research team focused their efforts on acquiring field mixes corresponding to binders used in the round-robin binder testing program administered through the Western Cooperative Test Group (WCTG). Loose mix samples collected from project locations in Oregon, Utah, Colorado and New Mexico were batched and compacted in preparation for mixture testing, which will occur in the next quarter. All asphalt mixture samples were compacted to 7% air voids, which are the expected in-place target air voids. Of the nine WCTG binders scheduled for testing in 2010-2011, UW-Madison has obtained four mix samples; three are on track for delivery, and two samples remain outstanding.

Other significant efforts focused on improving binder test reporting forms for the binder testing scheduled to begin in October 2010. Online and paper reporting forms have been revised to reflect comments from WCTG board members and affiliated laboratories. Changes to the report forms include increasing and highlighting the information related to Multiple Stress Creep and Recovery (MSCR) test procedures to identify sources of variability. Particular emphasis will be placed on identifying the make and model of Dynamic Shear Rheometers (DSRs) used by labs.

Additional efforts focused on understanding the use of PG-Plus binder tests throughout the country. Initial investigations suggest that while most states specify at least one PG-Plus test, with elastic recovery (ER) tests being the most common, specifications or test procedures often differ from state to state. Highlighting these differences remains a primary objective of this work element. In some cases, ER tests are used to validate polymer-modified mixtures from qualified contractors. Other states determine that DSR phase-angle measurements are sufficient for qualifying modified binders. Fewer states are using toughness and tenacity or softening point to provide additional binder characterization.

Significant Results

Four asphalt mixtures coming from field sections were connected to corresponding asphalt binders already tested during the round-robin testing. The loose mixtures coming from projects in the field were compacted and are currently being tested for dynamic modulus (E^*), flow number (FN) and fatigue. The effort to collect data from various labs and conduct analysis of variability and consistency of results among labs continues.

Significant Problems, Issues and Potential Impact on Progress

None.

Work Planned Next Quarter

The following activities are planned for the next quarter:

- *Mixture testing* will include dynamic modulus, fatigue and FN.
- *Binder testing* will begin in October 2010 and continue through June 2011. Standard binder tests, PG-Plus tests and tests recently developed at UW–Madison will be used.
- *Monthly conference calls* will continue with the WCTG board to define research priorities.
- The *Annual Meeting* of the Rocky Mountain Asphalt User/Producer Group will take place in Colorado in October 2010 and provide the opportunity to present ongoing strategies for improving specifications.

Work element V3b: Validation of the MEPDG Asphalt Materials Models Using New MEPDG Sites and Selected LTPP Sites (UNR, UWM)

Subtask V3b-1: Design and Build Sections (Start Year 1, Year 2, and Year 3)

Subtask V3b-2: Additional Testing (Start Year 2, Year 3, and Year 4)

Work Done This Quarter

None

Significant Results

None

Significant Problems, Issues and Potential Impact on Progress

Only two agencies have committed to the construction of MEPDG sites: the Washoe RTC in northern Nevada in 2008, The South Dakota DOT in 2009/2010. The researchers are facing significant hesitation from the DOTs to use the MEPDG to design and construct HMA pavements. The level of this work element has been reduced.

Work Planned Next Quarter

None

Subtask V3b-3: Select LTPP Sections (Start Year 1 thru Year 5)

Work Done This Quarter

In this quarter, the research team completed testing 28 binders from the LTPP program using the Linear Amplitude Sweep (LAS) accelerated fatigue test. Table V3b-3.1 presents the analysis of the LAS results for the LTPP binders using the framework of viscoelastic continuum damage (VECD). The fatigue field performance of the LTPP sections is also included in table V3b-3.1.

Table V3b-3.1. LAS results for LTPP binders.

SHRP ID	Sample Type	Climate Type	Fatigue Cracking, m ²	Testing Temp, °C	A ₃₅	B	N _f (2.5%)
300903	PG 64-22	DF	0	25	7.75E+06	-4.74	1.01E+05
370901	PG 64-22	WN	0	25	1.17E+07	-4.67	1.61E+05
370902	PG 64-22	WN	0	25	1.27E+07	-4.66	1.78E+05
370903	PG 70-22	WN	0	28	6.89E+06	-4.74	8.95E+04
09-0902	PG 64-28	WF	0	22	5.57E+06	-4.80	6.83E+04
37-0962	PG 76-22	WN	0	31	4.96E+07	-4.69	6.77E+05
090960	PG 58-28	WF	0.8	19	4.54E+06	-4.68	6.25E+04
09-0961	PG 58-34	WF	2.1	16	1.67E+07	-5.39	1.20E+05
120902	PG 64-16	WN	2.2	28	4.78E+07	-4.69	6.53E+05
090962	PG 58-28	WF	4.3	19	3.04E+06	-4.43	5.24E+04
090903	PG 64-22	WF	5	25	9.82E+06	-4.56	1.50E+05
89-A902	PG 52-40	WN	6.7	10	2.84E+07	-5.70	1.53E+05
89A901	PG 52-34	WN	8.8	13	4.93E+06	-4.91	5.49E+04
340902	PG 58-28	WF	11.4	19	3.65E+06	-4.76	4.68E+04
370963	PG 64-22	WN	12.7	25	1.67E+07	-4.78	2.10E+05
350903	PG 58-22	DN	15.7	22	1.38E+07	-4.87	1.59E+05
370965	PG 70-22	WN	17.7	28	1.36E+07	-4.76	1.74E+05
35-0902	PG 64-22	DN	32	25	2.07E+07	-5.16	1.82E+05
290963	PG 64-16	WF	37.9	28	2.29E+07	-5.23	1.90E+05
34-0901	PG 64-22	WF	49.5	25	6.41E+06	-4.73	8.44E+04
370964	PG 76-22	WN	51.1	31	4.52E+08	-5.00	4.61E+06
310902	PG 58-22	DF	65.5	22	3.96E+06	-4.87	4.57E+04
370960	PG 76-22	WN	73.1	31	5.93E+06	-4.52	9.46E+04
300902	PG 64-34	DF	76.2	19	1.43E+10	-6.79	2.87E+07
310903	PG 64-28	DF	175.5	22	1.72E+07	-4.92	1.90E+05
34-0961	PG 78-28	WF	178.8	28	1.28E+07	-5.13	1.16E+05
04-B901	PG 76-10	DN	328	37	4.96E+06	-4.49	8.12E+04
04B903	PG 70-10	DN	337.9	34	2.45E+06	-4.26	4.96E+04

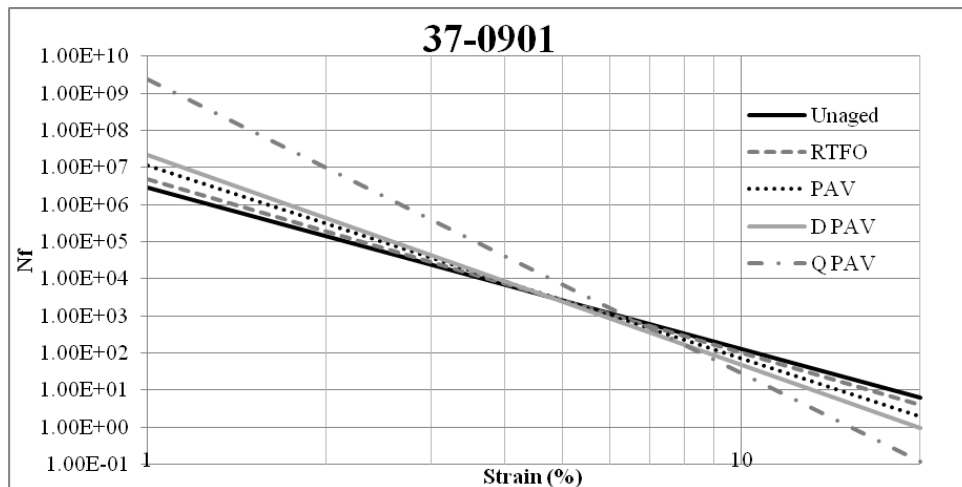
N_f= fatigue life. DF = dry-freeze. WN = wet-nonfreeze. WF = wet-freeze. DN = dry-nonfreeze.

There is no obvious trend between the N_f (2.5%) and the fatigue cracking reported. This is not surprising since the traffic volume, pavement thickness and climatic conditions need to be considered before a logical comparison should be made. The research team has started collecting the traffic and climatic data and also testing at local climate conditions.

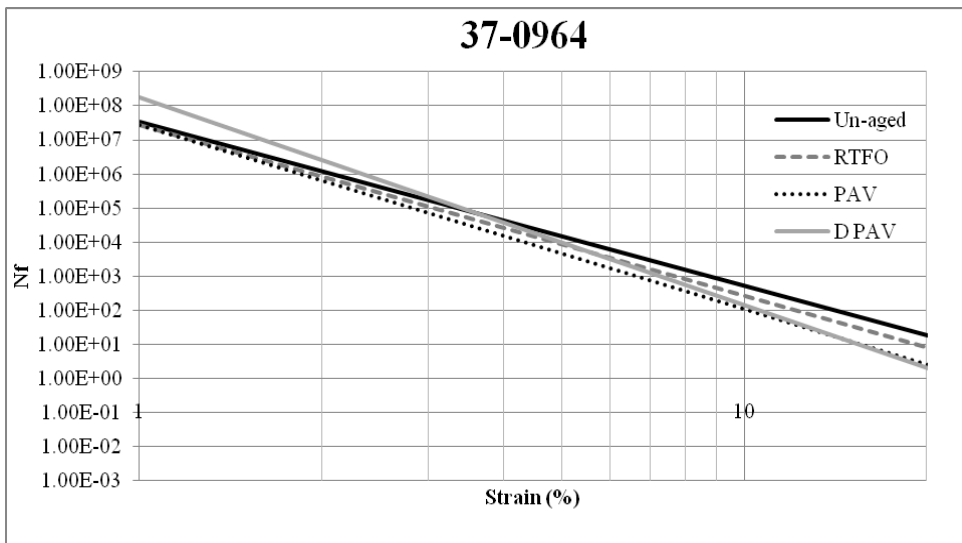
The effect of aging on the fatigue performance of asphalt binders using the LAS was also investigated in this quarter. Six LTPP binders were tested at five aging levels: un-aged, rolling thin film oven (RTFO)-aged, pressure aging vessel (PAV)-aged, double PAV-aged and quadruple PAV-aged. Double PAV-aged and quadruple PAV-aged consisted of 40 hours and 80

hours of pressure vessel aging, respectively. The results revealed that at low and high strain levels aging increases and decreases fatigue life, respectively. The modified binders exhibited small differences in fatigue performance with age, indicating that modification reduces the effect of aging. The fatigue law plots of two of the six binders tested at all age levels are presented in figure V3b-3.1. The 37-0901 binder is a neat binder for which aging is beneficial at low strains but detrimental at high strains.

Figure V3b-3.1 indicates that the 37-0964 modified binder is less sensitive to aging. Note that the 37-0964 binder was not tested at the quadruple PAV aging level due to its high stiffness and brittleness at this condition.



(a)



(b)

Figure V3b-3.1. Graphs. Effect of aging on LAS results for LTPP binders: (a) 37-0901; and (b) 37-0964. (D PAV = double PAV-aged; total of 40 hours aging. Q PAV = quadruple PAV-aged; total of 80 hours aging.)

Significant Results

LAS testing of the LTPP binders has been completed. The effect of aging on the fatigue life of LTPP binders was investigated. The results indicate that laboratory aging changes significantly and systematically the relationship between fatigue life (i.e., N_f , number of cycles to failure) and strain level. The changes are such that aging appears to improve binder fatigue resistance at low strain levels, but deteriorates fatigue resistance at high strain levels.

Significant Problems, Issues and Potential Impact on Progress

None.

Work Planned Next Quarter

The research team will develop limits for fatigue parameters A_{35} and B for specification purposes based on the comparison between LAS results and fatigue cracking field performance. The team will continue working on incorporating other pavement parameters such as pavement structure and traffic to improve the correlation between LAS results and field data. Also, the research team will continue data collection from LTPP sections for which low-temperature cracking and moisture damage performance is available.

Subtask V3b-4: Testing of Extracted Binders from LTPP Sections (Start Year 1)

Work Done This Quarter

None.

Work Planned Next Quarter

No work planned.

Subtask V3b-5: Review and Revisions of Materials Models (Start Year 2, Year 3, Year 4, and Year 5)

The reader is referred to subtask V3b-1.

Subtask V3b-6: Evaluate the Impact of Moisture and Aging (Start Year 3, Year 4, and Year 5)

The reader is referred to subtask V3b-1.

Work Element V3c: Validation of PANDA (TAMU)

Work Done this Quarter

Please refer to the details presented in work elements M4c, F1d-8, and F3c. These work elements outline what has already been accomplished in validating the constitutive models that are implemented in PANDA as well as the validation work that will be carried out in the coming quarter. At this stage, most emphasis is placed on validating the PANDA against the comprehensive ALF experimental data. The reader is referred to the following publications for more detail:

Darabi, M. K., Abu Al-Rub, R. K., Masad, E. A., Huang, C.-W., and Little, D. N. “A thermo-viscoelastic-viscoplastic-viscodamage constitutive model for asphaltic materials,” *International Journal of Solids and Structures* [DOI:10.1016/j.ijsolstr.2010.09.019](https://doi.org/10.1016/j.ijsolstr.2010.09.019).

Abu Al-Rub, R. K., Darabi, M. K., Little, D., and Masad, E. A., “A micro-damage healing model that improves prediction of fatigue life of asphalt mixes,” *International Journal of Engineering Science* [DOI: 10.1016/j.ijengsci.2010.09.016](https://doi.org/10.1016/j.ijengsci.2010.09.016).

Abu Al-Rub, R. K., Darabi, M. K., and Masad, E. A., “A straightforward numerical technique for finite element implementation of nonlocal gradient-dependent continuum damage mechanics theories,” *International Journal of Damage Mechanics* (in press).

Huang, C. W., Abu Al-Rub, R. K., Masad, E. A., and Little, D. N., “Three dimensional simulations of asphalt pavement performance using a nonlinear viscoelastic-viscoplastic model,” *ASCE Journal of Materials in Civil Engineering* [DOI:10.1061/\(ASCE\)MT.1943-5533.0000022](https://doi.org/10.1061/(ASCE)MT.1943-5533.0000022).

Significant Results

See the significant results sections in work elements M4c, F1d-8, and F3c.

Significant Problems, Issues and Potential Impact on Progress

See the significant results sections in work elements M4c, F1d-8, and F3c.

Work Planned Next Quarter

Focus will be placed on finishing the validation of PANDA using the ALF data.

Work Element V3d: Engineered Properties Testing Plan (TAMU)

Work Done this Quarter

The work completed this quarter relates to work described in Work Elements F1b-2, F2c, and E1a.

Work Planned Next Quarter

Please refer to Work Elements F1b-2, F2c, and E1a.

Validation Year 4

	Year 4 (4/2010-3/2011)												Team	
	4	5	6	7	8	9	10	11	12	1	2	3		
(1) Field Validation														
V1a: Use and Monitoring of Warm Mix Asphalt Sections														WRI
V1b: Construction and Monitoring of additional Comparative Pavement Validation sites														WRI
(2) Accelerated Pavement Testing														
V2a: Accelerated Pavement Testing including Scale Model Load Simulation on small test track (This work element will include all accelerated pavement testing)														WRI
V2b: Construction of validation sections at the Pecos Research & Testing Center														WRI
(3) R&D Validation														
V3a: Continual Assessment of Specification														UWM
V3a-1: Evaluation of the PG-Plus practices and the motivations for selecting the "plus" tests.														
V3a-2: Detailed analysis of all PG-Plus tests being proposed or in use today, documentation of benefits and costs of these tests, and comparison with new tests														
V3a-3: Development of protocols for new binder tests and database for properties measured				P										
V3a-4: Development of specification criteria for new tests based on field evaluation of construction and performance			P									JP		
V3a-5: Interviews and surveys for soliciting feedback on binder tests and specifications		P							JP					
V3b: Validation of the MEPDG Asphalt Materials Models and Early Verification of Technologies Developed by ARC using new MEPDG Sites and Selected LTPP sites														UNR/UWM/WRI
V3b-1: Design and Build Sections														UNR
V3b-2: Additional Testing (if needed)														
V3b-3: Select LTPP Sites to Validate New Binder Testing Procedures				DP	JP						P			UWM
V3b-4: Testing of Extracted Binders from LTPP Sections														
V3b-5: Review and Revisions of Materials Models														
V3b-6: Evaluate the Impact of Moisture and Aging														
V3c: Validation of PANDA														TAMU
V3d: Engineered Properties Testing Plan				P		P								TAMU

Deliverable codes

- D: Draft Report
- F: Final Report
- M&A: Model and algorithm
- SW: Software
- JP: Journal paper
- P: Presentation
- DP: Decision Point

Deliverable Description

- Report delivered to FHWA for 3 week review period.
- Final report delivered in compliance with FHWA publication standards
- Mathematical model and sample code
- Executable software, code and user manual
- Paper submitted to conference or journal
- Presentation for symposium, conference or other
- Time to make a decision on two parallel paths as to which is most promising to follow through

	Work planned
	Work completed
	Parallel topic

Validation Years 2 - 5

	Year 2 (4/08-3/09)				Year 3 (4/09-3/10)				Year 4 (04/10-03/11)				Year 5 (04/11-03/12)				Team
	Q1	Q2	Q3	Q4	Q1	Q2	Q3	Q4	Q1	Q2	Q3	Q4	Q1	Q2	Q3	Q4	
(1) Field Validation																	
V1a: Use and Monitoring of Warm Mix Asphalt Sections																	WRI
V1b: Construction and Monitoring of additional Comparative Pavement Validation sites																	WRI
(2) Accelerated Pavement Testing																	
V2a: Accelerated Pavement Testing including Scale Model Load Simulation on small test track																	WRI
V2b: Construction of validation sections at the Pecos Research & Testing Center																	WRI
(3) R&D Validation																	
V3a: Continual Assessment of Specification																	UWM
V3a-1: Evaluation of the PG-Plus practices and the motivations for selecting the "plus" tests.		P	D,F														
V3a-2: Detailed analysis of all PG-Plus tests being proposed or in use today, documentation of benefits and costs of these tests, and comparison with new tests				P	D												
V3a-3: Development of protocols for new binder tests and database for properties measured						JP				P							
V3a-4: Development of specification criteria for new tests based on field evaluation of construction and performance						D		P	P			JP	P		JP		
V3a-5: Interviews and surveys for soliciting feedback on binder tests and specifications									P		JP		P		D	F	
V3b: Validation of the MEPDG Asphalt Materials Models and Early Verification of Technologies Developed by ARC using new MEPDG Sites and Selected LTPP sites																	UNR/UWM
V3b-1: Design and Build Sections																	
V3b-2: Additional Testing (if needed)																	
V3b-3: Select LTPP Sites to Validate New Binder Testing Procedures					DP			P		JP, DP		P			D	F	
V3b-4: Testing of Extracted Binders from LTPP Sections																	
V3b-5: Review and Revisions of Materials Models																	
V3b-6: Evaluate the Impact of Moisture and Aging																	
V3c: Validation of PANDA																	TAMU
V3d: Engineered Materials Testing Plan											P(2)						TAMU

Deliverable codes

- D: Draft Report
- F: Final Report
- M&A: Model and algorithm
- SW: Software
- JP: Journal paper
- P: Presentation
- DP: Decision Point

Deliverable Description

- Report delivered to FHWA for 3 week review period.
- Final report delivered in compliance with FHWA publication standards
- Mathematical model and sample code
- Executable software, code and user manual
- Paper submitted to conference or journal
- Presentation for symposium, conference or other
- Time to make a decision on two parallel paths as to which is most promising to follow through

- Work planned
- Work completed
- Parallel topic

PROGRAM AREA: TECHNOLOGY DEVELOPMENT

Work element TD1: Prioritize and Select Products for Early Development (Year 1)

Work Done This Quarter

None. This work element has been completed.

Work Planned Next Quarter

None. This work element has been completed

Significant Problems, Issues and Potential Impact on Progress

None. This work element has been completed.

Work element TD2: Develop Early Products (Year 3)

Work Done This Quarter

Table TD2.1 summarizes the progress on the Products for Early Development. Work has been completed at WRI on the test method for Determination of Polymer in Asphalt. Work on the remaining products is expected to be completed by the end of 2010.

Table TD2.1. Summary of progress on early development products.

Product	ARC Research Program	Format	Estimated Completion Data	ARC Partner	Draft AASHTO Standard?
Simplified Continuum Damage Fatigue Analysis for the Asphalt Mixture Performance Tester	Prior	Test Method	12/31/2010	AAT	Yes
Wilhelmy Plate Test	Prior	Test Method	12/31/2010	TTI	Yes
Universal Sorption Device	Prior	Test Method	12/31/2010	TTI	Yes
Dynamic Mechanical Analysis	Prior	Test Method	12/31/2010	TTI	Yes
Automated Flocculation Titrimetric Analysis	Prior	Test Method	12/31/2010	WRI	Yes
Determination of Polymer in Asphalt	Prior	Test Method	Completed	WRI	Yes

Work Planned Next Quarter

Work will continue of the five Products for Early Development listed in Table TD2.1 with estimated completion dates of 12/31/2010.

Significant Problems, Issues and Potential Impact on Progress

None.

Work element TD3: Identify Products for Mid-Term and Long-Term Development (Years 2, 3, and 4)

Work Done This Quarter

The research team continued to review interim research results to identify potential mid-term and long-term products. A total of 29 mid- and long-term products were identified and brief descriptions of these products were included in the Revised Annual Work Plan for Year 4.

Work Planned Next Quarter

The research team will with continue to review interim research products to identify potential long-term development projects.

Significant Problems, Issues and Potential Impact on Progress

None.

Work Element TD4: Develop Mid-Term and Long-Term Products (Years 3, 4, and 5)

The research team will continue development on the 29 mid- and long-term products included in the Revised Annual Work Plan for Year 4.

Work Planned Next Quarter

The research team will with continue to review interim research products to identify potential mid-term and long-term development projects.

Significant Problems, Issues and Potential Impact on Progress

None.

PROGRAM AREA: TECHNOLOGY TRANSFER

CATEGORY TT1: OUTREACH AND DATABASES

Work element TT1a: Development and Maintenance of Consortium Website (Duration: Year 1 through Year 5)

Work Done This Quarter

The ARC website was maintained and updated. The ARC quarterly technical progress report, Apr 1- Jun 30, 2010, was uploaded to the ARC website. The following references were updated:

- List of Publications and Conference Proceedings under the “Publications” webpage.
- List of Presentations and Posters under the “Outreach” webpage.

The beta-version 1.2 of the *3D-Move Analysis* software was uploaded to the ARC website (figure TT1a.1) along with an update on the changes and modifications for the released version. A notification email for the new 3D-Move release was sent to all registered users. The announcement for the 3D-Move release was also posted to the 3D-Move Discussion Group forum. Additionally, responses to users’ questions were also posted to the forum.

Significant Results

None

Significant Problems, Issues and Potential Impact on Progress

None

Work Planned Next Quarter

Continue maintaining and updating the ARC website. Update the list of Publications and Conference Proceedings. Update the list of Presentations and Posters and the list of Theses and White Papers. Post information and new releases for 3D-Move. Maintain the 3D-Move Discussion Group Forum.

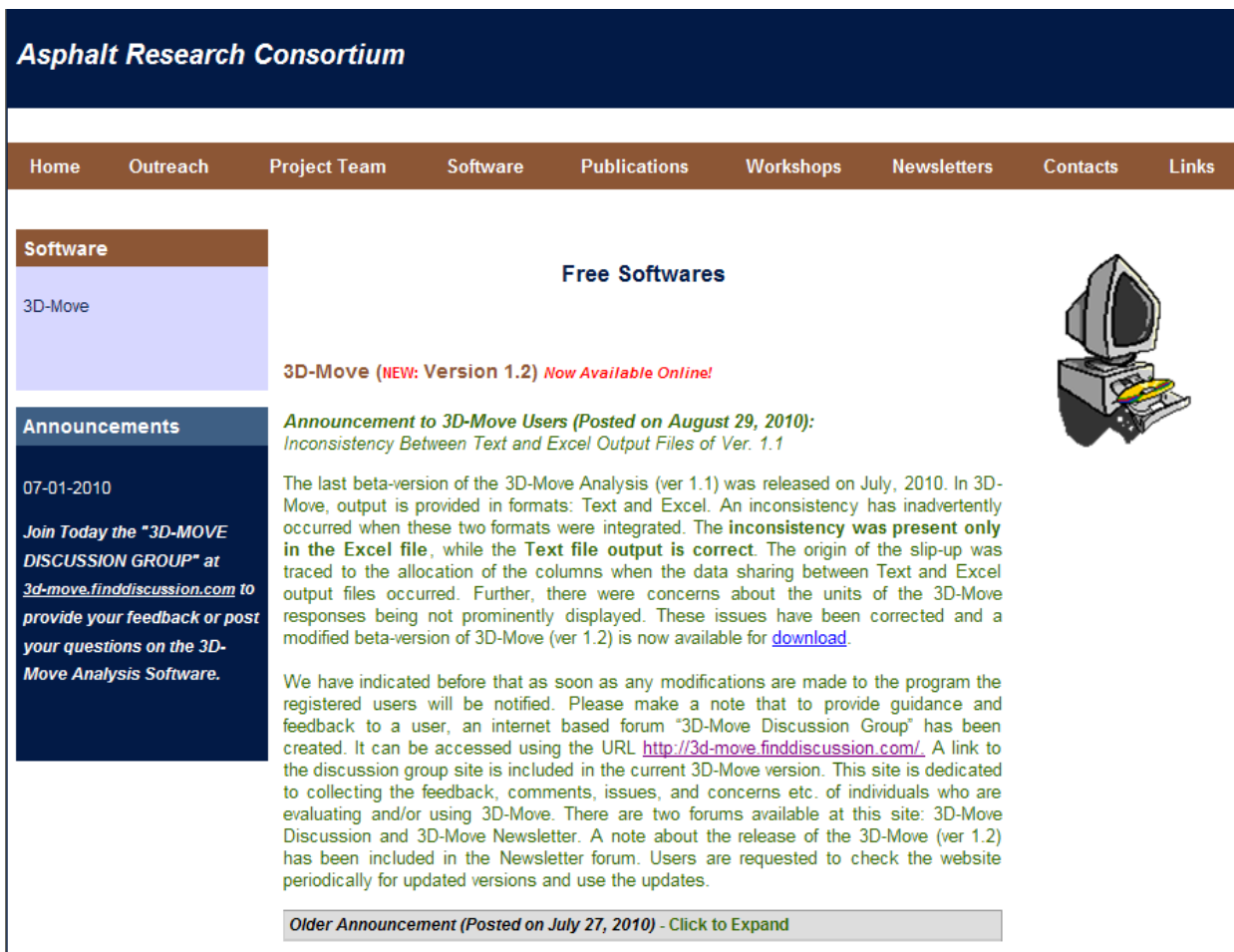


Figure TT1a.1. Screen capture for ARC Webpage “Software.”

Work element TT1b: Communications (Duration: Year 1 through Year 5)

Work Done This Quarter

Prepared and published the seventh ARC Newsletter (Vol. 4 Issue 2). UNR and UWM contributed to the Newsletter.

Significant Results

None

Significant Problems, Issues and Potential Impact on Progress

None

Work Planned Next Quarter

Prepare and publish the eighth ARC Newsletter.

Work element TT1c: Prepare Presentations and Publications

Presentations

Bahia, H., A. Hanz, and J. Meng, “Low Temperature Performance Prediction Methods for Emulsion Residues.” Presented to the Emulsion Task Force, Boston, MA, July 25-26, 2010.

Clopotel, C., “Modification of the Elastic Recovery Test of Binders and Its Relationship to Performance Properties of Asphalt Binders.” Masters Thesis Defense, University of Wisconsin-Madison, Madison, WI, 2010.

Hajj, E. Y., Updates on ARC Work Element E2d: Thermal Cracking Testing of Asphalt Mixtures. Presented to the FHWA Asphalt Mixture and Construction Expert Task Group, Madison, Wisconsin, September 21, 2010.

Hanz, A., H. Bahia, T. Miller, and P. Johannes, “ARC Emulsion Task Force Update – Improvement of Emulsions’ Characterization and Mixture Design for Cold Bitumen Applications.” Presented to the Emulsion Task Force, Boston, MA, July 25-26, 2010.

Harnsberger, P. M., and K. Maranchuk, “Construction and Initial Properties of the Manitoba High RAP Site.” Presented at the 2010 Petersen Asphalt Research Conference, Laramie, WY, July 12-14, 2010.

Luo, R., Y. Koochi, and R. L. Lytton, “Characterization of Field Cores of Asphalt Pavements.” Presented at the 2010 Petersen Asphalt Research Conference, Laramie, Wyoming, July 12-14, 2010.

Lytton, R. L., and R. Luo, “Characterization of Engineered Properties of Asphalt Mixtures as Inputs to PANDA.” Presented at the *Fundamental Properties and Advanced Models Expert Task Group of the Federal Highway Administration*, Madison, Wisconsin, September 23-24, 2010.

Swiertz, D., and H. U. Bahia, “Design System for HMA Containing High Percentage RAP and RAS: Analysis Procedure and Verification.” Presented to Asphalt Binder ETG, Madison, WI, September 22, 2010.

Publications

Abu Al-Rub, R. K., M. K. Darabi, D. Little, and E. A. Masad, “A micro-damage healing model that improves prediction of fatigue life of asphalt mixes,” *International Journal of Engineering Science* DOI: [10.1016/j.ijengsci.2010.09.016](https://doi.org/10.1016/j.ijengsci.2010.09.016).

Abu Al-Rub, R. K., M. K. Darabi, and E. A. Masad, “A straightforward numerical technique for finite element implementation of nonlocal gradient-dependent continuum damage mechanics theories,” *International Journal of Damage Mechanics* (in press).

Bahia, H., A. Meruva, and R. Velasquez, 2010, "Modification of the Penetration Test to Measure Rheological Properties of Binders." *Proceedings of the 4th Technical Week of Asphalt*.

Bahia, H., and R. Velasquez, 2010, "Understanding the Cause of Low Temperature Physical Hardening of Asphalt Binders." *Proceedings of the 55th Canadian Technical Asphalt Association Conference*.

Clopotel, C., E. Mahmoud, and H. Bahia, 2010, "Modification of the Elastic Recovery Test and its Relationship to Performance Related Properties of Modified Asphalt Binders." *90th Transportation Research Board Annual Meeting*, submitted.

Darabi, M. K., R. K. Abu Al-Rub, E. A. Masad, C.-W. Huang, and D. N. Little, "A thermo-viscoelastic-viscoplastic-viscodamage constitutive model for asphaltic materials," *International Journal of Solids and Structures* [DOI:10.1016/j.ijsolstr.2010.09.019](https://doi.org/10.1016/j.ijsolstr.2010.09.019).

Hanz, A., E. Mahmoud, and H. Bahia, 2010, "Asphalt Lubricity Test and Relationship to Mixture Workability." *90th Transportation Research Board Annual Meeting*, submitted.

Hanz, A., E. Mahmoud, and H. Bahia, 2010, "Impacts of WMA Production Temperatures on Binder Aging and Mixture Flow Number." *86th Association of Asphalt Paving Technologists Annual Meeting*, submitted.

Harnsberger, P. M., M. J. Farrar, S-C. Huang, and R. E. Robertson, 2010, "Comparative Field Performance Using Asphalts from Multiple Crude Oil Sources." *90th Transportation Research Board Annual Meeting*, submitted.

Hintz, C., R. Velasquez, Z. Li, and H. Bahia, 2010, "Effect of Oxidative Aging on Binder Fatigue Performance." *86th Association of Asphalt Paving Technologists Annual Meeting*, submitted.

Hintz, Cassie, Raul Velasquez, Carl Johnson, and Hussain Bahia, 2010, "Modification and Validation of the Linear Amplitude Sweep Test for Binder Fatigue Specification." *90th Transportation Research Board Annual Meeting*, submitted.

Huang, C. W., R. K. Abu Al-Rub, E. A. Masad, and D. N. Little, "Three dimensional simulations of asphalt pavement performance using a nonlinear viscoelastic-viscoplastic model," *ASCE Journal of Materials in Civil Engineering* [DOI:10.1061/\(ASCE\)MT.1943-5533.0000022](https://doi.org/10.1061/(ASCE)MT.1943-5533.0000022).

Johannes, P., E. Mahmoud, and H. Bahia, 2010, "The Sensitivity of the ASTM D7000 Sweep Test to Emulsion Application Rates and Aggregate Gradation." *90th Transportation Research Board Annual Meeting*, submitted.

Miller, T., A. Greyling, H. Bahia, and K. Jenkins, 2010, "Development of a Test Method for Determining Emulsion Bond Strength Using the Bitumen Bond Strength (BBS) Test." *2nd International Sprayed Sealing Conference*, accepted.

Miller, T., M. Mahmoud, and H. Bahia, 2010, “Comparing Surface Characteristics of Laboratory and Field Asphalt Mixtures.” *90th Transportation Research Board Annual Meeting*, submitted.

Moraes, R., R. Velasquez, and H. Bahia, 2010, “Measuring Effect of Moisture on Asphalt-Aggregate Bond with the Bitumen Bond Strength Test.” *90th Transportation Research Board Annual Meeting*, submitted.

Sousa, P., E. Kassem, E. Masad, and D. Little, 2011, “New Design Method of Fine Aggregates Mixtures and Automated Method for Analysis of Dynamic Mechanical Characterization Data”, The 90th Annual Meeting, Transportation Research Board, Washington, D.C., January 2011 (accepted for presentation).

Swiertz, D., E. Mahmoud, and H. U. Bahia, 2010, “Estimating the Effect of RAP and RAS on Fresh Binder Low Temperature Properties Without Extraction and Recovery.” *90th Transportation Research Board Annual Meeting*, submitted.

Tabatabaee, H., R. Velasquez, and H. Bahia, 2010, “Predicting Low Temperature Physical Hardening in Asphalt Binders.” *90th Transportation Research Board Annual Meeting*, submitted.

Velasquez, R., H. Tabatabaee, and H. Bahia, 2010, “Low Temperature Cracking Characterization of Asphalt Binders by Means of the Single-Edge Notch Bending (SENB) Test.” *86th Association of Asphalt Paving Technologists Annual Meeting*, submitted.

Work element TT1d: Development of Materials Database (Duration: Year 2 through Year 5)

Work Done This Quarter

Most of the work planned for this quarter has been completed. In addition to the planned work items, some unplanned work items were completed. These unplanned work items were required by the design changes discussed in last quarter’s report. The following list summarizes the effort made on these planned work items.

- The implementation of the user interface to support bulk editing of property measures is nearly complete and is undergoing final testing.
- The implementation of the enhanced material filtering has been completed.
- The concept of a sample run was introduced to allow for multiple test runs of a material sample from a validation site or other source.
- The infrastructure for the enhanced role-based authentication system is complete. The user interface elements for role-based system are complete for several forms and development is in progress for the remaining forms.
- Numerous enhancements have been made to the form to manage material properties
- Development of the revised file management system is under development.

- Validation site enhancements are underway.
- Several new support forms have been completed.
- Modifications were made to the software download application.

Significant Results

Property Measures – Bulk Editing

The rapid entry form (bulk measure editor) is nearly complete and is undergoing final testing. Much of the development time this quarter was dedicated to this task. Figure TT1d.1 shows the new bulk measure editor.

BI_GRADE_PG					
Property	Value	Unit	Final Results	Date	Select
PG_HIGH		°C	<input type="checkbox"/>		<input type="checkbox"/>
PG_LOW		°C	<input type="checkbox"/>		<input type="checkbox"/>
FP_COC		°C	<input type="checkbox"/>		<input type="checkbox"/>
ROT_VISC		Pa.s	<input type="checkbox"/>		<input type="checkbox"/>
MASS_LOSS	40	%	<input type="checkbox"/>	9/8/2010	<input checked="" type="checkbox"/>
ORIG_G*/sin(delta)		kPa	<input type="checkbox"/>		<input type="checkbox"/>
RTFO_G*/sin(delta)		kPa	<input type="checkbox"/>		<input type="checkbox"/>
PAV_G* sin(delta)	cheese	kPa	<input type="checkbox"/>		<input type="checkbox"/> ⚠
PAV_BBR_STIFFNESS		MPa	<input type="checkbox"/>		<input type="checkbox"/>
PAV_BBR_M-VALUE			<input type="checkbox"/>		<input type="checkbox"/>
PAV_DT_FAILURE_STRESS	9999999999999999	kPa	<input type="checkbox"/>	9/8/2010	<input checked="" type="checkbox"/> ⓘ
PAV_DT_FAILURE_STRAIN	-1	%	<input type="checkbox"/>	9/8/2010	<input type="checkbox"/> ⚠
PG_TRUE_HIGH		°C	The minimum allowable value for this property is 0. Record was NOT UPDATED.		
PG_TRUE_LOW		°C			
SPECIFIC_GRAVITY	100		<input type="checkbox"/>	burger	<input type="checkbox"/> ⚠

Figure TT1d.1. Multi-dimensional editor.

The following list describes the significant improvements to, and characteristics of, the new bulk editor:

- Entire groups of records can now be processed with a single button click.
- A date copying feature allows easy application of a common date to many measures, while permitting each measure to be assigned a different date if desired.

- Colored fields and feedback icons with mouse-over messages inform the user of the result of each process on a row-by-row basis.
- Successful processes are accompanied by a checkmark, with a tool-tip (mouse-over) stating what was completed.
- Invalid entries, such as text where a number or date should be are highlighted with a feedback icon stating that the row was not processed.

Custom min/max validation constraints are applied, which can be configured individually for each property by the database administrator. Violations of a “soft” min/max are marked in yellow an informational icon is displayed, with the row still being processed. Violations of a “hard” min/max (such as a percent less than zero) are marked in red. The text on the lower right side of figure TT1d.1 demonstrates this mouse-over message, including the specific value of the violated range.

The new bulk editor contains an additional feature to enable improved editing of multi-dimensional properties. Figure TT1d.2 shows the editor used to enter values for multi-dimensional properties. The example shows a two-dimensional grid while entering mixture phase angle by temperature.

Note that multi-dimensional properties are created using the multi-dimensional editor discussed in the previous quarter’s report.

Mixture Phase Angle		
Temperature, F	Hz	Value
40	25	
40	10	
40	5	
40	1	
40	0.5	
40	0.1	
<hr/>		
70	25	
70	10	
70	5	
70	1	
70	0.5	
70	0.1	
<hr/>		
100	25	
100	10	
100	5	
100	1	
100	0.5	
100	0.1	
<hr/>		
130	25	
130	10	
130	5	
130	1	
130	0.5	
130	0.1	

Add Blank Rows 3 Cancel Submit Changes

Figure TT1d.2. Multi-dimensional editor – entering measure values.

Material Filtering

Related to the topic of the enhanced measures bulk editor, the material filtering subsystem has been enhanced. Materials can now be selected (filtered) based on the following criteria:

- Work tasks including program area, program category, work elements, and work subtasks
- Material types
- Material categories
- The organization that created the material
- Material supplier

Figure TT1d.3 shows the material filters used to select materials for various measures. Note that the same material filters can be used to select data in other sections of the application.

Select Material To Edit From Tree:

Filters:

	Material Type	Material Category	Primary Organization	Supplier
<input type="checkbox"/> Work Tasks	[ALL]	[ALL]	[ALL]	[ALL]
<input checked="" type="checkbox"/> Validation Sections				

Show Detail

Select Validation Site: Shism Street

Select Validation Section: 32R101

Select Layer: 3

Filter By: Site Section Layer

Figure TT1d.3. Material filters.

Material Test Run

When a material sample is taken from a validation site, or other material source, that sample might be distributed to different consortium members for testing and processing. Thus, different measures will likely be recorded for the same sample. To account for the same sample being processed by different entities at different times, the concept of a *test run* was introduced. A test run is made up of a user-defined name and the date the run was performed. Test runs are then linked to material measures. The database enhancements and user control form to implement the test run are complete.

Role-based Authorization Enhancements

As discussed in last quarter's report, it was decided that the role-based authorization subsystem should be implemented such that users are categorized as standard users, organizational super users, and an administrator(s) or super user. Ordinary (standard) users cannot edit data created by others. Organizational super users can edit data created by standard users belonging to the same organization. An administrator can edit data created by any user. Ordinary (standard) users are allowed to view any and all data.

Development of the infrastructure to support this revised implementation is complete. New fields were added to the users and roles tables to support this functionality. In addition, fields were added to the necessary tables to indicate the user that created the record. In addition, new

infrastructure procedures were created that are used throughout the application to enforce this rules-based infrastructure. The following forms completely implement the new authorization scheme:

- Material types
- Contractors
- Contacts
- Property groups
- Administrative forms

Development is underway for the remaining forms and will be completed during the quarter ending December 31, 2010.

Material Properties

Several changes have been made the form to manage material properties. On this form, the user can now create property dimensions that are then used by the bulk measures editor. The administrator can now select a destination material type, and easily copy any number of properties to it, either by group or by selection. In addition, codes were added to aid in this process by notifying the administrator how each property is currently being applied in the database. Figure TT1d.4 shows the user interface for the multi-dimensional editor and copy properties facility.

Property Copy Destination Aggregate

CODES

1 -- Property assigned to at least one other Material Type
 2 -- Property assigned at least one Measure for this Material Type
 3 -- Property assigned at least one Measure for another Material Type

QUANTITATIVE PROPERTIES

BI_GRADE_AC									
Copy Selected Copy Group Remove Selected Remove Group Update Group Create New Property									
Property Name	Unit	S Min	S Max	H Min	H Max	Comment	Order		
VISI_GRADE	°C						10	Dims	<input type="checkbox"/>

BI_GRADE_PG									
Copy Selected Copy Group Remove Selected Remove Group Update Group Create New Property									
Property Name	Unit	S Min	S Max	H Min	H Max	Comment	Order		
PG_TRUE_HIGH	°C						10	Dims	<input type="checkbox"/> 2
PG_TRUE_LOW	°C						20	Dims	<input type="checkbox"/> 2
PG_HIGH	°C						20	Dims	<input type="checkbox"/> 2

Figure TT1d.4. Improved property editor.

File Management System

As the most pressing matters for this quarter were to complete the subsystems to enter data for materials, measures, and validation sites, along with the revised authorization system, the file management system is not complete at this time. With the other work items nearly finished, we will focus our efforts to complete this subsystem this quarter. The implementation goals were described in the last quarter's report.

Material-Validation Association

Previously, only one material could be assigned to each layer of a validation section, though that material could be composed of any number of other materials. This implementation was designed to represent the actual contents of that layer. It was decided that the ability to associate additional materials to each validation section and layer was necessary in order to identify materials to be tested that relate to the validation detail. Therefore, the database was extended and the interface modified to allow validation layers to be connected to any number of materials as shown in figure TT1d.5, while retaining the record of a single material representing the physical contents of a layer.

You may associate 0 or more Validation Sections with this material.

Show Detail

Select Validation Site: Shism Street

Select Validation Section: 32R101

Select Layer: 3 (Assigned To Material)

[Assign to Selected Material](#)

Figure TT1d.5. Validation association editor.

New Support Forms

During the initial development, some of the support forms were not complete. The following forms have been completed this quarter. In addition, the role-based infrastructure has been fully implemented for these new forms.

- The form to enter contractors responsible for validation sites has been completed.
- The form to enter contacts has been completed.

Figure TT1d.6 shows the form to create and modify contractors. The contacts form is not shown here as it is nearly identical.

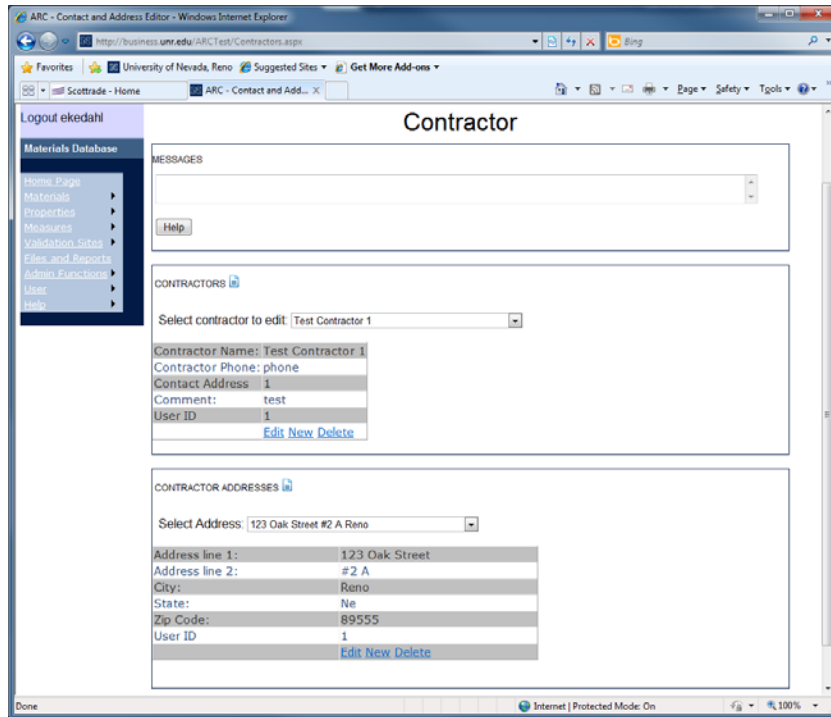


Figure TT1d.6. Contractor editing form.

3F-Move Software Download Application

The software download application was modified so that existing registered could enter their e-mail to download the software, rather than having to complete all of the registration information again.

Significant Problems, Issues and Potential Impact on Progress

None

Work Planned for Next Quarter

Our plan for the next quarter is to finalize those development tasks underway this quarter as follows:

- Finalize testing of the bulk editor.
- Finalize the implementation of the validation sites.
- Complete the implementation of the file management subsystem.

- Create the interface to allow the administrator to control display order of properties, with qualitative and quantitative properties intermixed.
- Complete the help system and documentation based on the above changes.
- Complete the user / super user system for the remaining forms and user interface elements.
- Clean test data and migrate that data to the production database version.

Work element TT1e: Development of Research Database (Duration: Year 2 through Year 5)

Work Done This Quarter

Uploaded the quarterly technical progress report to the ARC website. Updated the “Publications” and “Outreach” web pages.

Significant Results

None.

Significant Problems, Issues and Potential Impact on Progress

None.

Work Planned Next Quarter

Upload the ARC quarterly technical progress report to the ARC website. Publish the ARC newsletter on the ARC website.

Work Element TT1f: Workshops and Training

Work Done This Quarter

No activity this quarter.

Significant Results

None

Significant Problems, Issues and Potential Impact on Progress

None

Work Planned Next Quarter

None

Technology Transfer Year 4


	Year 4 (4/2010-3/2011)												Team
	4	5	6	7	8	9	10	11	12	1	2	3	
(1) Outreach and Databases													
TT1a: Development and Maintenance of Consortium Website													UNR
TT1b: Communications													UNR
TT1c: Prepare presentations and publications													UNR
TT1d: Development of Materials Database													UNR
TT1d-1: Identify the overall Features of the Web Application													
TT1d-2: Identify Materials Properties to Include in the Materials													
TT1d-3: Define the Structure of the Database													
TT1d-4: Create and Populate the Database													
TT1e: Development of Research Database													UNR
TT1e-1: Identify the Information to Include in the Research Database													
TT1e-2: Define the Structure of the Database													
TT1e-3: Create and Populate the Database													
TT1f: Workshops and Training													UNR

Deliverable codes

D: Draft Report
 F: Final Report
 M&A: Model and algorithm
 SW: Software
 JP: Journal paper
 P: Presentation
 DP: Decision Point

Deliverable Description

Report delivered to FHWA for 3 week review period.
 Final report delivered in compliance with FHWA publication standards
 Mathematical model and sample code
 Executable software, code and user manual
 Paper submitted to conference or journal
 Presentation for symposium, conference or other
 Time to make a decision on two parallel paths as to which is most promising to follow through

 Work planned
 Work completed
 Parallel topic

Technology Transfer Years 2 - 5

	Year 2 (4/08-3/09)				Year 3 (4/09-3/10)				Year 4 (04/10-03/11)				Year 5 (04/11-03/12)				Team
	Q1	Q2	Q3	Q4	Q1	Q2	Q3	Q4	Q1	Q2	Q3	Q4	Q1	Q2	Q3	Q4	
(1) Outreach and Databases																	
TT1a: Development and Maintenance of Consortium Website																	UNR
TT1b: Communications																	UNR
TT1c: Prepare presentations and publications																	ALL
TT1d: Development of Materials Database																	UNR
TT1d-1: Identify the overall Features of the Web Application																	
TT1d-2: Identify Materials Properties to Include in the Materials Database																	
TT1d-3: Define the Structure of the Database																	
TT1d-4: Create and Populate the Database							SW, v, β	SW									
TT1e: Development of Research Database																	UNR
TT1e-1: Identify the Information to Include in the Research Database																	
TT1e-2: Define the Structure of the Database																	
TT1e-3: Create and Populate the Database																	
TT1f: Workshops and Training																	UNR

Deliverable codes

D: Draft Report
 F: Final Report
 M&A: Model and algorithm
 SW: Software
 JP: Journal paper
 P: Presentation
 DP: Decision Point

Deliverable Description

Report delivered to FHWA for 3 week review period.
 Final report delivered in compliance with FHWA publication standards
 Mathematical model and sample code
 Executable software, code and user manual
 Paper submitted to conference or journal
 Presentation for symposium, conference or other
 Time to make a decision on two parallel paths as to which is most promising to follow through

 Work planned
 Work completed
 Parallel topic

